Fernando Aguilar-Galindo Rodríguez

Theoretical study of adsorption, excitation and resonant charge transfer of organic molecules on metal surfaces

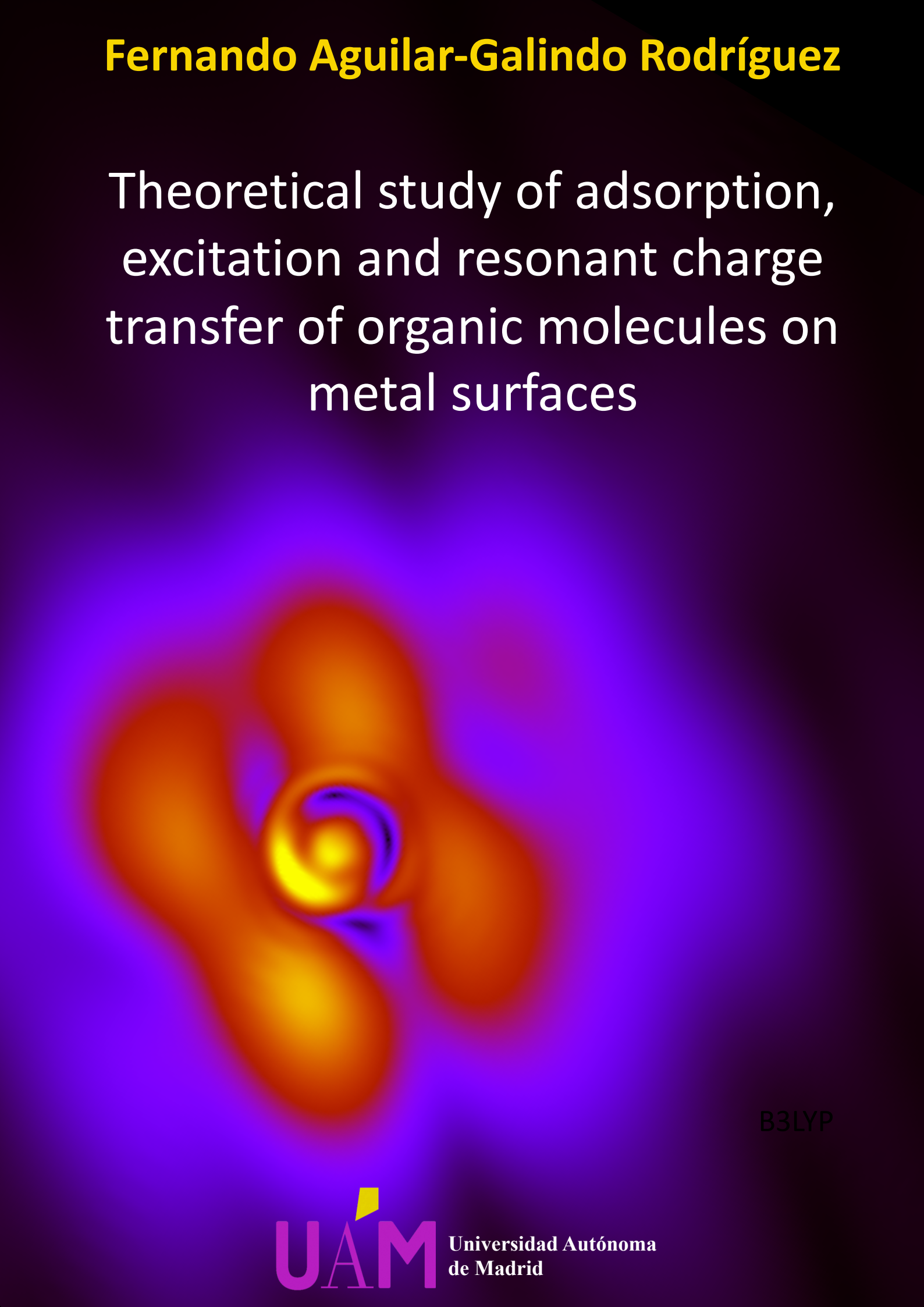

Universidad Autónoma de Madrid

Theoretical study of adsorption, excitation and resonant charge transfer of organic molecules on metal surfaces

Memoria que, para optar al título de Doctor en Química,
con mención de doctorado europeo presenta:

Fernando Aguilar-Galindo Rodríguez

Tesis dirigida por:
Dr. Sergio Díaz-Tendero Victoria

Madrid, 2019

FACULTAD DE CIENCIAS

Universidad Autónoma de Madrid

Theoretical study of adsorption, excitation and resonant charge transfer of organic molecules on metal surfaces

Fernando Aguilar-Galindo Rodríguez

Agradecimientos

Ésta es, probablemente, la parte más complicada de escribir de la tesis. Oficialmente se ha desarrollado entre los años 2015 y 2019, pero no habría llegado aquí sin mucho apoyo a lo largo de muchos años. Por eso es complicado recordar a toda la gente sin la cual no habría sido posible. Creo que por muchas páginas que escriba, no será suficiente para reconocer a todas esas personas que ahí han estado como creo que se lo merecen.

Empezaré dando las gracias al profesor Manuel Alcamí, porque sin el contrato FPI asociado a su proyecto, probablemente no habría hecho la tesis. O no al menos *esta* tesis. Manuel también me dio clase de informática en primero y me hizo pensar en simulaciones a raíz de una clase, ya por aquellos tiempos.

En segundo lugar, muchas, muchas gracias a mi director, el *Amado Líder*, Sergio Díaz-Tendero. Gracias por muchos motivos, por muchas *coshash*. Gracias por todo lo que he aprendido de ciencia, de "pixelar" figuras... Gracias también por darme vía libre en mis idas de olla ("Sergio, que quiero supervisar un TFG, ¿lo ofertamos?", "Sergio, que quiero meterme en este proyecto"...). Gracias, sobre todo, por el buen ambiente de trabajo. Será imposible encontrar alguien con quien me motive más ir a trabajar. No sé que me deparará el futuro, pero espero poder seguir trabajando contigo, aunque sea por las risas (que es para lo que estamos aquí). O al menos poder compartir de vez en cuando unos judiones o chocolate multilayer dopado.

Un "gracias" especial también a los profesores Manuel Yáñez y Otilia Mó. Sin ninguna duda, son los auténtitos culpables de que esté aquí ahora. Magníficos docentes, mejores personas. La clase de gente que hace falta en la Universidad. Manuel me dio clase en tercero de carrera y ahí fue cuando decidí dejar el camino de los matraces y seguir el camino de la Cuántica. Otilia, por su parte, siempre ha estado ahí, ayudando, aconsejando... La "madre" del departamento, siempre cuidando de sus "niños". Gracias a los dos.

Gracias también a todo el Departamento de Química. Creo que a casi todo el mundo en algún momento he ido a pedirle ayuda y no recuerdo ni una vez en la que me diesen largas (qué paciencia habéis tenido!). Gracias, por ello, a Inés, a Lara (siempre miraré los orbitales al hacer CASSCF!), a Alicia, a Cristina, a Sandra, a Michele, a Jesús, a Fernando, a Néstor, a Marisa...

Aquí quiero agradecer a dos personas también especialmente: a Merche y a Mohktar, que me supervisaron, respectivamente, los Trabajos de Fin de Grado y de Fin de Máster. Con ellos aprendí y tuve las ganas suficientes como para meterme en esta aventura que ha sido la tesis.

También es importante agradecer a quienes sin los cuales el departamento no se sostendría: Marga, Beatriz y Wilson (para mí, PAW no significa *Projected Augmented Wave* sino *Pregúntale A Wilson*, la frase más repetida (y útil) desde que empecé el máster).

Quiero agradecer también a todos aquellos profesores que durante el Grado contribuyeron a aumentar mi interés por la Química. En concreto, me gustaría citar a dos profesores. Primero, a Mariví, por la que pillé el gusto a la química orgánica, y que siempre tuvo abierta la puerta de su despacho para mí, desde primero de carrera hasta ahora. Y, segundo, a José Manuel López Poyato, con el que hemos empezado una colaboración muy divertida.

También me gustaría dedicar un lugar especial a Pilar Ocón, la cual ha demostrado muchísimas veces su (enorme) calidad no sólo docente e investigadora, sino también como persona. Sus consejos, su disponibilidad y su apoyo en etapas complicadas... Gracias, Pilar. Muchísimas gracias.

Este trabajo no se podría haber hecho si no hubiese habido un Centro de Computación Científica disponible 24/7 para lanzar cálculos. Gracias por eso a toda la gente del CCC, especialmente a Alberto y Pablo (con los cuales aprendí muchísimo de Linux!). Siempre llevaré a Anchuelo en el corazón.

Grazie mille, Ana e Michele (e tutte le persone del gruppo), per quei mesi a Napoli! Cuando llegué allí, un poco asustado por ser la primera vez que estaba tanto tiempo fuera de España, no me podía imaginar que la experiencia sería tan buena. Aprendí de superficies, de fotoquímica y de bases, pero además me abrísteis (literalmente) las puertas de vuestra casa, y hasta hicimos excursiones de fin de semana! Mi estancia allí fue magnífica por el gran ambiente que conseguísteis que hubiese en el grupo (y por las cookies de Ana!).

I would like to thank Prof. Andrei Borisov for allowing me to go to the ISMO (twice!). During my two stays there (and with his Skype calls and emails) I could learn A LOT about Quantum Mechanics and Solid State Physics. Also, I must thank him for all his support in all I could need and his interest in my period after the PhD. *Merci!* to Prof. Jean Pierre Gauyacq, who accepted me in his office during my second stay, for the fruitful scientific discussions. I can't forget about all the people from the ISMO who made great my time there, specially Valeria, Elisabetta and Marta, for many funny days and the nice lunches at Orsay!

Por supuesto, una pieza muy importante del ISMO fue Mario (gracias por animarme en tantos momentos!), que junto con la demás gente del *Colesp* hicieron esos meses en París algo inolvidable. Especialmente la gente con la coincidí los dos años, como Jorge (tenemos un Zombicide pendiente!), Mike (y nuestros días en la sala de estudio) y Felipe (con nuestras divagaciones sobre Química Cuántica y B-splines). Merci Naila, for showing me nice places to eat sweets and your friendship!

También quiero agradecer a las buenas gentes de IC el haber estado ahí desde hace ya unos cuantos años. Gente que ha contribuido a hacer ese pequeño "paraíso" donde, en unos días, se pueden cargar pilas para todo el año. Y gente con la que se puede contar en cualquier momento, desde para hacer un viaje para ver a los sevillanos (jamás olvidaremos la cara de Álvaro cuando nos plantamos allí), como para perdernos por islas suecas o montar nuestra propia *selección* de volley. Gracias a Fer y Gonlazito, a Irene y a Ana, por los momentos de gordura máxima; al equipo Arrow: Rafa (garrafa), Sara (la reina del mar) y Marian (de los Ángeles), por nuestros planes alternativos; a Ernesto, al que me une una amistad de 25 años, y a su capacidad de llegar a los sitios antes de la hora de salida; y a Silvia, que aunque llegó más tarde al equipo, ya hemos compartido unas cuantas quedadas en Madrid.

Desde hace muchos años me ha gustado la docencia. Esto ha sido en parte por lo que me marcaron muchos profesores de mi colegio, el Patrocinio de San José, durante toda esa larga etapa. Gracias por eso a Concha, a Fátima, a José María, a Mayte, a Alejandro, a Bárbara, a Tacha...

Especialmente entre los profesores del colegio tengo que mencionar a dos. Por un lado a Charo Cerezo, cuyo recuerdo me sigue empujando a ser mejor persona cada día. Espero que allá donde esté se sienta orgullosa. Y por otro lado a Javi, por quien finalmente me decanté por la Química en lugar de por la Física. Un ejemplo como profesor y como persona.

Gracias a la gente que ha hecho parte del camino conmigo en la universidad: 2m, que me lleva aguantando desde primer año de carrera. Un (literalmente) gran amigo. Y que compartamos muchos más cafés! Enrique, otro que me lleva aguantando unos añitos ya, muchas gracias por tu amistad, aunque seas medio experimental! También una mención al "esbirro", Guille, porque con sus ataques de risa me ha levantado el ánimo más de una vez.

También gracias a la gente que se fue incorporando más tarde, ya cuando había empezado mi etapa "entre ordenadores": al Dr. *moguri* Marcos del Cueto y al Dr. *laserino* Manuel Lara. Gracias, chicos, porque el máster y la tesis se llevó mejor con gente como vostros! De esta etapa también tengo que agradecer a la fuente de la sabiduría, a Octavio, que siempre estuvo ahí dispuesto a ayudar y apoyar, aunque estrictamente *no fuese su puto problema.* Gracias también a Arturo, que al menos con la música y los videojuegos tiene buen gusto.

Quiero agradecer también a gente que llegó algo más tarde, pero con quien también me he echado unas risas: Vani, que me mostró que la pizza NO es italiana, sino napolitana; Jorge (que no creí que sobreviviría hasta el día de depósito de la tesis); Darío; Eva; Noemí (aunque sea una chaquetera la apreciamos) y mi compañeros de despacho, Paula y Ransel, que me han aguantado mis reflexiones internas (o no tan internas) y muchas reuniones con el *Amado Líder*. Gracias por vuestra paciencia!

No puedo no mencionar a Sara: este final de tesis se ha llevado mucho mejor con esos mensajes que, con solo un icono de WhatApp, decían mucho.

Gracias a Sofía, que aunque se haya ido lejos sé que puedo contar con ella (y espero que vuelva a Europa!)

Un grupo muy, muy importante para mí en estos años ha sido el grupo de la parroquia, los micaelos. Gente con la que he tenido desayunos, noches de fiesta, viajes... Y con la que siempre he podido contar, en los momentos buenos y en los no tan buenos. Así que María, Loreto, Inés, Edu, Dani... muchas gracias! Gracias a mi doctora favorita, Amaya, por sus audios e invitaciones a la piscina y por demostrar tantas veces que se puede contar con ella. A Guille, por nuestros paseos, nuestras reflexiones filosófico-políticas y por tantas risas y sidras en el irlandés. Y gracias a mi ahijado, César, por estar ahí (generalmente *ahí*=Nuevos Ministerios media hora después de la hora de quedar), aunque no nos acompañase a Amaya, a Guille y a mí a nuestros paseos por la sierra. Y gracias, por supuesto, a Su Santidad, Jhonny, por su apoyo, su consejo y su amistad.

Gracias también a aquellas personas que no son de un grupo en concreto (o que son de varios) pero que han sido fundamentales. Gracias a Gorgio... digo a Giorgio, por su optimismo y más de 20 años de amistad. Gracias a Carmen, por todavía más años de amistad (¿desde 1992-1993?) y tantos y tantos buenos momentos (y la portada de la tesis! Que de no ser por tí habría sido muy sosa!). Gracias a Juan, por ya también unos cuantos añitos juntos. Rey de los memes y de los stickers. Gracias, por supuesto a Irene, que todo lo que le falta de melanina le sobra de corazón. Anda que no te he dado el coñazo... Gran psicóloga y mejor amiga!

De Luis, te mereces un párrafo a parte. Y todo lo que pueda escribir se me va a quedar corto. Colegio, carrera, parroquia... Has sido un amigo presente en casi todos los grupos importantes de mi vida. Es más, en parte estudié en la UAM porque es donde ibas a estudiar tú y tú fuiste quien me llevaste a la parroquia aquella tarde de viernes en 1º de carrera. Sólo por esa gente maravillosa que conocí gracias a ti, debería ser suficiente para estar agradecido. Pero gracias por muchas más cosas: por tu amistad incondicional, por estar ahí cada vez que la he liado (y han sido tantas veces...!), por el ánimo que me has dado durante la tesis, por tantas risas con tus comentarios sarcásticos en momentos de indignación... Gracias, gracias y mil veces gracias.

Por último, pero no por ello menos importante, quiero agradecer a mi familia el apoyo recibido durante todo este tiempo. Especialmente a mis abuelos, que tan importante han sido (y siempre serán) para mí. Gracias a mis padres que, aún siendo ajenos a la Química Teórica, nunca pusieron en duda mis decisiones y siempre me han animado a seguir hacia delante. Siempre han sido mi referencia. Llegar a ser como ellos, el motivo por el que me he exigido tanto a mí mismo (aunque quizás en el aspecto de orden me quedé bastante lejos). Gracias a mis hermanos, que aunque a veces tengamos nuestros roces, a la hora de la verdad puedo contar con ellos. También mencionar a Tiptup y a Tortugo, otros dos miembros de la familia que han sido un ejemplo de tranquilidad en los momentos de más tensión de la tesis.

Resumen

En esta tesis se presenta un estudio teórico de los procesos de adsorción y excitación de moléculas orgánicas depositadas sobre superficies metálicas. Los cálculos estructurales se han llevado a cabo en el marco de la teoría del funcional de la densidad (DFT por sus siglas en inglés), la más utilizada actualmente para este tipo de sistemas y que es compatible con condiciones periódicas de contorno, necesarias para describir correctamente el carácter metálico del sustrato.

Como moléculas orgánicas se han seleccionado tres derivados del vinilo: la acrilamida, el acrilonitrilo, y la acroleína, precursores de polímeros ampliamente utilizados en la industria. Las tres moléculas poseen un doble enlace C=C conjugado con distintos grupos funcionales que alteran el sistema π, tanto en deslocalización de la densidad electrónica como en energía de los orbitales moleculares. La presencia de un sistema π favorece la interacción con las superficies metálicas ya que estos estados, por su simetría, se encuentran espacialmente más accesibles para interaccionar con los estados de la superficie. Como sustrato se escogió una superficie de cobre. Se trata de un metal muy utilizado en aplicaciones tecnológicas (como electrodo en procesos electroquímicos, como base para catálisis heterogénea, etc.), por sus buenos resultados y su reducido precio. En concreto, se estudió la interacción de los derivados del vinilo con la cara (100), de simetría cuadrada y con la cara (111), de simetría hexagonal.

En la primera parte de la tesis, se realizó un estudio metodológico, con el fin de determinar como calcular óptimamente las propiedades de este tipo de sistemas. En concreto, y dado que en muchas ocasiones la interacción entre superficies metálicas y moléculas orgánicas se encuentra regida por interacciones débiles (típicamente fuerzas de van der Waals) un primer desafío a la hora de tratar estos sistemas es determinar cuál es la forma más adecuada de introducir estas interacciones en el cálculo, ya que muchos de los funcionales más utilizados no las reproducen correctamente. Por

ello, el primer objetivo planteado en esta tesis es determinar la influencia de las fuerzas de van der Waals en la adsorción de estas moléculas. Con esta finalidad, se probaron dos de las metodologías más utilizadas en la actualidad para modelizar las interacciones débiles: el método de Grimme (DFT-D2) y los funcionales de van der Waals (DFT-vdW).

La inclusión de periodicidad hace que los estados electrónicos presenten una dispersión con el momento lineal del electrón. La importancia de este efecto es mayor en los sistemas donde los electrones presentan una mayor movilidad, como es el caso de los metales. Por tanto, es necesario también determinar el grado de detalle de exploración del espacio recíproco (o espacio-K) requerido para tener unos resultados convergidos. Dado que las estructuras y energías de adsorción son pilares base para este trabajo, es crucial asegurar dicha convergencia.

Al tratarse de una superficie de energía potencial (PES, por sus siglas en inglés) de gran complejidad por el elevado número de grados de libertad presentes, existen multitud de formas de adsorción. Por ello, no resulta trivial localizar el mínimo más estable, donde se producirá mayoritariamente la interacción con la superficie. Se ha planteado una estrategia basada en la reactividad de los grupos funcionales y en la simetría de la superficie metálica para explorar la PES y encontrar dichos mínimos.

Una vez determinadas las geometrías de adsorción al nivel de precisión requerido, las interacciones molécula-metal son analizadas mediante diversas técnicas, tales como la teoría de átomos en moléculas, con la que se determina la transferencia de carga entre el metal y la molécula en la adsorción; la proyección de la densidad de estados sobre las distintas componentes de momentos angulares atómicos, de donde se extrae información sobre qué estados electrónicos participan en la interacción; y el análisis de la variación de densidad electrónica ($\Delta\rho$), que permite visualizar cómo por la adsorción se produce una redistribución de la densidad electrónica.

En la segunda parte de la tesis, se han estudiado los mismos derivados del vinilo sobre una superficie de Cu(111), con el fin de determinar la influencia de la simetría de la superficie en la interacción. En esta parte del trabajo, en la que se ha usado la experiencia previamente adquirida, se ha extendido el estudio a la obtención de los niveles vibracionales de las moléculas, comparándolos con las vibraciones en ausencia de interacción con el sustrato.

También sobre Cu(111) se ha realizado un estudio de dinámica molecular en el que se han considerado distintas cantidades de energía de excitación (6 o 12 eV)

inicialmente depositadas sobre la molécula. De esta forma, se ha estudiado la transferencia de energía térmica (cinética de los núcleos) de la molécula a la superficie a lo largo del tiempo, así como los canales de fragmentación a estas energías y como éstos se ven modificados por la interacción con la superficie metálica.

Una parte importante del trabajo realizado durante esta tesis ha consistido en desarrollar una metodología para estudiar dinámica electrónica de moléculas adsorbidas en superficies, basada en la resolución de la ecuación de Schrödinger dependiente del tiempo. Para ello, se ha programado un código para realizar propagación de paquetes de onda (WPP, del inglés *Wave Packet Propagation*). Dicho código, escrito en Fortran90, es totalmente general y puede ser usado para estudiar cualquier molécula, gracias a que se puede acoplar a programas de Química Cuántica o Física del Estado Sólido. En esta tesis también se ha desarrollado la interfaz mediante la generación de diversos códigos y scripts.

Con el software desarrollado, se calcularon los tiempos de vida y las energías de los aniones moleculares de los derivados del vinilo adsorbidos sobre Cu(100). Para ello, se usa la posición de adsorción más estable que se obtuvo para cada caso. Este estudio se extendió al nitroetileno, otro derivado del vinilo, para el cual también se incluyó la superficie de Cu(111), con el fin de analizar el efecto de la estructura electrónica del sustrato.

Finalmente, en la última parte de la tesis se evaluó cómo la inclusión de capas de aislante ultrafinas (1, 2 o 3 capas atómicas de espesor) son capaces de desacoplar la transferencia de carga entre molécula y superficie. Con el fin de obtener conclusiones lo más universales posibles, este estudio se realizó, además de en el nitroetileno, en una porfirina de Zn, un sistema muy diferente desde un punto de vista químico, que además es ampliamente utilizada en Nanotecnología.

Abstract

In this thesis we present a theoretical study of the adsorption and excitation processes of organic molecules deposited on metallic surfaces. The calculations of the structure have been carried out in the frame of the Density Functional Theory (DFT), which is the most used for this kind of systems and which is compatible with the Periodic Boundary Conditions (PBC) that are needed in order to describe properly the metallic character of the substrate.

Three derivatives of the vinyl have been considered: acrylamide (ACA), acrylonitrile (ACN) and acrolein (ACO), which are polymer precursors widely used in industry. The three molecules have a double C=C bond, which is conjugated with different functional groups that change the π electronic system, both the delocalization of the electronic density as well as the energy of the molecular orbitals. The presence of a π system favors the interaction with metal surfaces, since these states, due to their symmetry, are spatially accessible to interact with the states of the surface. A copper surface was chosen as substrate. It is a widely used metal for technological applications (as electrode in electrochemical processes, heterogeneous catalysis, etc.) due to its good performance and low cost. More specifically, the interaction of the vinyl-derivatives with the (100) surface (square symmetry), and with the (111) surface (hexagonal symmetry), have been studied.

In the first part of the thesis, a benchmarking study was carried, in order to determine the optimal methodology for this kind of systems. More specifically, since in many situations the interaction between metal surfaces and organic molecules is ruled by weak interactions (e.g. van der Waals forces) a first challenge to study these systems is to determine which is the most adequate way to introduce these interactions in the calculation, since many of the most used functionals do not reproduce them properly. For this reason, the first goal of this thesis is to determine the influence of van der Waals forces the adsorption of these molecules. With this purpose, two

of the most used methodologies to model weak interactions were tested: the method proposed by Grimme (DFT-D2) and the van der Waals functionals (DFT-vdW)

Due to the inclusion of periodicity, the electronic states present dispersion of the energy with the linear momentum of the electron. The importance of this effect is higher in systems where electrons presents a higher mobility, as in the case of metals. For this reason, it is also required to determine the degree of precision in the description of the reciprocal space (or K-space) needed to obtain converged results. Since the structures and adsorption energies are basic pillars of this work, it is crucial to ensure such convergence.

Since these systems have a very complex Potential Energy Surface (PES) due to the high number of degrees of freedom, there are plenty of adsorption geometries. For this reason, it is not trivial to locate the most stable minimum, where the molecule will interact with the surface. A strategy based in the reactivity of the functional groups and the symmetry of the metal surface was developed in order to explore the PES and to find the different minima, saving computational time.

Once the adsorption geometries have been determined at the required precision level, the metal-molecule interactions are analyzed through different techniques such as the theory of Atoms In Molecules (AIM), used to obtain the transferred charge between molecule and surface due to the adsorption; the projection of the Density Of States (DOS) on the different atomic angular momenta, which provide information on which electronic states are involved in the interaction; and the analysis of the change of the electron density ($\Delta\rho$), which allows us to visualize how a redistribution of this property is produced due to the adsorption.

In the second part of the thesis, we have studied the adsorption of the same vinyl-derivatives on a Cu(111) surface, in order to determine the influence of the symmetry of the surface. In this part of the work, in which the previously acquired experience has been used, the study has been extended to the obtaining of the vibrational levels of the molecules, in order to compare them with the vibrations in absence of interaction with the surface.

Also on Cu(111), a Molecular Dynamics (MD) study was carried out. In this study, different excitation energies (6 or 12 eV) were initially deposited on the molecule. In this way, we studied the transference of thermal energy (kinetic nuclear energy) from the molecule to the surface as a function of time, as well as the main fragmentation channels at these energies and how those channels are modified

due to the interaction with the metal substrate.

An important part of the work carried out during this thesis was to develop a methodology to study electron dynamics at molecules adsorbed on surfaces, based on the resolution of the Time-Dependent Schrödinger Equation (TDSE). To this, a software to carry out Wave Packet Propagation (WPP) has been developed. This code, written in Fortran 90, is totally general and it can be used to study any molecule, since it can be coupled to standard Quantum Chemistry or Solid-State Physics packages. In this thesis this interface was also developed, through different codes and scripts.

With the new software, lifetimes and energies of electronic resonances in molecular anions of the vinyl-derivatives adsorbed on Cu(100) were calculated. For this purpose, the most stable adsorption geometry in each case was used. We extended this study to the nitroethylene, another vinyl-derivative. For this molecule, the Cu(111) surface was also included, in order to get some insights of the effect of the electronic structure of the surface.

Finally, the last part of the thesis is a study of how the presence of ultrathin insulating films (1, 2 or 3 atomic layers width) are able to decouple molecule and surface. With the goal of obtaining general conclusions, this study was carried out with nitroethylene and Zn-porphyrin molecules, as very different system widely used in Nanotechnology.

Contents

List of Figures

List of Tables

Part I

Introduction

Chapter 1

Introduction

1.1 Nanoscience: an approach to an emerging (but consolidated) field

Nanoscience is the area of the science which studies the systems whose size is lower than a micrometer ($1\,\mu m = 10^{-6}$ m), in the range of the nanometers (nm, 10^{-9} m).

In 1959, in the meeting of the American Physical Society, Richard Feynman gave a talk entitled "There's Plenty of Room at the Bottom" [1, 2]. In that talk, Feynman thought about how the miniaturization of the system could induce a revolution in the technology. In order to do this, the ideal objective would be the manipulation of single molecules or atoms. These ideas would get popularity and they were the inspiration for a new emerging field. This can be considered as the birth of Nanoscience.

When the nanoscale regime is reached, several properties of the materials change, as the case of the melting point, lattice constants or the conductivity. These changes are mainly due to the discretization of the electronic levels, since with few atoms in the system bands are not formed, and due to the higher relation between surface (usually unstable) and volume.

The control of the synthesis of such small systems allows the design and fabrication of new materials with specific properties. For instance, a combination of an organic part (as a polymer) with an inorganic substrate (as a metal surface or nanoparticle) induces a charge transfer which changes the work function (energy re-

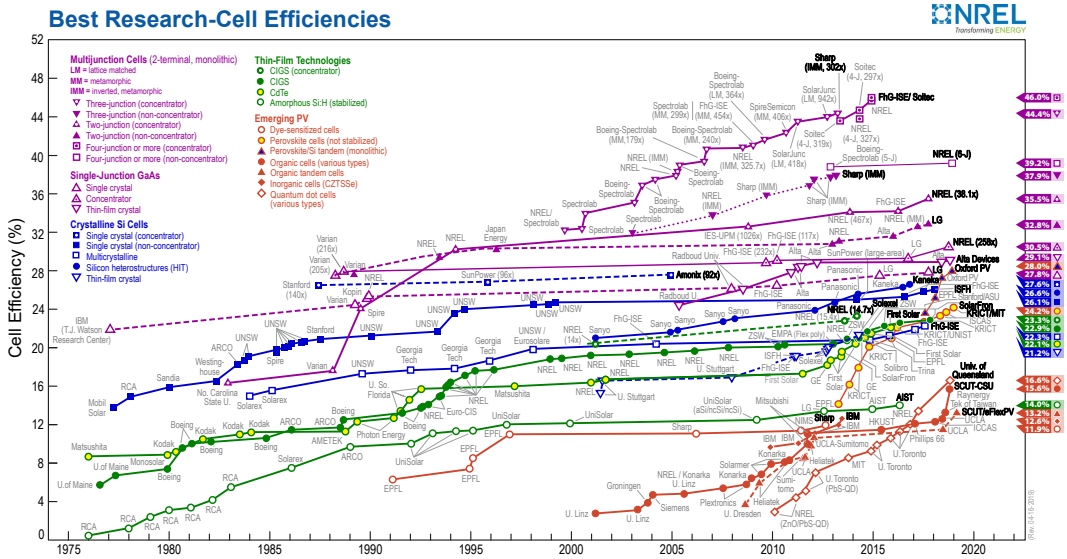

Figure 1.1: Evolution of the efficiency of the research solar cells. This plot is courtesy of the National Renewable Energy Laboratory, Golden, CO.

quired to extract an electron, the equivalent to the ionization potential for atoms or molecules) and the electron density in the system, leading to different conductivity and electronic structure, therefore changing their electronic properties. All these systems have multiple applications, such as optoelectronic devices, OLED (organic light-emitting diode), molecular spintronics, corrosion protectors...

The progresses in Nanoscience led to huge technological advances. As an example, in the decade of the 1960's, Gordon Moore declared what is call as "Moore's law": the number of transistors in a microprocessor will double each year [3]. Although later he changed the period to two years, the exponential grow was still valid. This is a direct consequence of the advances in the miniaturization of the electronic components, bounded to the advances in Nanotechnology.

Another example of application that reflects the development of Nanoscience concerns the exploitation of energy resources, in particular solar energy. The development of new materials, as well as the advances in their manipulation, caused an improvement of the solar cells whose efficiency has been growing during the last decades, from less than 25% to almost 50% (see Figure 1.1).

It is important to take into account that this enhancing of the efficiency is not only due to the advances in the previous technology (the single-junction cell effi-

ciency change from less than 24% to almost 30%) but to the development of new types of cells (as the multijunction cells, which are nowadays the ones with the best performance).

An important part of Nanoscience concerns the study of low dimensional materials. Since the first time graphene was obtained in 2004 by Novoselov *et al* [4], many other 2D materials have been subject of study: black phosphorus [5], hexagonal boron nitride [6], antimomene [7]... All these materials are promising for daily applications as touch screens, sensors...

The application of the Chemistry at the nanoscale leads to the field of the Nanochemistry.

1.2 Experimental techniques in Nanoscience

Due to the multiple applications of the Nanochemistry and the high interest that this field has experienced in the last years, several experimental techniques have been developed, which can be used to modify and measure multiple properties in the nanoscale.

In 1981 Gerd Binnig and Heinrich Rohrer developed the Scanning Tunnel Microscopy (STM). In 1982 the first real atomic structure of a Si surface was obtained and, for "their design of the scanning tunneling microscope" they were awarded with the Nobel prize in 1986. This huge breakthrough in microscopy is based in one of the most important effects in quantum mechanics, the tunneling. It is an effect which would not be observed if classical mechanics would apply to the microscopic world.

In this technique, a metallic tip is approached to the sample (a molecule, structure, surface...) which is deposited on a conductive substrate. The tip is connected to the substrate, in such a way that the Fermi level (highest occupied level in a solid, analogous to the HOMO orbital in isolated molecules) of the tip is aligned to the Fermi level of the structure. Thus, there is no net flux of electrons.

Between the tip and the substrate there is vacuum, which acts as a potential barrier, since an electron has no place to be attached (see scheme in Figure 1.2a).

Then, an electric field is applied between both parts of the system (tip and sample) and thus, the electron density flows from one part to the other (see Figure 1.2b), thus an electric current is established in a so-called tunneling regime.

The tunnel current, I_T, is proportional to:

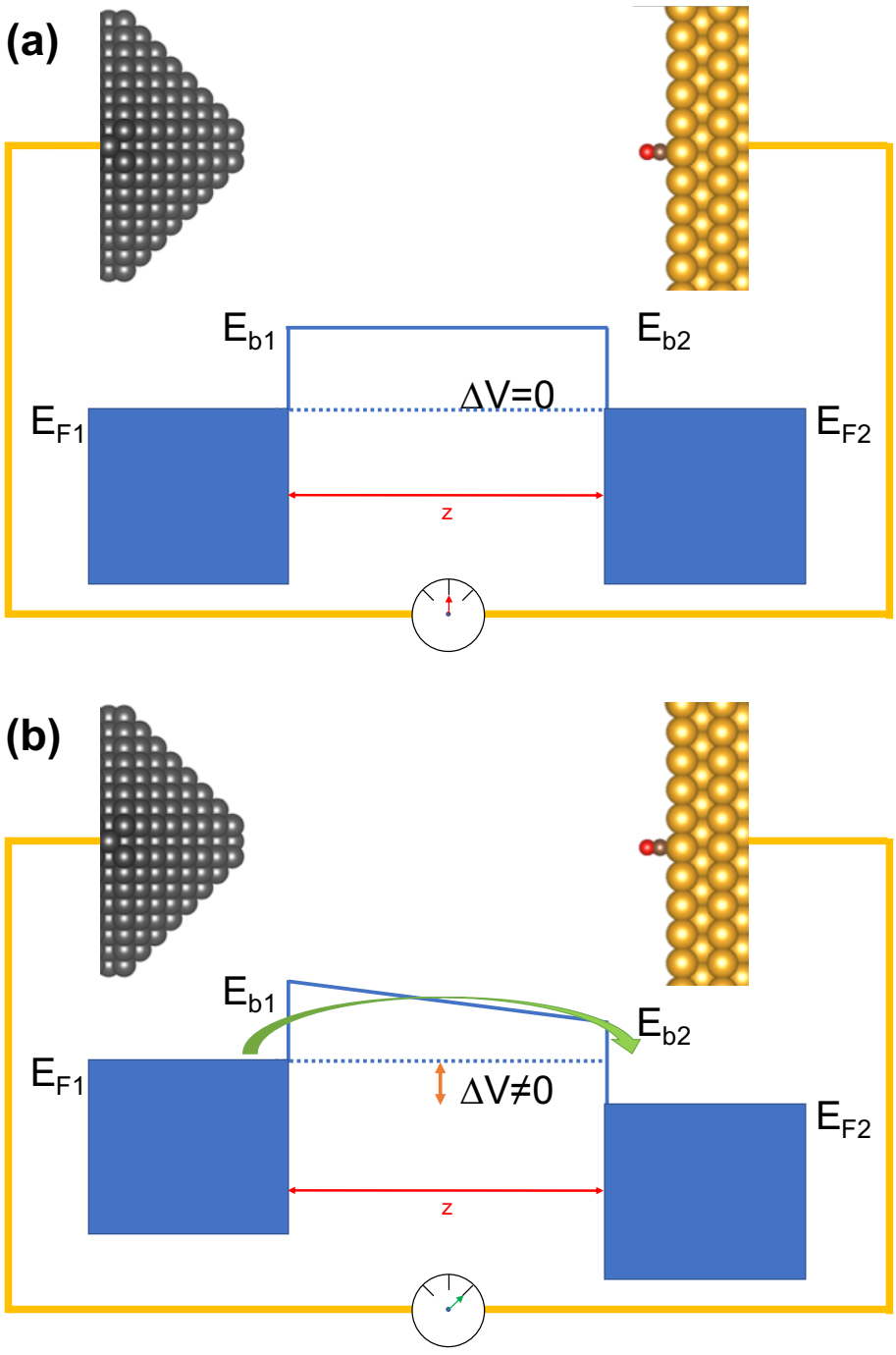

Figure 1.2: Scheme of the potential which would act on a electron in a STM experiment when there is no applied potential (a) and when the potential is active (b).

$$I_T \propto \frac{\Delta V}{z} e^{-kz\sqrt{\phi}} \tag{1.1}$$

where ΔV is the potential due to the electric field (difference between the potential of the tip and the potential of the sample), z is the tip-sample distance, k is a constant and ϕ is the average work function (energy difference between the Fermi level and the potential of the barrier).

STM is an excellent tool to obtain images from a solid surface with atomic resolution. It allows real space measuring: since the current is a function of the distance (with an exponential decay) it is possible to determine the structure of the sample with high precision.

The tunnel current is modified once the applied potential reaches the value of the empty level, in the case of a $\Delta V > 0$. If the potential is applied in the opposite direction ($\Delta V < 0$) then the intensity would change only when this value is enough to transfer electrons from an occupied level of the sample to the tip. Thus, recording the current intensity at different ΔV and calculating its derivative (dI/dV), it is possible to determine the energy of the electronic levels of the sample. In other words: dI/dV is proportional to the density of the states of the sample. Since the provided spectrum depends on the position of the tip, using STM is possible to determine the *Local* Density Of States (LDOS)

Once the value of the potential for a level of interest is determined, STM can be used to obtain the spacial distribution at that energy. An excellent example of this application is the work of Repp *et al* [8] in which they were able to compare the experimental density associated to a given energy and the theoretical results of a molecular orbital. I.e, in these experiments they were able to have a direct measure of the electronic density associated to a given molecular orbital in a single molecule.

With a STM tip, vibrational excitation can be induced, through the Inelastic Electron Tunneling Spectroscopy (IETS) [9]. In this technique, electrons traverse the sample, colliding in an inelastic way. Thus, part of their energy can be transferred to the molecule, inducing an excitation. At low energies, with IETS it is possible to populate vibrational excited states [10].

Also, this loss of energy can be used to promote the sample to a higher electronic state. In this case, after a certain time, the excited electron decays to the ground state with emission of light, in a process called *STM induced luminescence*. Recently, Doppagne *et al* used a STM to induce an electronic excitation and then to measure

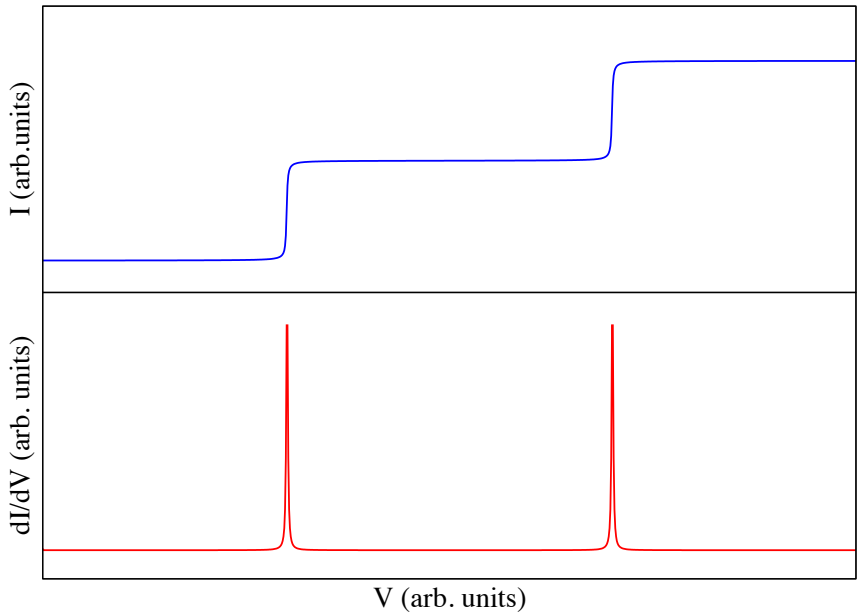

Figure 1.3: Example of an ideal STM experiment in which two discrete levels are explored.

the luminescence in single molecules [11].

STM can be also used to move atoms in order to build nanostructures, an application which has been used for the first time to write the smallest text in the History, the famous IBM logo [12]. In this way, systems with strong quantum effects can be constructed, such as quantum corrals [13], or atomic wires [14, 15] allowing a deeper understand in the most fundamental Physics: quantization of confined electrons (*particle-in-a-box*)

In addition to the information that a STM experiment can provide, other techniques are able to give complementary data. An excellent example is the 2-Photon-Photoemission (2PPE) in which two laser pulses are used (see Figure 1.4). The first one promotes an electron to an excited state and, after a certain time (time delay),

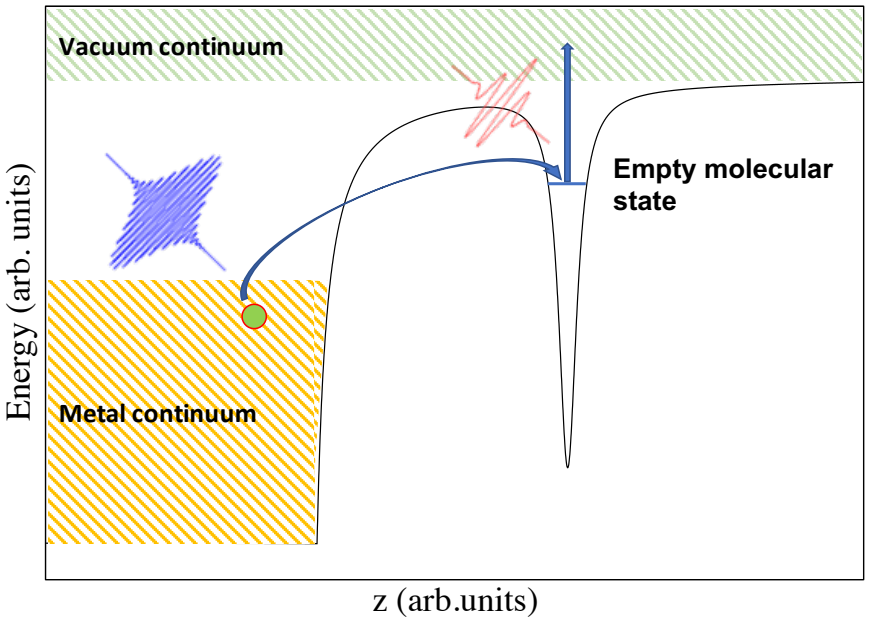

Figure 1.4: Scheme of a 2PPE experiment. A first pulse (blue) promotes an electron to an empty molecular state. Then, a second pulse (red) ionizes the system from that level. Time delay between pulses (Δt) allows to measure the lifetime of the molecular state.

which can be controlled with a huge precision, a second laser pulse ejects the excited electron. If the time delay is long enough, the system would be able to decay to the ground state and thus, the second pulse would not be able to ionize the sample. For this reason, through the use of time resolved 2PPE it is possible to obtain information about the lifetime of the excited states. [16, 17]). Angular-resolved 2PPE measures the angular distribution of the photoemitted electrons, providing information of the kind of excited state which is populated.

Some techniques can enhance their sensibility due to the coupling with surface plasmons in metallic surfaces. Plasmons are collective movements of electrons, with characteristic frequencies. They can induce excitation in molecules with transition in resonance with the plasmons. The use of this effect is the basis of some techniques

as Surface Enhanced Raman Spectroscopy (SERS) [18]. A STM tip can be used instead of a metal surface, technique known as Tip Enhanced Raman Spectroscopy (TERS) [19], etc. Due to the spatial location of the plasmon, some interesting effects can be observed, as a high importance of terms beyond dipole transitions [20], which are the most used to give explanation to light-induced excitations.

In this thesis, several theoretical methods have been used and/or developed to obtain the energy, lifetimes and shapes of the electronic states of molecules adsorbed on surfaces, as well as the energy of their vibrational states, giving explanation to many recent experiments and providing insights on the mechanisms behind fundamental processes such as excitation and de-excitation, molecular-substrate coupling and shifting of the electronic levels.

1.3 Theoretical Chemistry as a powerful tool

Many of the experiments that are being carried out do not have a clear interpretation. Due to the huge amount of molecules that are involved in a typical chemical experiment in a flask (of the order of the Avogadro number, $\sim 10^{23}$) many side reactions that are not taken into account occur and then the results are difficult to understand.

Also, despite the huge progresses than have been done in the last decades in experimental techniques, it is difficult (if not impossible) to carry out an experiment without noise which can perturb the obtained data. Even in the case of the state-of-the-art experiments which have been mentioned in the previous section, a total molecule-metal decoupling cannot be reached, and thus, it is not possible to study the intrinsic process that happens in a single molecule without external interactions.

For these reasons, the Theoretical Chemistry is a powerful tool whose use has experienced an enormous grow in the last decades. It provides explanation to many experimental results and also it is possible to study model systems (as totally isolated molecules). Also, a calculation is much less expensive than a sophisticated experimental setup. And, depending on the system, the results can be obtained in a faster way.

Theoretical Chemistry has been successfully applied to many fields in Chemistry in general and also to Nanoscience. There are multiple examples, but here only few of them are mentioned:

-It can be used to give explanations to chemical reactivity: for example, by the obtaining the reaction mechanism and activation barriers, synthetic chemists are able to understand why a given product is obtained even though it is not the more stable.

-In the field of Surface Chemistry, which has applications as important as heterogeneous catalysis, it is very difficult to determine experimentally exactly the adsorption position of a molecule on a surface. Also, in many cases defects play a crucial role in catalyzed reactions and the control of these defects is not trivial. Nevertheless, with theoretical calculations many defects and phases of the materials can be simulated in order to understand the mechanisms of the processes.

-Although in mass spectrometry experiments it is possible to determine the fragments that are being produced, the dynamical processes in which those charged species are formed are difficult to elucidate. However, through the use of simulations, some insights are obtained.

-Astrochemistry is also an area in which calculations have a great importance: although in a laboratory it is a huge challenge to mimic the conditions of the interstellar medium, these low pressure and temperature can be simulated.

1.4 Structure of this thesis

This thesis has been carried out in the framework of Quantum Chemistry to provide complementary information of Nanochemistry. In particular, interaction of organic molecules which are of high interest for industry (acrylamide, acrylonitrile and acrolein) with metal surfaces have been studied and analyzed. These interactions have been obtained for two different surfaces, (100) and (111), of the same metal, copper, which is widely used in heterogeneous catalysis. Also, different kind of excitations have been studied: thermal, vibrational and electronic. For this last process, a methodology have been developed and implemented in software coupled with Quantum Chemistry packages.

This manuscript is structured as follows:

The second part contains the theoretical background of this thesis. Specifically, Chapter 2 provides in a brief way the most usual concepts in Quantum Chemistry that have been used during the first part of the work (results in Chapters 4 and 5), including Density Functional Theory (DFT) and Periodic Boundary Conditions (PBC), which are key ideas in atomistic simulations of solids. In Chapter 3 the

basis of the Wave Packet Propagation (WPP) methodology is described, as well as its application, focused in the study of the electronic excited and anionic states of molecules adsorbed on surfaces, although this method can be extended to other systems (as molecules in the gas phase or materials). This chapter represents a key point of the thesis, since we have developed a general strategy to carry out WPP calculations based in the coupling with Quantum Chemistry packages.

In the third part of the manuscript (Chapters 4, 5 and 6), the obtained results are shown. Chapter 4 is a study of the adsorption on a pristine Cu(100) surface of the three vinyl-derivatives: acrylamide (ACA), acrilonitrile (ACN) and acrolein (ACO). Several aspects of the interaction (charge transfer, level alignment...) which can be used in order to understand the way in which the molecules interact and the strength of that interaction are analyzed and discussed. In this chapter, the importance of the weak interactions (dispersion, van der Waals) are also studied, as well as the way to introduce them in DFT, through two different schemes: the D2 method of Grimme [21] and the vdW-functionals [22].

Taking advantage of the optimal methodology for the study of the adsorption determined in Chapter 4, in Chapter 5 a study of the interaction of the vinyl-derivatives with a Cu(111) surface is presented. In this way, it is possible to study the effect of the orientation of the surface on the adsorption of organic molecules, even in the same metal. In this chapter the vibrational and thermal excitation are also studied, as well as the energy transfer between molecule and surface. For this last purpose, Molecular Dynamics (MD) simulations are used.

Finally, in Chapter 6, we discuss the results obtained with the WPP simulations of adsorbed molecules on metal surfaces, both clean and covered with ultrathin NaCl layers. This work has been carried out with the code that has been written during the thesis. With the results of the energies, lifetimes and shapes of the resonant wavefunctions we provide insights to relevant experimental works published recently [11, 23–29].

Part II

Methodology

Chapter 2

Methodoloy I: Electronic structure methods

2.1 Introduction

At the end of the 19th century, Newtonian Physics was unable to explain several experimental measurements. As an example, it could not describe the radiation emitted by a black body: at high frequencies, the classical model diverged from the spectrum that was obtained in the labs. Also, the model was not in agreement with the law of the conservation of energy.

In 1900, Max Planck proposed that black body emitted the energy not in a continuum way, but in small energy blocks that he called "quanta" and that were proportional to a constant, $\hbar$, called "Planck's constant" in his honor. With this assumption, Planck was able to propose a formula [30] that reproduced correctly the radiation of the black body. This discretization of the energy can be considered as the origin of the Quantum Mechanics.

Quantum Mechanics at big (macroscopic) scales, where the action is much larger than $\hbar$, converges to Classical Mechanics (Correspondence Principle), reason why for a long time nature could be described using Newton's laws. Nevertheless, for systems as atoms or molecules, whose action is of the order of $\hbar$, a quantum-mechanical treatment is required in order to have a correct description.

2.2 Schrödinger's equation

Neglecting relativistic effects, any quantum system is described by Schrödinger's [31] equation which, in atomic units ($\hbar = m_e = e = c = 1$) is:

$$i\frac{\partial}{\partial t}|\Psi(\vec{r},t)\rangle = \hat{H}|\Psi(\vec{r},t)\rangle \tag{2.1}$$

$\Psi(\vec{r},t)$ is what is called the *wavefunction*, which contains all the information of the system and in this case depends on $\vec{r}$, coordinates of all the considered particles and t, the time.

$\hat{H}$ is the "Hamiltonian operator". After applying it to one of its eigenfunctions, one obtains as eigenvalue the energy of the state. In the case of Ψ being a mixed state (linear combination of the eigenstates), after applying $\hat{H}$ to Ψ we obtain the average energy, which is the energy of the different eigenstates weighted by the contributions to the total wavefunction.
$\hat{H}$ can be decomposed as a sum of two operators:
-$\hat{T}$, the kinetic energy operator, defined in real space as $\hat{T} = \sum_i^n \frac{1}{2m_i}\nabla_i^2$, where n is the number of particles, ∇^2 is the sum of the second partial derivatives of the spatial coordinates ($\frac{\partial^2}{\partial x^2} + \frac{\partial^2}{\partial y^2} + \frac{\partial^2}{\partial z^2}$) and m_i the mass of the ith particle.
-$\hat{V}$, the potential energy operator. Its shape depends on the interactions between the particles of the system.

Now, let's suppose that the Hamiltonian operator does not depend on time. And let's write the wavefunction as a product of a function that only depends on time times another that only depends of the spatial coordinates of the particles: $\Psi(\vec{r},t) = \psi(\vec{r})\chi(t)$. If now, we substitute in 2.1:

$$i\frac{\partial}{\partial t}\psi(\vec{r})\chi(t) = E\psi(\vec{r})\chi(t) \tag{2.2}$$

$\psi(\vec{r})$ is a constant when we derivate respect time. Thus, we can divide both terms by this function and then group the χ and the t dependence in the following way:

$$\frac{1}{\chi(t)}d\chi(t) = -iE\ dt \tag{2.3}$$

Functions that satisfy this simple differential equation are the exponentials. There-

fore:

$$\chi(t) = e^{-iEt} \tag{2.4}$$

And thus, temporal evolution of the wavefunction is given by:

$$|\Psi(\vec{r},t)\rangle = e^{-i\hat{H}t}|\Psi(\vec{r},0)\rangle \tag{2.5}$$

This is only true if the Hamiltonian operator does not depend on time. If there is a temporal dependence, then the energy also depends on time and $\chi(t)$ has a different expression:

$$\chi(t) = e^{-i\int E(t)dt} \tag{2.6}$$

If we consider again a non time-dependent Hamiltonian, it is possible to expand the wavefunction at any time as a linear combination of the eigenstates, which neither depend on time. To this, it is necessary to solve the time-independent Schrödinger equation:

$$\hat{H}|\psi(\vec{r})\rangle = E|\psi(\vec{r})\rangle \tag{2.7}$$

where E is the energy of the system. To simplify the notation, we are going to use ψ to define stationary wavefunctions (without temporal dependence), whereas Ψ will be how we denote the whole wavefunction (including the temporal evolution)

For a molecule with N electrons and M nuclei, the Hamiltonian operator is:

$$\hat{H} = -\frac{1}{2}\sum_{i=1}^{N}\nabla_i^2 - \sum_{\alpha=1}^{M}\frac{1}{2m_\alpha}\nabla_\alpha^2 - \sum_{i=1}^{N}\sum_{\alpha=1}^{M}\frac{Z_\alpha}{r_{i\alpha}} + \sum_{i=1}^{N}\sum_{j>i}^{N}\frac{1}{r_{ij}} + \sum_{\alpha=1}^{M}\sum_{\beta>\alpha}^{M}\frac{Z_\alpha Z_\beta}{r_{\alpha\beta}} \tag{2.8}$$

The first two terms are the kinetic energy of electrons and nuclei. The third one is the (attractive) nucleus-electron interaction. The last two terms are the (repulsive) electrostatic interaction between electrons and between nuclei, respectively.

This Hamiltonian has no analytic solution due to the interaction between particles. As a first step to overcome this problem, in Quantum Chemistry the Born-Oppenheimer approximation is commonly used.

2.3 Born-Oppenheimer approximation

The lightest nucleus in the universe, the hydrogen (a single proton), has a mass about 1800 times the mass of the electron. That is why the movement of nuclei is much slower than the velocity of the electrons. The heavier the nuclei, the greater this difference is. The Born-Oppenheimer approximation [32] assumes that electrons move in the potential induced by the nuclei at a fixed position. Therefore, movement of nuclei and electrons are decoupled and the Schrödinger is simplified.

To this, we group the terms of the Hamiltonian in two blocks, $\hat{H} = \hat{H}_{nuc} + \hat{H}_{el}$. $\hat{H}_{nuc}$, the *nuclear Hamiltonian* contains the kinetic energy operator of the nuclei and $\hat{H}_{el}$, the *electronic Hamiltonian*, is defined as:

$$\hat{H}_{el} = -\frac{1}{2}\sum_{i=1}^{N}\nabla_i^2 - \sum_{i=1}^{N}\sum_{\alpha=1}^{M}\frac{Z_\alpha}{r_{i\alpha}} + \sum_{i=1}^{N}\sum_{j>i}^{N}\frac{1}{r_{ij}} + \sum_{\alpha=1}^{M}\sum_{\beta>\alpha}^{M}\frac{Z_\alpha Z_\beta}{r_{\alpha\beta}} \tag{2.9}$$

Now, since we have supposed that the nuclear coordinates are decoupled from the electronic ones, we write the wavefunction as a product of a function that only depends on the coordinates of the nuclei times a function that depends on the coordinates of the electron (although, parametrically, it depends on the nuclear positions):

$$\psi(\vec{r}) = \psi(\vec{r}_{el}, \vec{r}_{nuc}) = \phi(\vec{r}_{el}) \cdot \chi(\vec{r}_{nuc}) \tag{2.10}$$

In this way:

$$\hat{H}\psi(\vec{r}) = (\hat{H}_{nuc} + \hat{H}_{el})\phi(\vec{r}_{el}) \cdot \chi(\vec{r}_{nuc}) \tag{2.11}$$

$$(\hat{H}_{nuc} + \hat{H}_{el})\phi(\vec{r}_{el}) \cdot \chi(\vec{r}_{nuc}) = \hat{H}_{nuc}\phi(\vec{r}_{el}) \cdot \chi(\vec{r}_{nuc}) + \hat{H}_{el}\phi(\vec{r}_{el}) \cdot \chi(\vec{r}_{nuc}) \tag{2.12}$$

Under the action of $\hat{H}_{el}$, $\chi(\vec{r}_{nuc})$ is constant. The same happens with $\hat{H}_{nuc}$ and $\phi(\vec{r}_{el})$. So, if we define E_{el} as the result of applying $\hat{H}_{el}$ to $\phi(\vec{r}_{el})$:

$$\hat{H}_{nuc}\phi(\vec{r}_{el}) \cdot \chi(\vec{r}_{nuc}) + \hat{H}_{el}\phi(\vec{r}_{el}) \cdot \chi(\vec{r}_{nuc}) = \phi(\vec{r}_{el}) \cdot (E_{el} + \hat{H}_{nuc})\chi(\vec{r}_{nuc}) \tag{2.13}$$

Since this is equal to apply the full Hamiltonian to the whole wavefunction:

$$\phi(\vec{r}_{el}) \cdot (E_{el} + \hat{H}_{nuc})\chi(\vec{r}_{nuc}) = E\phi(\vec{r}_{el}) \cdot \chi(\vec{r}_{nuc}) = \phi(\vec{r}_{el})E \cdot \chi(\vec{r}_{nuc}) \tag{2.14}$$

if we divide by $\phi(\vec{r}_{el})$ (no operator is acting on this function anymore), we obtain:

$$(E_{el} + \hat{H}_{nuc})\chi(\vec{r}_{nuc}) = E\chi(\vec{r}_{nuc}) \tag{2.15}$$

So, as a conclusion, under the Born-Oppenheimer approximation, the total energy of the system can be calculated through the wavefunction of the nuclei, which move in the potential generated by the electrons. This potential is assumed to be adapted instantaneously for each set of nuclear coordinates.

This approximation breaks down in some cases, as for the situations where several electronic states are close in energy.

2.4 Antisymmetry and Pauli exclusion principle

An intrinsic property of the particles, without classical analogue, is the spin.

Although spin appears naturally in the development of the quantum field theory (that includes also relativistic effects) in a non-relativistic approach, as the case of this thesis, it is necessary to postulate it.

Depending on the value of the spin, particles can be classified in fermions (case of half-integer spin) or bosons (integer spin). The spin-statistics theorem establishes that, depending on to which family a particle belongs, it follows a Bose-Einstein statistic (bosons, as photons or some nuclei) or a Fermi-Dirac statistic (fermions, as electrons, protons or neutrons)

A consequence to the fact that electrons are fermions is that their wavefunction must be antisymmetric respect to the exchange of two particles:

$$\psi(x_1, x_2) = -\psi(x_2, x_1) \tag{2.16}$$

So, if we suppose $x_1 = x_2$, which means that both particles are in the same quantum state,

$$\psi(x_1, x_2) = -\psi(x_2, x_1) = \psi(x_2, x_1) \tag{2.17}$$

This implies that ψ is necessarily zero and thus, there is no particle. That is why two fermions cannot be in the same quantum state simultaneously. This is known as *Pauli exclusion principle* [33].

2.5 Molecular wavefunction. Hartree-Fock method

In the development of the Born-Oppenheimer approximation, a given spatial distribution of the nuclei is required to get the electronic wavefunction.

As a first step, we write the all-electron wavefunction as a product of N single-electron wavefunctions, ϕ_i, which we call *spin-orbitals*:

$$\psi_{el}(\vec{r}_1, \vec{r}_2 ... \vec{r}_N) = \prod_i^N \phi(\vec{r}_i) \tag{2.18}$$

where $\vec{r}$ contains the spin and the spatial coordinates x, y, z. The product $\prod_i^N \phi(\vec{r}_i)$ is usually known as *Hartree product*.

Remembering that electrons are fermions, their wavefunction must be antisymmetric. Nevertheless, equation 2.18 does not satisfy this.

If two functions are solution of a given differential equation (as the case of the Schrödinger equation) with the same eigenvalue, a linear combination of those eigenfunctions will be also a solution with the same eigenvalue. Taking this into account we can define a linear combination of Hartree products such that it satisfies the antisymmetry of the wavefunction.

John C. Slater proposed [34] a simple way of doing this, through what are called *Slater determinants*:

$$\psi_{el}(\vec{r}_1, \vec{r}_2 ... \vec{r}_N) = \frac{1}{\sqrt{N!}} \begin{vmatrix} \phi_1(\vec{r}_1) & \phi_2(\vec{r}_1) & \cdots & \phi_N(\vec{r}_1) \\ \phi_1(\vec{r}_2) & \phi_2(\vec{r}_2) & \cdots & \phi_N(\vec{r}_2) \\ \vdots & \vdots & \ddots & \vdots \\ \phi_1(\vec{r}_N) & \phi_2(\vec{r}_N) & \cdots & \phi_N(\vec{r}_N) \end{vmatrix} \tag{2.19}$$

The factor $\frac{1}{\sqrt{N!}}$ is the normalization constant.

Since this wavefunction is built as a determinant, it is easy to check that it is antisymmetric. If we exchange two columns we obtain two functions that only differ in two electrons. And, as a property of the determinants, this exchange changes the sign of the determinant.

Using the variational principle, it is possible to obtain the best wavefunction based in a single Slater determinant. This is the aim of the known as *Hartree-Fock method* [35,36]. To this, it is necessary to introduce some parameters, which are going to be used to minimize the energy (and therefore, to improve the wavefunction). Since the Slater determinant is define by the spinorbitals, they must be obtained variationally. This can be done defining them as a linear combination of atomic orbitals (LCAO), which is only a change of basis of the vector space. In this way, the i-th molecular orbital is linked with the atomic orbitals through the following expression:

$$\phi_i(\vec{r}) = \sum_{\lambda=1}^{M} c_{i\lambda}\xi_\lambda(\vec{r}) \tag{2.20}$$

where $\xi_\lambda(\vec{r})$ denotes the λ-th atomic orbital. Due to the infinite dimension of the Hilbert space, it is necessary to truncate the expansion and thus include only M atomic orbitals. The value of M is related with the size of the *basis* of the calculation (see corresponding section for a more detailed information).
So the parameters to optimize variationally are the coefficients $c_{i\lambda}$.

The Hartree-Fock method proposes to substitute the instantaneous electron-electron interaction by an *average* interaction. In this way, each electron moves in the average field generated by the other electrons. This makes simpler the resolution of the problem.

The implementation of this method is done, in the case of systems with paired spins, through the resolution of the Roothaan-Hall equations [37, 38], which give the linear combination of atomic orbitals that minimize the energy of the Slater determinant and, at the same time, makes the Fock operator diagonal: the *canonical* molecular orbitals are then obtained.

2.6 Electron correlation. Beyond Hartree-Fock

The substitution of the instantaneous electron-electron interaction in the Hartree-Fock method produces a partial loss of the total energy of the system. We define as *electronic correlation energy* the difference between the exact energy (neglecting relativistic effects) and the Hartree-Fock limit, the energy obtained with an ideally complete basis:

$$E_{corr} = E_{exact} - E_{HF} \tag{2.21}$$

There are methods to take into account this correlation energy, as the post-Hartree-Fock methods. They are called in this way because they try to correct a wavefunction previously obtained at a Hartree-Fock level. In this thesis two families of methods have been employed: the Möller-Plesset (MP), based in perturbation theory, and the Coupled Cluster (CC).

2.6.1 Perturbation theory

In perturbation theory the Hamiltonian operator of the system, for which there is no exact solution, is written as a sum of a simpler Hamiltonian than can be solved (which is known as unperturbed Hamiltonian, $\hat{H}_0$) and a term known as the "perturbation" ($\hat{V}$), which we consider as *small* respect $\hat{H}_0$:

$$\hat{H} = \hat{H}_0 + \hat{V} \tag{2.22}$$

If $\hat{V}$ has no time dependence, this perturbative treatment is known as *Rayleigh-Schrödinger Perturbation Theory* (RSPT). In this case, since $\hat{H} \approx \hat{H}_0$, we can assume that the eigenfunctions of $\hat{H}$ and the eigenfunctions of $\hat{H}_0$ must be similar.

Now, we expand the wavefunction and the energy as a Taylor series. To do this, we introduce the λ parameter, which allows us to include progressively the action of the perturbation:

$$\psi_n = \psi_n^{(0)} + \lambda\psi_n^{(1)} + \lambda^2\psi_n^{(2)} + ... \tag{2.23}$$

$$E_n = E_n^{(0)} + \lambda E_n^{(1)} + \lambda^2 E_n^{(2)} + ... \tag{2.24}$$

where ψ_n is the total wavefunction, eigenfunction of $\hat{H}$, $\psi^{(0)}$ is the wavefunction at zeroth order (eigenfunction of $\hat{H}_0$) and $\psi^{(k)}$ is the k-th order correction. Analogously, E_n is the total energy, $E_n^{(0)}$ is the energy at zeroth order and $E_n^{(k)}$ is the k-th order correction to the energy. In this notation, everything is referred to the n-th state, so this treatment is not limited to the ground state and can be extended to higher states.

If we define $\psi_n^{(0)}$ in such way that $\langle\psi_n^{(0)}|\psi_n\rangle = 1$ (which is usually known as *intermediate normalization*) and also $\langle\psi_n^{(0)}|\psi_n^{(k)}\rangle = \delta_{0,k}$ it is possible to use the closure relation, once the terms of same order of λ are grouped. In this way, the expression of the correction to the energy up to the second order is:

$$E_n \approx E_n^{(0)} + \langle\psi_n^{(0)}|\hat{V}|\psi_n^{(0)}\rangle + \sum_{m\neq n} \frac{\left|\langle\psi_n^{(0)}|\hat{V}|\psi_m^{(0)}\rangle\right|^2}{(E_n^{(0)} - E_m^{(0)})} \tag{2.25}$$

In the case of the application to molecular systems, the most used perturbative treatment is the Møller–Plesset (MP) [39], where the Hartree-Fock wavefunction is the unperturbed wavefunction. $\hat{H}_0$ is defined as the sum of the one electron operators and $\hat{V}$ is the difference between the real electron-electron interaction and the average interaction that is used in the Hartree-Fock method.

The correction to the second order (MP2) takes into account a good fraction of the electronic correlation in a totally *ab initio* way. If the Hartree-Fock is a good starting wavefunction (the single Slater determinant is a good approximation to the total wavefunction), MP2 is able to give accurate molecular geometries with a reasonable computational effort.

2.6.2 Coupled Cluster

Another way to recover the correlation energy is through the *Coupled Cluster* method [40]. In this case, the wavefunction is defined as:

$$\psi_{CC} = e^{\hat{T}}\psi_{HF} \tag{2.26}$$

where $\hat{T} = \hat{T}_1 + \hat{T}_2 + ...$, being $\hat{T}_n$ the operator that generates the n-excitations on the reference (Hartree-Fock) wavefunction. The $\hat{T}$ operator is usually truncated to

include only the single and double excitation operators (which is known as CCSD, *Coupled Cluster Singles and Doubles*). Nevertheless, since those operators are in an exponential, the tri- and tetra- excitations are also included. For this reason, CC is a highly precise method.

It is possible to add the action of $\hat{T}_3$ in a perturbative way, methodology known as CCSD(T), in order to reduce the computational effort of this operator. This method is usually used as benchmark due to extremely high precision (its error are usually lower than 1kcal/mol), reason why CCSD(T) is consider as the *gold standard*.

CC, in the different variations, has two limitations:

-Since it is a correction based on the Hartree-Fock wavefunction, if this reference is not adequate, the results may be wrong, as in the case of MP.

-Due to the computational effort, it cannot be applied to large systems.

A widely used alternative to introduce the electron correlation is the Density Functional Theory (DFT), explained in detail in section 2.8

2.7 Basis functions

For all the previously described methods, it is required to describe mathematically the molecular orbitals. Since there is no analytic solution for the atomic orbitals (AO), with the only exception of the hydrogen-like atoms, it is necessary to write them in some way, usually as a linear combination of a set of functions, which is known as *basis*. The quality of the results strongly depends on the choice of the basis: the larget it is, the more flexibility will have the variational process to optimize the molecular orbitals.

2.7.1 Slater type orbitals

The presence of point charges in the Hamiltonian operator produces a discontinuity in the electrostatic potential in the positions where there is a nucleus. As a consequence, the electronic density must have a discontinuity in its first derivative, which is known as *cusp theorem*, demonstrated by Kato [41]. The *Slater Type Orbitals* (STO) are functions that satisfy this requirement and have the following mathematical expression:

$$\phi_{\zeta,n,l,m}(r,\theta,\varphi) = NY_{l,m}(\theta,\varphi)r^{n-1}e^{-\zeta r} \tag{2.27}$$

On the other hand, these functions have a disadvantage: the three- and four-center bielectronic integrals cannot be calculated analytically and thus, their application requires a huge computational effort. That is why this kind of functions is usually used only in high-level calculations for small systems, as atoms or diatomic molecules. They are also employed in calculations where those integrals are omitted, as the case of semi-empirical methods.

2.7.2 Gaussian type orbitals

An alternative to the STO functions is the use of what is called GTO, *Gaussian Type Orbitals* [42]. In this case, the basis functions have the following shape:

$$\phi_{\alpha,n,l,m}(r,\theta,\varphi) = NY_{l,m}(\theta,\varphi)r^{n-1}e^{-\alpha r^2} \tag{2.28}$$

The behavior in the area close to the nuclei is not the correct one (they do not satisfy the cusp theorem) and the decay at long distances is too fast in comparison with the STO. Nevertheless, these problems can be overcome by including a higher number of basis functions. Also, the GTOs allow an analytic integration, which makes the calculation much faster, even though the basis is larger. That is why this kind of basis is the most extended in gas phase molecular calculations.

2.8 Density Functional Theory

In 1964, P. Hohenberg and W. Kohn demonstrated [43] that, in the case of the ground state, the energy is a functional of the electron density. It means that, if the density is known, it is possible to determine exactly the energy and all the other properties of the system. This is shown in the two Hohenberg-Konh theorems:

First theorem

Any observable in a non-degenerated ground state can be calculated through the electron density of the system. In other words: any observable of the ground state can be described as a functional of the electron density.

Second theorem

Given a external potential $v(r)$, the density of the ground state minimizes the energy functional.

The external potential $v(r)$, in the case of molecules, is the electrostatic potential induced by the nuclei.

In that way, the electronic energy can be expressed as the sum of the kinetic energies of the electrons plus the potential energy of the (repulsive) electron-electron and the (attractive) electron-nucleus interactions:

$$E[\rho] = T[\rho] + V_{ee}[\rho] + V_{ne}[\rho] \tag{2.29}$$

Nevertheless, although these theorems show the existence of a universal functional, they are not able to determine *the expression* of the functional.

2.8.1 Kohn-Sham method

A first approach to deal with the Density Functional Theory was proposed by Kohn and Sham [44]. It is based in a fictitious system of non-interaction electrons, whose density (ρ_s) is equal to the density of the real (interacting) system (ρ).

In this case, the energy would be:

$$E[\rho_s] = T[\rho_s] + V_{ne}[\rho_s] \tag{2.30}$$

where the first term can be easily calculated if we introduce orbitals and we write the wavefunction as a Slater determinant:

$$T[\rho_s] = \sum_{i}^{occ} \langle \phi_i | -\frac{1}{2}\nabla^2 | \phi_i \rangle \tag{2.31}$$

The second term, the interaction electron-nuclei is also easy to calculate in terms of the density and the electrostatic potential of the nuclei, $v(\vec{r})$:

$$V_{ne}[\rho_s] = \int \rho_s(\vec{r}) v(\vec{r}) d\vec{r} \tag{2.32}$$

In terms of the density, the expression of the Coulomb interaction is:

$$J[\rho] = \frac{1}{2}\int\int \frac{\rho(\vec{r}_1)\rho(\vec{r}_2)}{|\vec{r}_1 - \vec{r}_2|} d\vec{r}_1 d\vec{r}_2 \tag{2.33}$$

Now, we can write equation 2.29 as:

$$E[\rho] = T_s[\rho] + (T[\rho] - T_s[\rho]) + V_{ne}[\rho] + J[\rho] + (V_{ee}[\rho] - J[\rho]) \tag{2.34}$$

The terms in parenthesis are the difference between the kinetic energy of the non-interacting electrons are the real ones and the energy difference between the real electron-electron interaction pure Coulomb interaction, respectively. These differences are the terms that we do not know how to calculate easily. We can group those terms in what we call exchange-correlation:

$$V_{xc}[\rho] = (T[\rho] - T_s[\rho]) + (V_{ee}[\rho] - J[\rho]) \tag{2.35}$$

And thus, eq. 2.29 becomes:

$$E[\rho] = T_s[\rho] + V_{ne}[\rho] + J[\rho] + V_{xc}[\rho] \tag{2.36}$$

The molecular orbitals used in this procedure, known as *Kohn-Sham orbitals* are obtained in a self-consistent way, as in the case of the Hartree-Fock method. Nevertheless, the orbitals in both methods are not the same, since the Hamiltonian operator is not the same.

2.8.2 Functionals

The big limitation of DFT lies in the fact that $V_{xc}[\rho]$ is unknown. For this reason, it is compulsory to use approximate functionals, which built in base of simplifications, or physical models. These functionals, which usually include external parameters in order to reproduce experimental or high level calculations, can be classified in four families:

-Local Density Approximation (LDA): In this case, the $V_{xc}[\rho]$ term depends exclusively of the density, in such a way that the system is treated as an uniform electron gas. This assumption is more realistic in the case of metals, where LDA

behaves better than for non-metallic solids or molecules.

-Generalized Gradient Approximation (GGA): For finite systems and/or with some regions where the electron density changes drastically, a way to improve $V_{xc}[\rho]$ is to make it depend not only of the density, but also on its gradient ($\nabla\rho$). The PBE (Perdew-Burke-Ernzerhof) functional [45] is an excellent example of the GGA family and has been widely used in calculations of both molecules and solid state.

-Meta-GGA: The natural step after the GGA is to include not only the gradient of the density, but further derivatives. In this way the functional enhances its flexibility and then one can obtain, in principle, better results. M06-L, one of the Minnesota functionals [46], belongs to this family.

-Hybrid functional: In the Hartree-Fock method there is no interaction of the i-th electron with itself due to the fact that the Coulomb and the exchange integrals cancel themselves. Nevertheless, this is not guaranteed in the Kohn-Sham formulation of the DFT, which produces the *self-interaction error*. Due to this fictitious interaction, the electron density tends to be too delocalized and thus the band gap of the system is underestimated. A way to fix this error, at least partially, is through the introduction of the exact Hartree-Fock exchange (although calculated with the Kohn-Sham orbitals). The functionals that introduce this term are known as *hybrid*. Their computational cost is higher, but they are able to predict in a better way some properties as the band gap. As an example of this type of functionals, one of the most used in the last years is the B3LYP [47, 48].

2.8.3 Weak interactions and Density Functional Theory

One of the problems with the current functionals is the fact that usually they do not take into account weak interactions, such as van der Waals (vdW) forces. Although DFT gives accurate bond energies and distances, in non-covalent interactions the results provided by most of the functionals are far from the correct values.

The interactions that rule this kind of systems come from changes in the electron density, which are cause by charge fluctuations. This is due to the instantaneous electron-electron interactions: the dynamic electron correlation.
This fraction of the energy is contained in the V_{xc} part of the functional. But it is difficult to find expressions that converges to the (already known) asymptotic behaviors at short *and* long distances.

In order to overcome this problem, several approaches have been developed to

consider weak interactions [49]. During this thesis, based in the adsorption of organic molecules on surfaces (systems in which weak interactions play a crucial role) two different alternatives have been used: the DFT-D method of Grimme [21,50] and the vdW-DF, proposed by Dion [22].

-Grimme's model is based in a simple and pragmatic idea: adding a term in order to correct the Kohn-Sham energy. There are different ways in which this term is calculated. The most simple way (and the one that we have used in this framework) is the DFT-D2. In this case, the extra term that represents the dispersion is calculated through a pair-wise force field, which is given by the following expression:

$$E_{disp} = -s_6 \sum_{i=1}^{N_{at}-1} \sum_{j=i+1}^{N_{at}} \frac{C_6^{ij}}{R_{ij}^6} f_{dmp}(R_{ij}) \tag{2.37}$$

where s_6 is a scaling factor which depends on the functional that is used, R_{ij} is the distance between the nuclei (taking into account the atomic radii), f_{dmp} is a damping function used to avoid singularities and C_6^{ij} is the dispersion coefficient. This last term is calculated through:

$$C_6^{ij} = \sqrt{C_6^i C_6^j} \tag{2.38}$$

where the factors inside the square root are the coefficients defined for each element of the periodic table.

The two main advantages of this method are it is very fast to compute and also its behavior is correct at long distances $1/R^6$. On the other hand, the drawback of DFT-D2 lies in the excessive simplicity of the model, which does not take into account the chemical environment or screening effects. For this reason, usually the dispersion energies are overestimated. That is why, to study adsorption energies we only include the D2 correction to the first layer of the surfaces.

-VdW-DF is a more sophisticated approach to dispersion forces. In this case, this term is included in an approximate way in the functional as a non-local correction. In this way, weak interactions depends on the electron density, without empirical factors. For this reason, it is possible to use this method to calculate dispersion energies for any arbitrary system. The main disadvantage of wdW-DF is the computational effort that it requires, which is higher than in the case of the Grimme's model.

2.9 Periodic Boundary Conditions

In 1928, F. Bloch demonstrated [51] that, in the case of a periodic potential (as the case of the solids), the wavefunction ψ of the system can be expressed as:

$$\psi(\vec{r}) = e^{i\vec{k}\vec{r}}u(\vec{r}) \tag{2.39}$$

where u is a function with the same periodicity of the potential. u is known as *Bloch function.*

This means that, if we find the u function that satisfies the Schrödinger equation for the periodic region, automatically we will know the wavefunctions that are compatible with the system. These wavefunctions, will be defined as the combination of u with all the plane waves whose wave vectors are compatible with the periodicity of the system.

The necessity of including periodic boundary conditions is huge in the case of some systems as solids: macroscopic systems, although they are finite, have properties that are closer to conceptually infinite system than to the small cluster models that can be calculated nowadays if periodicity is not included.
In the case of metals this is specially important: the metallic character, the existence of empty levels that are accessible for electrons just above the energy of the highest occupied level of the system (known as *Fermi energy* or *Fermi level*) is a consequence of the periodicity. In the case of a finite system, its edges would limit the movement of the electrons, which would produce a quantization of the energies and the continuum would not exist anymore.

2.9.1 Plane waves and pseudopotentials

Localized basis, briefly explained in section 2.7 are compatibles with the Kohn-Sham method. It is the most common way of proceed when we are interested in carrying out DFT calculations in isolated molecules.

Nevertheless, there is a basis that is specially convenient when we want to study periodic systems: plane waves. These basis functions are defined as:

$$|\vec{k}\rangle = e^{i\vec{k}\vec{r}} \tag{2.40}$$

where $\vec{k}$ is a vector of the reciprocal space of the cell to replicate. They are an ensemble of orthogonal functions:

$$\langle k|k'\rangle = \delta_{\vec{k},\vec{k}'} \tag{2.41}$$

And moreover is an infinite ensemble, which means that plane waves are a complete basis that can be used to define any function inside the periodic cell.

These functions are also eigenfunctions of the kinetic energy operator. Thus, they are eigenfunctions of the Hamiltonian operator, if the potential is constant:

$$\hat{T}e^{i\vec{k}\vec{r}} = -\frac{1}{2m}\nabla^2 e^{i\vec{k}\vec{r}} = \frac{|\vec{k}|^2}{2m}e^{i\vec{k}\vec{r}} \tag{2.42}$$

Due to the fact that this ensemble is infinite, it is necessary to truncate the expansion, in order to make it computationally accessible. To this, it is possible to consider all the $\vec{k}$ that, being compatibles with the periodicity of the cell, have an energy lower than a selected value, proportional to $|\vec{k}|^2$, known as *cut-off energy*. With this rule to choose which plane wave are introduced in the expansion for the calculation, it is possible to assure that the basis is the same, independently of the number of atoms inside the cell. That is why this basis does not have problems related with the so-called basis set superposition error (BSSE).

One of the disadvantages of using plane waves as basis is that, due to the fact that they are delocalized over the whole space, it is required to use a huge amount of basis functions in order to localize a density, as the case of very bounded states in atoms (as core electrons). Since these electrons are strongly attracted by the nucleus, they are barely affected by the rearrangement due to changes in chemical bonds. That is why, since they are mainly inactive, it is possible to replace them by an effective potential (known as *pseudopotential*). In this way, although these electrons are not taken into account explicitly, the more external (valence) electrons, which participate in chemical bonding have the same (or almost the same) energy and wavefunctions than the one that they would have if all the electrons are fully included in the calculation.

2.10 Molecular Dynamics

Generally, all the theory and methods previously described are used to obtain the geometry that minimizes the energy of the system and then, using that spatial distribution of the atoms, to determine all the properties of interest: dipole, charges, frequencies...

The idea of using a single geometry to study a system is justified. Statistically, molecules are usually in the distribution of minimum energy: given an electronic state, the ground state of the nuclear wavefunction has a maximum at that conformation, so the probability of finding the system there is high. This assumption is specially valid in those cases where the internal energy of the system is low (which macroscopically means low temperature) and thus only the ground state is populated.

Nevertheless, there are occasions where the potential energy surface is widespread along one or more internal coordinates, as when weak interactions are involved. For example, in van der Waals complexes or physisorption of molecules on surfaces. In these cases, the system has easy access to other places in the potential energy surface.

Moreover, even in systems with well-defined energetic minima, when the internal energy of the system is high enough, it is able to evolve through paths that are different to the minimum energy one.

In these cases, the information that can be extracted in the energetic minimum or the zero-gradient points would be not enough and thus it is required to explore other regions of the potential energy surface. In order to do this, it is possible to use what is called *molecular dynamics* (MD) simulations.

Taking into account the fact that the masses of the nuclei are much larger than the electrons, as a first approach to study the temporal evolution of a molecular system is to consider nuclei as a classical particles that move in the potential generated by the electrons, which is obtained through quantum-mechanical calculations. This kind of molecular dynamics simulations are known as *Born-Oppenheimer Molecular Dynamics* (BOMD) [52, 53], because they are based in the same considerations than the Born-Oppenheimer approach.

BOMD is a powerful tool to explore different regions of the potential energy surface that are accessible at a given energy (or temperature in the case of an ensemble)

or to study the temporal evolution of a system. To do this, the procedure is:

1) The electronic wavefunction is converged for the current nuclear geometry.

2) With this wavefunction, the potential that the nuclei feel is calculated.

3) Since $F = -\nabla V$, the acting forces are obtained.

4) A classical propagation of the nuclei, using Newton's laws, is done, using the previously calculated forces. Since it is done numerically, this forces act only during a given time step. Then, come back to step 1)

Since for each time step it is required to converge the electronic wavefunction, this kind of calculations can be extremely computational demanding, although the electronic wavefunction of the previous step can be used as initial guess in order to make the convergence faster. That is why, this methodology is generally limited to small systems (up to few hundreds of atoms, depending on the level of theory) and short times (up to few picoseconds).

Although this has been the methodology used in this thesis, there are other approaches to treat the temporal evolution.

If we increase the complexity, we can treat quantum-mechanically the full system, even nuclei. Although then the systems than can be studied are smaller (as well as the time scale), it allows to take into account some processes as tunneling, which can not be considered if nuclei are described as classical particles.

On the other hand, if we are interested in long-time processes or huge systems (as proteins), then it is necessary to decrease the computational effort in each time step. To this, it is possible to use previously computed potentials, as force fields, which allows to avoid the resolution of the Schrödinger's equation.

2.11 Analysis tools

2.11.1 Projected Density Of States (PDOS)

In solid state calculations, instead of the "molecular orbital" idea, which is widely used in gas-phase calculations, it is usually used the idea of "band". The periodicity given by imposing periodic boundary conditions produces a more diffuse energetic spectrum, which is not discrete anymore. That is why, it is defined the *Density of States* (DOS) as the number of states which a given energy:

$$DOS(E) = \rho(E)dE \tag{2.43}$$

By observing the DOS it is possible to determine properties as the band gap of the system (difference between the Fermi level and the first unoccupied state).

If we write the electron density in terms of a basis, by projecting the density on part of the basis, it is possible to determine the different contributions to the whole DOS. This is known as *Projected Density Of States* (PDOS). If the basis used to do the projection is the one formed by the atomic orbitals, it is possible to determine which atoms (and which orbital) contribute to each state. This can be used to locate interactions, as chemical bonds.

2.11.2 Quantum Theory of Atoms In Molecules (QTAIM)

At the beginning of the decade of 1990, Richard Bader proposed what is known as the Quantum Theory of Atoms in Molecules (QTAIM) [54, 55], a methodology to separate conceptually a molecule in the atoms that form the system. It is based in the topology of the electron density.

In the framework of the QTAIM, an atom is defined as a region of the real space delimited by zero-flux surfaces, which are two-dimensional surfaces where the density is a minimum in the direction of the surface vector.

Since the density in the proximity of a nucleus is maximum, in the case of periodic boundary conditions, all the atoms inside the cell are delimited and thus their volume is finite. Through the integration of these atomic volumes it is possible to determine the electron density that belongs to the different atoms and, by difference of the number of electrons inside and the nuclear charge, it possible to assign a value of the atomic charge.

One huge advantage of QTAIM is the fact that it is based in the density, which is a physical observable (in contrast to other partitionings based in orbitals, which are not observables).

Through the analysis of the electron density, we are able to determine not only the presence of interactions, but their nature (ionic or covalent) and the strength. For these properties, it is enough to study the Bond Critical Point (BCP), a particular point of the space which delimits the different atoms and is a maximum of the density in two directions and a minimum in a third one (the direction which connects the interacting atoms).

Chapter 3

Methodology II: Wave Packet Propagation

3.1 Introduction

Methods described in Chapter 2 are usually used to study static properties or bound states of systems where the Hamiltonian is a time-independent operator. For the states which are embedded in a continuum (resonances) or time-dependent potentials the applications of these methods is not straightforward, although they can be used to extract the scattering matrix and then study resonances.

Nevertheless many methodologies have been developed to study explicitly the Time-Dependent Schrödinger Equation. One of them is the Wave Packet Propagation (WPP) [56–58], which is widely used to study different kind of problems in Physics and Chemistry. In particular, WPP is used to study dynamical processes taking into account some effects that are missed in semi-classical dynamics (as tunneling in chemical reactions, using the wave packet to represent the nuclear dynamics [59]), electron dynamics or photoionization if the wave packet represents an electron [60]... In general, it is a powerful methodology to study temporal evolution processes with a complete quantum-mechanical description. Also, WPP can be applied to time-dependent potentials, as the interaction of matter with light. In this case, one can obtain not only the energies of all the states that are involved in the process, but their population before, during and after the interaction.

An additional advantage of the Wave Packet Propagation is that it describes

correctly (if the basis is adequate) the continuum states and the resonances. In this case, using WPP it is possible to obtain the lifetime of these states [58], something that is not possible using other methodologies that are restricted to obtain only the energies.

When we are dealing with multi-electron systems, as molecules beyond H_2^+, we cannot treat explicitly all the electrons with a reasonable computational effort and thus we are restricted to a single active electron approach.

In this thesis we study the energy and lifetime of anions and excited states of molecules adsorbed on metal surfaces through the use of WPP. To this end, we have developed a code in which a single electron wave packet is propagated. Since the potential is obtained through the Density Functional Theory, the interaction between the active electron and the rest of the electrons of the system is taken into account in the sum of the Hartree and the exchange-correlation potential. These potentials are calculated using Quantum Chemistry codes and given to our software as an input.

3.2 Time Dependent Schrödinger Equation

As we have mentioned in Section 2.2, the time evolution of a quantum system is given by the Time Dependent Schrödinger Equation (TDSE):

$$i\frac{\partial}{\partial t}\Psi(\vec{r},t) = \hat{H}\Psi(\vec{r},t) \tag{3.1}$$

If the wavefunction is known at a given time, which we denote as $t = 0$ for simplicity, the exact wavefunction at $t = t$ is

$$|\Psi(\vec{r},t)\rangle = \hat{U}(t)|\Psi(\vec{r},0)\rangle \tag{3.2}$$

where $\hat{U}$, the *time evolution operator* is defined as

$$\hat{U}(t) = e^{-i\hat{H}t} \tag{3.3}$$

If we express the Hamiltonian of the system as a combination of k states with energy E_k and eigenvectors ϕ_k

$$\hat{H} = \sum_k E_k|\phi_k\rangle\langle\phi_k| \tag{3.4}$$

we can write $\hat{U}$ as

$$\hat{U}(t) = e^{-it\sum_k E_k|\phi_k\rangle\langle\phi_k|} \tag{3.5}$$

or, if we expand the exponential as a Taylor series in order to extract the projector $|\phi_k\rangle\langle\phi_k|$ from the exponential,

$$\hat{U}(t) = \prod_k \{1 + |\phi_k\rangle\langle\phi_k|(e^{-itE_k} - 1)\} \tag{3.6}$$

From the last expression, if we expand a given wavefunction as a linear combination of the (orthonormal) eigenstates,

$$|\Psi(\vec{r}, 0)\rangle = \sum_j c_j(0)|\phi_j\rangle \tag{3.7}$$

being $c_j(0) = \langle\phi_i|\Psi(0)\rangle$ (projection of the initial wavefunction on the i-th eigenfunction), we can write the wavefunction at any time as

$$|\Psi(\vec{r}, t)\rangle = \hat{U}(t)|\Psi(\vec{r}, 0)\rangle = \sum_j c_j(0)e^{-itE_j}|\phi_j\rangle = \sum_j c_j(t)|\phi_j\rangle \tag{3.8}$$

For time-independent Hamiltonians, the time evolution of a wavefunction can be described as the change of the coefficients used to expand the wavefunction in the basis of the (time-independent) eigenfunctions. Assuming short time propagation, $\Delta t \approx 0$, we use locally the eigenstates for the propagation.

3.3 Basis for the propagation

Formally, anytime we define the wavefunction as a linear combination of eigenfunctions of the Hamiltonian, we are using an infinite expansion. This is due to the fact that these eigenfunctions form a basis of the Hilbert space of the wavefunctions and, since there is no upper limit to the energy, this space has an infinite dimension.

Obviously, due to technical limitations, it is impossible to use an infinite basis in a calculation and thus we have to truncate the expansion. It should not affect the quality of the results since extremely high energy functions do not contribute so much to the states that we are usually interested in. And even in the case we want to study highly excited systems, we only have to include more terms in the expansion to achieve the desired accuracy.

Once we are not forced to use infinite expansions to have an accurate enough description of the systems of study, we can use a change of basis and the properties would remain constant. Since we rarely know *a priori* the eigenfunctions of the system in which we are interested, this is not, definitively, a good choice. As an alternative solution we would think about using the basis described in section 2.7, as Gaussian or Slater functions. Nevertheless, although these functions can be used to describe continuum states and resonances [61] they are not the best choice in our case.

There are better alternatives to have a correct description of delocalized states. In this thesis we have used the pseudo-spectral grid approach. We expand the wavefunction in a plane-wave basis and then we impose the grid to have the correct values. An homogeneous grid provides also a straightforward way to deal with propagations, reason why it is the chosen basis in for the code he have developed.

3.4 Propagation schemes

It is not necessary to know the exact expression of the eigenfunctions to study the temporal evolution of a wavefunction. In general, with few exceptions (as a free particle), there is no analytical solution to the TDSE and then it is required to use approximate numerical methods to solve it. In these cases, the time cannot be a continuum variable and thus it must be replaced by a *time step*, Δt, defined by the user. The stability and the convergence of the propagation strongly depend on the choice of Δt

The main differences between the numerical methods for the TDSE lay in the way in which the $\hat{U}$ operator is approximated o applied. Although many alternatives have been developed (Lanczos [62, 63], Crank-Nicholson [64], etc.) in this thesis we have used the *split-operator technique* [65]. To this, the Hamiltonian operator is written as the sum of the kinetic energy operator, $\hat{T}$, and the potential energy operator, $\hat{V}$. Since $\hat{T}$ and $\hat{V}$ do not commute, the consecutive application of the exponentials of the two operators is not equal to the action of the exponential of the total Hamiltonian:

$$e^{-i\hat{H}\Delta t} = e^{-i(\hat{T}+\hat{V})\Delta t} = e^{-i\hat{T}\Delta t}e^{-i\hat{V}\Delta t} + [\hat{T},\hat{V}]O(\Delta t^2) \tag{3.9}$$

There is other way to define $\hat{U}$ in terms of $\hat{T}+\hat{V}$, in which the error is lower for

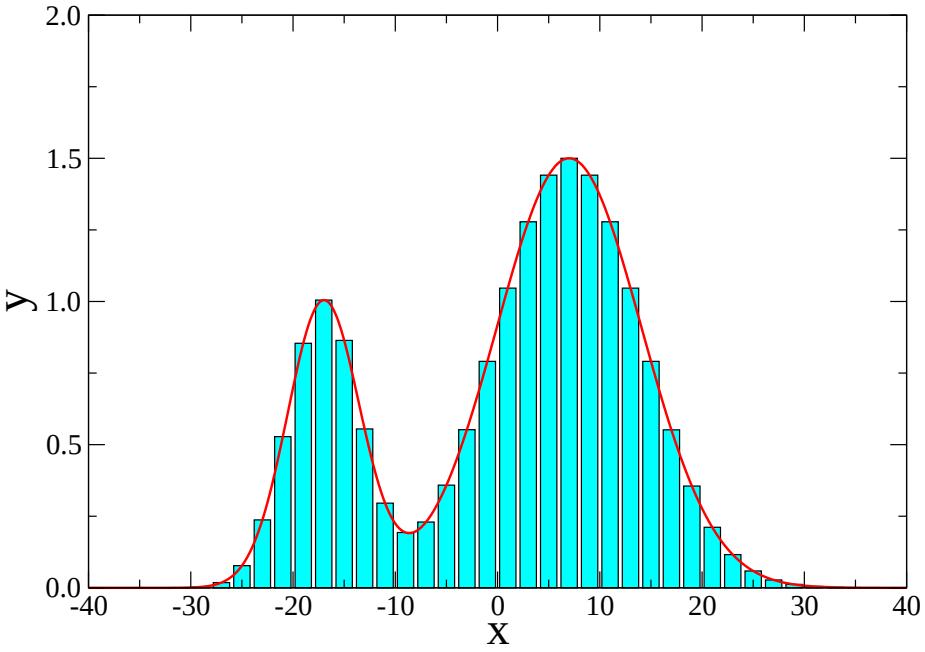

Figure 3.1: An example of a grid representation (cyan rectangles) being used to describe a function (red line)

small Δt:

$$e^{-i\hat{H}\Delta t} = e^{-i\hat{V}\frac{\Delta t}{2}} e^{-i\hat{T}\Delta t} e^{-i\hat{V}\frac{\Delta t}{2}} + [\hat{T}, \hat{V}]O(\Delta t^3) \tag{3.10}$$

The reason why it is convenient to split the Hamiltonian in terms of $\hat{T}$ and $\hat{V}$ lies in the fact that a local operator (as the potential energy operator) is diagonal in a grid representation, as it was pointed out by Kosloff [66]. Indeed, if we denote ϕ_i as the i-th basis function (mesh point), V_{ij} is:

$$V_{ij} = \langle \phi_i | V | \phi_j \rangle = \int \phi_i(x) V(x) \phi_j(x)\, dx = V(x_i)\delta_{ii} \tag{3.11}$$

Since a grid basis behaves as Dirac delta, at least one of the functions $\phi(x)$ is zero at any position of space, unless both functions are located in the same region. In that case, the solution of the integral is the value of the potential at that position.

Nevertheless, in the real space representation of the Schrödinger equation, the kinetic energy operator is not local since it involves a derivative. But, if we perform a Fourier transformation (denoted as $\mathcal{F}$) on the whole equation:

$$\mathcal{F}\Big[-\frac{1}{2m}\frac{d^2}{dx^2}\psi(x)+V(x)\psi(x)\Big]=\mathcal{F}\Big[E\psi(x)\Big] \tag{3.12}$$

using the properties of the Fourier transformation such as the linearity, we get:

$$\frac{p^2}{2m}\tilde{\psi}(p)+\int dp'\tilde{V}(p-p')\tilde{\psi}(p')=E\tilde{\psi}(p) \tag{3.13}$$

where $\tilde{\psi}(p)$ is the representation of the wavefunction in the momentum space and the integral denotes the convolution of $\tilde{\psi}(p)$ and $\tilde{V}(p)$, potential in momentum representation. Now, the kinetic energy becomes a local operator and thus, it is diagonal in our grid basis. The generalization to the 3D case is straightforward.

Since a transformation from real to reciprocal space does not change the wavefunction, it is possible to switch from one representation to another at any time. Through the use of the FFT (Fast Fourier Transform) [67, 68] the direct and backward transformations in a grid are performed with an extremely high computational efficiency. Thus, the complete propagation scheme used during this thesis is:

$$\Psi(\vec{r},t+\Delta t)=e^{-i\hat{V}\frac{\Delta t}{2}}FFT^{-1}\Big[e^{-i\hat{T}\Delta t}FFT[e^{-i\hat{V}\frac{\Delta t}{2}}\Psi(\vec{r},t)]\Big] \tag{3.14}$$

In each representation application, the corresponding operator is diagonal. The exponential of a diagonal matrix is also diagonal, so this scheme is very fast to compute, since the exponentials have to be calculated once at the beginning of the calculation (if the Hamiltonian does not contain any time-dependent term) and after that the propagation consist in a term-by-term multiplication and change of representation of the wavefunction by using the FFT.

3.5 Potential for the propagation

The kinetic energy is an operator which does not depend on the system of study (although its shape depends on the coordinate system chosen), but the potential is different for each case. This is the reason why, although WPP is an adequate methodology to study properties such lifetimes or excitation energies, it should be

adequated to each system by computing the potential. With the only exception of systems with analytical potentials (as hydrogen-like atoms) or systems where the potential can be calculated through the wave packet with a reasonable computational effort (few electrons systems), we need an external source for the potential.

The potentials used in this thesis, where the systems of study are molecules adsorbed on surfaces, are expressed as a sum of several terms that are going to be described in the following sections.

As a first approximation, the potential of the system can be written as the sum of the potential due to the molecule, V_{mol}, and the potential of surface. In this thesis, we have used an analytical potential, described in section 3.5.1. Since it is a model potential, we denote this term as V_{surf}^{mod}:

$$V = V_{mol} + V_{surf}^{mod} \tag{3.15}$$

This potential would describe correctly the states of the metal, including band structure, surface state and image states. In the same way, it would describe the molecular states perturbed by the surface. Some of these states appear as resonances, reason why WPP is an excellent methodology to study the active electron.

Nevertheless, in some cases, as chemisorption process or when there is an important charge transfer, the electron density around the molecule on the surface is very different to the density if the surface is not present, even if we are considering the same molecular geometry. Then, it is necessary to use a more sophisticated description of the potential.

To this end, we add the charge rearrangement due to the interaction, ΔV, define as the difference of the potential of the whole system minus the potential of the surface and the molecule by separate:

$$\Delta V = V_{mol+surf} - [V_{mol} + V_{surf}] \tag{3.16}$$

Now, with this new scheme, the total potential would be:

$$V = V_{mol} + V_{surf}^{mod} + \Delta V = V_{mol} + V_{surf}^{mod} + V_{mol+surf} - [V_{mol} + V_{surf}] \tag{3.17}$$

If we write this last equation in a different way and we cancel the two V_{mol} terms:

$$V = [V_{molecule+surface} - V_{surface}] + V_{surface}^{mod} \tag{3.18}$$

The potential inside the brackets represents the molecule perturbed by the surface and includes all the changes in the electron density due to the interaction, in the molecule and in the surface. This term is mainly located around the molecule and tends to vanish at few atomic units. Thus, at large distances the potential can be approximated to the surface model.

In this approach, the calculations of the whole system and the isolated surface potentials are carried out using exactly the same geometry (the one of the adsorption). This is a key point, because in this way the inner electrons of the surface are totally cancelled, as well as the effect of the pseudopotentials, if they have been used.

3.5.1 Metal surface model potential

If we are studying surfaces or molecules on surfaces, the standard codes based on DFT are able to deal with enough atoms to describe properly many of the processes of interest (adsorption, charge transfer...). Typically, 4-5 atomic layers are enough for a proper description of these properties. Nevertheless, other phenomena, such as coupling with the metallic continuum or electron decay towards the bulk or along the surface state, require a much larger cell, which would contain a huge number of atoms. The computational effort is such as these systems are not accessible nowadays.

As an alternative, the surface-electron interaction can be described through model surfaces, which can be analytical. This is the case of the model surface potential developed by Chulkov *et al* [69], which is used in this thesis.

It is a potential that recover the most important characteristics of the surfaces: energies and lifetimes of surface and image states, as well as the projected band gap at the $\bar{\Gamma}$ point. This gap is very important in the decay and coupling of atomic or molecular states [70]. The potential is analytical and it depends only on a few parameters, which are specific for each surface.

Provided this potential, we can generate a big enough grid to describe correctly the continuum states. To this end, it is possible to calculate the potential of the molecule (with the adsorption geometry) using a regular-size supercell (which is known as *DFT cell*) and then, add the Chulkov potential and, at the same time, generate a larger grid (*WPP cell*). This expansion is not a problem, since the potential generated by the molecule should be negligible in the limit of the DFT cell in the coordinate parallel to the surface (molecular effect is screened inside the metal). That is why, the results should be the same than if we would have used a larger cell

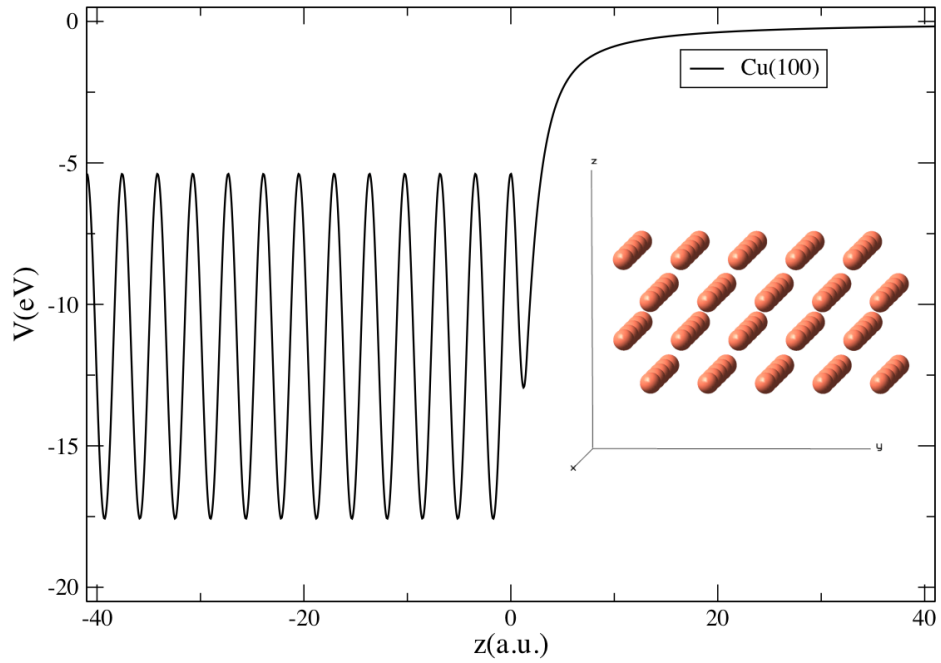

Figure 3.2: Chulkov potential of the Cu(100) surface and 4-layers slab of this surface.

for the DFT calculation.

Of course, if the system of interest is periodic (self-assembled monolayers, for example) the periodicity of the DFT cell is correct and thus the total cell in the WPP must have the same size.

3.5.2 Molecular potential

One of the most important advantages of the methodology that has been developed in this thesis is the fact that it is able to treat any molecule, importing the information from Quantum Chemistry packages. In this case, the molecular potential contains several parts that are described in the following sections.

Local potential

Although in Quantum Chemistry WPP techniques are usually applied to study temporal evolution of nuclei, in this thesis we are considering fixed nuclei and single-electron wave packets, which are going to be affected mainly by electrostatic forces.

Describing the interaction between the electron and the nuclei in a point $\vec{r_i}$ of the grid is easy: this part of the potential is only the sum of the individual potentials generated by each of the M nucleus at that coordinate:

$$V(\vec{r_i}) = \sum_{\alpha}^{M} -\frac{Z_\alpha}{|\vec{r_i} - \vec{r}_\alpha|} \tag{3.19}$$

If we are dealing with non-punctual charge distributions of the nuclei, as in the case of pseudopotentials, the interaction of the electron with a nucleus requires the use of the use of the Gauss Law for the electric field:

$$\oint \vec{E} d\vec{s} = \frac{Q}{\epsilon_0} \tag{3.20}$$

Knowing that the pseudopotentials have a radial distribution of the function that describe the nuclei, that we denote as $\rho(r)$, where r is the distance from the center of the pseudopotential, by substitution in the Gauss Law:

$$\oint \vec{E} d\vec{s} = \frac{\int_0^r \rho(r')dr'}{\epsilon_0} \tag{3.21}$$

so, for $r < r_{cut}$, where r_{cut} is the maximum distance for which the pseudopotential is defined, the electric field is:

$$E(r) = \frac{\int_0^r \rho(r')dr'}{4\pi r^2 \epsilon_0} \tag{3.22}$$

For $r \geq r_{cut}$, all the charge is contained inside the radius and then we can recover the simple Coulomb expression.

In the case of the electrostatic interaction between the active electron and the others, we do not have an analytical expression of the electron density and thus the calculation of this term of the potential becomes more difficult.

Nevertheless, it is possible to use the Poisson equation, which shows the relationship between the electron density and the electrostatic potential:

$$\rho(\vec{r}) = -\frac{\nabla^2 V(\vec{r})}{4\pi} \tag{3.23}$$

The sum of the potential generated by the electron density and the potential

generated by the nuclei is known as *Hartree potential* and it is a very important part of the total potential.

Nevertheless, since we are working in the frame of the Density Functional Theory, the electron correlation is introduced through the *exchange-correlation potential*, V_{xc}. Thus, the total local potential is the sum of the Hartree potential and the exchange-correlation potential. This term can be easily extracted from different Quantum Chemistry or Solid-State Physics packages. In this thesis, we have used Abinit [71] for this purpose.

It is possible to add to this local potential other terms in order to take into account other interactions, for example, the interaction with an external electromagnetic field.

Norm-conserving pseudopotentials

In our implementation, the local potential is extracted from standard codes based in the Density Functional Theory. Since we are mainly interested in the interaction of molecules with metal surfaces, we have to use periodic boundary conditions to describe these systems properly, as we discussed in Section 2.9.

Those softwares are usually based in plane waves and they use pseudopotentials in order to decrease the computational effort. To carry out an electron propagation, the norm in the pseudopotential region must be the same that the one that it would have if all the electrons were considered explicitly. Otherwise, the norm of our wave packet would change artificially during the propagation, which is unphysical and would invalidate the obtained results.

For this reason, in this thesis we have used Abinit, which uses norm-conserving pseudopotentials [72]. These pseudopotentials, in addition to the local part (which is taken into account in the local potential of the propagation) they have a non-local part (V_{NL}) that is responsible of the correct energy position of the calculated states. The non-local part must be taken into account also in the propagation. Its action is defined as:

$$V_{NL} = \sum_{k} \sum_{l} \sum_{m} \sum_{\sigma} |\phi_{klm\sigma}\rangle V_{klm\sigma} \langle \phi_{klm\sigma}| \tag{3.24}$$

where l and m denote the angular momentum and magnetic quantum number of each pseudofunction, k is introduced for those angular momenta in which more than one pseudofunction is needed for the atom σ. $V_{klm\sigma}$ is the shift in the energy of the

(normalized) eigenfunction $\phi_{klm\sigma}$ to place it at the correct position in the spectrum. These $\phi_{klm\sigma}$ are orthonormal:

$$\langle\phi_{klm\sigma}|\phi_{klm\sigma}\rangle = \delta_k\delta_l\delta_m\delta_\sigma \tag{3.25}$$

Thus, the action on the wavefunction of the non-local part can be described as the successive action of the different non-local pseudopotentials:

$$e^{-iV_{NL}\Delta t} = e^{-i\Delta t\sum_\alpha V_\alpha\hat{P}_\alpha} = \prod_\alpha e^{-i\Delta t V_\alpha\hat{P}_\alpha} \tag{3.26}$$

where α denotes the different non-local components (k, l, m, σ) and $\hat{P}_\alpha = |\phi_\alpha\rangle\langle\phi_\alpha|$.

The best way to define the action of this kind of potentials in a split-operator scheme requires to extract the projectors from the exponential. As it was done in equation 3.6 with the Hamiltonian operator, we can write the exponential as a Taylor series. For the α-th projector:

$$e^{-i\Delta t V_\alpha\hat{P}_\alpha} = \sum_{n=0}^{\infty}\frac{(-i\Delta t V_\alpha\hat{P}_\alpha)^n}{n!} \tag{3.27}$$

Now, if we extract from this summation the term $n = 0$, which is just 1, and taking into account that $\hat{P}^n = \hat{P}$ (which is fulfilled for any projector, since they are idempotent by definition),

$$e^{-i\Delta t V_\alpha\hat{P}_\alpha} = 1 + \hat{P}_\alpha\sum_{n=1}^{\infty}\frac{(-i\Delta t V_\alpha)^n}{n!} \tag{3.28}$$

Adding and subtracting $\hat{P}_\alpha$,

$$e^{-i\Delta t V_\alpha\hat{P}_\alpha} = 1 - \hat{P}_\alpha + \hat{P}_\alpha\left(1 + \sum_{n=1}^{\infty}\frac{(-i\Delta t V_\alpha)^n}{n!}\right) \tag{3.29}$$

The term inside the parenthesis is equal to an exponential, so the expression becomes:

$$e^{-i\Delta t V_\alpha\hat{P}_\alpha} = 1 + \hat{P}_\alpha(e^{-i\Delta t V_\alpha} - 1) \tag{3.30}$$

Also, for each α and Δt, the term inside parenthesis is constant, so can be calculated once at the beginning of the calculation.

Since the projector is localized in the region of the space surrounding the corresponding atom, out of the region $\hat{P}_\alpha = 0$ and thus the non-local operator becomes the unity operator and its action can be skipped. In this way, it is possible to calculate the projection $\hat{P}_\alpha|\Psi(\vec{r},t)\rangle$ only in a certain volume, reducing the computational effort.

3.5.3 Correction to energy: molecular projectors

If the propagation is carried out using only the local DFT potential and the non-local potential to treat correctly the effect of the pseudopotentials, the energies obtained in a WPP simulation must be the same of the DFT calculation: the KS energies (if convergence in dt and dx is reached).

Nevertheless, despite of the huge improvements in the development of functionals, we are far from a correct description of the excited states, electron affinities or ionization energies in term of the Koopmans' theorem [73].

As an alternative, it is possible to introduce a correction in order to shift the state of interest, which we denoted as ϕ_α. To this, and if we consider that the shape of the state is correct, we can define a new Hamiltonian operator which is the same that we have used until now but with an extra term:

$$\hat{H}' = \hat{H} + U|\phi_\alpha\rangle\langle\phi_\alpha| \tag{3.31}$$

where U is the difference between the KS energy of the orbital that represents the active electron and the correct energy, which can be calculated using high level ab initio calculations.

In this thesis we have considered two processes:

-(Single) electronic excitation: once we have characterized the state of interest (especially the orbital where the active electron is located), we calculate the excitation energy using EOM-CCSD [74], with a triple-ζ basis.

-(Single) molecular anion: if we are interested in the ground state of the anion, we consider that wavefunction of the extra electron has the same shape than the LUMO. The energy of this state (the electron affinity) is calculated as the energy difference of the anion and the neutral molecule, using CCSD in both cases and a triple-ζ basis too.

In both cases all the orbitals that are involved in this calculation (the HF used in the coupled cluster calculations and the KS of the DFT) must be characterized,

to avoid other states (as Rydberg states) which could appear at lower energies, especially if large basis set with diffuse functions are used. For these calculations, we have used Gaussian09 [75]

These orbitals for the projectors are calculated for the isolated molecule. For this reason, the correction to the Hamiltonian operator is not diagonal when the surface is considered and it allows partial mixing between the states in which there is a molecular contribution. That is why the shifting in the energy is not exactly the same as the U value and why the shape of the wavefunctions can change (if the new term of the Hamiltonian is diagonal the shape will be exactly the same).

The way in which this correction is included is the same as the action of the non-local part of the pseudopotential.

3.5.4 Absorbing potential

The use of the Fourier grid Hamiltonian approach introduces naturally periodicity in the calculation. In many situations we want to take it into account, as in the case of SAMS, high surface coverage, etc. Nevertheless, there are other systems in which, in order to reproduce the electron escape, we have to introduce outgoing wave boundary conditions in the limit of the mesh. The study of a single molecule on a surface (low coverage regime) or electron scattering in an isolated molecule in the gas phase are two examples of systems without translational symmetry. In these cases, the outgoing wave and the incoming wave of the next cell would interfere, producing a fake quantization of the levels, which would shift the energy and change the lifetime of the electronic state artificially.

To avoid this effect, it is possible to use a simulation box big enough to extract all the information of interest before an important part of the wave packet reaches the boundary.

There is a (more practical) alternative: the use of absorbing potentials. These are imaginary potentials that, when they are applied in the complex exponential in the split-operator scheme, become real. Those real exponentials are not unitary transformations and thus, the norm of the wavefunction in the regions of the space where they are acting decreases. In this way, the wavefunction would vanish before entering in the closest replica.

Let $f(x)$ be a real function, with $f(x) \geq 0 \, \forall \, x$ considered. In this case, $V_{abs}(x) = -if(x)$ is a pure imaginary function, with $\Im\{V_{abs}\} \leq 0 \, \forall \, x$ too. The action of V_{abs}

in a complex exponential on a wavefunction, as in the split-operator scheme is:

$$e^{-iV_{abs}(x)\Delta t}\psi(x) = e^{-f(x)\Delta t}\psi(x) \tag{3.32}$$

Since outwave boundary condition is not hermitian, the Hamiltonian operator becomes not hermitian. Thus, in the region where the absorbing potential acts (where $f(x)$ is not zero) this exponential vanish the wavefunction and, for this reason, there is a loss of the norm of the total wavefunction.

During this thesis we have used a quadratic absorbing potential, which acts only in the proximity of the edge of the simulation cell. In this region, the potential is defined by:

$$V_{abs}(x) = -i\lambda\,(x - x_{lim})^2 \tag{3.33}$$

where x_{lim} is the value where this potential starts to act. Thus $x - x_{lim}$ is the distance from the starting point of the potential. λ is a factor that controls the shape of the potential. A high value might cause a reflection of the wavefunction, whereas if a small λ is used, the absorbing potential would need to act in a large region of the space in order to be effective vanishing the outgoing waves.

An equilibrium should be found to achieve potentials that absorb efficiently both high and low frequency parts of the wavefunction.

3.6 Obtaining of lifetimes, energies and wavefunctions

All the information of a system is contained in its time-dependent wavefunction. Nevertheless, extracting this information is not immediate, especially if we do not have an analytic expression of the wavefunction, but a numerical solution, as in our case. In this section we show how to obtain the properties of our interest in this thesis: the energies and lifetimes of the electronic states and their corresponding wavefunctions.

We start from the autocorrelation function, $A(t)$, defined as:

$$A(t) = \langle \Psi(t) | \Psi(0) \rangle \tag{3.34}$$

where $\Psi(t)$ is the wavefunction at time t and $\Psi(0)$ is the initial wavefunction we have set for the propagation. If we expand the wavefunctions in terms of the eigenstates,

we get:

$$A(t) = \sum_i c_i^*(t)\langle\phi_i^*(t)| \sum_j c_j(0)|\phi_j(0)\rangle \tag{3.35}$$

Since these eigenstates are orthonormal ($\langle\phi_i^*| \phi_j\rangle = \delta_{ij}$),

$$A(t) = \sum_i c_i^*(t)c_j(0) \tag{3.36}$$

The temporal evolution of the coefficients is given by:

$$c_i(t) = c_i(0)e^{-iE_it} \tag{3.37}$$

If now we replace 3.37 in 3.36, we get:

$$A(t) = \sum_i |c_i|^2 e^{iE_it} \tag{3.38}$$

The Fourier Transform of the autocorrelation function,

$$n(E) = \int A(t)e^{-iEt}dt = \sum_i |c_i|^2 \int e^{iE_it}e^{-iEt}dt = \sum_i |c_i|^2\delta(E - E_i) \tag{3.39}$$

is the density of states, projected in the initial wavefunction. Selecting different initial functions, we get different $|c_i|^2$ and thus different projected density of states. That is why the choice of the initial wavefunction is extremely important: we can populate different states by using different $\Psi(0)$. This is useful to focus in specific states by the symmetry or the spatial distribution. In the systems of interest in this thesis, molecules adsorbed on metal surfaces, if we choose for the propagation as the initial wavefunction an eigenfunction obtained for the molecule in the gas phase, we can determine to which states of the whole system contributes the gas phase wavefunction.

If the potential contains an imaginary part (absorbing potential), the Hamiltonian operator is not hermitian anymore and thus some of the eigenvalues, the ones related with resonant states, are complex. In those cases, in the projected density of states the peaks are not delta functions anymore, since the states acquire a width, Γ, which are the inverse of the lifetime of that state, τ.

In this case, the autocorrelation function can be written as a linear combination of bounded and decaying states [58]:

$$\mathcal{A}(t) = \sum_{j=1}^{J} a_j e^{-i\left(E_j - i\frac{\Gamma_j}{2}\right)t} = \sum_{j=1}^{J} a_j e^{-iE_j t} e^{-\frac{\Gamma_j}{2}t} \tag{3.40}$$

This expression can be used to fit the autocorrelation function. The fitting parameters are the amplitudes a_j, the energies E_j and the widths Γ_j. If states with long lifetimes are populated, it allows us to avoid the long propagations which would be required to converge the spectrum.

Now, if we are interested in the wavefunction at a given energy E_α, wavefunction which we denoted as ψ_α, it is possible to get it in the following way:

$$\psi(\vec{r})_\alpha = \int_0^\infty e^{iE_\alpha t} \Psi(\vec{r}, t) dt \tag{3.41}$$

The exponential $e^{iE_\alpha t}$ acts as a filter on the time-dependent wavefunction, annihilating the contributions with an energy different from E_α, being this annihilation more effective with the states which are far in energy from E_α.

In this way, with short propagation times we are able to "purify" the wavefunction from very high (or low) energies, while cleaning the wavefunction from states that are close in energy would require longer propagations.

To know the values of E_α it is necessary to carry out a previous propagation in order to get the energy spectrum.

As an illustrative example of this effect, we have calculated the energy and the lifetime of the π^* anion of the carbon monoxide (CO), adsorbed on a pristine Cu(100) surface. We have used two approaches to compute the potential: (i) just the sum of the potential of the surface and the molecule (ii) taking into account the rearrangement of the electron density due to the interaction. Comparison of the results with both potentials allows to study the influence of the charge transfer. The local potential along the molecular axis in both cases is shown in figure 3.3.

There are two main differences between the potentials.

-The first one is the value around the minima (position of the nuclei): in the case in which we have taken into account the charge transfer (black line) in this area

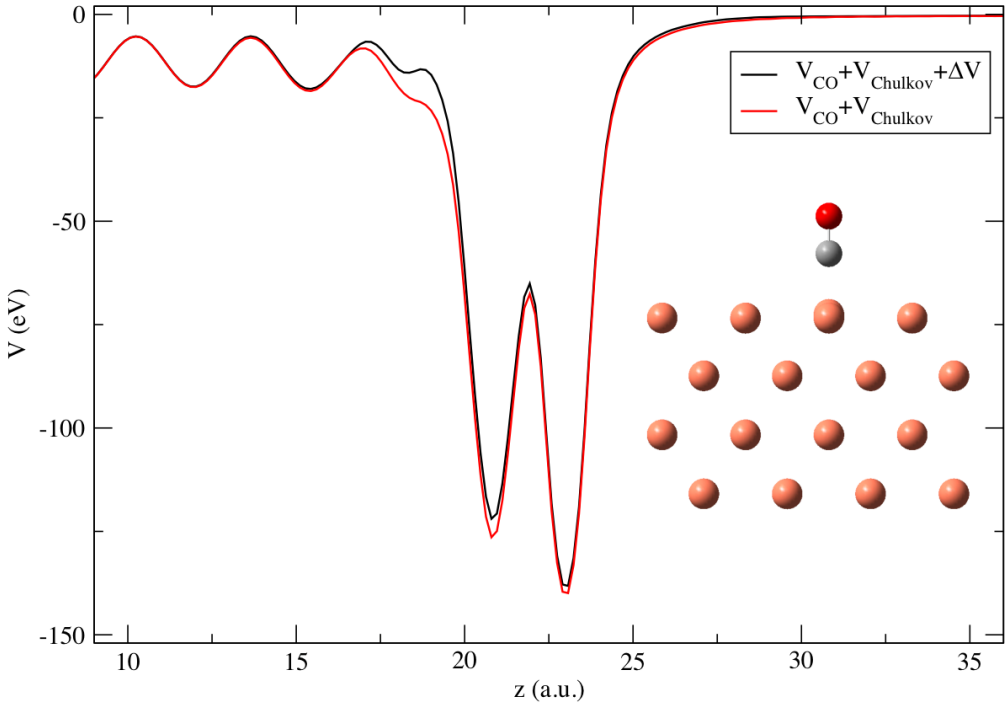

Figure 3.3: Comparison between the potential calculated with (black) and without (red) the charge transfer (black) in the CO/Cu(100) system

the potential is less attractive. This is due to the fact that the additional electron density due to the charge transfer generates an extra electron screening and thus, the active electron is less attracted by the nuclei.

-The second one is the appearance of a new local maximum at $z \approx 19$ a.u. if the charge transfer is considered. It is due to the rearrangement of the electron density near the surface.

The effect of extra screening shifts the electronic states to less negative (or even positive) energies. In the case of the anion of CO on Cu(100), the energy changes from -2.54 eV if charge transfer is not considered, to $+1.13$ eV using the full potential (with respect to the vacuum level, $E_{vac} = 0$ eV). On the other hand, the barrier that appears in the metal surface blocks the decay of the molecular states towards the metal, stabilizing those states and thus decreasing their widths. In this particular case, where the charge transfer shifts to a positive energy the molecular anion, the

width changes from 1.28 eV (lifetime $\tau = 0.51$ fs) without charge transfer, to 3.25 eV ($\tau = 0.20$ fs) if charge transfer is considered, due to the extra available decay channel towards the vacuum. Nevertheless, if there is no extra channel, considering the electronic rearrangement due to the interaction increases the lifetime.

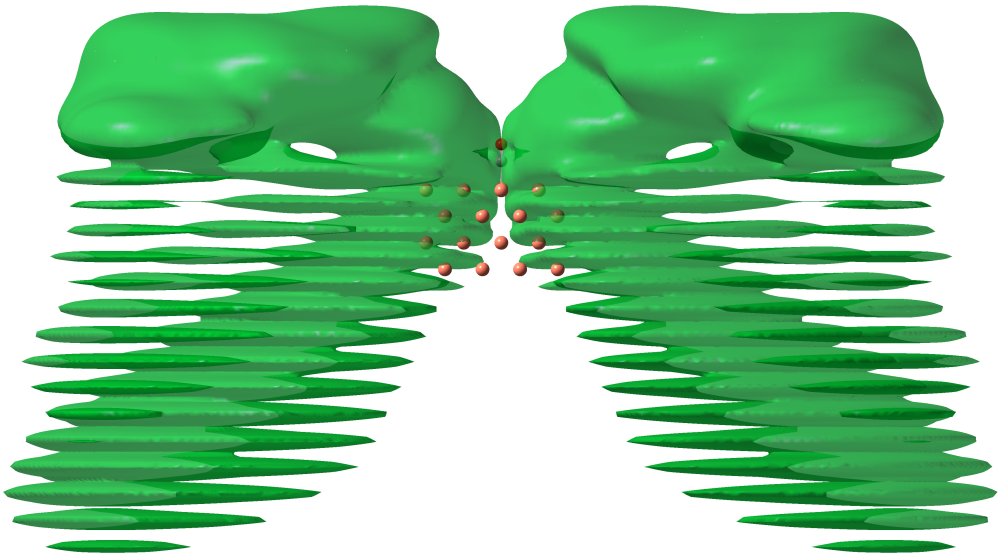

Figure 3.4: Electron density of the resonant wavefunction of CO adsorbed on Cu(100). Isovalue=0.001

3.7 Interaction with electromagnetic fields

We are dealing with excited electronic states and we may be interested not only in the properties of those states, but in how we can populate them. Since experiments are very often based on pump-probe fs lasers, in order to have a better comparison with the experimental results, we have included in the code the possibility of simulate the action of laser pulses. In our propagation scheme it is possible to add new terms in a very simple way, as it was discussed in section 3.5.2.

The expression of the potential, V_{ext}, produced by a monochromatic wave coming along the z axis is given by:

$$V_{ext}(t) = E_0 \cdot z \cdot cos(\omega t + \theta) \tag{3.42}$$

where E_0 is the amplitude of the field, ω is the angular frequency of the field and θ is a phase factor.

In many experimental techniques as 2PPE (2photon-photoemission) the incident radiation is not a continuous wave, but a laser pulse with a width. This kind of light sources exert a potential in the electrons that can be described as:

$$V_{ext}(t) = E_0 \cdot z \cdot cos(\omega t + \theta) \cdot exp\left[-\frac{(t-t_0)^2}{2\sigma^2}\right] \tag{3.43}$$

where σ is the width of the Gaussian envelope and t_0 is the time around the pulse is centered (and when it acquires the maximum value if the phase factor is zero).

Due to the uncertainty principle, this last pulse is not a monochromatic light anymore: the presence of the envelope introduces a width in the energy spectrum. That is why, the longer the pulse duration, the better defined its energy is.

In a formal development, using an infinite expansion, the eigenstates of the time-independent potential (when the pulse is not acting) form a complete basis of the Hamiltonian. Thus, the eigenstates of the complete Hamiltonian, when the pulse is acting, can be written as a linear combination of the eigenstates without the laser field.

Using the perturbation theory up to first order, the transition probability per unit of time P from an initial state $|i\rangle$ to a set of final states $|f\rangle$ with a density of states $n(f)$, due to the action of the time-dependent part of the Hamiltonian $\hat{H}$ (in our case, the laser field) is given by the Fermi's golden rule:

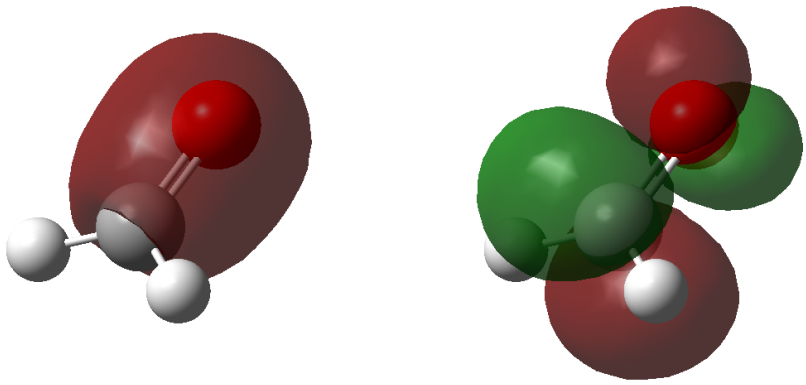

Figure 3.5: Wavefunctions (isovalue=0.05 a.u.) of the two selected states of the formaldehyde for the laser-induced transitions: σ_{CO} (left) and π^*_{CO} (right). Red and green colors denote different phases.

$$P_{i\to f} = \frac{2\pi}{\hbar}|\langle i|\ \hat{H}|f\rangle|^2 n(f) \tag{3.44}$$

This expression only considers one-photon absorption. Multiphotonic process would require further order in the perturbative expansion.

Since we are not dealing with analytic expression, but numerical solutions of the TDSE, we use the full expression of the laser field. Then, we determine the final population after the pulse action by projecting the final wavefunction on the eigenstates that we previously obtained in a propagation without time-dependent potential.

Thus, the role of the laser pulse is just coupling the time-independent eigenstates to allow the change of their populations.

In order to show the action of the laser, we have selected the formaldehyde. It is a planar molecule, which states with a well-defined symmetry. Using our WPP code we have obtained two states: the inner σ_{CO} and the π^*_{CO}, which are shown in figure 3.5.

These states have been chosen in order to analyze the effect of the symmetry. Placing the molecule in the xy plane and with a field that oscillates along z, the $\sigma \to \pi^*$ transition should be active at first order, since one of the states involved is symmetric and the other is antisymmetric with respect to z.

The evolution of the population of the states which are involved in the transition

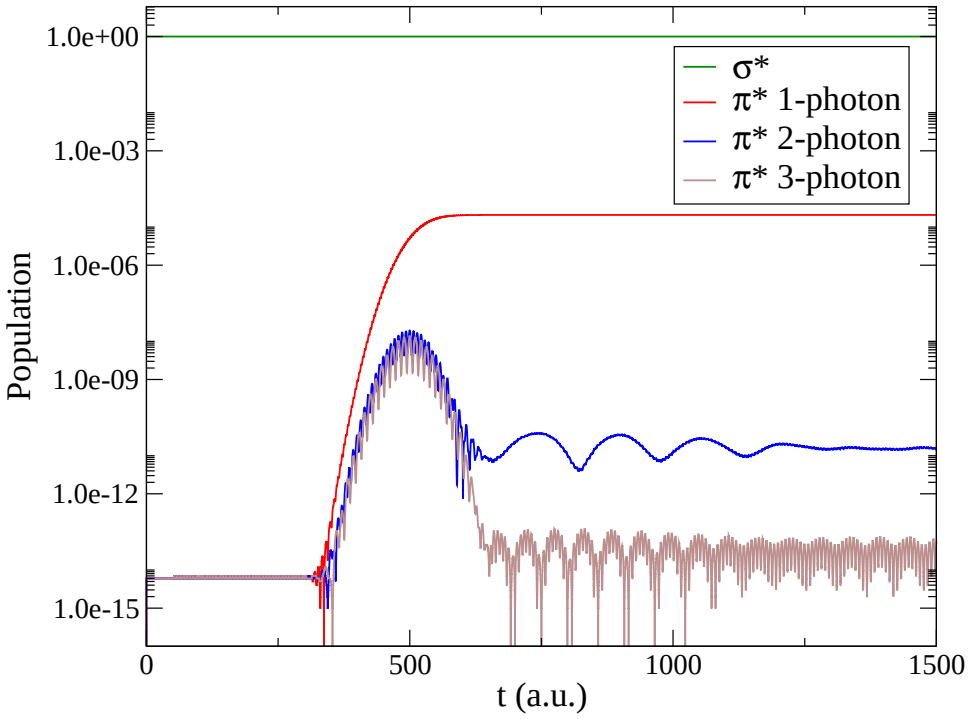

Figure 3.6: Population of the π^* state, after excitation from the σ state, using 1, 2 or 3 photons (red, blue and brown lines, respectively). Population of the σ state (green line) barely changes.

are shown in figure 3.6. The amplitude of the laser pulse, centered at $t = 500$ a.u. is 0.002 a.u. The σ value is 40 a.u. In each case the frequency is the equal to energy difference between the states or divided by a factor 2 or 3 (for the 2 and 3 photon absorption respectively).

In order to get the populations of the different states, the wavefunction at each time is projected on the different functions ϕ (in this case, eigenstates) that are given to the code. The population is the square of the absolute value of this projection:

$$P_i(t) = |c_i(t)|^2 = |\langle \phi_i | \Psi(t) \rangle|^2 \tag{3.45}$$

Despite the numerical noise (mainly due to the numerical accuracy in the local potential) the eigenstates can be obtained with few contribution of other states and

WPP can be used to study transitions with our code.

3.7.1 Theoretical electron detector. Simulating experiments

In those cases where the time-dependent potential populates bound states, calculating the final populations is straightforward. We can obtain the coefficients of the eigenstates after the action of the laser pulse. On the other hand, if continuum states are populated, this process becomes more difficult. We cannot wait the system to reach an equilibrium since the part of the wavefunction in which we are interested would vanish. Part of the wavefunction would reach the end of the mesh and vanish in the absorbing potential during the action of the pulse.

However, we can place a theoretical detector to determine the fraction of the wave packet that goes out of our simulation box and the energy and momentum contributions of the wave packet over the continuum states. In this way, we are able to determine also the time that would take to those outgoing waves to leave the system. Since the kinetic energy of the ejected electrons is a quantity than can be measured, we can have a comparison with the experiment.

We are going to place our theoretical detector as a xy plane, parallel to the surface, in the cases we consider it.

For $z \gg z_{molecule}$, in the asymptotic region, we suppose that the potential only depends on the z coordinate. Due to our methodology in which we expand the DFT box with an analytical potential (in the case of surfaces) or vacuum (isolated molecules) this is formally correct.

Now, in a very good approximation for the Chulkov potential at large distances, we set $V = V_0 = 0$.

In this way, in this region the eigenfunctions ϕ_i of the Hamiltonian (free particle) are plane waves:

$$\phi_{\vec{k}}(\vec{r}) = e^{i\vec{k}\vec{r}} \tag{3.46}$$

where $\vec{k} = (k_x, k_y, k_z)$

Now, the wavefunction can be written as:

$$\Psi(\vec{r}, t) = \sum_{\vec{k}} c_{\vec{k}} e^{-iE_{\vec{k}}t} e^{i\vec{k}\vec{r}} \tag{3.47}$$

Since we are interested in the z direction, we group $\vec{k}_{||} = (k_x, k_y)$ and separate k_z. Analogously, we define $\vec{r}_{||} = (x, y)$. With this new notation, equation 3.47 can be written as:

$$\Psi(\vec{r}, t) = \sum_{\vec{k}_{||}, k_z} c_{\vec{k}_{||}, k_z} e^{-iE_{\vec{k}_{||}} t} e^{-iE_{k_z} t} e^{i\vec{k}_{||}\vec{r}_{||}} e^{ik_z z} \tag{3.48}$$

The waves with $\vec{k}_{||} = 0$ are:

$$\Psi(\vec{r}, t)_{\vec{k}_{||}=0} = \sum_{k_z} c_{0,k_z} e^{-iE_{k_z} t} e^{ik_z z} \tag{3.49}$$

Now, after we have imposed $\vec{k}_{||} = 0$, we solve for the plane of the detector, z_0. We denote this time-dependent result as $A(z_0, t)$

$$A(z_0, t) = \langle \Psi(x, y, z_0, t)_{\vec{k}_{||}=0} | \Psi(x, y, z_0, t) \rangle = \int\int dxdy\, \Psi(x, y, z_0, t) \tag{3.50}$$

So, the integral of Ψ in the z_0 plane gives us directly the information of the waves with $\vec{k}_{||} = 0$ that goes through the detector at each time.

We define now $\Phi(z_0, \omega)$ as the Fourier transform of $A(z_0, t)$:

$$\Phi(z_0, \omega) = \int dt\, e^{i\omega t} A(z_0, t) \tag{3.51}$$

If we calculate $\Phi(z_0 + dz, \omega)$ by doing the same in the following point of the grid, we can obtain $\Phi(z_0 + \frac{dz}{2}, \omega)$ by interpolation and its derivative. With these two quantities, we can obtain the flux, and thus, the energy distribution of the outgoing electrons:

$$J = \Im \left\{ \Phi^*(z_0, \omega) \frac{d\Phi(z_0, \omega)}{dz} \right\} \tag{3.52}$$

In order to show how this capability is implemented in our code, we have studied the ionization of the formaldehyde molecule from the deepest σ state. To this, we have used a laser pulse centered in $t = 500$ a.u., with a width $\sigma = 40$ a.u., an amplitude equal to 0.002 a.u. and a frequency of 1.2 a.u., which is enough to ionize from the initial state (whose energy is -0.97915 a.u.). Since in this case we know the energy of the initial state and the energy of the laser pulse, we know *a priori* the

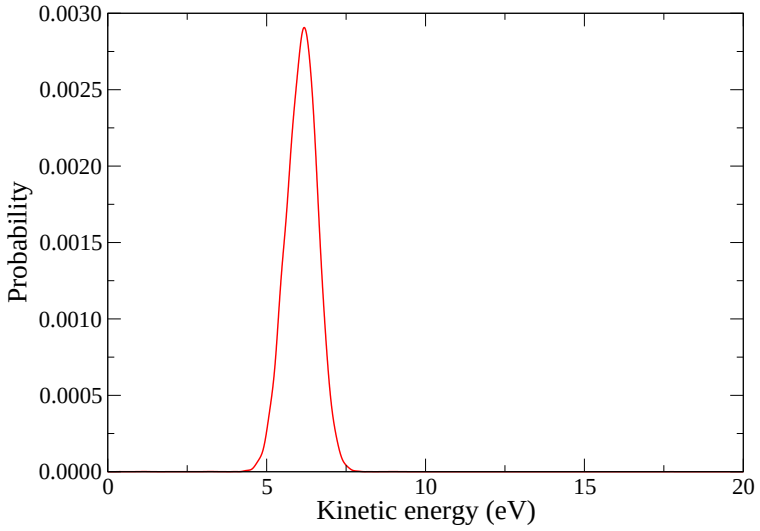

Figure 3.7: Distribution of the kinetic energy of the ejected wave packet after the laser pulse.

kinetic energy of the ejected wave packet: $1.2 - 0.97915 = 0.22085$ a.u. (around 6 eV), which is in agreement with the spectrum, shown in figure 3.7.

Part III

Results

Chapter 4

Adsorption of vinyl derivatives on Cu(100)[1]

Abstract We present a thorough theoretical study of the adsorption of acrolein (ACO), acrylonitrile (ACN), and acrylamide (ACA) on a Cu(100) surface. For this purpose, we have used the Density Functional Theory (DFT), imposing Periodic Boundary Conditions (PBC) to have a correct description of the electronic band structure of the metal and including dispersion forces through two different schemes: the D2 method of Grimme and the vdW-DF.

We have found several adsorption geometries. In all of them, the vinyl group together with the amide (in ACA), cyano (in ACN), and carbonyl (in ACO) groups, is highly involved. The highest adsorption energy is found for acrylamide, followed by acrolein and the lowest for acrylonitrile.

We show that a strong coupling between the π electronic system (both occupied and virtual orbitals) and the electronic levels of the metal is mainly responsible of the chemisorption. As a consequence, electronic density is transferred from the surface to the molecule, whose carbon atoms acquire a partial sp^3 hybridization. Lone-pair orbitals of the cyano, amide and carbonyl groups also play a role in the interaction. The simulations and following analysis allow to disentangle the nature of the interaction, which can be explained on the basis of a simple chemical picture: donation from the occupied lone pair and π orbitals of the molecule to the surface and backdonation from the surface to the π^* orbital of the molecule ($\pi-$backbonding).

[1]This chapter is based on J.Phys.Chem.C, 122, 27301 (2018)

4.1 Introduction

Adsorption of organic molecules on metal surfaces is a process of high interest due to the large number of technological applications in which it is involved: heterogeneous catalysis [76–82], hybrid metal-organic materials [83–92], photovoltaic organic nanodevices [93–96], ultrathin optoelectronics [97–101], organic solar cells [94, 96, 102, 103], molecular spintronics [104–107], corrosion protectors [99, 108–111], etc. The interaction of the organic molecules between them and with the substrate favors specific orientations, which can lead to the formation of Self-Assembled Monolayers, SAMS [112–118]. The coupling between the metal and the molecules in the SAMS causes the appearance of electronic properties that both parts do not present separately [119]. This is a key point of the hybrid materials. Furthermore, these surface-molecule interactions modify the electronic structure of the adsorbed molecules, weakening some chemical bonds and enhancing the reactivity, which can be applied in heterogeneous catalysis. In the adsorption, some organic groups are specially involved. However, the molecule-substrate affinity does not depend only on the group, but also on the nature of the surface (chemical composition and topology), as well as on the conjugation or proximity to other groups in the molecule. Acrolein, acrylonitrile and acrylamide present different groups and are thus excellent candidates to study the interaction between organic molecules and metal surfaces (see structures in Fig. 4.1). These molecules are polymer precursors, reason why they have an important technological interest. Their common structural characteristic is the presence of a vinyl group, with a double C=C bond, which is usually involved in strong adsorptions (chemisorption) with the surface [120,121]. This bond is conjugated with different functional groups in each of the three molecules, so they can be used to study how the electronic delocalization due to conjugation affects a substituted alkene interacting with a metal surface, and its adsorption ability.

Experimental works on similar molecules adsorbed on Cu(100) surface have been carried out: Temperature-programmed desorption and near-edge X-ray absorption techniques were used to study the decomposition reactions to generate vinyl groups from vinyl bromide and vinyl iodide on Cu(100) [122]. The same techniques were used to study the bonding and reactivity of allyl groups (CH_2CHCH_2) on a Cu(100) surface [123]. And more recently, the combination of temperature-programmed reaction/desorption and reflection-absorption infrared spectroscopy has been employed to study reactions of CH_2 = CHBr and CH_3CHBr_2 on Cu(100) [124]. Linking of

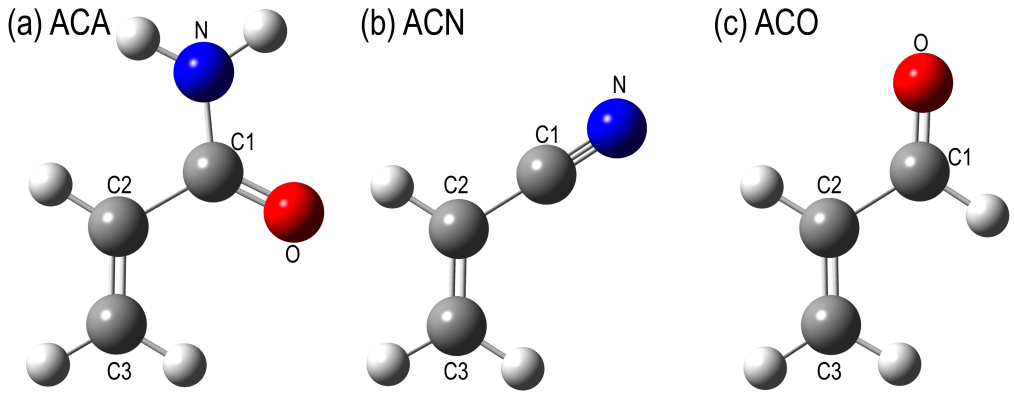

Figure 4.1: The three vinyl derivative molecules studied in this chapter: (a) acrylamide (ACA), (b) acrylonitrile (ACN), and (c) acrolein (ACO). Labels of atoms in each molecule correspond to those used in Tables 4.1, 4.2 and 4.3.

the vinyl group to the surface is a key aspect to understand the reactivity of these experiments.

Over the last decades, different experimental techniques have been developed to probe properties of adsorbed molecules (as adsorption energy and geometry, electronic and vibrational levels, etc.). Adsorption geometries can be measured with high precision using atomic force microscopy (AFM) [125, 126] or scanning tunneling microscopy (STM) [127–129], being this last technique able to study also the electronic structure near the Fermi level. X-ray standing wave (XSW) [130] is an extremely powerful technique for obtaining information of surfaces and interfaces on the atomic scale, by combining diffraction with other spectroscopic techniques. PhotoElectron Diffraction (PED) [131, 132] takes advantage of the scattering response of photoexcited electrons to obtain accurate information on the structural information on surfaces. The strength of the molecule-surface interaction (adsorption energy) can be obtained through temperature programmed desorption (TPD) [133, 134] experiments. X-ray spectroscopy [135, 136] allows to evaluate the change in the electronic density associated to charge transfer processes or changes in the vicinity of the atoms due to newly formed bonds. Nevertheless, although these methods provide valuable data, the interpretation of the results is sometimes difficult and theoretical calculations arise as an excellent approach to help in the interpretation of experimental measurements. Also, the study of some properties is a real challenge from the experimental point of view, whereas by means of theoretical simulations this information

can be obtained.

From a fundamental point of view, the theoretical description of these systems is a challenge [137], in particular their electronic structure: whereas metals have a continuum energy spectrum, molecules present discrete levels. The interaction of the two subsystems causes a coupling of the electronic levels, which generates charge transfer processes and gives a certain lifetime to the molecular states, becoming resonances (discrete levels immersed in a continuum) [58, 138–141]. Another issue to describe the interaction between organic molecules and metal surfaces is that this process is frequently ruled by weak interactions [142–148]. These forces are crucial in certain cases, in particular when in the adsorption process covalent bonds are not formed and molecule and surface keep their previous identities (physisorption). This kind of interactions (as dispersion or van der Waals forces) is related with the so-called "dynamic" electronic correlation. There are some alternatives to recover this correlation, as the Configuration Interaction (CI) methods or the ones based on perturbation theory (MPn family). Nevertheless, all of these post-Hartree-Fock methods require a huge computational effort so their use is restricted to small systems. As an alternative, it is possible to use Density Functional Theory (DFT). This methodology scales much better than the post Hartree-Fock methods, so it can be used for larger systems (hundreds of atoms) with an affordable computational time. The different methods developed for including dispersion forces in DFT can be clasified into three families: (i) A pairwise-additive correction to the total energy, proposed by Grimme [21, 50, 149]. In these methods the dispersive energy is described by damped interatomic potentials of the form C_6R^{-6}. (ii) The Van-der-Waals density functionals (vDW-DF) are density derived methods [22, 150] that explicitly include in the Hamiltonian a non-local functional of the electron density to account for the dispersion forces; optPBE-vdW [151] and vdW-DF-cx [152, 153] are successful implementations of this family. (iii) The third family merges the ideas of the two previous ones; i.e. the methods in this category compute the vdW parameters such as atomic C_6 coefficients, vdW radii R, and static atomic polarizabilities α_0 as functionals of the chemical environment and the electron density. Robust developments of this idea are the DFT+XDM approach [154–156] originally proposed by Becke and Johnson, and the DFT+vdW approach of Tkatchenko and Scheffler [157]. In a review [158] an exhaustive analysis of the use of these methods for the description of hybrid inorganic/organic systems can be found. We compare results obtained with the D2

method [21] and with the optPBE functional [151].

In this work, we present a Density Functional Theory study of the absorption of acrolein, acrylonitrile and acrylamide on a pristine Cu(100) surface. Density Functional Theory has been probed to give excellent results in the description of interactions between organic molecules and metal surfaces (see e.g. [120,144,147,148, 159–163]). Although in the study of isolators, cluster models are usually good enough to describe correctly the electronic distribution of the system, in the case of metals finite clusters are not adequate, since the spatial confinement of the electronic density produces a spurious quantization of the electronic levels that is not present in the real metal. To avoid this, periodicity must be taken into account and we introduce it by imposing Periodic Boundary Conditions (PBC) in our simulations. We first present a comparison between different approaches to include weak interactions, which are not taken into account in most of the DFT functionals. Then, we deepen in the understanding of the adsorption process, through the analysis of the changes in the electronic levels of the molecule (coupling with the metallic continuum and shifting in the energy spectrum), as well as the study of the transferred charge (value and spatial distribution) due to the interaction. The thorough theoretical analysis presented here, allows to characterize the nature of the interaction between the molecules and the metal surface.

4.2 Computational details

All the calculations were done in the framework of the Density Functional Theory (DFT) using the Vienna Ab initio Simulation Package (VASP) [164, 165], which uses Periodic Boundary Conditions (PBC). The use of PBC is required in order to describe the metallic character of the surface. The exchange-correlation (XC) potential was calculated in the generalized gradient approximation (GGA), using the Perdew-Burke-Ernzerhof (PBE) [45] functional. The interaction between ions and electrons has been described through the projector augmented wave (PAW) pseudopotentials of the VASP database. The electronic density is expanded in a plane wave basis set up to a kinetic energy cutoff of 750 eV, value for which convergence of absolute energy is reached. The periodic supercell contains a metal slab made by a four−layer (5×5) surface unit cell of copper atoms, the adsorbed molecule and a vacuum distance of $\sim$20 Å in the direction perpendicular to the surface, defined

as $z-$axis. The size of the supercell makes the interaction of the molecule with the $z-$closest replica surface negligible (for practical purposes, vacuum is imposed along this direction). The cell is big enough in the x, y directions to neglect also the interactions with the molecules of the replicas, so we work in the low$-$coverage regime, since single molecule adsorption is considered.

To sample the Brillouin zone, which is strongly related with the computational effort that the calculation requires and the quality of the results, we used the $\Gamma-$centered Monkhorst-Pack scheme, with two different meshes: $1 \times 1 \times 1$ (only $\Gamma-$point) and $3 \times 3 \times 1$. This gives us three levels of theory, used to find a good compromise between computation time and accuracy:

(1) Use of $\Gamma-$point only to optimize the geometry. Also, the energy is obtained at this level.

(2) Single point with the $3 \times 3 \times 1$ mesh on the top of the $\Gamma-$point optimized geometry, denoted as "331/Γ".

(3) Geometry and energy obtained with the $3 \times 3 \times 1$ K-points mesh.

In the optimization calculations, a first-order Methfessel-Paxton scheme was used, with a σ value of 0.2 eV. In the extraction of the Partial Density Of States (PDOS) a gaussian smearing with a σ value of 0.1 eV was used. The electronic self-consistent convergence was set to 10^{-5} eV in order to have accurate energies and gradients. For the convergence criteria in the optimization, we impose all of the Hellmann-Feynman forces to be lower than 0.005 eV Å^{-1} for the geometrical coordinates that we allow to relax (x, y, z of the atoms in the molecule and the z coordinate of the atoms in the first layer of the metal surface).

We have explored the influence of weak interactions (e.g. Van der Waals forces), which are important to describe accurately geometries and energies in adsorption processes, in two different ways:

- DFT-D2 method of Grimme [21]. To avoid the overestimation of the dispersion energies, we included the Grimme's scheme only in the molecule and in the first layer of the metal. This approach has been successfully used in the past. [147, 148]

- Inclusion of these interactions in the exchange-correlation functional, through the use of the optPBE functional. [22, 150, 151, 166]

We have checked the importance of relaxing the geometry of the second layer of Cu atoms. To this, we have reoptimized the geometries of all studied structures, including geometry relaxation of the first two layers using the optPBE functional and a $1 \times 1 \times 1$ K-mesh (only $\Gamma-$point). Single point energy calculations were done over the new optimized geometry using the same functional and a $3 \times 3 \times 1$ K-points mesh. Adsoption energies are typically $\sim 1\%$ larger than in those cases where only one layer of Cu atoms was relaxed (always smaller than 5% in all cases). Relevant distances between atoms in the molecule-metal surface interaction barely change: for instance, the distances between the carbon atoms of the vinyl group and the Cu atoms in the surface typically change in 0.005 Å, and never more than 0.013 Å, for the most stable structure found in each molecule.

To analyze the charge transfer, we have used the Quantum Theory of Atoms in Molecules (QTAIM) by Bader [54, 55], with the code developed by Henkelman et al. [167–169]

The initial geometries were chosen by placing functional groups of the molecules on top, bridge and hollow positions of the Cu(100) surface. Due to the high symmetry of the surface, different rotations and translations were considered as initial guess of the geometry to include several kinds of interactions in the exploration of the potential energy surface. In particular, for acrylonitrile we selected two initial guess geometries corresponding to those previously described in the literature [120, 170–172]. They show interactions between the C=C bond and the C≡N bond with the metal surface in two different orientations. For acrolein we started from different positions of the C=C bond: top, bridge and with carbon C3 on top. We combine these positions with different rotations to maximize other possible interactions of the molecule with the substrate. In the case of the acrylamide rotation of the molecule keeping the C=C bond on top, leads to three possible interactions: (i) O and N on top, (ii) O and C-N on bridge (iii) O and C-N on top. We also considered the case with C3 on top and O on bridge.

4.3 Results and discussion

We present the obtained results in four sections analyzing different aspects: adsorption geometries, interaction energies, charge transfer and changes in the electronic structure and bonding.

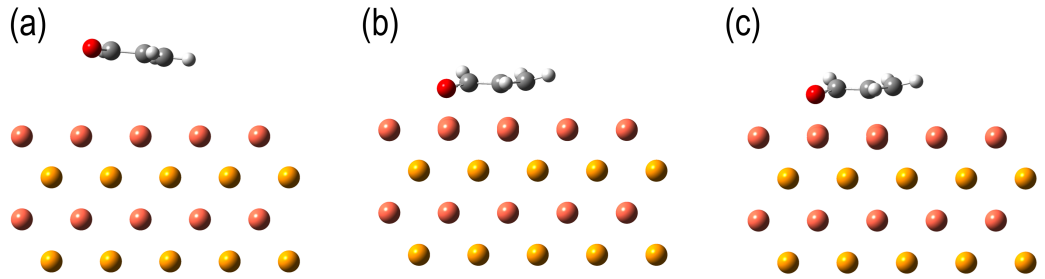

Figure 4.2: Side view of an optimized structure of acrolein adsorbed on a Cu(100) surface, obtained with (a) PBE, (b) PBE+D2, (c) OPTPBE. Two colors for the two different relative orientations of Cu layers are used.

4.3.1 Geometry

We first analyze the effect of introducing van der Waals forces to study the geometry of adsorbed molecules on metal surfaces. To this, starting from the same initial geometry we optimized acrolein on Cu(100) at level 1 (Γ point) using the pure PBE -without van der Waals corrections-, PBE+D2 and OPTPBE functionals. The lateral views after geometry optimization are shown in Fig. 4.2. The geometry changes dramatically if weak interactions are not included (the molecule-surface distance is increased by 2 Å) and, accordingly, the adsorption energy is much smaller (52 meV at a 331/Γ level). We thus corroborate that including weak interactions is crucial to study adsorption of organic molecules on a metal surface.

After the search of possible adsorption posibilites starting with different initial geometries with the previously explained strategy, we have found two minima for the adsorption of acrylamide on Cu(100), structures "ACA-1" and "ACA-2" (see Fig. 4.3); also, two for acrylonitrile ("ACN-1" and "ACN-2", Fig. 4.4); and three for acrolein ("ACO-1", "ACO-2" and "ACO-3", Fig. 4.5). Since the methods that include vdW forces, Grimme's D2 and OPTPBE, provide very close geometries, regardless of the K-points mesh used in the optimization, with negligible differences at sight, we only show in the figures those obtained geometries using the OPTPBE functional.

In the adsorption of acrylamide, the oxygen atom interacts directly with one copper atom of the surface, placed on top position in both adsorption geometries. A second common characteristic in both cases is the location of the double C=C bond, also on top position. The main difference between ACA-1 and ACA-2 is the planarity of the molecule: in ACA-2 the nitrogen is further from the plane defined

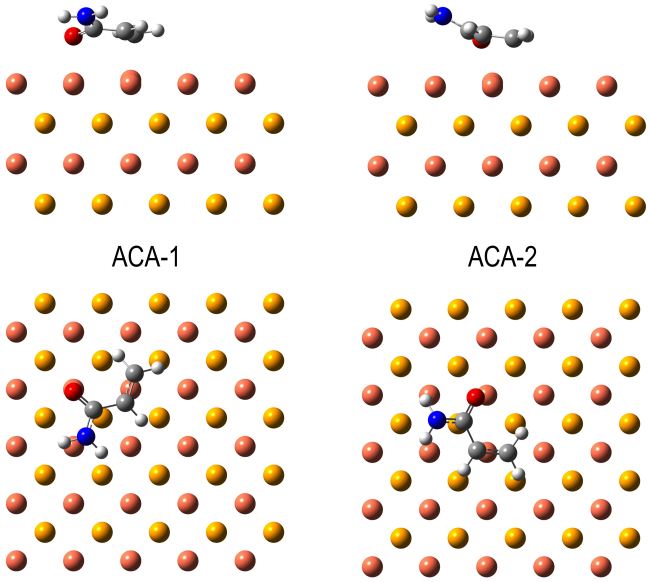

Figure 4.3: Top and side views of the two minima found for acrylamide adsorbed on a Cu(100) surface. Two colors for the two different relative orientations of Cu layers are used.

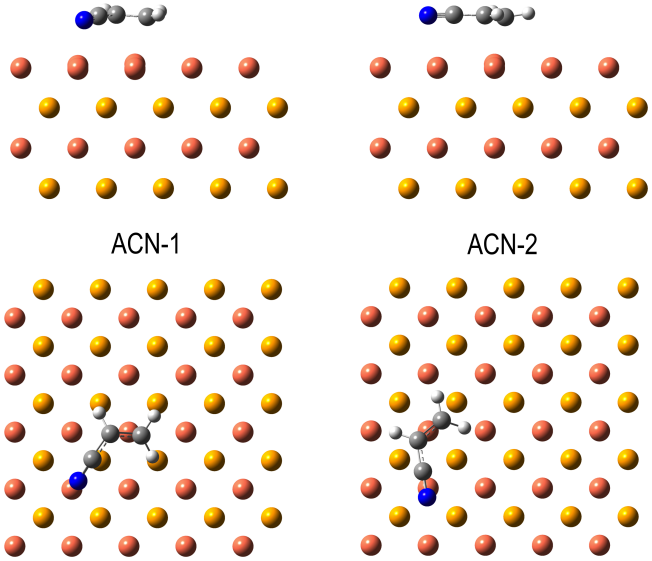

Figure 4.4: Top and side views of the two minima found for acrylonitrile adsorbed on a Cu(100) surface. Two colors for the two different relative orientations of Cu layers are used.

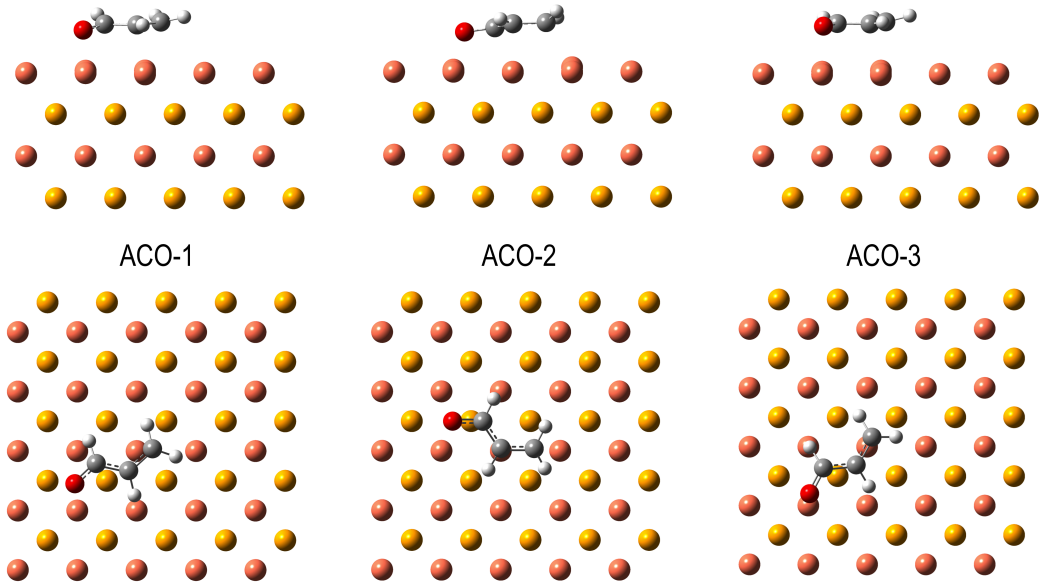

Figure 4.5: Top and side views of the three minima found for acrolein adsorbed on a Cu(100) surface. Two colors for the two different relative orientations of Cu layers are used.

by the double C=C bond and the oxygen atom, with the amino group pointing toward the vacuum. The reason is that in ACA-1 the molecule−surface linkage is mainly localized on the oxygen atom (a strong σ O−Cu interaction is observed as detailed below), while in ACA-2 the Cu−C distance is lower than in ACA-1, showing that the interaction through the double C=C bond has a greater importance (as we will show below charge transfer to the π^*_{CC} orbital occurs). In a simple chemical picture, the carbon atoms would acquire stronger sp^3 character in ACA-1. Thus, the $-NH_2$ group points out the surface explaining the difference observed after geometry optimization. The electronic structure analysis provides further details and confirms the validity of this picture.

As in the case of acrylamide, the two minima found in acrylonitrile exhibit a clear direct interaction between the double C=C bond and a copper atom of the first layer. The main difference between both structures is the relative orientation of the molecule on the surface, which determines the copper atoms that interact with the molecule. While in ACN-1 the nitrogen atom is located in top position, in ACN-2 the C≡N bond interacts with the Cu atom. The relative orientation in

ACN-1 makes also possible an interaction between the carbon atom of the cyano and a copper atom located in the second layer (in hollow position with respect to the first layer). In ACN-2, the two copper atoms of the first layer that interacts with the molecule are closer, so there is no hollow position available, and the molecule does not interact with atoms of the second layer. In ACN the hydrogen atoms also go out of the molecular plane and the carbon atoms do not have anymore a pure sp^2 hybridization. These geometrical distortions point out chemisorption, as detailed below.

Acrolein shows three different adsorption possibilities. ACO-1 and ACO-2 do not show the C=C bond in top position. The relative orientation of the C=O bond with respect to the surface in ACO-2 indicates that the local molecular dipole of this bond is pointing toward the surface, thus interacting in an electrostatic manner with the substrate rather than with a chemical bond. ACO-3 keeps the C=C as well as the oxygen atom in top position. ACO-1 has its oxygen atom in bridge position and also pointing to the surface, thus the dipole of the molecule plays a role in this adsorption geometry. As in the other two systems, sp^3 character is observed in the C atoms of the three adsorption geometries. This indicates that the interaction is not only pure dispersion in this case, but also shows some covalent character, chemisorption.

More detailed information on the geometry is presented in Tables 4.1, 4.2 and 4.3; bond distances have been extracted after the optimization at the different levels of theory for the three molecules. For comparison, we also include those of the isolated molecules in the gas phase. At the light of the numbers, the first conclusion is that the way in which the dispersion forces are included does not change the geometry of the molecule (bond distances barely change ~ 0.01 Å), but it affects the surface-molecule distances, where values can differ up to ~ 0.2 Å). The surface-molecule distances are usually underestimated when the D2 correction is included because this method lacks screening effects inside the metal and thus, it overestimates the molecule-surface interactions. Nevertheless, since the C_6 parameters of the atoms in the molecules (H, C, N, O) are much lower than the one of Cu (0.14-1.75 *vs.* 10.82), the D2 correction has a small effect in the molecule. However, screening of dispersion interactions within the metal does not always lead to an increase in the molecule-surface distances. Since the screening reduces effective C_6 coefficients and vdW radii, distances can be significantly reduced by screening. This has been observed when comparing the Tkatchenko-Scheffler vdW method and the correctly screened vdW^{surf}

Table 4.1: Most relevant distances, in Å, of the minima found for acrylamide adsorbed on a Cu(100) surface after geometry optimization at the different levels of theory employed. Gas phase distances are also included for comparison.

		PBE+D2		OPTPBE	
		Γ	331	Γ	331
ACA	C1-N	1.371	1.371	1.375	1.375
	C1-O	1.234	1.234	1.236	1.236
	C1-C2	1.495	1.495	1.496	1.496
	C2-C3	1.336	1.336	1.336	1.336
ACA-1	C1-N	1.358	1.359	1.360	1.361
	C1-O	1.274	1.273	1.272	1.271
	C1-C2	1.461	1.462	1.466	1.468
	C2-C3	1.409	1.405	1.394	1.389
	C1-Cu	2.718	2.729	2.788	2.804
	C2-Cu	2.183	2.203	2.310	2.376
	C3-Cu	2.136	2.153	2.212	2.237
	N-Cu	3.040	3.052	3.166	3.171
	O-Cu	2.066	2.081	2.107	2.124
ACA-2	C1-N	1.359	1.361	1.360	1.361
	C1-O	1.277	1.278	1.273	1.273
	C1-C2	1.456	1.454	1.464	1.464
	C2-C3	1.424	1.421	1.404	1.401
	C1-Cu	2.819	2.797	2.911	2.923
	C2-Cu	2.112	2.126	2.222	2.239
	C3-Cu	2.183	2.210	2.225	2.267
	N-Cu	3.237	3.186	3.415	3.447
	O-Cu	2.071	2.093	2.106	2.137

method [158, 173]. We also realize that the changes when one increases the K-mesh from Γ to $(3 \times 3 \times 1)$ are almost negligible. A 331 optimization requires a huge computational effort and barely changes the atomic positions. Since the supercell in the real space is quite large, its small reciprocal space is small enough to be accurately described with a single k-point. Regardless of the functional and k-mesh it is possible to appreciate common trends in the bond distances. In any molecule and adsorption geometry, the C1-C2 distance decreases after the interaction, whereas C2-C3 and C1-X (X=N for ACN, and X=O for ACA and ACO) get larger. This is what one would expect in the case of population of the lowest unoccupied molecular orbital (LUMO), which has a bonding character between C1 and C2, and antibonding between C2 and

Table 4.2: Most relevant distances, in Å, of the minima found for acrylonitrile adsorbed on a Cu(100) surface after geometry optimization at the different levels of theory employed. Gas phase distances are also included for comparison.

		PBE+D2		OPTPBE	
		Γ	331	Γ	331
ACN	C1-N	1.169	1.169	1.167	1.167
	C1-C2	1.424	1.424	1.427	1.427
	C2-C3	1.342	1.342	1.342	1.342
ACN-1	C1-N	1.190	1.189	1.186	1.185
	C1-C2	1.401	1.401	1.403	1.404
	C2-C3	1.421	1.420	1.406	1.403
	C1-Cu	2.749	2.776	2.771	2.802
	C2-Cu	2.218	2.242	2.386	2.435
	C3-Cu	2.135	2.151	2.211	2.242
	N-Cu	2.063	2.071	2.101	2.110
ACN-2	C1-N	1.188	1.188	1.181	1.181
	C1-C2	1.411	1.410	1.415	1.416
	C2-C3	1.409	1.409	1.395	1.392
	C1-Cu	2.359	2.348	2.500	2.517
	C2-Cu	2.183	2.206	2.293	2.333
	C3-Cu	2.174	2.179	2.264	2.295
	N-Cu	2.243	2.268	2.377	2.426

C3 and between C1 and X. As we show below, in the LUMO region of the molecule an increase of the electronic density is indeed appreciated due to the interaction between the molecule and the surface, which also explains the sp^3 character of the C atoms involved in the bonding.

4.3.2 Adsorption energies

The adsorption energy is defined as:

$$E_{ads} = E_{mol/surface} - (E_{mol} + E_{surface}) \tag{4.1}$$

Where $E_{mol/surface}$ is the energy of the whole molecule+surface system, E_{mol} is the energy of the optimized molecule in the gas phase and $E_{surface}$ is the energy of the isolated bare surface. The results of the adsorption energies for all the studied structures, computed with the different levels of theory here considered, are shown

Table 4.3: Most relevant distances, in Å, of the minima found for acrolein adsorbed on a Cu(100) surface after geometry optimization at the different levels of theory employed. Gas phase distances are also included for comparison.

		PBE+D2		OPTPBE	
		Γ	331	Γ	331
ACO	C1-O	1.225	1.225	1.226	1.226
	C1-C2	1.471	1.471	1.472	1.472
	C2-C3	1.342	1.342	1.342	1.342
ACO-1	C1-O	1.311	1.309	1.302	1.294
	C1-C2	1.436	1.435	1.440	1.441
	C2-C3	1.416	1.410	1.407	1.405
	C1-Cu	2.258	2.267	2.343	2.426
	C2-Cu	2.114	2.156	2.177	2.235
	C3-Cu	2.160	2.164	2.212	2.200
	O-Cu	2.098	2.111	2.113	2.089
ACO-2	C1-O	1.332	1.333	1.330	1.333
	C1-C2	1.424	1.418	1.426	1.419
	C2-C3	1.448	1.456	1.443	1.455
	C1-Cu	2.379	2.390	2.447	2.447
	C2-Cu	2.069	2.099	2.112	2.138
	C3-Cu	2.180	2.158	2.246	2.190
	O-Cu	2.114	2.135	2.139	2.142
ACO-3	C1-O	1.289	1.291	1.284	1.285
	C1-C2	1.443	1.441	1.445	1.443
	C2-C3	1.410	1.410	1.404	1.404
	C1-Cu	2.387	2.414	2.518	2.547
	C2-Cu	2.175	2.200	2.243	2.265
	C3-Cu	2.128	2.139	2.184	2.200
	O-Cu	2.032	2.036	2.061	2.066

in Table 4.4.

The obtained values after the use of only the Γ−point and the single point 3×3×1 on the top of the Γ−point geometry show that Γ−point is not enough to have correct energies. In particular, by using the PBE+D2 functional, adsorption energies change in average 63.0 meV, with a maximum difference of 84.0 meV. OPTPBE is however less affected by the different K-Point mesh: in average, the adsorption energy changes in 45.0 meV, with a maximum change of 62.0 meV. Nevertheless, the obtained results with levels (2) and (3) are very similar. The largest difference in adsorption energies

Table 4.4: Adsorption energies (in eV) of the acrylamide, acrylonitrile and acrolein on Cu(100) computed at the different levels of theory and with the two functionals employed.

	E_{ads} (eV)					
	(1) Full Γ		(2) 331/Γ		(3) Full 331	
	PBE+D2	OPTPBE	PBE+D2	OPTPBE	PBE+D2	OPTPBE
ACA-1	-1.225	-0.930	-1.154	-0.879	-1.157	-0.879
ACA-2	-1.240	-0.932	-1.157	-0.872	-1.157	-0.868
ACN-1	-0.940	-0.644	-0.856	-0.590	-0.882	-0.601
ACN-2	-0.809	-0.525	-0.774	-0.483	-0.780	-0.496
ACO-1	-1.063	-0.736	-0.980	-0.674	-0.995	-0.696
ACO-2	-1.019	-0.677	-0.992	-0.670	-1.006	-0.687
ACO-3	-1.056	-0.740	-0.998	-0.701	-1.006	-0.704

from $3 \times 3 \times 1/\Gamma$ to full $3 \times 3 \times 1$ is 26.0 meV (PBE+D2) and 22.0 meV (OPTPBE). Average differences in adsorption energies do not change much either between levels (2) and (3): 10.3 meV (PBE+D2) and 10.0 meV (OPTPBE). This indicates, as we have mentioned before, that the geometries obtained with $\Gamma-$point are almost the same than the ones provided by the $3 \times 3 \times 1$ mesh, but with an important gain in computational effort. Therefore, we conclude that the best compromise between accuracy and computational time is the $3\times3\times1/\Gamma$ level. If one compares the absolute adsorption energy of the most stable structure in each molecule at the $3 \times 3 \times 1/\Gamma$ and full $3 \times 3 \times 1$ levels (see Table 4.4), then it can be seen that changes are 0 meV (ACA-1), 11meV (ACN-2) and 22meV (ACO-1).

Table 4.4 shows that, except in the case of the acrylonitrile, the different adsorption structures are almost degenerate in energy, regardless of the method used to include the weak interactions and the K sampling. At the $3 \times 3 \times 1/\Gamma$ and full $3 \times 3 \times 1$ levels, both PBE+D2 and OPTPBE functionals predict the same structure as the most stable one. The only exception is the acrylamide, although the stability difference is lower than the error of the method.

Our results also show that the adsorption energy is systematically overestimated by the PBE+D2 method with respect to the OPTPBE one in approximately 300 meV, regardless of the level. While in Grimme's D2 approach the dispersion is included through a semi-empirical way, in OPTPBE it is included in the functional, OPTPBE results can be considered, in principle, more reliable. For the archetypal

widely studied example of benzene on Cu(111), experimental values of adsorption energy are in the range 57 – 78 kJ/mol [144,174,175]. PBE-D2 also overestimates the binding energy in this case 97 kJ/mol [176], while vdW-DF slightly underestimates it ($\sim$ 53 kJ/mol) [174, 177].

The most stable structure in the three molecules (ACA-1, ACN-1 and ACO-3) shows a common characteristic: it always corresponds to a geometry with direct interaction between the C=C bond with a Cu atom on top potion and also direct interaction between the N atom (ACN) or O atom (ACO and ACA) with a Cu atom on top position. This similarity confirms the nature of the interaction and can be considered as a general behavior.

The stability of the organic molecules on metal surfaces upon adsorption is crucial for electronic nanodevices, since the coupling of the molecular states is effective only at short ranges, thus a strong anchoring (high E_{ads}) increases the efficiency of charge transfer through the linking sites.

4.3.3 Charge transfer

To go deep into the understanding of the metal-molecule interaction, we have also studied the charge transfer between molecule and surface upon adsorption (Δq). Several methods have been developed to evaluate atomic charges. Among them, the Mulliken population analysis (MPA) [178], the Hirshfeld population analysis (HPA) [179], Quantum Theory of Atoms In Molecules (QTAIM) [54,55], Natural Population Analysis (NPA) [180], and Voronoi Deformation Density method (VDD) [181] are the most popular ones. They can yield drastically different absolute values [182] and one has to be caution with the interpretation of the results. Our analysis has been carried out using the QTAIM method. The computed values of the transferred charge in the different adsorption geometries of each molecule are shown in Table 4.5.

We do not observe a clear relation between the charge transfer, Δq, and the adsorption energy. Acrolein is the molecule with the highest value of Δq, with a large difference with respect to the others, and its adsorption energy is located between that of acrylonitrile and acrylamide. There is no relation either between the different adsorption geometries of each molecule obtained with the two methods and Δq. Nevertheless, there is a clear trend in the values: ACO has the greatest value in Δq, followed by ACN and being ACA the molecule that takes less charge

Table 4.5: Transferred charge from the surface to the molecule (in atomic units) for the different molecules and adsorption geometries, computed at the level 2 (single point energy calculation with a 331 K-mesh over the geometry optimized with a Γ point).

	PBE+D2	OPTPBE
ACA-1	0.264	0.188
ACA-2	0.324	0.222
ACN-1	0.369	0.286
ACN-2	0.323	0.233
ACO-1	0.573	0.496
ACO-2	0.684	0.648
ACO-3	0.478	0.416

transferred from the surface. This fact can be understood in terms of electronic structure; in particular analyzing the energies of the lowest unoccupied molecular orbital (LUMO) of each molecule in gas phase. The energy of this orbital with respect to the Fermi level is 1.47 eV in ACO; 1.69 eV in ACN and 2.14 eV in ACA. Thus, a simple explanation arises: higher the electron affinity of the molecule larger the charge transferred from the surface.

As in the analysis of the adsorption energies, the PBE+D2 functional gives higher values for Δq than the OPTPBE one. Since OPTPBE includes the weak interactions in the Hamiltonian (in the self-consistent optimization of the electronic density), charges given by this method should be more accurate. Consequently, the following analysis, related with the spatial redistribution of the electronic density, has been carried out using the OPTPBE results. To this, we define the change in the electronic density upon adsorption as:

$$\Delta\rho = \rho_{molecule/surface} - (\rho_{molecule} + \rho_{surface}) \tag{4.2}$$

where $\rho_{molecule/surface}$ is the electronic density of the whole system, and $\rho_{molecule}$ and $\rho_{surface}$ are the densities of the molecule and surface computed keeping the adsorption geometry. The results (Fig. 4.6) reveal a high similarity between the regions where there is a gain of electronic density (in green) with the LUMO orbital of the corresponding molecule in the gas phase. It is reasonable to assume that, in the adsorption of these molecules on a Cu(100) surface the interaction leads to a charge transfer from the metal to the LUMO orbital of the molecule. The Δq

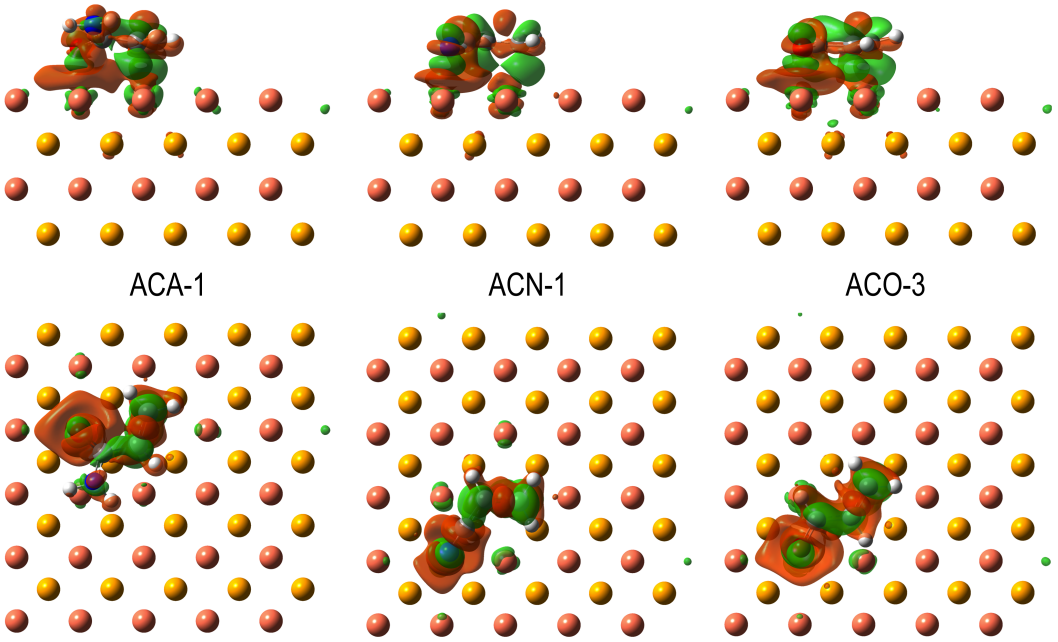

Figure 4.6: Change in the electronic density upon adsorption ($\Delta\rho$, isovalue=0.01) for the most stable adsorption structures of the three vinyl derivatives on Cu(100) surface. Green shows positive $\Delta\rho$ and red shows negative $\Delta\rho$.

regions also reflect the partial covalent character of the interactions, highlighting the linkage sites. The depletion of electron density in regions where there is no nodal plane in the π system, in addition to the mentioned gain in the LUMO, is explained in terms of a simple chemical picture: electron donation from the π orbital of the molecule to the surface and backdonation from the surface to the π^* orbital of the molecule ($\pi-$backbonding). We can also observe donation from lone pairs (LP) orbitals; typically from LP orbitals on the N atom in the cyano, and on the O atoms in the amide and carbonyl groups. Thus from the $\Delta\rho$ analysis we can infer $\pi \rightarrow$ Cu and LP $\rightarrow$ Cu donation and Cu $\rightarrow \pi^*$ backdonation. This phenomenon has been previously observed in a large variety of systems such as simple molecules [183–185], organic molecules with aromatic rings and functional groups [186, 187] or phthalocyanines [188] interacting with metal surfaces. The electronic structure analysis in the next section confirms this scenario.

The electronic properties of organic charge transfer (CT) compounds depend on the amount of charge transferred from the donor (D) to the acceptor (A) species. It

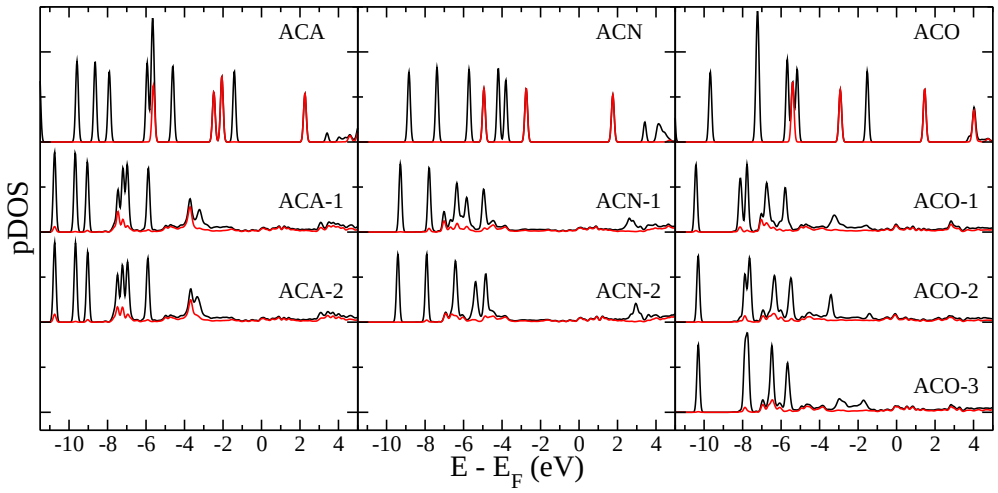

Figure 4.7: Density Of States projected on the atoms of the adsorbed molecules. Results of the molecule far from the slab, non interacting with the surface, is also shown for comparison - upper curves in each panel. Red shows the pz-projection, which allows to identify the π contribution to the pDOS.

has been shown that the CT process can be tuned by controlling the stoichiometry of the D and A quantities when they are forming self-assembled monolayers on metal surfaces [189] and proceeds through the metal. Thus, the electron transport in hybrid organic-metal nanodevices depends on the charge transfer efficiency.

4.3.4 Electronic structure: energy levels alignment

Further information on the interaction nature is obtained by computing the projected Density Of States (pDOS). Decomposing the total Density Of States (DOS) in the contributions of the different angular momenta of each atom allows to analyze in detail the electronic structure and thus to determine the kind of interaction established between the molecule and the surface. For the different adsorption geometries of each molecule we present in Fig. 4.7 the DOS projected on all the atoms of the corresponding molecule. For comparison, the pDOS when the molecule is placed far enough from the surface to avoid interactions (typically $\sim$ 10Å), is presented as well in each case. The low energy region of the DOS is not shown because inner bands (which correspond to bonding σ molecular orbitals) barely change their position in energy after adsorption. They are just slightly shifted to lower energies due to the

transferred charge and are not relevant since they do no contribute to the linkage.

Comparing the pDOS of the molecules far from the slab with those interacting with the surface the main difference is found in the loss of resolution in the bands corresponding to the π and π^* orbitals in the isolated molecule and the lone pairs of the O and N: LP and π orbitals show the maximum hybridization with the metal states and are the responsible of the interaction. In general, broadening of the bands due to the interaction is observed also for other orbitals, although to a lesser extent. The observed change in the molecular states is a well known phenomenon [190] and other theoretical works have previously pointed it out in the interaction of organic molecules with metal surfaces (see e.g. [191]). Understanding this effect has consequences in the mechanisms that determine the optoelectronic properties of high-performance organic materials [192], in particular in the rate of charge transfer between the active species (molecules) and the conductor (metal). As expected after the results obtained of the location of the transferred charge, the LUMO orbital of the three studied molecules is shifted below E_F becoming an occupied state with a bonding character and strongly contributes to the linkage of the molecule to the surface [91].

A further analysis has been carried out by representing the change in the electronic density upon adsorption ($\Delta\rho$) in two-dimensional projections (see Figs. 4.8, 4.9 and 4.10). We obtain a complementary picture of the orbital hybridization due to the the charge transfer (mainly lone pair and π orbitals), i.e. the states involved in the donation/backdonation to/from the copper surface. Figure 4.8 shows 2D cuts of $\Delta\rho$ containing the π^* and the LP (O and N) orbitals of ACA. As previously mentioned, after the pDOS results, we observe an increase of the electronic density between C1 and C2 (backdonation from the surface to the π^*) and a depletion of the charge in the LP (dative interaction from the molecule to the surface). The change transfer is higher in the oxygen than in the nitrogen atom, and can be simply explained in terms of distance, the NH_2 group is further away from the surface than the carbonyl (C=O) and therefore the interaction is less favored. As in the case of the ACA, the 2D cuts of ACO clearly show the dative interaction $LP_O \rightarrow Cu$ (depletion of the charge in the lone pair of the oxygen) and the backdonation from the Cu to the π^* (enhancement of the electronic density in this orbital). ACN is similar to ACA and ACO: the electron density between C1 and C2 increases upon adsorption ($Cu \rightarrow \pi^*$), while the charge in the LP of the N atom decreases ($LP_N \rightarrow Cu$).

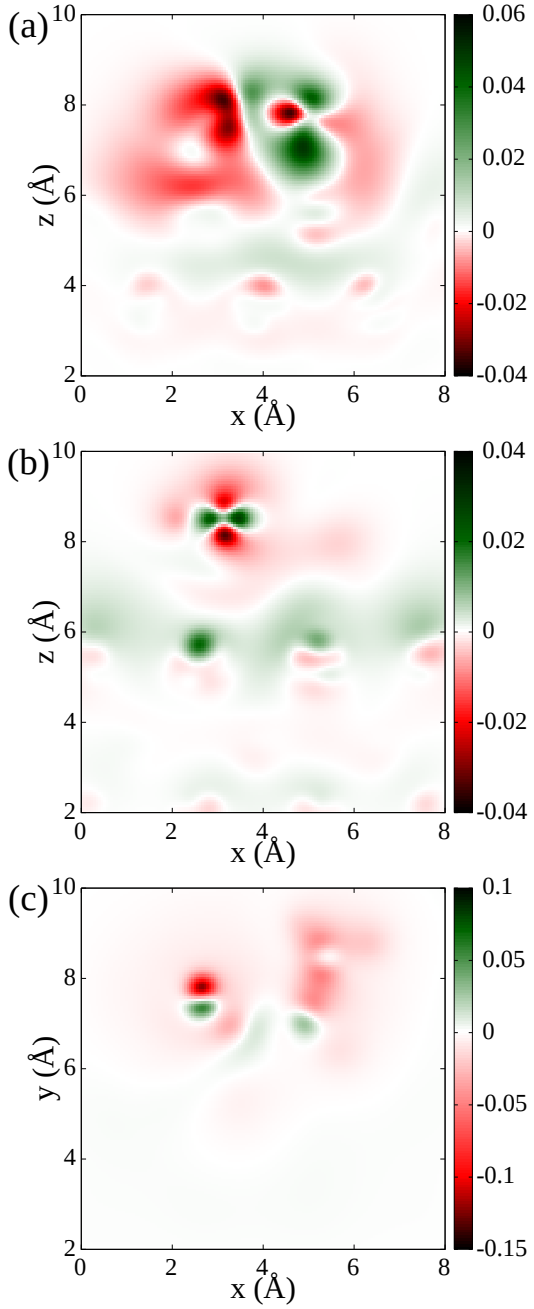

Figure 4.8: Two-dimensional cuts of the change in the electronic density upon adsorption ($\Delta\rho$) in ACA-1: (a) xz plane located between C_1 and C_2 showing the π^* density; (b) xz plane containing the N atom and showing its lone pair orbital; (c) xy plane which containing the O atom and showing its lone pair orbital.

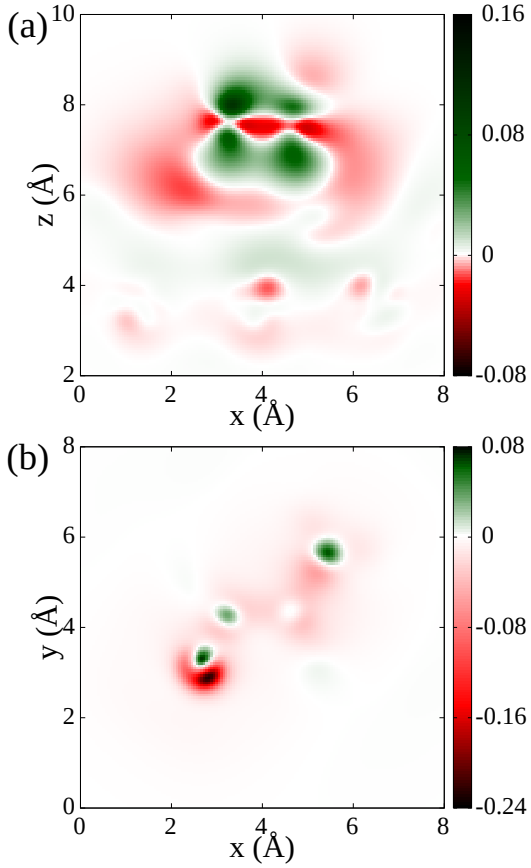

Figure 4.9: Two-dimensional cuts of the change in the electronic density upon adsorption ($\Delta\rho$) in ACO-3: (a) xz plane located between C_1 and C_2 showing the π^* orbital; (b) xy plane containing the O atom and showing its lone pair orbital.

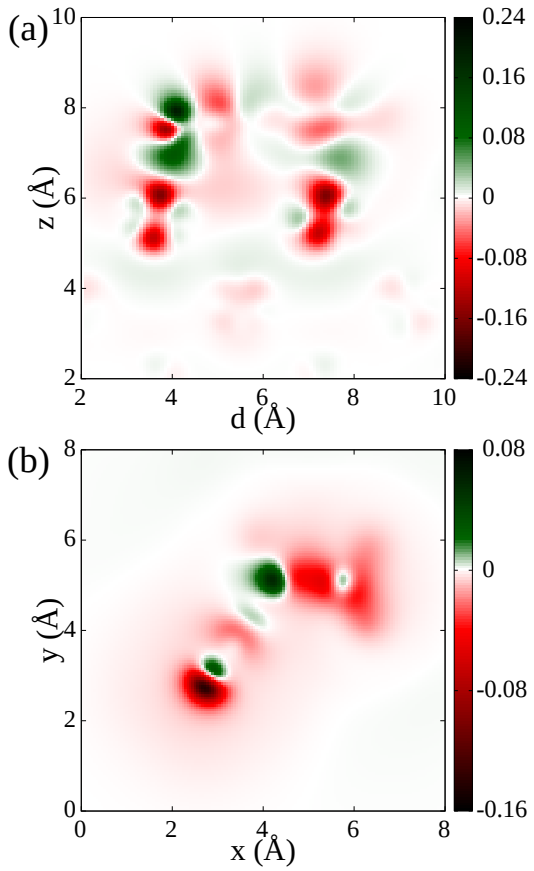

Figure 4.10: Two-dimensional cuts of the change in the electronic density upon adsorption ($\Delta\rho$) in ACN-1: (a) xz plane located between C_1 and C_2 showing the π^* orbital; (b) xy plane that containing the N atom and showing its lone pair orbital.

4.4 Conclusions

We have presented a detailed Density Functional Theory study of vinyl derivatives molecules (amide, aldehyde and cyano as substituents) adsorbed on a pristine Cu(100) surface. Our calculations also include periodic boundary conditions, in order to take into account a correct description of the metallic character of the surface. Weak interactions were included in the PBE functional through two different schemes: the Grimme's D2 model and the OPT-DFT (OPTPBE). Differences in the results obtained with both methods mainly arise from the fact that D2 approach does not take into account the screening inside the metal and overestimates the interaction forces between the molecule and the metal surface. For the three organic molecules here studied, several stable structures were found, being these isomers almost degenerated in energy except in acrylonitrile, whose isomers have an energy difference of about 100 meV. In the three cases the most stable isomers have two common structural characteristics: the double C=C bond and an atom with a lone pair (oxygen in acrolein and acrylamide, and nitrogen in acrylonitrile) are placed on top position. This arrangement favors the interaction of the π orbital in the C=C bond of the molecule with the d orbital of the Cu atom, and the interaction of the lone-pair orbital in N and O with d orbitals of the Cu atom. The nature of the interaction between these molecules and the surface is verified with the analysis of the projected density of states and the charge transfer; both show a donation from the π_{CC} and from the lone pair orbitals to the surface and a backdonation to the π^*_{CC} orbital. This type of interaction and the relation between the energy of the LUMO orbital and the amount of transferred charge from the surface to the molecule seem to be a common characteristic of the vinyl derivatives adsorbed on metal surfaces.

As a general conclusion, the interaction of organic molecules with π orbitals (typically in C=C double bonds) and lone pair orbitals (in oxygen or nitrogen atoms) is expected to happen with metal substrates with "d" orbitals in the manner we present in this work. The donation - backdonation is a synergic process that leads to the so called $\pi-$backbonding [193] and drives the adsorption of organic molecules in metal surfaces. The nature of the interactions described in this work might be also responsible for the stabilization of small metal clusters surrounded by organic molecules [194, 195] and help in the synthesis of new metal-polymer nanocomposites [196, 197].

Chapter 5

Adsorption of vinyl derivatives on Cu(111)[1]

Abstract Here we present a theoretical study of the interaction, chemisorption and thermal decomposition of three vinyl derivatives (acrolein, acrylonitrile, and acrylamide) on a pristine Cu(111) surface. To this we have carried out density functional theory simulations, including weak van der Waals forces, in the framework of periodic boundary conditions. The results have shown strong anchoring between the molecules and the surface through the vinyl group, with the different functional groups driving molecular orientation. We explain the chemisorption with a simple chemical picture: donation from the occupied lone pair and π orbitals of the molecule to the surface and backdonation from the surface to the π^* orbital of the molecule (π-backbonding). *Ab initio* molecular dynamics simulations highlight the efficient energy exchange in excited adsorbed molecules and energy dissipation through the interface, which takes place in a few hundreds of femtoseconds. The study of the dynamics also allows to comprehend the catalytic effect of the chemisorption, which is reflected not only in the larger amount of fragmentation but also in the much richer spectrum of fragments observed with respect to the molecular decomposition in the gas phase.

[1]This chapter is based on J.Phys.Chem.C, 123, 19625 (2019)

5.1 Introduction

Interaction of organic molecules with metal surfaces has been studied for a long time (see e.g. [137, 198, 199]). Nevertheless it still remains as a hot topic due to the recent experimental developments that allow high precision in single molecule measurements and due to the number of applications in which it is involved [200–202]. In the case of transition metal substrates, the *d*-band of the surface is able to mix with some of the molecular states, in particular with the π states, since they are typically close in energy and are spatially accessible, as stated in the *d-band center theory* [138, 203–206]. These interactions can be explained with simple chemical models in terms of electron donation and back-donation [207] and are responsible for the appearance of new properties in hybrid organic-metal materials, which are not present in the organic parts nor in the metal separately. For this reason, this kind of composite systems has been proposed as promising candidates in several areas such as hybrid metal-organic materials [83–92], photovoltaic organic nanodevices [93–96], ultrathin optoelectronics [97–101], organic solar cells [94, 96, 102, 103], molecular spintronics [104–107], corrosion protectors [99, 108–111], etc. In addition, the organic-metal interface is also responsible for the rearrangement of the molecular electron density that weakens some chemical bonds, while others become stronger, thus changing the intrinsic reactivity. This is the key aspect behind heterogeneous catalysis [76–82]. Other aspect that must be considered for catalytic applications is the anchoring of the molecule to the surface: as it has been recently pointed out by Jiang and Huo [208], relative orientations of the adsorbed reactants and/or changes in the molecule-surface interaction energies enhance reaction rates; they further show the importance of the dynamics in these processes.

Excitation of vibrational modes is an excellent way to promote the system to higher energy states that are close to the so-called transition state (TS) point in the potential energy surface (PES), facilitating the reaction by increasing its rate. Nowadays it is possible to use light sources (typically ultrashort laser pulses) to selectively probe vibrational excited states that populate a given mode and, thus, to drive the reaction through a specific path (the so-called quantum control [209–216]). For example, combination of different lasers allowed us to probe the dynamics of all adsorbed molecules in a sample and selectively probe only different subsets of the adsorbed molecules in the same experiment [217]. Laser pulses have been also used to observe electronic structure changes in molecule-metal surface bond break-

ing employing a pump probe scheme [185]; the delay between the pump and the probe pulses allows measuring of molecular desorbtion dynamics. Scanning tunneling microscopes (STM) have been also utilized in the promotion and control of single-molecule chemical reactions adsorbed on surfaces [218] through inelastic electron scattering processes: *cis-trans* isomerization [219, 220], molecular dissociation [221], bond cleavage [222, 223], and dehydrogenation [224] are examples of single-molecule reactions induced with an STM. The intermediate excited state created with the electric current of the STM is the key point to control these reactions. Recent experiments have studied in detail these electronic excited states in different systems [11, 23, 28]. Photo-assisted activation of selected bonds in individual molecules adsorbed on metal surfaces within the junction of an STM has been recently reported [225]; the mechanism behind this achievement consists of the coupling of photons with bond activation through a resonant photo-assisted tunneling process.

Another important aspect that must be considered in the excitation of molecules that interact with metal surfaces is the energy relaxation mechanisms, that is, the energy transfer from the molecule to the substrate. Vibrational relaxation lifetimes of molecules adsorbed at metal surfaces have been measured to be in the range of a few picoseconds [226–228] or even longer [229]. The response of vibrationally excited adsorbed molecules on metals and the energy relaxation mechanisms have been the matter of study during the last decades [230–234]. Electron-hole pair excitations have been found to be one of the dominant channels of vibrational energy dissipation of chemisorbed molecules. Novko et al. have recently investigated [235] the early stage dynamics of excited carbon monoxide molecules adsorbed on Cu(100) unveiling the microscopic processes behind the vibrational spectroscopic changes induced by femtosecond laser pulses. In a recent work [236], Ge et al. showed competition between two channels in the vibrational energy relaxation dynamics of rhenium based catalysts adsorbed on metal surfaces: intramolecular vibrational relaxation and electron-hole pair mechanisms were shown to occur in the same time scale.

Despite the experimental and theoretical efforts many questions still remain open, such as the mechanisms of the vibrational relaxation of excited molecules in direct energy transfer to substrate vibrational modes (phonons), the influence of the anchorage, the presence of different functional groups in these mechanisms, and the behavior of highly vibrationally excited organic molecules chemisorbed on metal surfaces. We provide insight into these questions in this work by means of theoretical

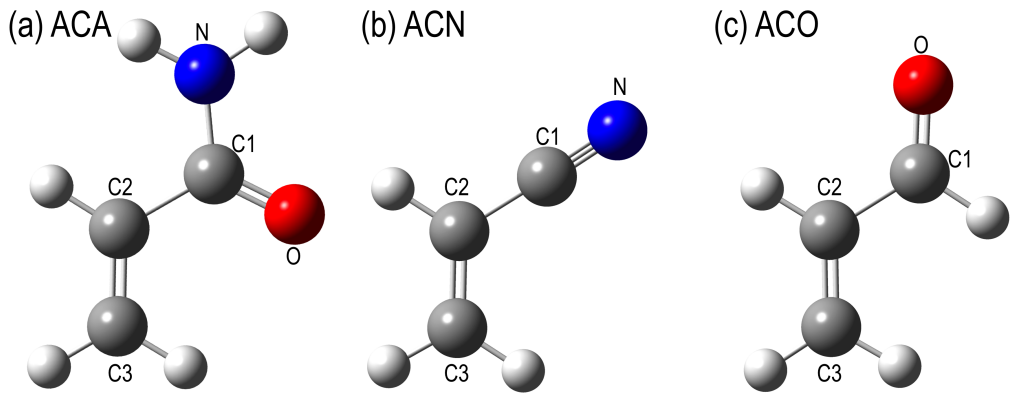

Figure 5.1: The three vinyl derivative molecules studied in this chapter: (a) acrylamide (ACA), (b) acrylonitrile (ACN), and (c) acrolein (ACO). Labels of atoms in each molecule correspond to those employed in the text and tables.

simulations based on Density Functional Theory (DFT) and *Ab Initio* Molecular Dynamics (AIMD). We present an exhaustive study of the adsorption of three vinyl-derivatives (acrylamide, ACA; acrylonitrile, ACN and acrolein, ACO) on a pristine Cu(111) surface. These molecules have a common skeleton (a terminal double C=C bond) and they differ in their substituents, which are able to conjugate with the vinyl group, thus changing the electron density distribution along the skeleton (see Fig. 5.1). The metallic character of the surface is correctly described due to the inclusion of Periodic Boundary Conditions (PBC) in the simulations, avoiding spurious quantization of the electron density due to the finite size of the system. The combination of DFT+PBC has been successfully used to study this kind of systems (see e.g. [120, 144, 147, 148, 159–163, 207]). Weak interactions (such as van der Waals forces), which have been proved to be crucial in the adsorption of organic molecules on metal surfaces, [142–148, 207] are taken into account through the methodology developed by Dion et al. [22, 150, 151]

We have structured our work in three parts: (i) first we present a static study including adsorption energies and geometries, charge transfer and electronic structure; (ii) then, vibrational modes of the adsorbed molecules on the metal surface are presented, focusing mainly on the role of the interaction to understand frequency shifts with respect to the gas-phase; and (iii) finally, *ab initio* molecular dynamics simulations on the highly-excited molecules (6 and 12 eV of internal energy) show energy dissipation dynamics, molecular cleavage processes and decomposition kinet-

ics. All these results aim to provide insights for the future development of efficient heterogeneous catalysts and new catalytic strategies.

5.2 Computational details

Both, static and dynamic calculations, were performed with the Vienna Ab initio Simulation Package (VASP) software [164, 165], which is based in the Density Functional Theory (DFT) and take advantage of the Periodic Boundary Conditions (PBC), essential to account for the periodicity of the system and thus to properly describe the metallic character of the surface. The optPBE functional [22,150,151,166] was chosen for this work, since it has been shown to provide accurate results for the interaction of organic molecules with metallic surfaces (see e.g. [137, 207, 237, 238]). The interaction between ions and electrons is described by using the Projector Augmented Wave (PAW) pseudopotentials [239,240], obtained from the VASP database. The electronic density is calculated with a plane-wave expansion, up to a kinetic energy of 750 eV for the static calculations. In the case of the molecular dynamics simulations, due to the higher computational effort, the cutoff was set to 500 eV, enough to converge the adsorption energies. We have used in all the calculations the same periodic supercell; it consists of a four-layer slab with 5×5 copper atoms in each of the directions that define the hexagonal (111) surface. A vacuum of 20 Å is included in the $z-$axis, direction perpendicular to the surface, in order to avoid the interaction with the closest replica and to give the system enough space to evolve in the molecular dynamics simulations. This supercell size has been shown to provide converged results [120, 207]. The Brillouin zone was sampled by using the $\Gamma-$point in the optimization. Optimized geometries are used in single point calculations using a $\Gamma-$centered Monkhorst-Pack scheme [241] with a $3 \times 3 \times 1$ K-point sampling to have more accurate adsorption energies. This methodology was previously used with success in [207], with a typical error in adsorption energies smaller than ~ 10 meV. To determine the partial occupancies, we have used the first-order Methfessel-Paxton scheme [242], with a σ value of 0.2 eV. The electronic self-consistent convergence was set to 10^{-5} eV to have highly accurate energies and gradients. In the case of the molecular dynamics simulations, this value was set to 10^{-4} eV. For the convergence criteria in the geometry optimizations, we have imposed all the Hellmann-Feynman forces to be lower than 5×10^{-3} eV/Å for the geometrical variables to be relaxed

(x, y, z of all the atoms in the molecule and the z coordinate of the first layer of the slab).

Atomic charges have been computed by using the Quantum Theory of Atoms In Molecules (QTAIM) [54,55]. For this purpose, and taking advantage of the numerical grid which VASP uses to store the electron density, we have employed the code developed by Henkelman et al. [167–169] to perform the grid integration.

To characterize the surface-molecule interactions, we have also carried out a projected Density Of States (pDOS) analysis. To do this, we project the total Density Of States (DOS) on the different angular momenta of every atom inside the supercell. With all these contributions, one can easily determine which states contribute on each projection. This technique is useful to identify the molecular orbitals that are mixed with substrate states leading to molecule-metal interactions.

Vibrational frequencies have been evaluated under harmonic approximation. In this case, we have performed a central difference calculation. Each degree of freedom of the molecule and the z coordinate of the atoms of the first metal layer are moved ± 0.015 Å from the equilibrium position in order to obtain the Hessian matrix. Then, the matrix is diagonalized and the normal modes (eigenvectors) and energies (eigenvalues) are obtained. We have benchmarked the vibrational results obtained with VASP using as reference those computed at the PBE/aug-cc-pVTZ level of theory for the neutral molecule in the gas phase using the Gaussian09 code [75]. The greater difference between both codes in stretching modes is of $\sim$16 cm^{-1} (C1-C2 stretching in acrolein).

For the *ab initio* molecular dynamics simulations, all the coordinates of the molecule and the first, second and third atomic metal layers were allowed to move. In each trajectory the initial excitation energy (6 or 12 eV) was randomly distributed among the nuclear coordinates of the molecule. These are the typical values of multiple bond dissociation energies (see e.g. [243]) We run several trajectories for each considered molecule and each excitation energy value and then statistics were performed on them (a total of 180 trajectories for molecules adsorbed on a metal surface, and 90 trajectories for molecules on the gas phase were run). To ensure adiabaticity in the simulations, the time step was set to 0.3 fs, and we propagated the trajectories up to $\sim$ 0.5 ps (those with excitation energy of 12 eV) or $\sim$1 ps (those with an excitation energy of 6 eV). These simulations were performed in the microcanonical ensemble.

5.3 Results and discussion

5.3.1 Adsorption, interaction energies and charge transfer

In the search for molecular adsorption sites we have carried out a systematic exploration of the potential energy surface. To this, we have selected several structures as an initial guess in the geometry optimization. The choice was done by placing the molecule, whose geometry was pre-optimized in the gas phase, in a parallel orientation with respect to the surface and at a distance of ∼2 Å. Then, we scanned the relative orientation of the molecule with respect to the surface keeping the parallel orientation, using different rotational angles, and taking advantage of the high symmetry of the hexagonal surface. With this strategy we have selected 100 initial geometries to optimize. During the optimization process, similar structures were discarded using geometrical and energetic criteria, that is, when two of them lead a similar configuration (in a visual inspection) and with a relative energy between them that is smaller than 5 meV. We finally obtained six possible adsorption structures for acrylamide, four for acrylonitrile and two for acrolein, named hereafter ACA[1-6], ACN[1-4] and ACO[1-2] respectively. The high symmetry of the surface and the limited molecular anchorage sites are probably responsible for the low number of structures found. Fig. 5.2 shows the geometry of the optimized structures and Table 5.1 shows the adsorption energy E_{ads} of these structures, defined as:

$$E_{ads} = E_{mol/surface} - (E_{mol} + E_{surface}) \tag{5.1}$$

where $E_{mol/surface}$ is the energy of the total system (molecule adsorbed on the surface), E_{mol} is the energy of the molecule without any interaction with the surface (optimized in the gas phase) and $E_{surface}$ is the energy of the pristine slab.

In the obtained structures for the three studied molecules, the vinyl group plays a crucial role in the interaction with the surface. In a simple visual inspection, loss of planarity of the terminal CH_2 group is observed in all cases. This is the consequence of the strong interaction between the C atom and the surface which implies charge transfer and chemisorption, as we will show below. It can be easily explained within the hybrid orbital model: charge transfer from the molecule to the surface leads to a change in hybridization in the terminal C atom from sp^2 in the gas phase to sp^3 in the adsorbed structure, forming a new chemical bond between the molecule and the surface (see the dihedral angles in Table 5.2). Indeed, in the energetically most

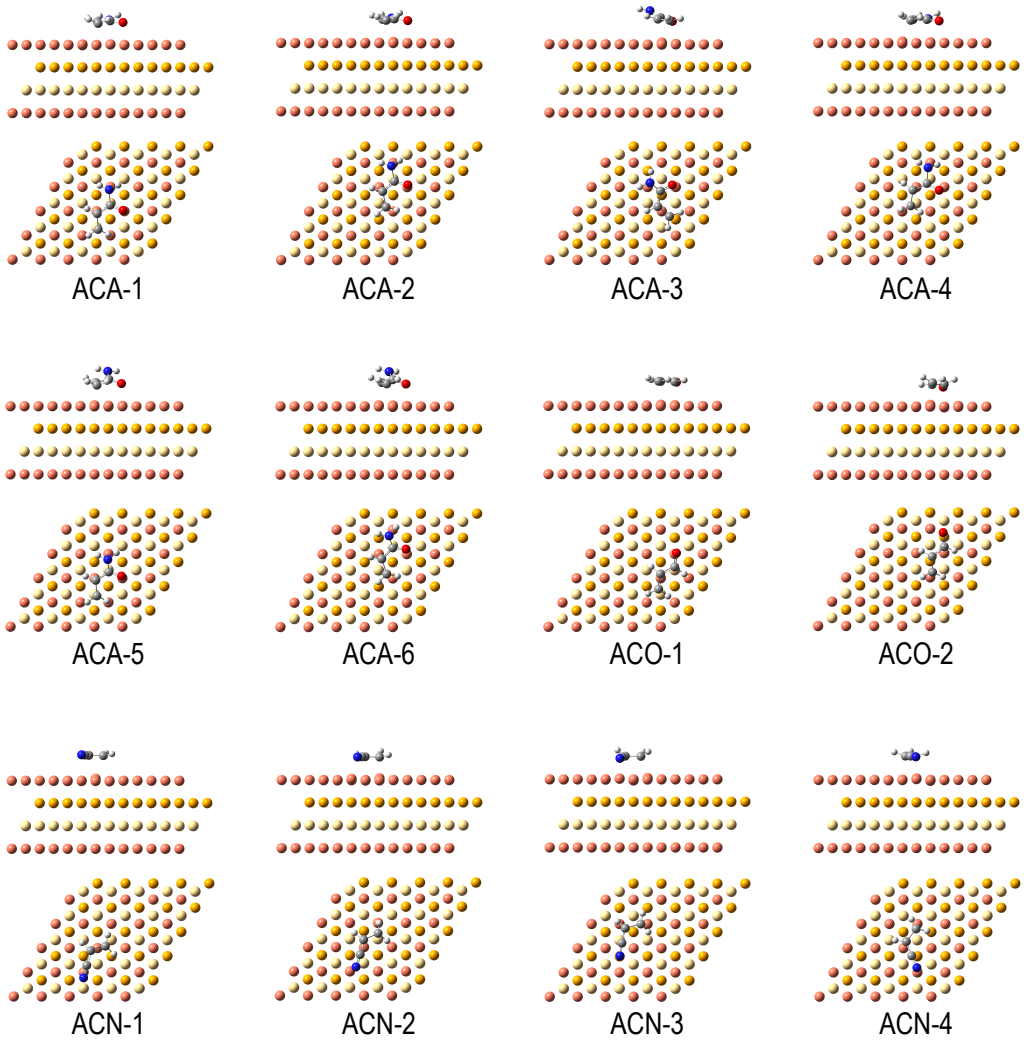

Figure 5.2: Top and side views of the minima found for acrylamide (ACA), acrylonitrile (ACN) and acrolein (ACO) adsorbed on a Cu(111) surface. Three colors for the different (non-equivalent) Cu layers are used.

favorable structure found for the three molecules (ACA-3, ACN-1 and ACO1) the terminal C=C bond lies on top of a Cu atom of the surface forming an $\eta^2 - \mathrm{Cu}$ bond, thus showing that the vinyl–surface interaction is the main anchorage point and key stabilizing factor. In the case of Cu(100) we also found that the most stable structures of the considered vinyl-derivatives are those in which the double C=C bond is on top of a Cu atom of the surface [207].

Table 5.1: Adsorption energy E_{ads} of acrylamide (ACA), acrylonitrile (ACN) and acrolein (ACO) on a Cu(111) surface. Several structures were obtained for each molecule (see Fig. 5.2). Relative energy ΔE between the structures in each system. All values are in eV.

	E_{ads} (eV)	ΔE (eV)
ACA-1	-0.520	0.208
ACA-2	-0.477	0.251
ACA-3	-0.728	0.000
ACA-4	-0.466	0.262
ACA-5	-0.637	0.091
ACA-6	-0.569	0.159
ACN-1	-0.354	0.000
ACN-2	-0.145	0.208
ACN-3	-0.135	0.219
ACN-4	-0.271	0.083
ACO-1	-0.456	0.000
ACO-2	-0.442	0.014

The adsorption structures that we have found for ACA show in common a direct, on top, interaction between the oxygen atom of the molecule and a Cu atom of the surface, with relative energies between them of up to ~ 260 meV. In ACA-1, ACA-2 and ACA-4 we also distinguish direct interaction between the N atom and a Cu atom of the surface (N$\rightarrow$Cu$_{\text{top}}$); in these cases, hybridization also changes in the N atom from sp^2 to sp^3 and the geometry is accordingly distorted. However in ACA-3, ACA-4, ACA-5 and ACA-6 planarity in the amide group is observed; in these cases hybridization is not altered and the resonant amide structure O-C=NH_2 is preserved. The geometrical changes upon adsorption are also reflected in the electronic structure and discussed below.

In the case of ACN, the cyano and vinyl groups change the position in each adsorption geometry (on top of a Cu atom and on hollow between Cu atoms in the surface), showing differences in the adsorption energy of up to ~ 220 meV. ACO-1 and ACO-2 are nearly degenerated ($\Delta E = 14$ meV). Interestingly, the less stable one (ACA-2) shows a stronger interaction between the O atom and the Cu one (the distance between O and the surface is 1.8 Å; while in ACA-1 is 2.2 Å) and presents a higher distortion of the molecule upon adsorption (e.g. the dihedral angle H-C-C-C is 146° in ACO-2 and 163° in ACO-1, being planar in the gas phase with an angle

Table 5.2: Most relevant C−C distances (in Å), dihedral H − C2 − C3 − H angles in adsorption (in degrees, hydrogen atoms in *trans*) and transferred charge from the surface to the molecule (in atomic units) of the most stable minima found for acrylamide, acrylonitrile and acrolein adsorbed on a Cu(111) surface after geometry optimization. Gas phase distances are also included for comparison.

	C1 − C2		C2 − C3		Dihedral	Δq
	Gas	Ads.	Gas	Ads.	angle	
ACA-3	1.497	1.462	1.337	1.414	153.6	-0.224
ACN-1	1.427	1.416	1.342	1.411	157.7	-0.244
ACO-1	1.473	1.444	1.342	1.412	161.6	-0.388

of 180°). It suggests that in ACO-2 the deformation energy (with respect to the gas phase structure) is countered with the adsorption one, but not enough to become the most stable conformation.

We now analyze in more detail the nature of the molecule–surface interaction focusing on the most stable structure of each studied system (ACA-3, ACN-1 and ACO-1). The adsorption leads to charge transfer from the surface to the molecule in the three cases (see Table 5.2). However, no relation between the charge transfer and adsorption energy is observed. The highest charge transfer from the surface to the molecule is observed in acrolein, followed by acrylonitrile and acrylamide. We obtained similar trends and absolute values in the adsorption of the same molecules on the Cu(100) surface [207], which points out that the charge transfer does not depend on the crystal orientation but on its chemical composition and on the adsorbed organic molecule.

Charge transfer can be further studied by analyzing the change in the spatial redistribution of the electronic density upon adsorption, which is defined as:

$$\Delta\rho = \rho_{molecule/surface} - (\rho_{molecule} + \rho_{surface}) \tag{5.2}$$

where $\rho_{molecule/surface}$ is the electronic density of the whole system, and $\rho_{molecule}$ and $\rho_{surface}$ are the electronic densities of the molecule and surface computed keeping the adsorption geometry. Fig. 5.3 shows that the charge is mainly transferred to the vinyl group in the three molecules, i.e. from the surface to the lowest unoccupied molecular orbital (LUMO), which has π^* character. Therefore, the π system in the molecule becomes more homogeneous due to the adsorption and this is reflected on changes in

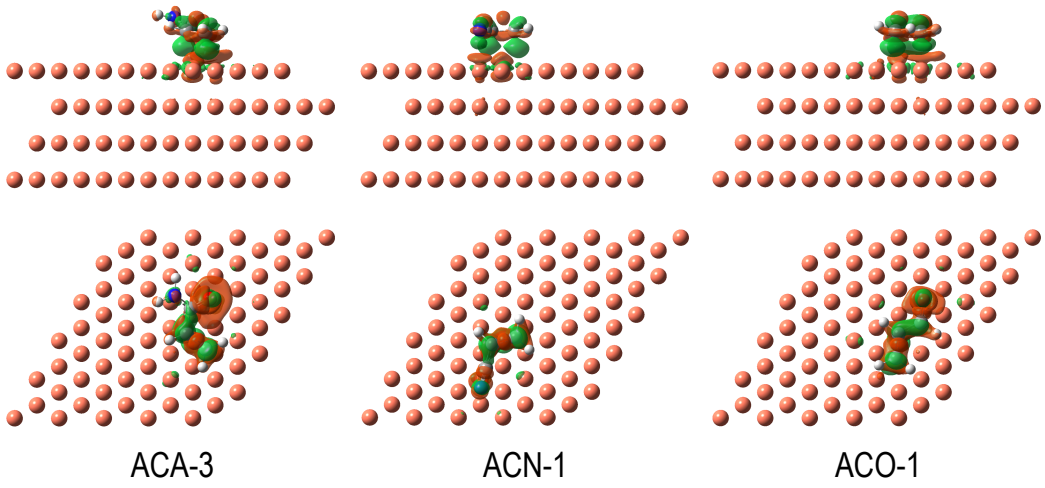

Figure 5.3: Change in the electronic density upon adsorption ($\Delta\rho$, isovalue=0.02) for the most stable adsorption structures of the three vinyl derivatives on the Cu(111) surface. Green color shows positive $\Delta\rho$ and reddish orange color shows negative $\Delta\rho$. All the Cu atoms in this figure are shown in the same color.

the geometry. Indeed, the C1-C2 bond (single C-C bond in the gas phase) is shortened, while the C2-C3 bond (double C=C bond in the gas phase) lengthens, as can be observed in Table 5.2. The distortion of the molecular skeleton upon adsorption is the direct consequence of the stronger electronic delocalization. The distortion in the molecular geometry, especially those changes in the C-C bond distances and the loss of planarity in the vinyl group, together with the charge transfer results, confirm the nature of the molecule–surface interaction as chemisorption. As shown before for vinyl derivatives adsorbed on Cu(100) [207], the depletion of electron density in regions where there is no nodal plane in the π system and the gain in the LUMO orbital is explained in terms of a simple chemical picture: electron donation from the π orbital of the molecule to the surface and backdonation from the surface to the π^* orbital of the molecule ($\pi-$backbonding). This phenomenon was also observed in other molecules of different nature adsorbed on metal surfaces [183–188].

In order to get a deeper information on the changes in the electronic structure upon adsorption and on the nature of the interaction, we have analyzed the density of states projected on molecular states: projected Density Of States (pDOS). They are shown, for the most stable adsorption conformer, in Fig. 5.4. Due to the different

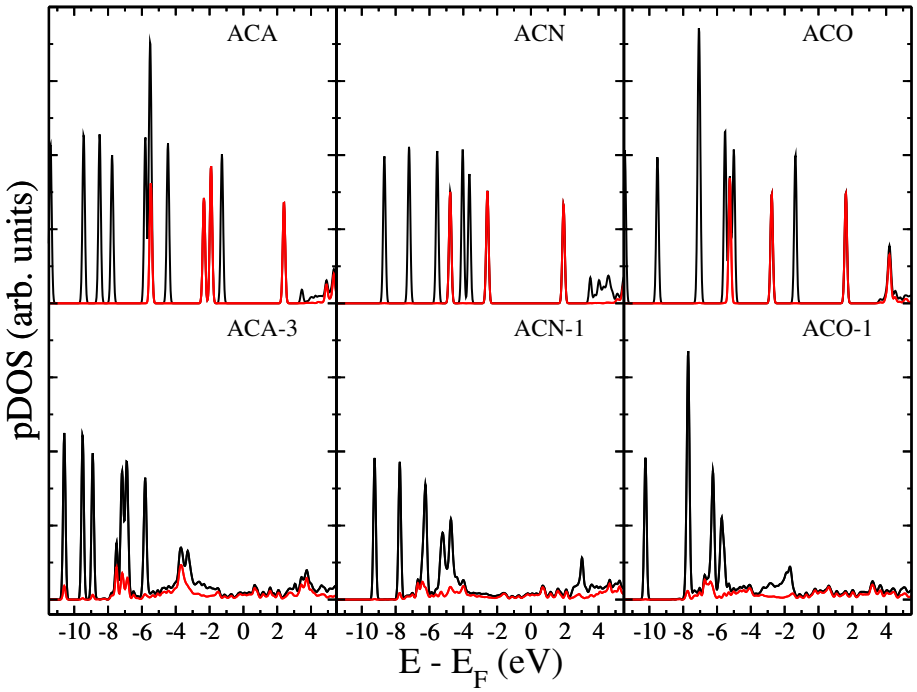

Figure 5.4: Density Of States projected on the atoms of the adsorbed molecules. Results of the molecule far from the slab, non-interacting with the surface, are also shown for comparison - upper curves in each panel. Black curve, total pDOS; red curve, pz-projection, which allows us to identify the π contribution to the pDOS.

Fermi levels of the molecule and surface separately, when they interact, there is an energy alignment which induces a charge transfer from the metal to the organic molecule [91,244]. For this reason, since the molecule has a partial negative charge, its nuclei have an extra screening, shifting its electronic levels. This is a common feature of all the molecular states, regardless of their symmetry. As we have explained, charge transfer takes place mainly through the π orbitals of the molecule; due to their spatial orientation, the overlap with the metal states is more favorable and thus, these orbitals are able to mix more efficiently with the surface. This is clearly appreciated in the pDOS: the π states (in red) are the ones that have a higher change upon molecular adsorption: they are the only molecular states that do not keep their previous identity showing a larger broadening and higher energy shift. This observation confirms the nature of the chemical interaction: donation from the occupied lone pair and π orbitals of the molecule to the surface and backdonation from the surface to the π^* orbital of the molecule ($\pi-$backbonding).

Table 5.3: Wavenumbers (in cm^{-1}) associated to the stretching modes of the acrylamide (ACA), acrylonitrile (ACN) and acrolein (ACO), in the gas phase (neutral and anion) and in the most stable adsorption geometry on Cu(111).[(a)]In the case of the acrolein, the frequency at 910.92 cm^{-1} is strongly coupled with other mode at 1149.93 cm^{-1}. Although Hamada et al. [245] assigned the C1-C2 stretching to this band (1158 cm^{-1} in their work), an analysis of the contributions of the normal modes shows that this internal coordinate contributes approximately equal to both bands. In this work we propose this new assignment since it is consistent with the other vinyl-derivatives and with the shift after the adsorption. Frequencies of anionic molecules in the gas phase have been computed with Gaussian09 [75].

stretching mode	Gas Phase		Molecule/Cu(111)
ν	ACA neutral	ACA anion	ACA-3
NH_2 asymmetric	3627.01	3477.66	3578.58
NH_2 symmetric	3494.81	3356.24	3448.05
CH_2 asymmetric	3166.46	3155.30	3142.67
CH_2 symmetric	3082.50	3069.88	3053.34
C-H	3065.00	3039.22	3079.02
C=O	1680.84	1586.16	1483.68
C2=C3	1624.43	1468.19	1417.15
C-N	1256.36	1257.72	1274.84
C1-C2	796.87	813.85	1383.82
ν	ACN neutral	ACN anion	ACN-1
CH_2 asymmetric	3182.71	3162.84	3167.93
C-H	3101.47	3060.99	3087.59
CH_2 symmetric	3086.79	3071.03	3074.74
C≡N	2253.28	2078.32	2094.58
C2=C3	1613.95	1454.19	1455.07
C1-C2	871.42	866.63	1350.37
ν	ACO neutral	ACO anion	ACO-1
CH_2 asymmetric	3159.48	3127.58	3143.39
C-H (vinyl)	3100.49	3020.88	3052.93
CH_2 symmetric	3067.72	3045.11	3047.44
C-H (aldehyde)	2790.37	2682.81	2818.41
C=O	1688.45	1466.86	1427.86
C2=C3	1618.60	1466.86	1457.79
C1-C2	910.92[(a)]	1197.22	1321.07

5.3.2 Vibrational frequencies

We now present how the molecule-surface interaction, characterized in the previous section, influences the vibrational properties of the studied molecules. This is a first step toward the understanding of their behaviour upon thermal excitation (see next section). In particular, we have computed the harmonic vibrational frequencies of the most stable adsorption structure for each vinyl-derivative. We present in Table 5.3 the computed frequencies of the most relevant vibrational modes. For comparison, vibrational frequencies of the same modes for the neutral and anion molecules in the gas phase are also shown.

The three vinyl-derivatives exhibit the same trends after the adsorption. The C1-C2 stretching mode increases its frequency in several hundreds of cm^{-1} in the adsorbed structures, which indicates a stronger bond. On the other hand, the double C2=C3 bond decreases its characteristic frequency from $\sim$ 1620 to $\sim$ 1460 cm^{-1}. In this way, in the adsorbed molecules the difference between both frequencies (C1-C2 and C2-C3 stretching modes) is much smaller than in the gas phase. This is the consequence of the higher electron delocalization in the molecular skeleton, as stated in the previous section. Accordingly, changes in the C1-C2 and C2-C3 bond lengths in the adsorbed structures lead to very similar distances after the adsorption (1.4 Å). Also, both the symmetric and antisymmetric $\nu(CH_2)$ frequencies are red-shifted, which is consistent with the change of hybridization of the terminal C3 atom due to the interaction with the surface: the atom adopts a partial sp^3 character and the frequencies decrease $\sim$ 20 cm^{-1}.

In the substituent groups (C=O for ACO, C≡N for ACN, and NH_2C=O for ACA) variations in the frequencies of the stretching modes can be also explained in terms of charge transfer and molecular chemisorption to the metal surface. The amide group of acrylamide has an important contribution to the Lewis structure in which the electron lone pair of the nitrogen atom migrates to form a double bond with the carbon, thus shifting the pair in the C=O to the oxygen atom. In this resonant form, a partial negative charge is placed on the oxygen atom (see Fig. 5.5). In the adsorption a non negligible part of the transferred charge is accommodated on the oxygen atom (see $\Delta\rho$ in Fig. 5.3) thus decreasing the weight of this resonant structure. Consequently, the lone pair of the nitrogen does not participate on the resonant structure and is thus available to link the molecule to the surface. The N atom adopts an sp^3 character, causing a red-shift in both symmetric and antisymmetric

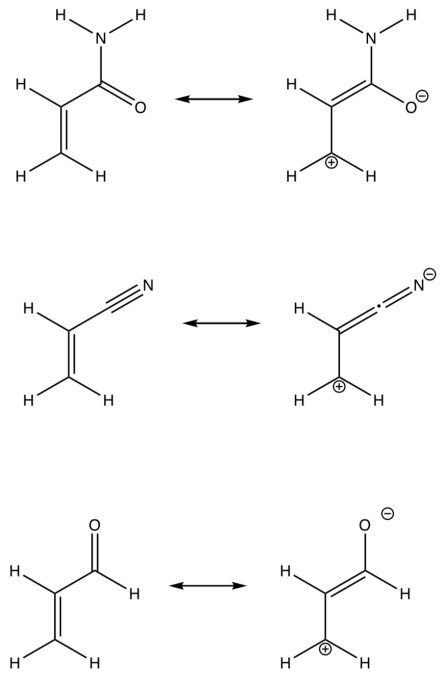

Figure 5.5: Resonance forms of acrylamide (up), acrylonitrile (middle) and acrolein (down). The two relevant structures for the discussion are shown for each molecule.

$\nu(NH_2)$ stretching frequencies. In addition, since larger electron density is hosted in the molecule, the oxygen atom does not form a pure double C=O bond anymore and, consequently, the corresponding stretching frequency is also red-shifted.

In acrylonitrile, the C $\equiv$ N bond in the cyano group becomes more labile in the adsorption because (i) part of the electron density initially located on this bond is now participating in the linkage with the surface ($\pi \rightarrow$ Cu donation) and (ii) the extra transferred charge populates the π^* orbital (Cu $\rightarrow \pi^*$ backdonation) [207]. Thus, red-shifting is also observed in the stretching frequency of this bond, as shown experimentally [246].

Finally, the acrolein has two internal stretching modes: the double C=O bond, which behaves as the CO bond of the amide group (red-shift due to the adsorption)

and the C-H bond of the aldehyde. This last frequency is blue-shifted after the interaction with the surface. This change can be also explained by the high electron transfer from the metal to the molecule. An internal rearrangement of the electron density is observed and although the molecule hosts globally 0.39 e^- from the surface, locally in the C1-C2 bond 0.46 e^- is distributed. The charge excess strengthens the bond and therefore it becomes shorter, causing an increase in the frequency of the $\nu(C1-H)$ stretching mode.

Although changes observed in some modes upon adsorption point in a similar direction to those in the negatively-charged molecules in the gas phase, the trends in a few modes follow an opposite behavior [$\nu(C-H)$ in ACA, $\nu(C1-C2)$ in ACN and $\nu(C-H_{aldehyde})$ in ACO]. This indicates that the new vibrational leves are affected not only by charge transfer effects, but also by the covalent interactions with the surface that strongly anchor the molecule, thus hindering certain atomic displacements.

5.3.3 *Ab initio* Molecular Dynamics

Finally we have studied the behavior of excited vinyl derivatives (ACA, ACN and ACO) adsorbed on a Cu(111) surface by means of *ab initio* molecular dynamics (AIMD). To this we have computed several trajectories for each system assuming two values of excitation energy ($E^* = 6$ and 12 eV) randomly distributed among the nuclear degrees of freedom of atoms in the molecule. During the propagation we allow the movement of all the atoms (except the last layer inside the metal bulk). For comparison, AIMD simulations on the molecules in the gas phase were also carried out.

We first analyze the excitation energy distribution and transfer dynamics. Fig. 5.6 shows the energy decomposition as a function of time: potential energy, kinetic energy in atoms of the molecule, kinetic energy in atoms of the metal and total kinetic energy. Each curve corresponds to an average over all the computed trajectories (with fluctuations of $\sim 7-25\%$). In all cases (regardless the molecule or the excitation energy) a similar behavior is observed: During the first ~ 20 fs, the excitation energy is gradually transferred from kinetic energy in the molecule to potential energy; i.e the energy is very rapidly redistributed and the system suffers strong deformations from its departure point in the optimized geometry. Then, it reaches a pseudo-equilibrium in which $\sim 50\%$ of the kinetic energy has been transferred to potential

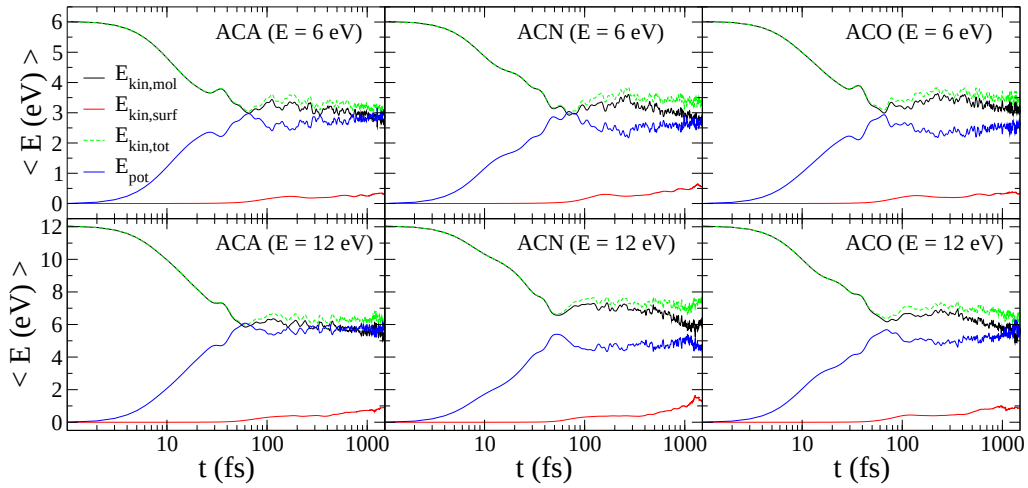

Figure 5.6: Energy exchange among the kinetic energy of the atoms in the molecule ($E_{kin,mol}$), kinetic energy of the atoms in the surface ($E_{kin,surf}$), total kinetic energy ($E_{kin,tot}$) and potetial energy (E_{pot}), as a function of the time in the *ab initio* molecular dynamics simulations. Each energy contribution has been averaged in time over the trajectories. Acrylamide (ACA), acrylonitrile (ACN) and acrolein (ACO) with 6 and 12 eV of initial excitation energy have been considered.

energy. From this point on, the kinetic energy remaining in the atoms of the molecule is slightly transferred into kinetic energy of the atoms in the surface. The highly-excited molecules evolve breaking bonds (molecule-surface or intramolecular bonds) during the first femtoseconds in the propagation and transfer of thermal energy from the molecule to the surface is only effective when the atoms of the molecule have cooled down. The main reason is the difference in mass between them: since the copper atoms on the surface are (at least) four times heavier than the atoms of the molecule inelastic collisions are only effective at a low velocity; that is, from the remaining atoms of the molecule that still interact with the substrate, the transfer of momentum to the metal atoms takes place in a kind of friction process. A deeper analysis on the movements of Cu atoms reveals that the coordinates in these atoms are frozen during the first part of the propagation, even if they are allowed to move; only when the potential energy has reached a maximum the Cu atoms begin to move from their original positions. This result indicates that all the potential energy gain is in the form of molecular deformation or desorption.

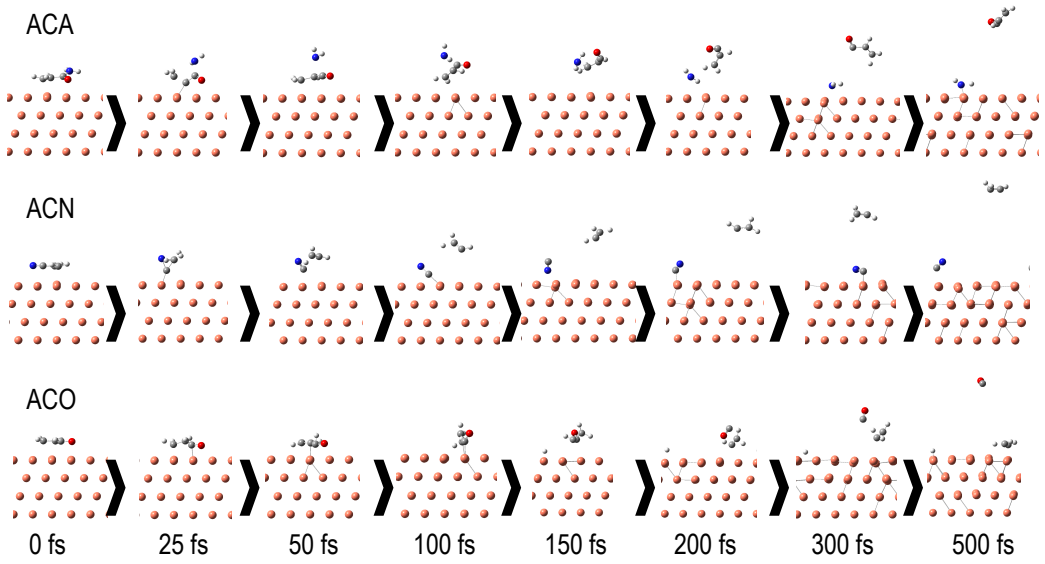

Figure 5.7: Snapshots of *ab initio* molecular dynamics trajectories for acrylamide (ACA), acrylonitrile (ACN) and acrolein (ACO) with an initial excitation energy of 12 eV. The selected trajectories show molecular breaking leading to (i) $NH_{2(Ads)}$ + $CHOCH_2$ for ACA; (ii) $CN_{(Ads)}$ + CH_2CH for ACN; (iii) $H_{(Ads)}$ + $CH_2CH_{(Ads)}$ + CO for ACO

We now focus on the chemical processes taking place after excitation. To this we analyze the final products obtained after the molecular dynamics propagation. We first analyze the three main processes that we have observed:

- Adsorption: The molecule is still interacting with the surface. Most probably it has been moved from its original adsorption site. In this process, isomerization can be also observed.

- Desorption: The molecule is desorbed and does not interact with the surface any more. In this process, isomerization is also observed.

- Break: Bonds in the molecule suffer cleavage producing two or more fragments (see examples of trajectories following this kind of dynamics in Fig. 5.7).

Fig. 5.8 shows the probability of these processes in the three studied molecules (molecular breaking in the gas phase with $E^* = 12$ eV is also shown for comparison). When the molecule breaks, the produced fragments can desorb or stay interacting

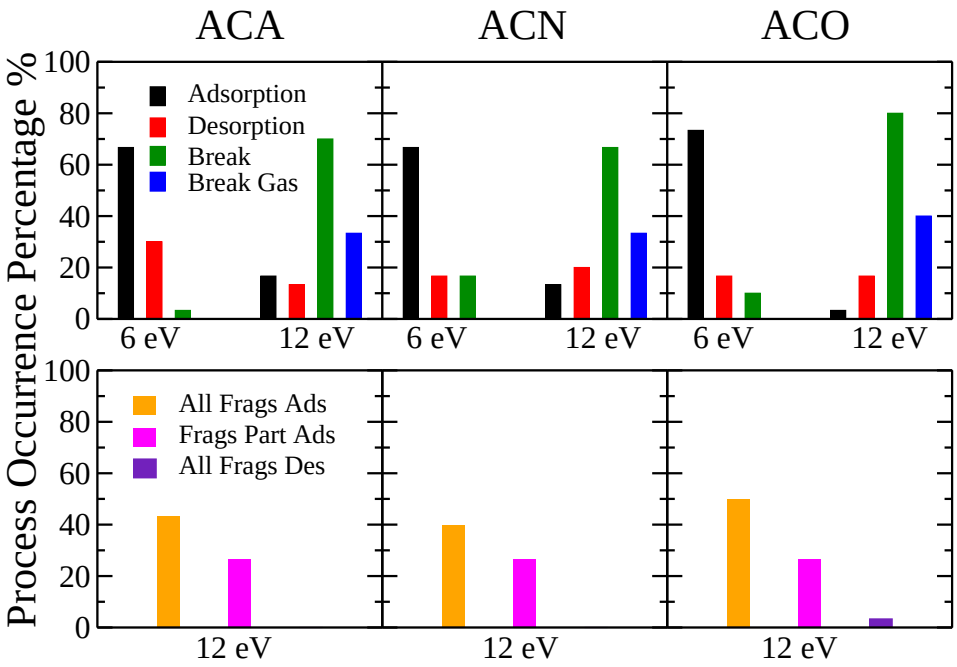

Figure 5.8: Percentage of the process occurrence obtained in the molecular dynamics for the three studied molecules acrylamide (ACA), acrylonitrile (ACN) and acrolein (ACO). Upper panels (excitation energes 6 and 12 eV): The molecule remains adsorbed (Adsorption); the molecule desorbs (Desorption); the molecule is broken (Break). Lower panels (excitation energy 12 eV): when the molecule is broken, all produced fragments remain adsorbed (All Frags Ads), all produced fragments desorb (All Frags Des), part of the fragments remains adsorbed and the rest desorb (Frags Part Ads). In the upper panels the results for the molecular breaking percentage of the molecules in the gas phase at 12 eV are also shown.

with the surface (part of them or all of them). This information is also shown in the figure. The general trends are similar in the three studied molecules (although percentages differ from one to another). The probability of finding trajectories with molecular adsorption decreases with the energy, from $\sim 70\%$ at 6 eV to $\sim 10\%$ at 12 eV. Acrylamide shows larger desorption at 6 eV than at 12 eV (most probably because we found much less molecular breaking at 6eV in comparison with 12 eV). In acrylonitrile and acrolein similar amount of molecular desorption is found at 6 and 12 eV ($\sim 15 - 20\%$). Molecular breaking is the dominant process at 12 eV in

the three molecules adsorbed with the surface ($\sim 70 - 80\%$). It is worth noting that the amount of molecular breaking observed in the molecules in the gas phase with the same excitation energy (12 eV) is half of those observed in the adsorbed systems. Even if part of the excitation energy is transferred to the metal surface, the probability of finding molecular fragments is much larger. The reason is that the interaction of the molecule with the metal surface weakens the bonds between atoms in the molecule. In particular, the charge transferred in the chemisorption is mainly located on the LUMO orbital of the molecule, with a strong π^* antibonding character: larger π conjugation but making C=C bonds much more labile. We observe larger probability of molecular breaking in the surface when all the produced fragments remain adsorbed on the substrate. A negligible amount of desorption of all the produced fragments is appreciated. But the catalytic effect of the metal surface is not only observed in the larger amount of fragmentation produced when the molecule is interacting with the substrate, but also in a much wider spectrum of produced fragments (see Tables 5.4, 5.5 and 5.6). Some of the observed fragments in the gas phase are not present in the adsorbed systems, but a much richer fragmentation behavior is observed. In general:

- Atomic hydrogen is widely observed in the adsorbed molecules while almost negligible in the gas phase.
- In gas phase stable molecular species are mainly produced, such as ethylene $H_2C = CH_2$, acetylene $HC \equiv CH$, molecular hydrogen H_2, hydrogen cyanide HCN, or carbon monoxide CO.
- The vinyl moiety C_2H_3, coming from a direct cleavage of the central C-C bond is one of the most observed fragments. Since the charge transferred is accommodated on the LUMO it increases the π delocalization reinforcing the central C-C bond; this strengthening is reflected in the less amount of vinyl fragments observed in the adsorbed molecules.

In particular for each molecule:

- In acrylamide NH_2 is much more observed in the adsorbed molecule being the dominant fragment (50%).
- In acrylonitrile HCN is the most abundant fragment in the gas phase and it is not observed on the adsorbed molecule, where the CN fragment is largely the

dominant one (60%).

- In acrolein HCO and C_2H_3 are common fragments in the gas phase. While C_2H_3 is also one of the most abundant fragments in the adsorbed molecule, HCO almost disappears, with CO being much more probable now.

5.4 Conclusions

In summary, we have presented a deep theoretical study of organic-metal interfaces, focussing on the electronic properties and thermal stability of potential candidates for composite hybrid materials. In particular we have performed density functional theory (DFT) simulations of the vinyl derivative polymer precursors acrylamide, acrylonitrile and acrolein, interacting on a pristine Cu(111) surface. The modeling highlighted anchoring mechanisms and the preferred arrangement of the molecules on the surface. Interestingly, the vinyl group acts as the binding site and the functional groups in each molecule drive the relative adsorption orientation. Linkage with the surface can be explained with a simple chemical picture: $\pi \rightarrow$ Cu donation and Cu $\rightarrow \pi^*$ backdonation. Changes in the electronic structure associated with this kind of interaction show stronger electronic delocalization and consequently distortion of the molecular skeleton. Molecular anchoring (through the vinyl group) and structural changes (bond elongations and dihedral angle modifications upon adsorption) suggest the possibility of controlled polymerization in given crystal orientations. The *ab initio* molecular dynamics simulations have shown a very efficient energy redistribution (shared between the kinetic energy of atoms in the molecule and atoms in the surface and potential energy in a short time of ~ 100 fs). Molecular decomposition shows a much more varied spectrum when the molecule is adsorbed on the surface and, notably, a catalytic effect with a larger amount of fragmentation with respect to molecules in the gas phase. These findings may help achieve a deeper comprehension of the properties of ultra-thin organic coating of metal surfaces, a promising two dimensional kind of hybrid material with potential applications in many areas.

Table 5.4: Percentage of *ab initio* molecular dynamics trajectories where the corresponding fragment of the acrylamide (ACA) molecule is produced. Results when the molecule is adsorbed on Cu(111) and for the molecule in gas phase are given, both with initial excitation energy 12 eV.

Fragment	ACA/Cu(111)	Gas Phase
H	23.33	–
ACA-H	3.33	–
NH_2	50.00	13.33
ACA-NH_2	13.33	3.33
CH_2	13.33	–
ACA-CH_2	0.00	–
O	10.00	–
ACA-O	3.33	–
C_2H_3	16.67	20.00
C_2H_2	13.33	–
CO	26.67	10.00
OC_2H	10.00	–
NH_2C_2H	3.33	–
NHC_3H_3	3.33	–
$OCNH_2$	6.67	–
CH	3.33	–
NH_2COH	–	3.33
NH_2CO	–	10.00
CH_2CH_2	–	3.33
CHCH	–	3.33
HNCO	–	3.33

Table 5.5: Percentage of *ab initio* molecular dynamics trajectories where the corresponding fragment of the acrylonitrile (ACN) molecule is produced. Results when the molecule is adsorbed on Cu(111) and for the molecule in gas phase are given, both with initial excitation energy 12 eV.

Fragment	ACN/Cu(111)	Gas Phase
H	33.33	–
ACN-H	6.67	–
C_2H_2	23.33	3.33
CN	60.00	13.33
C_2H_3	30.00	13.33
CH	3.33	–
CH_2	6.67	–
C	3.33	–
CHCH	–	13.33
HCN	–	16.67

Table 5.6: Percentage of *ab initio* molecular dynamics trajectories where the corresponding fragment of the acrolein (ACO) molecule is produced. Results when the molecule is adsorbed on Cu(111) and for the molecule in gas phase are given, both with initial excitation energy 12 eV.

Fragment	ACO/Cu(111)	Gas Phase
H	56.67	3.33
ACO-H	3.33	–
CH_2	6.67	–
ACO-CH_2	3.33	–
CO	36.67	13.33
C_2H_2	10.00	3.33
C_2H_3	33.33	30.00
CH	6.67	–
OC_2H_2	3.33	–
O	13.33	–
CH_2CCH_2	3.33	–
OH	6.67	–
C_3H_3	10.00	–
OCHCCH	3.33	–
C_2H	3.33	–
C_3H_2	3.33	–
$OCCH_2$	3.33	–
CHO	6.67	–
CHCH	–	6.67
HCO	–	26.67
H_2	–	6.67

Chapter 6

Molecular anions on surfaces

Abstract

In this chapter we present a study of anionic states of molecules adsorbed on surfaces. To this, we have used Wave Packet Propagation, a methodology that allows us to follow the dynamics of the extra (active) electron. From these simulations, we can extract the energy, lifetime and decay channels of these states. Different molecules (acrylamide, acrolein, acrylonitrile and nitroethylene) and surfaces (Cu(100) and Cu(111)) have been considered in order to determine, respectively, the effect of the molecule and the surface in the properties of interest. In the last part of this study, we include ultrathin ionic layers between the molecule and the metal substrate, in particular atomically thin layers of NaCl. The results show the importance of the coupling between the molecule and the substrate as a crucial aspect that affects the behavior of the whole system. The similarity of the results with very different molecules points out the universality of the trends that have been observed in this work.

6.1 Introduction

In the previous chapters we discussed results on the adsorption of the vinyl-derivatives on two different copper surfaces: Cu(100) (Chapter 4) and Cu(111) (Chapter 5). These studies were carried out for the molecules in the electronic ground state using state-of-the-art DFT methods. Nevertheless, although the results are robust and consistent, a direct comparison with experimental measurements could be challenging, especially in the cases where weak interactions (typically van der Waals forces) between the molecule and the surface rule the adsorption.

There are many experimental techniques to study surface supported nanostructures in general, and adsorbed molecular species in particular. Some of them, such as the Scanning Tunneling Spectroscopy (STS) or the Time-Resolved Two-Photon-Photoemission (TR-2PPE), are able to provide an information on the energies and lifetimes of the decaying quasistationary electronic states of the molecules adsorbed on metal surfaces. Due to their role in surface reactivity, and due to the possible application of the adsorbed molecules as single photon sources, characterization of the anionic and/or excited states is of paramount importance. In particular the lifetime of a molecular state is a key property which would control the efficiency of the reaction mechanism [247], or, if one is interested in the fluorescence, the decay to the ground state might compete with the migration of the electron towards the substrate. [11, 24, 248, 249]

In this chapter we show the results of the quantum time-dependent calculations describing the evolution of the wave function of an active electron in the charge transfer between the molecule an the metal, initially localized as a molecular anion for different organic molecules adsorbed on a metal surface. We address: the previously studied acrylamide (ACA), acrylonitrile (ACN) and acrolein (ACO); nitroethylene (NET), also a vinyl derivative with a highly stable anion; and Zn-porphyrin as an example of this wide family of molecules that have been used in last years in many applications (solar cells, molecular materials, etc.).

The calculations are carried out with the wave packet propagation (WPP) technique as explained in Chapter 4. The WPP calculations within one-active-electron approximation not only yield the energies of the quasistationary electronic states localized on the molecules, but also the rates of their population decay via energy-conserving electron transfer towards continuum of unoccupied electronic states of the metal (Resonant Charge Transfer, RCT). In the case, where the RCT dominates the

decay of the molecular localized electronic state, its lifetime τ can be determined as an inverse of the RCT rate Γ: $\tau = 1/\Gamma$. With the WPP simulations we also compute the wavefunctions of the quasistationary states, allowing their total characterization. The molecules cited above are interesting for this kind of calculations since their Lowest Unoccupied Molecular Orbital (LUMO), which is the one that would accept the electron, has π^* character. As it was shown in Chapter 4, these orbitals are able to hybridize with the states of the metal substrate. Due to the strong coupling, the decay via RCT towards the metal is fast. The new molecules that are included in this chapter also present this character. For the four vinyl-derivatives (ACA, ACN, ACO and NET), since the LUMO has an antibonding $\pi^*C_2{-}C_3$ character, populating this state would make weaker the (formally) double C=C bond, opening new horizons in surface reactivity and catalysis.

6.2 Computational details

All the Wave Packet Propagation simulations are performed using the code developed during this thesis.

For the acrylamide, acrylonitrile and acrolein adsorbed on Cu(100), the calculations are performed with two different sizes of the uniformly spaced 3D mesh: $nx = ny = nz = 512$ (regular box) and $nx = ny = 1024, nz = 512$ (large box). While the regular box is used routinely, the large-box-computations are performed for some of the data points to check the convergence of the results. The mesh spacing $dx = dy = dz = 0.169$ a.u. is set such that, for the free standing molecule, the Kohn-Sham (KS) energies of molecular orbitals obtained from WPP converge to better than 0.1 meV. Simultaneously, the difference between the WPP results and the KS energies of molecular orbitals obtained from the quantum chemistry code (Abinit) also differ by less than 0.1 meV. Along the z-coordinate perpendicular to the surface the computation box covers 55 a.u. inside metal (approx. 17 copper layers), and 30 a.u. of the vacuum region above the surface. The electron interaction with pristine Cu metal is represented with the model potential developed by Chulkov *et al.* [69].

The complex absorbing potentials $V_{abs}(x, y, z)$ are introduced at the boundaries of the computational box. This allows to avoid artificial effects linked with super-cell geometry, to impose the outgoing wave boundary conditions, and to represent the situation of the single molecule absorbed on the semi-infinite metal surface. The

complex absorbing potential is defined as:

$$V_{abs}(x,y,z) = -i\lambda\left(\upsilon(x)+\upsilon(y)+\upsilon(z)\right), \tag{6.1}$$

where

$$\upsilon(\xi) = \begin{cases} (\xi-\xi_{lim^+})^2 & \text{if } \xi > \xi_{lim^+}, \\ (\xi_{lim^-}-\xi)^2 & \text{if } \xi < \xi_{lim^-}, \\ 0 & \text{otherwise.} \end{cases} \tag{6.2}$$

The potential strength $\lambda = 2\cdot 10^{-4}$ a.u. ,and ξ_{lim^+} and ξ_{lim^-} define the size of the absorption-free space. In practice we used: $x_{lim^+} = y_{lim^+} = x_{lim^-} = y_{lim^-} = 20$ a.u. for the regular computation box, and $x_{lim^+} = y_{lim^+} = x_{lim^-} = y_{lim^-} = 40$ a.u. and for the large computation box. In both cases $z_{lim^+} = 3$ a.u. and $z_{lim^-} = 25$ a.u.

Given an initial wave function $\Psi(\vec{r}, t=0) = \Psi_0(\vec{r})$, the time-dependent wave function of an active electron $\Psi(\vec{r},t)$ is obtained from the time-dependent Schrödinger equation applying the WPP technique. The propagation time step $dt = 0.018$ a.u. is used allowing to reach better than 0.1 meV convergence in KS energies of molecular orbitals for the free-standing molecule. The energies and widths of the quasi-stationary states are extracted from the analysis of the autocorrelation function, $A(t)$, defined as following:

$$A(t) = \iiint \Psi_0^*(\vec{r})\Psi(\vec{r},t)\; d^3\vec{r}. \tag{6.3}$$

Two resonance extraction schemes are possible (see ref [58]). First one is based on the analysis of the density of electronic states $n(E)$ projected on initial state $\Psi(0)$.

$$n(E) = \mathrm{Im}\left\{\int_0^T A(t)\; e^{iEt} dt\right\}, \tag{6.4}$$

where $\mathrm{Im}\{\mathrm{Z}\}$ stands for the imaginary part of the complex number Z, $t=0$ is the initial time of the time-propagation, and T is the finite, albeit large propagation time. The decaying (quasi-stationary) molecular states appear as resonances in $n(E)$. The energy positions and widths of the resonances in $n(E)$ are associated with energies and RCT decay rates of the corresponding molecular states. This approach is robust, but it is difficult to apply in the case when the long-lived states are present in the system. This is because very large propagation times T are then needed to converge

the Fourier transform.

In such situations an alternative scheme is used. The autocorrelation is sought in the form (see ref [58]):

$$\mathcal{A}(t) = \sum_{j=1,...n} a_j e^{-iE_j t} e^{-\frac{\Gamma_j}{2}t}. \tag{6.5}$$

I.e. it is represented as a linear combination of the contributions from quasistationary states with energies E_j and decay rates Γ_j. Some of the states are the actual resonances of the system and some are the "effective" resonances that represent the contribution of the conduction band states, surface state continuum, and free-propagating states above the vacuum level. The least square fit of the autocorrelation function $A(t)$ obtained from the WPP by the analytical form $\mathcal{A}(t)$ given by Eq. (6.5) yields the complex energies (E_j, Γ_j) of the resonances in the system. The results for the actual resonances converge as function of the calculation time T and number of states n.

The reason why $A(t)$ is not evaluated at every time-step is because the spatial integral involved in its calculation is quite time-consuming. It was checked that there is no loss of accuracy if only one of each three steps are used.

Since $A(t)$ depends on $\Psi_0(\vec{r})$, the choice of the initial wavefunction might significantly ease or harm extraction of the resonance characteristics. For this reason, initial conditions must be carefully chosen and, depending on the states of interest, several propagations with different initial wavefunctions might be required. For the study of the anionic and/or excited states in which the LUMO orbital has a large contribution, this orbital obtained in the gas phase (where the energy is known from the quantum chemistry calculations) is chosen as an initial state for the time-propagation.

In order to obtain $\Psi_0(\vec{r})$, a time propagation is performed for the free-standing molecule in the gas phase. We are interested in the π^* orbital which is at the origin of the sought resonances for the molecules adsorbed at metal surface. For the free-standing molecule, the π^* is antisymmetric with respect to the molecular plane. Therefore, as an initial state for the WPP in this case we use a gaussian function centered out of the molecular plane so that its projection on π^* is non-zero. Since the KS energy, E_α, of the π^* orbital is known from the quantum chemical calculation, we can get the state in which we are interested by the time-to-energy Fourier Transform

(see Section 3.6 for further details):

$$\Psi_0(\vec{r}) = \int_0^\infty e^{iE_\alpha t}\Psi(\vec{r},t)dt \tag{6.6}$$

Once the wavefunction $\Psi_0(\vec{r})$ is obtained in the gas phase, we use it as an initial wavefunction in the following time-propagation including the surface.

Finally, to get the resonant wavefunction we carry out a final propagation asking for the wavefunction at the energy of interest.

In the calculations addressing the molecules adsorbed on metal surfaces covered with some monolayers (ML) of ionic crystal (here: NaCl) we use a modified model of the substrate. In addition to the model potential of Chulkov and co-authors describing interaction of an electron with metal, we use the model potential representing an electron interaction with NaCl films developed by Díaz-Tendero *et al* [139]. This is a self-consistent 3D potential which is able to describe an electron interaction with ions at crystal lattice cites. In this case, for computational convenience, we use the same grid spacing ($dx = dy = dz = 0.114$ a.u.) as in earlier publication by Díaz-Tendero *et al* [139]. To compensate the reduction of the grid spacing in these calculations as compared to the clean metal case, we use the largest possible size of the mesh with $nx = ny = nz = 1024$ knots in each direction. In this way, for the NaCl films of 3ML thickness, we address similar depth inside metal and similar vacuum part at positive z, as in the calculations performed for the molecules adsorbed on clean metal surface.

The interaction potential between an active electron and a molecule, $V_{molecule}$, is obtained through a single point calculation in the frame of the Density Functional Theory as implemented in the Abinit code [71]. For the plane wave expansion we use a cut-off energy of 32 a.u., and a convergence criterion of 10^{-9} a.u. in energy. The reciprocal space was sampled using Γ-point. For the molecules adsorbed directly on the metal, the potential includes the effect of the charge transfer, as described in Chapter 3. In the calculations addressing metal surface covered with NaCl film the (local) potential is defined as:

$$V = V_{molecule} + V_{metal}^{\text{Chulkov}} + V_{\text{NaCl}}^{\text{Diaz-Tendero}}, \tag{6.7}$$

where $V_{molecule}$ has been obtained for the free-standing molecule in vacuum while using the optimized adsorption geometry; $V_{metal}^{\text{Chulkov}}$ is the model potential for the

electron-metal interaction proposed by Chulkov and co-authors [69]; $V_{\mathrm{NaCl}}^{\mathrm{Diaz-Tendero}}$ is the model potential representing an active electron interaction with NaCl film [139].

This approach, based on the $V_{molecule}$ potential representing an electron interaction with free-standing molecule is adequate in the molecule/ionic crystal/metal surface systems, because the charge transfer between the molecule and the substrate is found to be very small. From DFT studies with VASP (with the same computational details than in previous chapters), in addition to the geometries, we obtained a transfer of 0.06 (1ML of NaCl) and 0.07 (3ML of NaCl) of an electron from the surface to the molecule. Thus, in accord with earlier findings [148], the decoupling of the molecule from the metal is effective even with a single monolayer of NaCl.

6.3 Results

6.3.1 Energies and lifetimes of acrylamide, acrylonitrile and acrolein anions adsorbed on a Cu(100) surface

Starting from the molecular π^* orbital obtained from the gas-phase WPP calculations, we carried out the WPP studies of the dynamics of an active electron in the RCT between an adsorbed molecule and a metal surface. The details on the extraction of the wavefunction of the π^* orbital can be found in Chapter 3. In order to impose the correct affinities of the molecular species in the gas-phase, a non-local term is been added to the one-electron Hamiltonian describing the molecule/surface system. Since, according to the Koopman's theorem, the LUMO states are the ones where an extra electron would be located, as explained in Section 3.5.3, we can use a correction:

$$\hat{H}' = \hat{H} + U|\phi\rangle\langle\phi| \tag{6.8}$$

where $\hat{H}'$ is the full Hamiltonian. It is given by the original Hamiltonian, $\hat{H}$, plus the non-local correction $U|\phi\rangle\langle\phi|$, where $\phi(\vec{r}) = \Psi_0(\vec{r})$, and $\Psi_0(\vec{r})$ is the wave function of KS LUMO orbital of the free-standing molecule, obtained from the WPP. The energy shift of the LUMO orbital is given by the constant U. The U values are 3.539, 3.652 and 3.728 eV for the acrylamide, acrylonitrile and acrolein, respectively. This energy shift was obtained as the difference of the electron affinity (calculated at CCSD/cc-pVTZ level with Gaussian09 [75]) and the KS energy of the orbital in the gas phase, calculated with Abinit using the same parameters as in the calculation of

the molecule+surface system.

In order to get more precise values of the energies and lifetimes, consecutive propagations are required. To this end: (1) We run the WPP to define the energy E_j of the quasistationary state; (2) We rerun the WPP to extract the resonance wavefunction at E_j via Fourier transform of the electronic wave packet; (3) We use it as an initial state for the subsequent WPP run and we repeat the iteration cycle. The procedure is initiated with WPP performed for the adsorbed molecule, and using as an initial wavefunction the LUMO orbital extracted in the gas phase. Note that for this gas-phase calculation we use a molecular geometry (an atomic arrangement) obtained from the *ab initio* calculations for the absorbed molecule. Using an iterative procedure described above we progressively increase the contribution of the quasistationary state in the initial wave function $\Psi(0)$ which eases the extraction of the energy and the decay rate of the molecular localized resonance.

We illustrate the performance of the above iterative procedure with an example of the acrylamide molecule adsorbed on Cu(100). The two consecutive time-propagations are applied. First one is performed using the gas-phase LUMO orbital as an initial state, and provides an initial state for the second time propagation. In Figure 6.1 we show the time evolution of the occupation of the initial state, $|A(t)|^2$, and in Figure 6.2 we show the electron density of states projected on initial state of the time propagation. As described earlier, the pDOS is obtained from the Fourier analysis of the autocorrelation amplitude $A(t)$. To better understand the results presented in Figure 6.1 and in Figure 6.2 it is important to recall that the time dependent wave function obtained in the wave packet propagation can be expressed via development over the basis of the eigenstates φ_k of the Hamiltonian $\hat{H}'$:

$$\Psi(\vec{r},t) = \sum_k \; e^{-iE_k t} \; \langle \varphi_k | \Psi_0 \rangle \; \varphi_k(\vec{r}), \tag{6.9}$$

where E_k is an eigenenergy. Note that the index k runs over both: continuum and bound states. The $\langle \varphi_k | \Psi_0 \rangle$ coefficients provide a population of various eigenstates by the choice of initial condition, and thus the contribution of these eigenstates into the time propagation.

If only the decaying quasistationary state is populated by the choice of initial conditions one would expect an exponential decay of the population, $|A(t)|^2$, of the initial state. This is what is observed in results corresponding to the "refined"

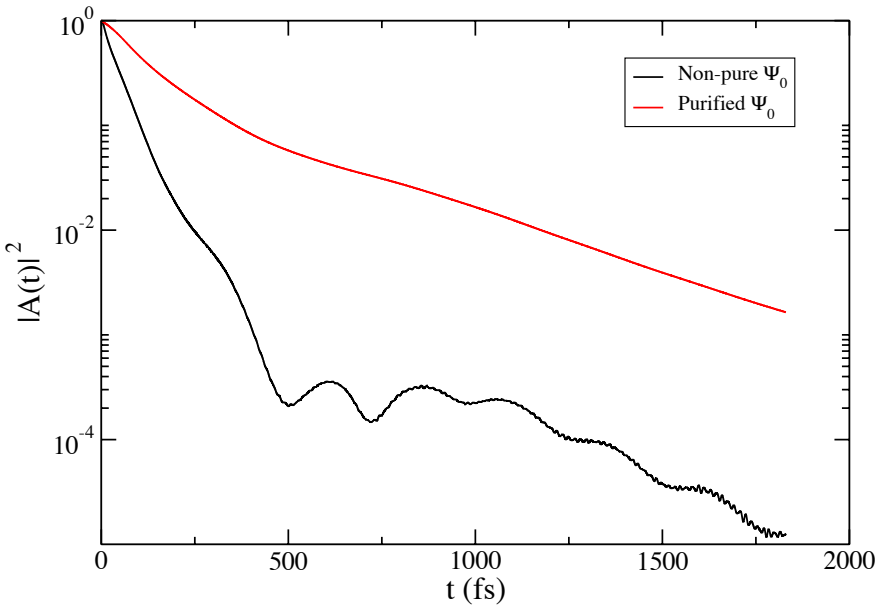

Figure 6.1: Square of the autocorrelation function of the acrylamide using two different initial wavefunctions. Black: gas phase wavefunction. Ref: "refined" wavefunction.

initial state and shown with red curve in Figure 6.1. At variance, using the gas-phase orbital as an initial state in the time propagation (black curve in Figure 6.1) leads to the strong population of metal continuum states within the broad energy range. In turn, this results in the fast drop of the inittial state population at short propagation times. At longer propagation times we retrieve an exponential decay of the quasitationary state, however with some oscillations. The oscillating pattern results from the interference between different stationary and quasistationary states of the system (molecular orbitals and resonances different from the one associated with the LUMO orbital) populated by the choice of the initial state. This analysis is further supported by the pDOS shown in Figure 6.2. The pDOS obtained in the propagation with "refined" initial state features single Lorentzian peak corresponding to the quasistationary state originating from the LUMO molecular orbital hybridized with metal surface. If the gas-phase LUMO orbital is used as an initial state, along

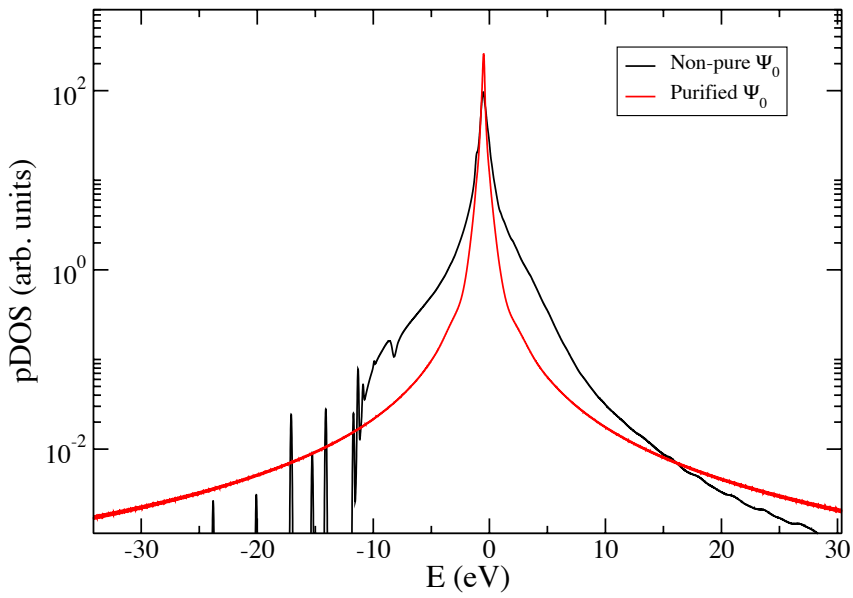

Figure 6.2: Fourier transform of the autocorrelation functions shown in Figure 6.1. In addition to a broader peak at the energy of interest, other states appear in the spectrum when the non-refined (gas-phase) wavefunction is used.

with the main peak corresponding to the sought quasistationary state, the pDOS shows a broad feature extending from approx -12 eV to large positive energies. This feature reflects the contribution of the continuum of electronic states in metal valence band and in vacuum populated with the initial wave packet. The discrete peaks below the valence band bottom (below -12 eV) emerge owing to various molecular orbitals with high binding energies.

Computed energies, widths and lifetimes of the anionic states in the three studied molecules are shown in Table 6.1 (regular box) and Table 6.2 (large box).

Both simulation cells provide results with differences lower than 0.1 fs in lifetimes and 0.03 eV in energies (which represents less than 5% in all the cases). Thus, we conclude that the regular box can be used to describe the energy and the decay dynamics of the molecular induced resonances at surfaces.

In the three cases, the surface strongly stabilizes the extra electron around the

Table 6.1: Energy, width and lifetime of the molecular anion of the three vinyl-derivatives adsorbed on Cu(100), using the regular box.

	ACA	ACN	ACO
E(eV)	-0.580	-0.475	-0.655
Γ (eV)	0.41	0.63	0.59
τ (fs)	1.61	1.04	1.12

Table 6.2: Energy, width and lifetime of the molecular anion of the three vinyl-derivatives adsorbed on Cu(100), using the large box.

	ACA	ACN	ACO
E(eV)	-0.582	-0.466	-0.679
Γ (eV)	0.42	0.65	0.59
τ (fs)	1.53	1.01	1.12

molecule: the obtained energies for the anionic states are negative (i.e., below the vacuum level), whereas in the gas phase the energy of the anion is positive with respect to the neutral molecule (the anion is thus, a resonance). With these energies, the extra electron would not be able to scape towards the vacuum and thus, the options would be remain around the molecule (which would be a bound state) or decay towards the metal.

All the three anionic states have energies which are above the Fermi level of the surface. For this reason the electron transference from the molecule to the substrate is energetically favourable. This is why the electron finally escapes from the molecule, whose anion becomes a resonance.

The RCT is extremelly efficient because of the strong interaction of the molecular states with the surface. As was previously shown in Chapters 4 and 5, the π states of the vinyl derivatives (both occupied and unoccupied) are mixed with the metal, which is a very effective decay channel towards the susbtrate. Because of this large coupling the lifetimes are extremelly short. The fact that the three anions exhibit a similar width ($\sim$ 0.5 eV) reflects that the decay channel is, in all the cases, due to the π-metal coupling path. Interestingly, the energies of the anions do not correlate with their lifetimes. Thus, the RCT efficiency (and width of the state) is given by the effectivity of the molecule-metal coupling. As it is shown in Chapter 4, in the acrylonitrile and the acrolein adsorbs in a almost total parallel orientation with respect to the metal surface. However, the NH_2 group of the acrylamide is oriented

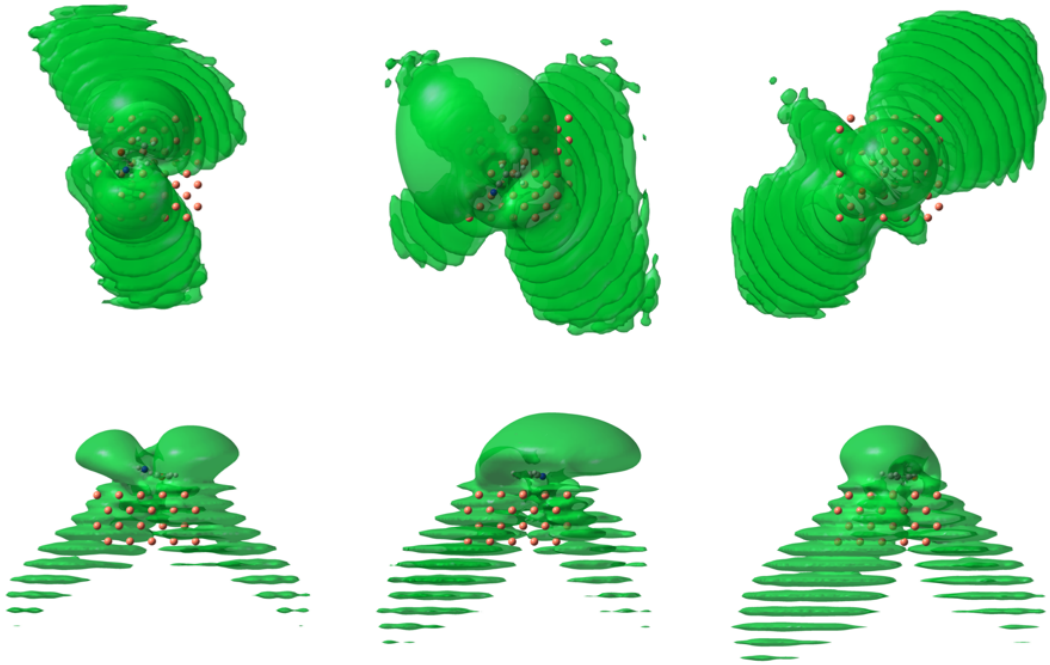

Figure 6.3: Density (isovalue=0.0025 a.u.) associated to the resonant wavefunctions of the molecular anion of the vinyl-derivatives on Cu(100). Top and lateral views are shown for acrylamide (left), acrylonitrile (center) and acrolein (right).

towards the vacuum. Then, the π^* orbital is not oriented totally perpendicular to the substrate and thus, for this reason, the coupling is less efficient.

The densities, modulus square of the resonant wavefunctions at $E = E_\alpha$, $|\psi(\vec{r})_\alpha|^2$, associated to the corresponding energies of the π^* of the three vinyl-derivatives on Cu(100) are shown in Figure 6.3.

In the three cases $|\psi(\vec{r})_\alpha|^2$ is characterized by the hybridization between the molecular LUMO orbital and valence band states of the metal: part of the density is localized on the molecule and the rest is spread in a decaying tail inside the metal. The density localized in the organic part retrieves the lobes as in the π^* molecular orbital in the gas phase. The decaying tail inside metal corresponds to the flux of electrons escaping from the decaying quasistationary molecule-localized state into the metal continuum. It presents oscillations due to the metal atomic layers. In addition, the flux of electrons outgoing from the molecule into the metal shows a well pronounced directionality. Thus, electrons escape from the molecule not along

the direction perpendicular to the surface plane, which is a shortest path to the metal, and intuitively, the easiest direction of an electron transfer. In contrast to this simple minded picture, the flux of escaping electrons is oriented at some angle with respect to the surface normal. To understand this behavior we have to analyze the electronic structure of the metal surface and the coupling with the π^* molecular orbital.

The model potential that we have used to model the metal depends only on the z-coordinate, the one perpendicular to the surface. The image potential for an electron in vacuum in front of the surface is smoothly matched with a periodic function inside metal bulk, where the periodicity is given by an arrangement of atomic planes parallel to the surface. The specific shape of the potential depends on the surface under study. The eigenfunctions of metal electrons can be writen in the form:

$$\psi_{\vec{k}_{||},E_z}(x,y,z) = \frac{1}{2\pi} e^{ik_x x} e^{ik_y y}\ \chi(E_z,z) = \frac{1}{2\pi} e^{i\vec{k}_{||}\vec{r}_{||}}\ \chi(E_z,z), \tag{6.10}$$

being the wave vector parallel to the surface $\vec{k}_{||} = (k_x, k_y)$, and $\vec{r}_{||} = (x, y)$. The energies of metal electrons are given by:

$$E = E_x + E_y + E_z = \frac{k_x^2 + k_y^2}{2} + E_z = \frac{k_{||}^2}{2} + E_z. \tag{6.11}$$

The metal states are characterized by the parabolic bands in the direction parallel to the surface, and the projected band structure effects are associated with an electron motion along the z-coordinate (see Figure 6.4). At $k_x = k_y = 0$, which is known as $\bar{\Gamma}$ point, the energy spectrum is given by E_z. The quantum number E_z runs over the continuous and discrete values corresponding to the metal bulk bands and surface localized states. Indeed, because of the periodic variation of the potential an electron propagation perpendicular to the surface is impossible inside metal within certain electron energy range. The projected energy gap opens in the metal band structure (*projected band gap*). Within the projected band gap, the 1D Schrodinger equation describing an electron motion along the z-coordinate admits solutions at discrete energies E_z with bound state wave functions localized at the surface. In 3D, the corresponding electron is moving freely parallel to the surface, and it is trapped in z-direction. Among the surface localized states one distinguishes the surface state (SS) and the image potential states (IPSs) [58, 69, 250]. The IPSs are the equivalent to Rydberg states in atoms and molecules, and emerge due to the image potential

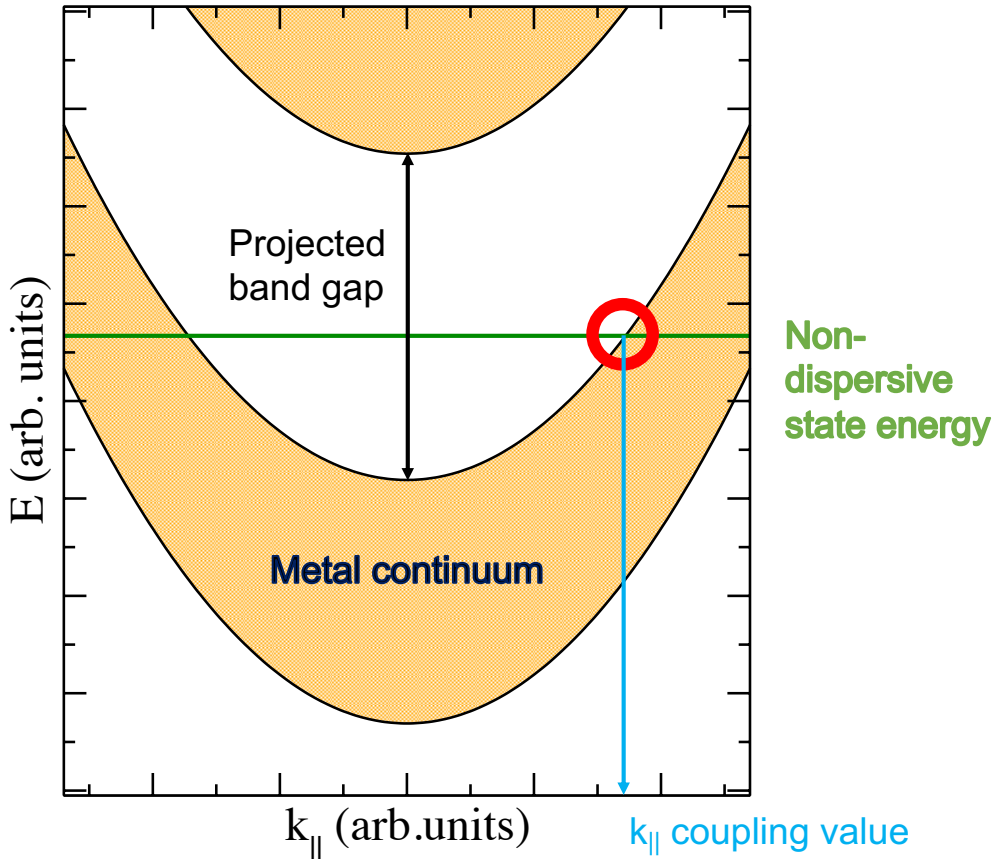

Figure 6.4: Scheme of the coupling of a localized (non-dispersive) state, in green, embedded in the projected band gap (white) with a dispersion relation proportional to $k_{||}^2$ in a free-particle model. At a given value of $k_{||}$, the localized state enters in the metallic continuum and is able to couple with the states of the metal.

tail outside the metal. In certain cases the SS and IPSs fall outside projected band gap and are broadedned into the resonances because of the possible electron escape into the bulk.

In the cases of the three molecules studied in this section the energy of the π^* molecular state of interest lies inside the projected band gap (X-gap of the Cu(100) surface, which is located between -3.02 eV and +3.08 eV with respect to the vacuum level). Thus, for the quasistationary molecular localized state, associated with π^* orbital, the decay via electron transfer towards the bulk states with $k_{||} = 0$ propagat-

ing perpendicular to the surface is impossible. An electron needs to take a different path, with a higher $k_{||}$ enough to reach the metal continuum. This is observed in all the three vinyl-derivatives. In Figure 6.4 we show a scheme of this situation.

For the Cu(100) model given by the 1D Chulkov potential, the value of the electron momentum parallel to the surface, $k_{||}$, needed to reach the energy resonance between the valence band state characterized by the energy E_z, and molecule localized state, can be calculated as $k_{||} = \sqrt{2(E_{\pi^*} - E_z)}$. In particular, the smallest possible value $k_{||}^{cv}$ (which we call *coupling value*) is given by $k_{||}^{cv} = \sqrt{2(E_{\pi^*} - E_{GB})}$, where E_{GB} is the energy of the bottom of the projected band gap taken at $\bar{\Gamma}$ point of the projected band structure. For the fixed E_z, different final momenta $\vec{k}_{||} = (k_x, k_y)$ are allowed as far as $(k_{||})^2 = k_x^2 + k_y^2$. The energy resonance conditions are isotropic regarding final electron momentum parallel to the surface with no preferential direction. Thus, the orientation of the decay along the well defined directions seen in Figure 6.3 arise from the properties of the molecular state. In this case, the π^* states have two nodes, whose influence extends inside the metal, reason why an angular dependence in the decay is observed (see upper part of Figure 6.3).

We have performed a deeper analysis of the decay channels of the resonant states associated with the π^* orbital. To this end, we looked at the contribution of final states characterized by $k_x = k_{||}\, cos(\alpha)$ and $k_y = k_{||}\, sin(\alpha)$ momenta into the outgoing wave packet in the asymptotic region inside the metal. Here α is an angle between the positive direction of the x-axis and the projection of an electron momentum on the plane parallel to the surface. The x-axis is directed along the $C_1{-}C_2$ molecular bond. The asymptotic region is characterized by the complete screening of the molecule induced potential so that only electron metal interaction potential determines the wave packet dynamics. The contribution of the different final states in the outgoing wave packet is given by:

$$c(k_x, k_y) = \int\int \psi(x, y, z_0)\, e^{ik_x x}\, e^{ik_y y} dx\, dy \tag{6.12}$$

As well, the analysis can be carried out in terms of $k_{||}$ and α,

$$c(k_{||}, \alpha) = \int\int \psi(x, y, z_0, t)\, e^{ik_{||} cos(\alpha)\, x}\, e^{ik_{||} sin(\alpha)\, y} dx\, dy \tag{6.13}$$

These studies are carried out for the calculations with "refined" initial state, when only the decaying molecular resonance contributes to the time dependent wave

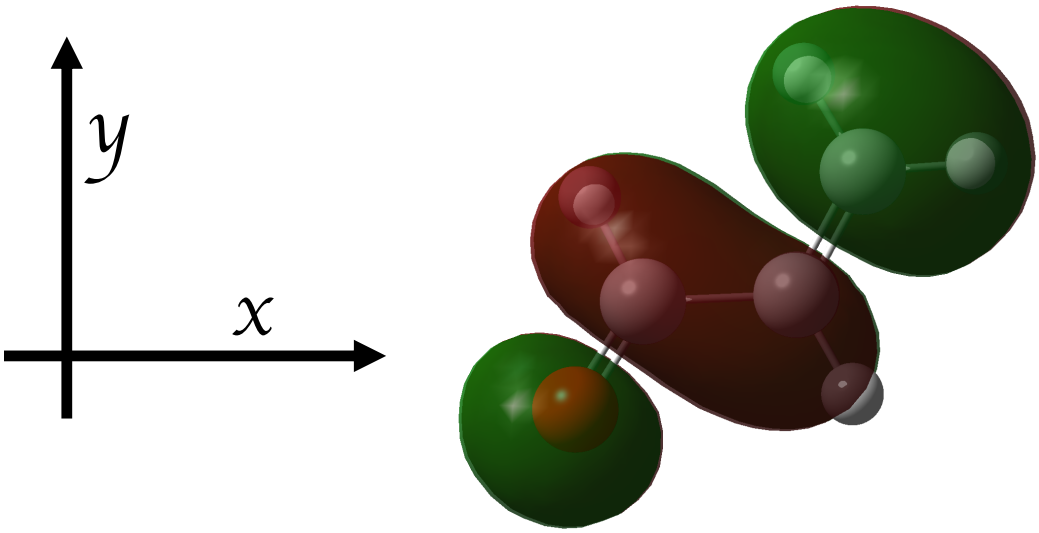

Figure 6.5: LUMO orbital of the acrolein. Red an green denotes different phases.

packet. We then obtained that while the amplitude of the projection coefficients varies in time according to the exponential decay low, their functional dependence on k_x, k_y becomes nearly time-independent as it is defined by the quasistationary state (see below).

Along with an asymptotic expansion (z_0 is taken in the assymptotic region inside metal), for the sake of comparison, we have also calculated the plane wave decomposition of the molecular π^* orbital of each molecule on the surface and in the gas phase (with the adsorption geometry). The molecular plane is not a good choice in this case since states with π symmetry have a nodal plane at this position. Therefore, for the angular analysis of the wavefunction the z value was chosen 1 atomic unit above the center of the $C_1{-}C_2$ bond. This choice provides good resolution of the coefficients. The corresponding $c(k_{||}, \alpha)$ coefficients are shown in Figures 6.6, 6.7 and 6.8 for the situation, when the absolute value of the wave vector parallel to the surface is fixed equal to $k_{||}^{cv}$. The resulting shape of the dependence on the angle α can be explained in terms of interference of decaying waves. At 45° respect to the axis defined by the $C_1{-}C_2$ bond (which are the two adjacent atoms that have the same phase in the π^* state) there is a maximum, due to the presence of the terminal atom. It acts as a focal point that is not annihilated with any other wave, since the atoms with the opposite phase are closer to the center of the molecule and thus, at large

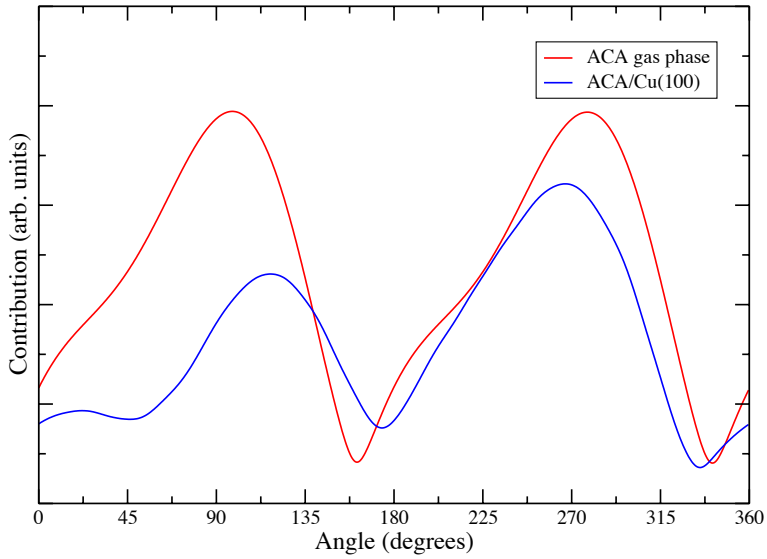

Figure 6.6: Weight of the plane waves with given modulus of $k_{||}$, as function of the angle, for the acrylamide.

distances, the terminal atom dominates. On the other hand, at 135^o with respect to the same axis, the central atoms and the terminal ones (with opposite phase), generate a destructive interference. In this general trend, some small deviations are observed due to the asymmetry of the molecule. In order to illustrate this, in Figure 6.5, we show the LUMO of the acrolein indicating the definition of the axis.

In the analysis of the wavefunctions of the molecules adsorbed on the surface, the minima are still in approximately the same angle. Some shifts are observed due to the rearrangement of the electron density, which affects the linear combination of the atomic orbitals to define the state. This is due to the dative interaction of the lone pairs with the surface and the back donation to the molecule, as described in Chapter 4.

In the case of the acrylonitrile and the acrolein, the gas phase and the adsorbed profiles are very similar. The transferred charge is distributed between the four non-hydrogen atoms which compose the molecule. Thus, these four focal points change in a similar way their emission. On the other hand, in the case of the acrylamide the nitrogen atom is slightly out of the plane pointing to the vacuum. For this reason, the weights of the p_z orbitals in the wavefunction are not the same with and without

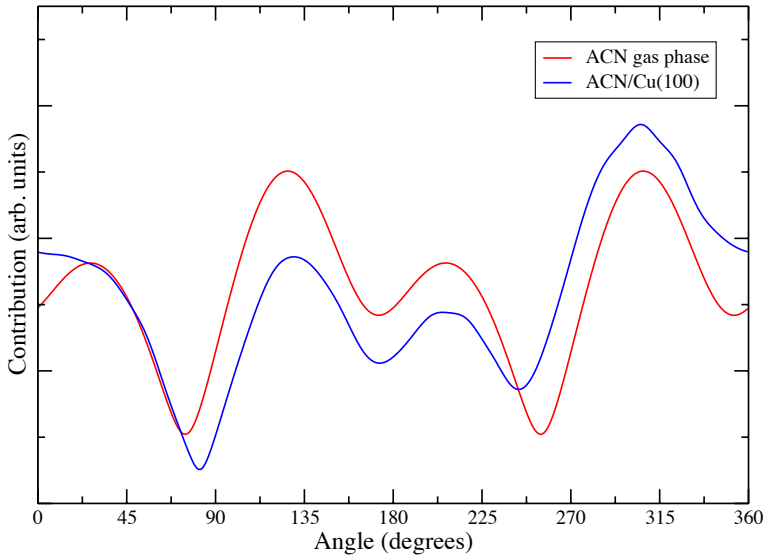

Figure 6.7: Weight of the plane waves with given modulus of $k_{||}$, as function of the angle, for the acrylonitrile.

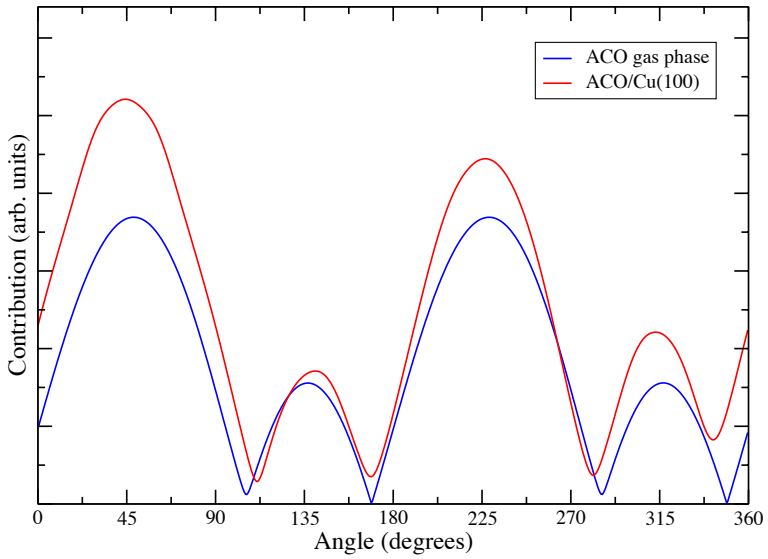

Figure 6.8: Weight of the plane waves with given modulus of $k_{||}$, as function of the angle, for the acrolein.

interaction with the metal and thus the angular profile is modified.

This analysis does not have to be restricted to a given $k_{||}$ and we can extend it to other values. The 2D maps of the $c(k_{||}, \alpha)$ coefficients calculated in the $(k_{||}, \alpha)$ plane are shown in Figure 6.9 (ACA), Figure 6.10 (ACN) and Figure 6.11 (ACO). In these analysis three different heights have been considered: z_0 = between molecule and metal, z_0 = the first metal surface layer, and z_0 = 6 a.u. below the first metal layer. Similar pattern is observed at any z: the decaying wave imprints the $k_{||}$ decomposition of the molecular orbital behind the resonance. This result can be understood using the Bardeen transfer hamiltonian theory [251–253]. routinely applied to explain the STM images or to address an electron transfer between atomic or molecular species and surfaces. Within this approach, the decay rate of the molecule in front of the surface is given by the golden rule equation

$$\Gamma = 2\pi\Sigma_{\vec{k}_{||},E_z} \left| M_{\vec{k}_{||},E_z} \right|^2, \tag{6.14}$$

The transition matrix elements, $M_{\vec{k}_{||},E_z}$ between the localized molecular state $\Psi_0(x,y,z)$ and metal states $\psi_{\vec{k}_{||},E_z}(x,y,z)$ are given by

$$M_{\vec{k}_{||},E_z} = \frac{1}{2} \iint_S \left[\psi_{\vec{k}_{||},E_z} \nabla\Psi_0^* - \Psi_0^* \nabla\psi_{\vec{k}_{||},E_z} \right], \tag{6.15}$$

where the integration runs over any surface in the potential barrier that separates a molecule from the metal. Obviously, the $\vec{k_{||}}$ structure of the transition matrix elements defining the electron flux in different $\vec{k_{||}}$ decay channels reflects the decomposition of the molecular orbital in the basis of plane waves parallel to the surface.

The main difference between the three z heights is that the waves with low value of $k_{||}$ have less contribution inside the metal. This is due to the fact that the outgoing wave is mainly located in the proximity of the molecule. In this region the bounded part of the wavefunction, which has a higher contribution of waves with low $k_{||}$ values, dominates. At deeper z, the effect of the molecule on the potential vanishes. Thus, there is no contribution of waves with $k_{||} = 0$, since the energy is inside of the projected band gap of the Chulkov potential.

If we would not have included the energy correction, the π^*-orbital would have a lower energy and thus, would be immersed into the continuum of electronic states

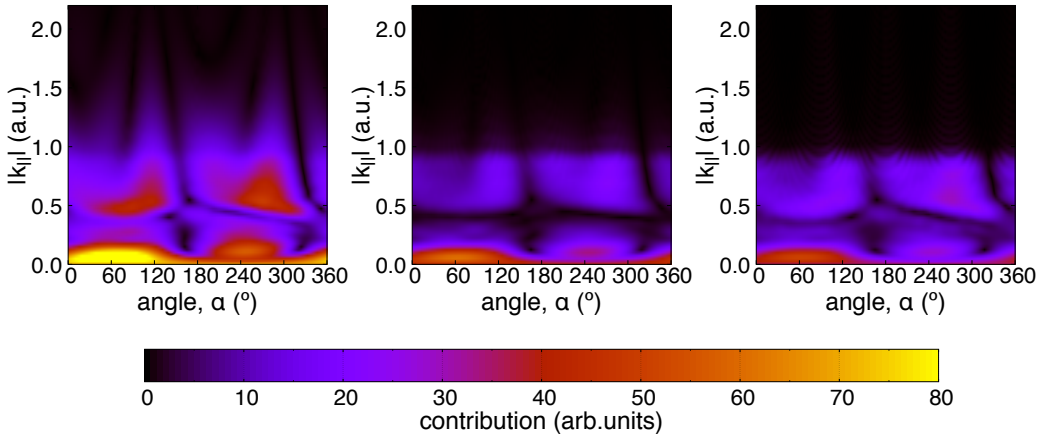

Figure 6.9: $|k_{||}|$-α analysis for the acrylamide between the molecule and the surface (left) in the first layer of the model (middle) and 6 a.u. below the first layer (right).

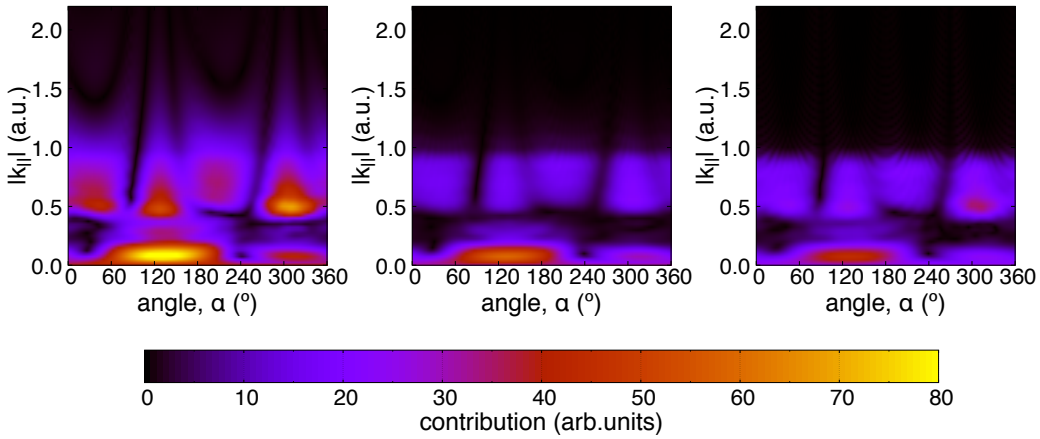

Figure 6.10: $|k_{||}|$-α analysis for the acrylonitrile between the molecule and the surface (left) in the first layer of the model (middle) and 6 a.u. below the first layer (right).

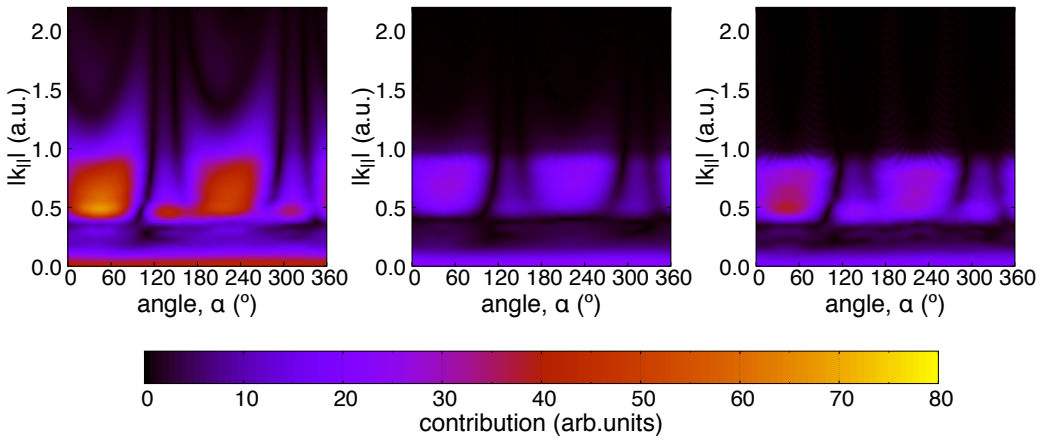

Figure 6.11: $|k_{||}|$-α analysis for the acrolein between the molecule and the surface (left) in the first layer of the model (middle) and 6 a.u. below the first layer (right).

of the metal below the projected band gap. This implies no restriction for the $k_{||} = 0$ decay, and the electron would be able to escape from the decaying state into the metal along the surface normal, which is the easiest direction of the electron transfer. In order to verify this, we have performed a propagation in the acrolein without the molecular projector. In this case the stabilization effect of the projected band gap which blocks the decay of the molecular localized state by an electron escape along the surface normal is absent. The computed width of the π^* resonance (its decay rate) increases to 0.65 eV, corresponding to the reduced lifetime of 1.01 fs. The new resonant wavefunction, where the $k_{||} = 0$ decay is dominant, is shown in Figure 6.12. This shows the huge importance of including the molecular projector in the Hamiltonian; not only to obtain a correct position in the spectrum but also to properly describe the coupling with the metal and thus to provide reliable values of the lifetime and decay paths.

For a deeper analysis, we have decomposed the wavefunction inside the metal (4 a.u. below the surface) in its k_x-k_y components for the cases of the acrolein adsorbed on Cu(100) with/without molecular projector (see Figure 6.13). This decomposition shows that, in the absence the correction, since the energy of the state lies in the metal continuum, even at $k_{||} = 0$ the coupling is possible, reason why there is a large contribution of the waves with $k_x = 0, k_y = 0$. On the other hand, if the energy is corrected, the energy of the resonant wavefuncion is inside the gap and thus, a higher

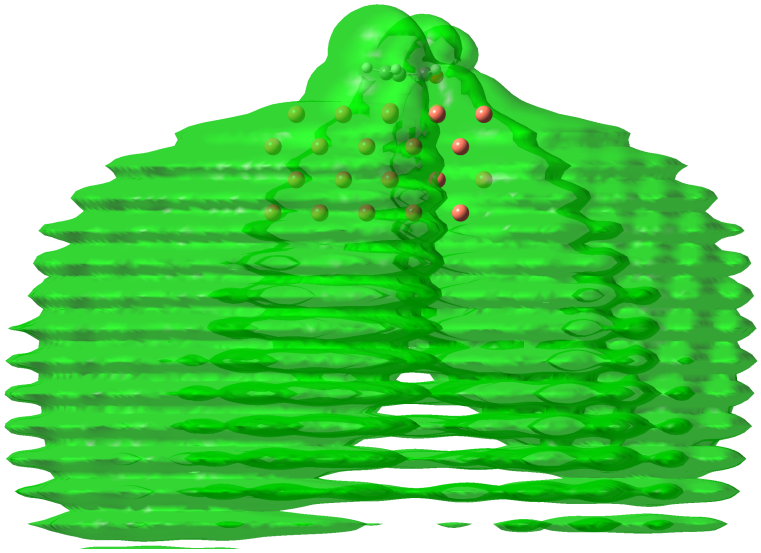

Figure 6.12: Decay of the π^* state of the acrolein in absence of the molecular projector (isovalue=0.001 a.u.).

value of $k_{||}$ is needed to reach the continuum and to have an effective coupling.

6.3.2 Effect of the substrate: energies and lifetimes of nitroethylene anion on different metal surfaces.

Through the study of the acrylamide, acrylonitrile and acrolein on Cu(100), we deeply analyzed the effect of the molecule. Despite the common character of the state (π^*), the three vinyl derivatives show different energies, lifetimes and angular patterns in their decay.

In order to understand the role of the surface, we have studied the nitroethylene anion on different surfaces: Cu(100), Cu(111) and a *jellium* model surface, which does not present a projected band gap. Nitroethylene is an appropriate molecule to carry out this study, since the molecular anion is a highly bound state and it falls

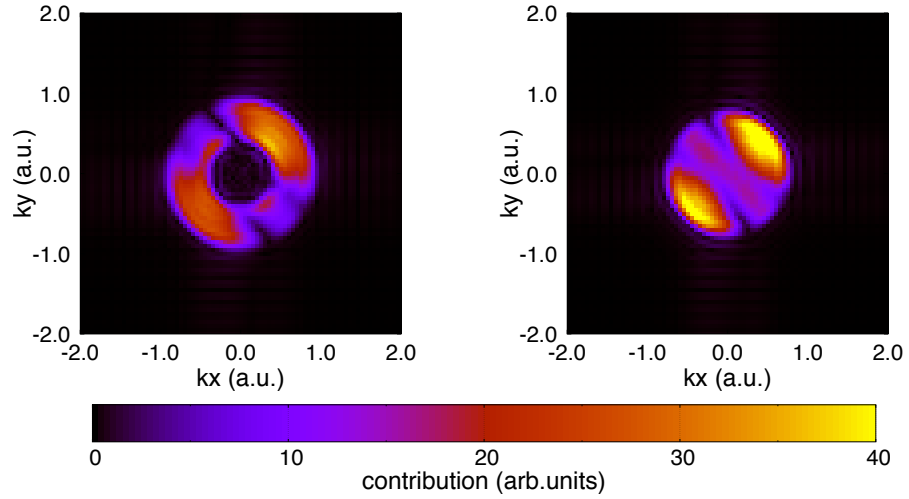

Figure 6.13: $k_x - k_y$ decomposition of the acrolein with (left) and without (right) molecular projector.

into the projected band gap (L-gap) of the Cu(111) surface.

We have used as initial wavefunction the π^* orbital of the molecule in the gas phase (this orbital hosts an extra electron for the negative molecular ion). To this end, using the Abinit code we performed a single point DFT calculation for the isolated molecule in the gas phase. The molecular geometry is set identical to that of the molecule adsorbed on the metal surface. The absorption geometry is determined from Density Functional Theory calculations with VASP, as in the case of the previously studied molecules.

A molecular projector was applied to the π^* state in order to correct the energy. The U parameter is 3.527 eV for the Cu(100) and the *jellium* surface (since we used the adsorption geometry of the Cu(100) to build the *jellium* model) and 3.454 eV for the Cu(111) surface. The slighly different value for the molecule on Cu(111) arises from the (small) change in the orbital energy due to the different molecular geometry on this substrate.

The results for the energies and lifetimes of the different molecular anions are summarized in Table 6.3, and the wavefunctions of the molecule localized quasistationary state obtained for different surfaces are shown in Figure 6.14.

If we analyze the lifetime on the three surfaces, we observe that the *jellium* surface shows the lowest lifetime, i.e. the fastest decay of the molecular anion by resonant

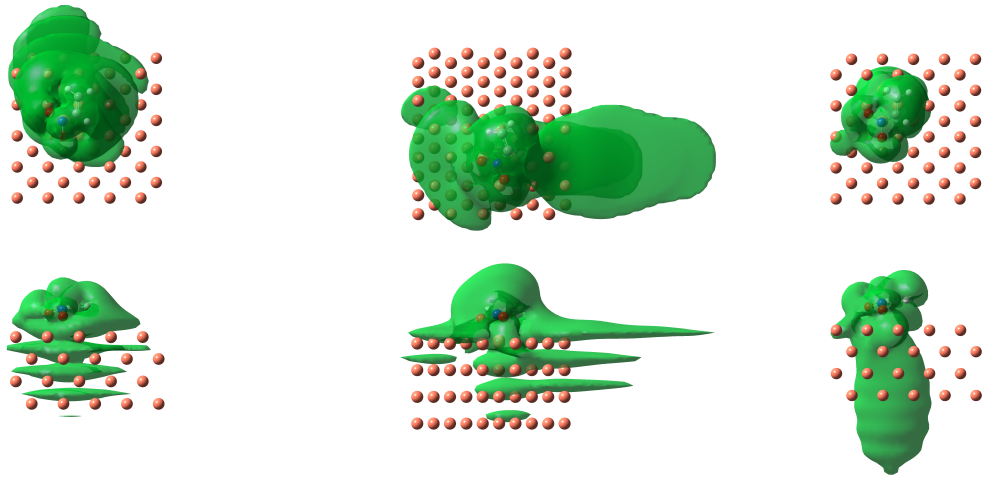

Figure 6.14: Top and lateral views of the density associated to the resonant wavefunction of the nitroethylene molecular anion on Cu(100) (left), Cu(111) (center) and the free electron surface (right). Isovalues=0.005 a.u.

energy conserving electron transfer from the molecular orbital into the continuum of valence band states of the metal. Indeed, no blocking effect of the projected band gap is present in this case, so that an electron can escape from the molecular potential well into the metal continuum along the surface normal. This is the most efficient direction for an electron transfer because of the shortest path with lowest potential barrier. This is nicely seen in Figure 6.14 which shows that in the *jellium* metal case the outgoing flux of electrons inside metal is strongly confined within the narrow cone around the direction perpendicular to the surface.

Among the two surfaces with a gap, the larger decay rate is obtained for Cu(111) surface. This is despite at $\bar{\Gamma}$ point, the negative ion resonance appears higher an energy from the gap bottom in Cu(111) as compared to Cu(100). As follows from

Table 6.3: Energy, width and lifetime of the nitroethylene molecular anion adsorbed on the different surfaces.

	Cu(100)	Cu(111)	*jellium*
E (eV)	-1.656	-1.024	-1.421
Γ (eV)	0.37	0.46	0.59
τ (fs)	1.78	1.43	1.12

Figure 6.15, which shows a scheme of the different $k_{||}$ states in resonance with molecular orbital in both cases, higher $k_{||}$ is required in order to reach the energy resonance with metal continuum states for Cu(111) surface as compared to Cu(100) surface. One would then expect stronger stabilization of the quasistationary state by the projected band gap effect for the Cu(111)-case. The reason for this apparent controversy consists in the contribution of the surface state continuum to the anion decay. Absent for Cu(100), the surface state of Cu(111) corresponds to am electron trapped at the metal vacuum interface and moving parallel to the surface. Because of the surface localization this state is strongly coupled with π^* orbital of the adsorbed molecule and represents an extremely efficient decay channel of the quasistationary state (similar findings have been reported for the decay of the H^- ion and quasistationary states localized on alkali adatoms on Cu surfaces [254, 255]. The corresponding panel of Figure 6.14 nicely illustrates the dominating decay channel of the molecular localized state into the surface state continuum with an outgoing electron flux moving parallel to the surface and the z-dependence of the wave function reflecting that of the surface state. Note that the contribution of the metal bulk to the decay is not visible at the scale of the figure.

As compared to the molecule localized states considered in the previous section, the energy of the negative ion resonance of the nitroethylene molecular ion on Cu(100) surface appears closer to the bottom of the gap. For this reason, a much lower $k_{||}$ is required in order to reach the resonance with metal continuum states. Te projected band gap effect leading to an electron escape into the metal at some angle with respect to the surface normal is then not seen in Figure 6.14 in sheer contrast to Figure 6.3.

All over, comparing results obtained here with different metals, the stabilization of the adsorbate localized electronic states by the projected band gap calculated for the molecular adsorbates is much less important than that found for alkali adatoms [255]. We explain this result by the different electronic structure of the adsorbate. The high polarizability of alkali atoms leads to the formation of the long-lived hybridized state pointing in z-direction outwards from the metal surface which enhances the band gap effect. This hybridized state is absent for molecular species addressed in our work.

Further insights can be gained from the plane wave decomposition of the wavefunctions in the plane parallel to the surface shown in Figure 6.16. According with

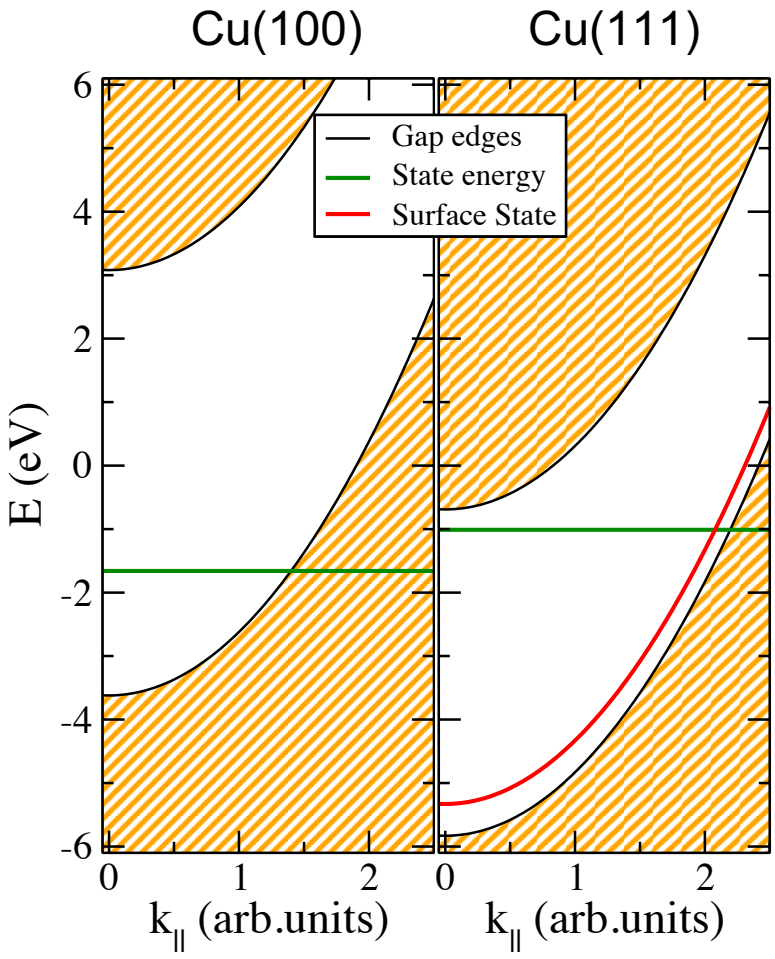

Figure 6.15: Energy diagram of the Cu(100) and Cu(111) surfaces coupled with the anion of the nitroethylene.

the energy position of the molecular anion resonance within the projected band gap, in the case of the Cu(111) surface there is a larger contribution of waves with high absolute values of $k_{||}$ as compared to the Cu(100) surface.

Moreover, this analysis also retrieves the angular distribution of the resonant wavefunction. This pattern can be explained by the interference of the p orbitals

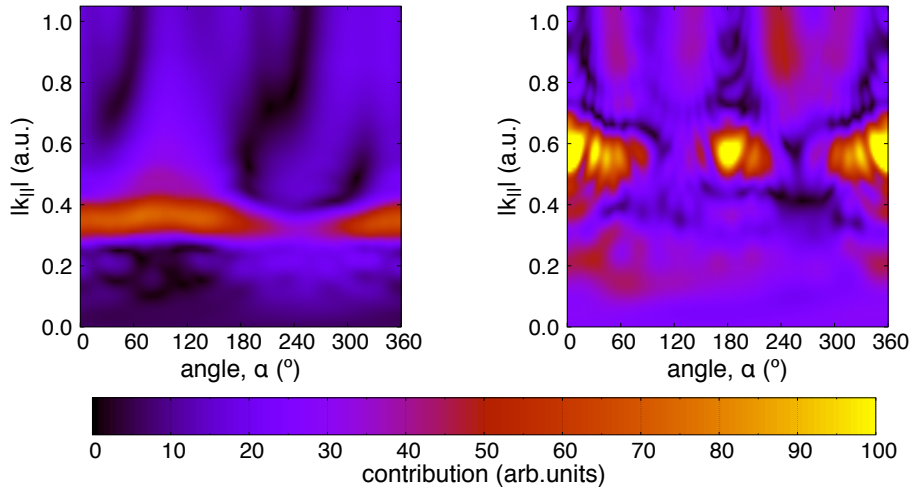

Figure 6.16: $|k_{||}|$-α analysis for the nitroethylene between the molecule and the surface on the Cu(100) (left) and the Cu(111) (right) surfaces.

which compose the π system (in Figure 6.17 this state is shown in the gas phase, in absence of interactions for comparison). To obtain further information, we have plotted (see Figure 6.18) the real part of the resonant wavefunction in the analysis plane for both surfaces, in order to get the phases of the focal points. In this way, we can understand the nature (constructive or destructive) of the interference.

Since in the case of the Cu(100) the coupling is given at low $k_{||}$, there is few spreading of the function parallel to the surface and thus, the emission in this direction has less intensity. On the other hand, on the Cu(111) surface, the most important contribution of the wavefunction is given in the surface state, enhancing the effect of the interference parallel to the surface.

The shape of the resonant wavefunctions, which are shown in Figure 6.14, exhibit a totally different behavior in the decay, depending on the surface (see Figure 6.16). In the case of the Cu(100) surface, few angular dependence is observed, although the contribution of $k_{||} = 0$ is small. On the other hand, in the Cu(111) the decay is mainly along the surface state, with a clear orientation. This can be attributed to the fact that the π^* state on the Cu(111) has an energy closer to the gap edge. Thus, a higher value of $k_{||}$ is required to reach the continuum or, as in this case, the surface state. Thus, the efficiency interference of the p_z orbitals of the π system is different.

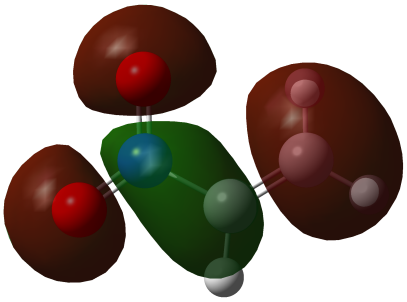

Figure 6.17: π^* state of the nitroethylene in the gas phase. Red and green denote different phases.

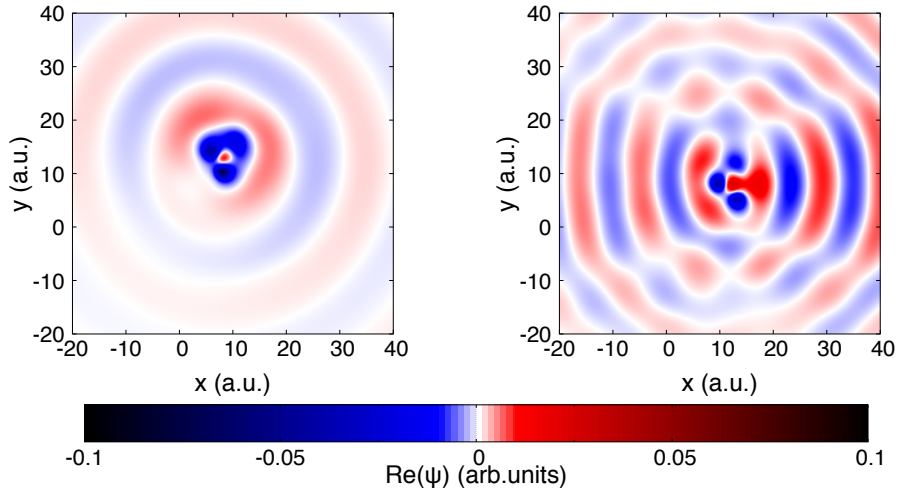

Figure 6.18: Phase (real part) of the wavefunctions between the nitroethylene and first metal layer. Left: Cu(100) surface. Right: Cu(111) surface.

6.3.3 Decoupling molecule and metal surfaces with ultrathin ionic films.

In previous sections it has been shown that usually anionic molecular states have a very short lifetime. Although depending on the molecule and the substrate the lifetime changes, the resonant electron transfer into the metal is extremely efficient in quenching the population of molecular localized states with energies above the Fermi level. As a consequence, this might inhibit many processes associated with these states as intermediates such as surface reactivity and luminescence, for example.

The way around this difficulty is to (partially) decouple electronic states localized on surface supported molecule from the continuum of the electronic states of the metal so that the lifetimes of the molecular resonances are increased. In practice, one can use a configuration where organic molecules are adsorbed on the ultra thin ionic crystal films deposited at metal surfaces or on other molecules [8, 256–258]. In these systems, owing to its broad band gap, an ionic crystal film plays a role of the "buffer" or decoupling layer. Then, if the anionic and/or excited molecular state is populated using photoexcitation or STM (scanning tunnel microscopy) techniques [11, 248, 249, 259], the active electron can be kept for sufficiently long time on a given molecular orbital. In this case, the energy that was acquired as an electronic excitation can induce atomic rearrangement, including bond breaking, or photon emission [222, 260, 261]. Although many experimental works routinely rely nowadays on this approach, efficiency of which has been proven empirically, the theoretical description of the decay of the population of the molecule localized states in these systems is completely missing. Some insights can be gained from the 2PPE experiments and theoretical studies of the lifetimes of the image potential and interface states for the metal surfaces covered with rare gas or ionic crystal films [262–264]. However these studies address the electronic states delocalized in the direction parallel to the surface. As to the adsorbed molecules, most of the theoretical work focused so far on a static picture, such as the DFT studies of adsorption geometries and charge transfer processes [147, 148, 265, 266] in the ground state.

Our aim is, using the WPP studies of the dynamics of the active electron in the molecule/ionic-crystal-film/metal system, to get a deeper understanding of the decoupling process. We particularly focus on the change of the lifetime of the molecular localized resonances owing to the band gap of the ionic crystal film which can be associated with a potential barrier between the molecule and the metal. As an ionic crystal we consider NaCl, which is often used in the experimental studies as a decoupling layer.

As a molecular specie for this study we use the nitroethylene molecule. As we have explained previously in Section 6.3.2, this choice is made because the free-standing molecular anion is a highly bounded state. In difference to negative ion resonances, there is no decay towards the vacuum. An absence of the population decay channels different from the electron transfer to the metal makes the nitroethylene molecule an ideal candidate to study the effect of the decoupling from the metal associated

with presence of insulating layers, such as sodium chloride.

For the molecular adsorption on the metal surfaces covered with ionic crystal films, the ground state calculations have demonstrated that the charge transfer between the molecule and the substrate is drastically reduced even for the 1 ML thick ionic crystal film [147,148]. This implies that an adsorbed molecule shows nearly the same distribution of electron density as the molecule in the gas phase (if changes in geometry are small, which is the most common case). Therefore, for the calculations of the decay of the quasistationary molecule-localized electronic states, the total potential $V(x, y, z)$ seen by an active electron in the adsorbed molecule/NaCl/metal system can be described as the sum of several terms:

$$V = V_{mol}^{DFT} + V_{\mathrm{NaCl}} + V_{\mathrm{Cu(100)}}. \tag{6.16}$$

Here, V_{mol}^{DFT} is the electron-molecule interaction potential derived, as explained in the main theory chapter, from the ab initio DFT calculations of the individual molecule in the gas phase using an absorption geometry (atomic arrangement within the molecule). Potentials for the NaCl films of several ML thickness, V_{NaCl}, are calculated using the model developed by S. Díaz-Tendero *et al* [139], which has been shown to provide an excellent results for the image potential and interface states for metal surfaces covered with ionic crystal films. Finally, the last term in Eq. (6.16) stands for the model potential of an electron interaction with metal surface proposed by Chulkov and collaborators [69]. Since the Cu(100) surface was used in the previous chapters to study the effect of the molecular specie on the lifetimes of the molecular localized states, we use the same surface to analyze the effect of the decoupling.

Along with the energy and lifetime of the anionic nitroethylene deposited on Cu(100) surface covered with several ML thick NaCl film, we have also obtained the energy and lifetime of the nitroethylene on pristine Cu(100) surface using model potential given by Eq. (6.16) where we set $V_{NaCl} = 0$. Note, that in contrast with procedure developed for the molecules adsorbed on metal surfaces in the main theory chapter and used in preceding sections, this approach does not account for the change redistribution between an adsorbed molecule and metal surface due to the interaction.

We neglect this effect purposely here, which allows to perform a direct comparison with results obtained for the molecule/NaCl/metal system, and to elucidate the role played by the NaCl layer in dynamics of quasistationary sates.

Table 6.4: Energy, width, decimal logarithm of the width and lifetimes of the anionic nitroethylene on the Cu(100) surface, clean and covered by 1, 2 and 3 NaCl monolayers.

# NaCl ML	Energy (eV)	Γ (eV)	$log_{10}(\Gamma)$	τ (fs)
0 (no $\Delta\rho$)	-5.950	$4.50 \cdot 10^{-1}$	-0.347	$1.46 \cdot 10^{0}$
0 (with $\Delta\rho$)	-1.656	$3.70 \cdot 10^{-1}$	-0.432	$1.78 \cdot 10^{0}$
1	-2.539	$3.43 \cdot 10^{-3}$	-2.465	$1.92 \cdot 10^{2}$
2	-2.445	$4.48 \cdot 10^{-5}$	-4.349	$1.47 \cdot 10^{4}$
3	-2.231	$1.53 \cdot 10^{-6}$	-5.815	$4.30 \cdot 10^{5}$

Our results are summarized in Table 6.4.

There is an evident difference in the values of the energy of the nitroethylene anion adsorbed on the clean Cu(100), without NaCl, depending whether a simplified form $V = V_{mol}^{DFT} + V_{\mathrm{Cu(100)}}$, or the full potential model developed in Chapter 3 is used in the WPP calculations of the active electron dynamics. Indeed, as discussed in Chapter 3 in the adsorption ground state there is a partial electron transfer between a molecule and the surface (this stationary redistribution of an electron density in the ground state not to be mixed with electron dynamics in excited states at the core of our work.) An adsorbed molecule acquires electron density from the surface and thus, the extra electron evolving in the quasistationary orbital of molecular anion has lower binding energy because of the higher screening of the nuclei. For this reason, account for the partial electron transfer from the metal to the molecule with associated electron density change $\Delta\rho$ changes drastically the WPP value of the resonant energy. The corresponding definition of the potential seen by an active electron is outlined in great details in Chapter 3. In the case of the nitroethylene, due to the huge electronegativity of the nitro group, this effect is of special importance.

The widths of the nitroethylene anion adsorbed on the clean Cu(100), without NaCl coverage are less sensitive to the effect of the charge transfer, with globally very fast decay of the population of the π^* orbital towards the metal. One can notice however that when the $\Delta\rho$ effect is accounted for the clean Cu(100) surface (0 ML coverage), the energy of the quasistationary state falls within the projected band gap of Cu(100). Then the gap stabilization effect is operative and the decay rate of the molecule localized resonance is smaller than for the calculation neglecting the charge redistribution in the ground state $\Delta\rho = 0$, where the anion resonance falls energetically below the X-gap of the Cu(100) surface.

Compared to this small variation above, when the NaCl film is introduced between the molecule and metal surface it inhibits the molecule-surface resonant electron transfer and leads to the orders of magnitude smaller decay rate of the molecular anion population with corresponding increase of the lifetime.

Basically, every added monolayer results in 10^2 times decrease of the width of the molecular localized resonance with π^* character. This exponential dependence is clearly seen in Figure 6.19, where we show the decay rate Γ as a function of the number of NaCl atomic layers between the Cu(100) surface and the nitroethylene. The calculated widths fit an exponential function (a line if the logarithm of the width is plotted), which is in good agreement with the experimental measurements that point out a huge stabilization of the resonant states even with few insulator monolayers. For 0 layers (clean surface), both results, with and without $\Delta\rho$ effect, are plotted. These results are quite similar and the trendlines considering one or the other are essentially the same. This is due to the fact that even the case where the effect of the charge transfer is expected to be higher (no NaCl monolayer) the width barely changes.

In Figure 6.20, 2D cuts of resonant wavefunctions of nitroethylene on Cu(100) with 0, 1, 2 and 3 NaCl layers are shown.

Increasing the number of salt layers decouples the molecule from the surface. The decay rate of the quasistationary π^*-anionic state becomes smaller and thus the flux of the electrons leaving the molecule localized orbital and moving inside metal is strongly reduced with each subsequent ML of NaCl. For the 3ML coverage the decay rate becomes so small that we basically deal with a localized bound state wave function without the continuum part. The narrow width of the resonance explains the difficulty to address the system with standard quantum chemistry approaches within the supercell geometry. Indeed, the size of the cell has to be very large so that several quantized states would fall within the energy range given by the resonance width allowing its determination.

Consider the simple model of the molecule-surface charge transfer. Lets express the wave function of the decaying state in the basis of molecule and surface states

$$\psi = \Lambda \left(\phi_{\pi^*} + \sum_{\vec{k}} c_{\vec{k}} \phi_{\vec{k}} \right) \tag{6.17}$$

where ϕ_{π^*} and $\phi_{\vec{k}}$ are, respectively, the eigenfunctions of the molecule and the sub-

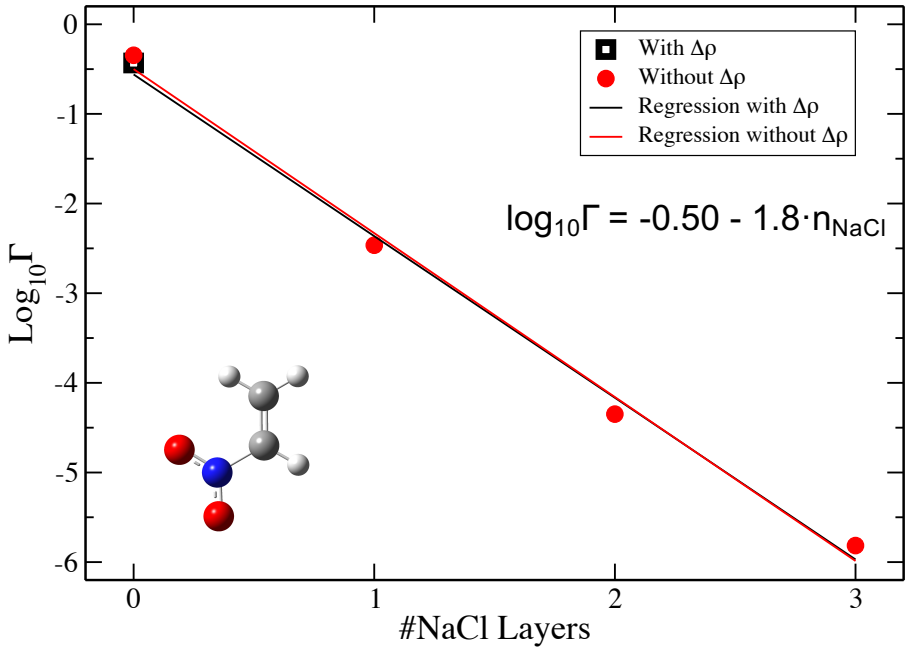

Figure 6.19: Logarithm of the width of the π^*-anionic state of the nitroethylene on nNaCl/Cu(100) as function of the number of salt layers. The mathematical expression corresponds to the trendline considering all the points without $\Delta\rho$.

strate in absence of interaction (Λ is here a normalization constant). The decaying quasistationary state can be associated with an eigenfunction of the molecular surface Hamiltonian satisfying outgoing wave boundary conditions. Where, within the basis of the ϕ_{π^*} and $\phi_{\vec{k}}$ states, the Hamiltonian of the system can be expressed as:

$$H = \begin{pmatrix} E_{\pi^*} & V_{m-s} \\ V_{m-s}^* & E_s \end{pmatrix} \tag{6.18}$$

Here E_{π^*} is the energy of the π^* orbital, E_s is the diagonal matrix with energies of the $\phi_{\vec{k}}$ states, and V_{m-s} is the coupling matrix between the molecular localized and substrate states. Reduction of the continuum part in the resonance wave function ψ with increasing number of salt layers is thus linked with decrease of V_{m-s}.

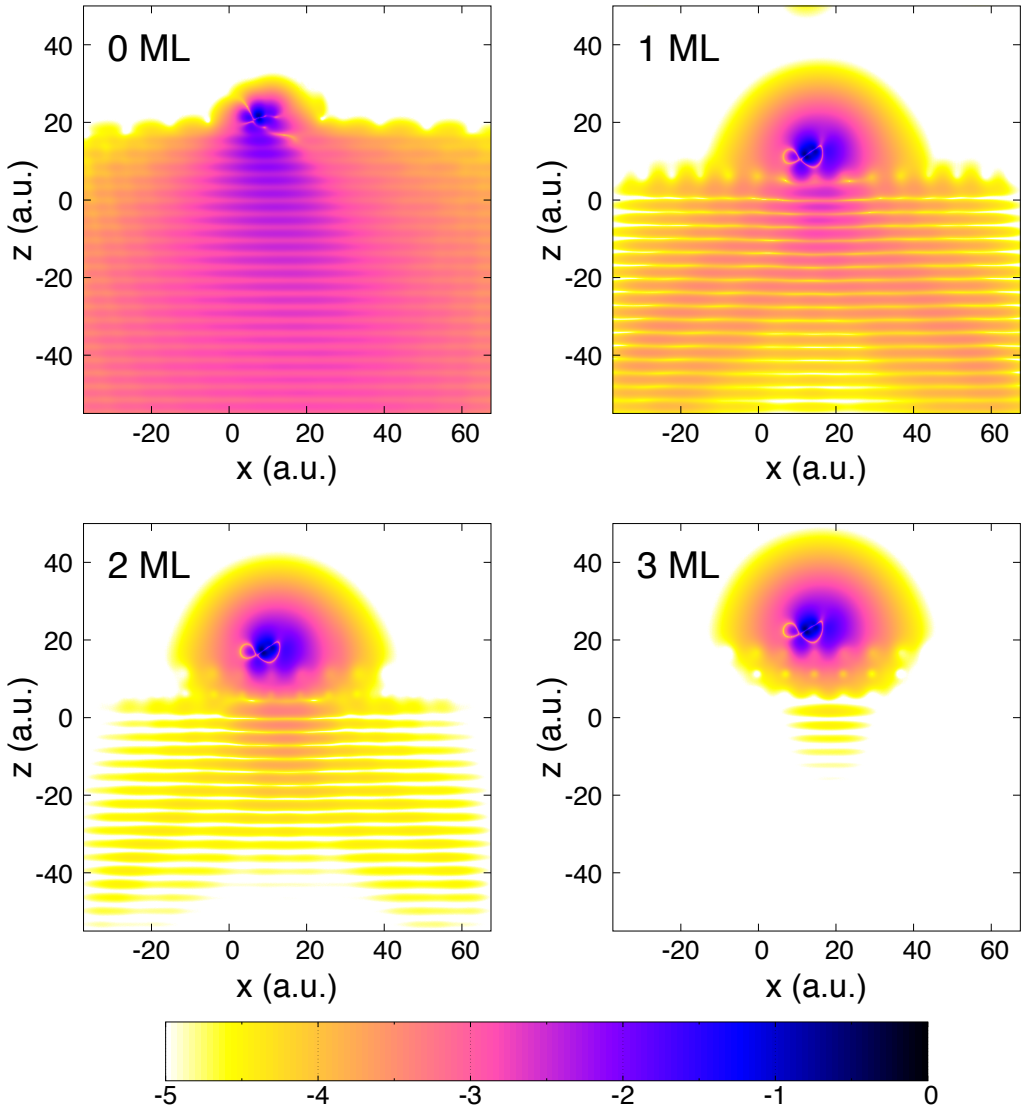

Figure 6.20: 2D cut (xz plane) of the logarithm of the density associated to the resonant wavefunction for the nitroethylene on Cu(100), covered by 0, 1, 2 and 3 NaCl layers. The value of the y coordinate is the one that contains the nitrogen atom.

Recently, single-molecule fluorescence induced by a scanning tunnel microscope (STM) has been measured experimentally [267,268]. In these works, different authors probed the enhancing of the signal due to decoupling induced by insulator layers. In these cases, the lifetime is a key factor: if an excited electron escapes from the molecular orbital into the continuum of metal states on a time scales much shorter than those of optical transitions, the fluorescence is quenched. Thus, the presence of ionic layers decouples molecule and metal surface enhancing the lifetime of the excited or anionic molecular state.

One of the systems that has been used in the STM induced luminescence experiments is the Zn-phthalocyanine [11]. Apart from the studies cited above, this molecule has a remarkable scientific interest for the wide range of applications, such as optoelectronics, nanodevices, molecular photovoltaics... [269–271].

For this reason, along with the nitroethylene anion, we have also carried out the WPP study of the Zn-porphyrin on the clean Cu(100) surface and Cu(100) surface covered with 1ML, 2ML, and 3ML NaCl films. Porphyrin is a molecule similar to the phthalocyanine and it presents the same kind of interactions with the surface (through the π system and the metallic center). In this system there is no intrinsic dipole, in contrast with the large dipole in nitroethylene. For the free-standing molecule, the extra-electron forming molecular anion is delocalized in a very extended spatially π orbital. Extending our work to Zn-porphyrin allows us to study if there is a common trend of the decoupling due to the salt layers. Since both molecules (porphyrin and phthalocianyne) are expected to behave in a similar way, we expect to obtain results allowing direct comparison with findings reported in the STM induced luminescence experiments [11, 24, 248]. Our main interest in this system is the evolution of the lifetime with the number of spacer NaCl mono-layers. This property barely changes with the inclusion of $\Delta\rho$ effect, as it was shown with the study of the nitroethylene. Therefore, we neglected the charge transfer in the ground state system associated with molecular adsorption. The 2D cuts (xz) densities of the resonant wavefunctions are shown in Figure 6.21, the numerical values of the calculated quantities are given in Table 6.5, and the in Figure 6.22 we show the evolution of the resonance decay rate with number of NaCl spacer mono-layers with emphasis on the exponential dependence of Γ on the thickness of the salt film.

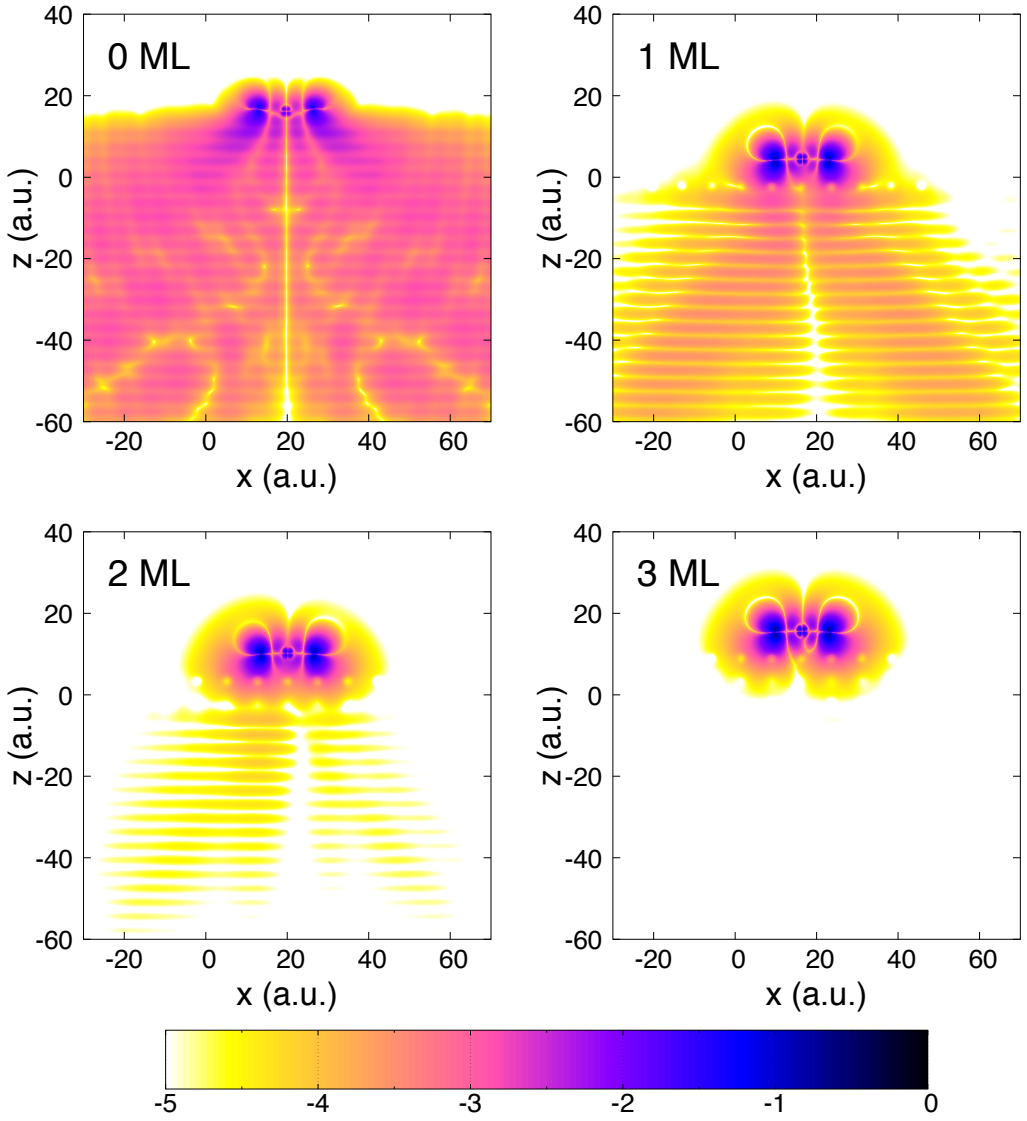

Figure 6.21: 2D cut (xz plane) of the logarithm of the density associated to the resonant wavefunction of the Zn-porphyrin on Cu(100), covered by 0, 1, 2 and 3 NaCl layers. The value of the y coordinate is the one that contains the Zn atom.

Table 6.5: Energy, width, decimal logarithm and lifetimes of the width of the anionic porphyrin on the Cu(100) surface, clean and covered by 1, 2 and 3 NaCl monolayers.

# NaCl ML	Energy (eV)	Γ (eV)	$log_{10}(\Gamma)$	τ (fs)
0	-5.405	$5.35 \cdot 10^{-1}$	-0.272	$1.23 \cdot 10^{0}$
1	-2.826	$1.97 \cdot 10^{-3}$	-2.706	$3.34 \cdot 10^{2}$
2	-2.689	$1.55 \cdot 10^{-5}$	-4.810	$4.25 \cdot 10^{4}$
3	-2.510	$1.22 \cdot 10^{-6}$	-5.914	$5.40 \cdot 10^{5}$

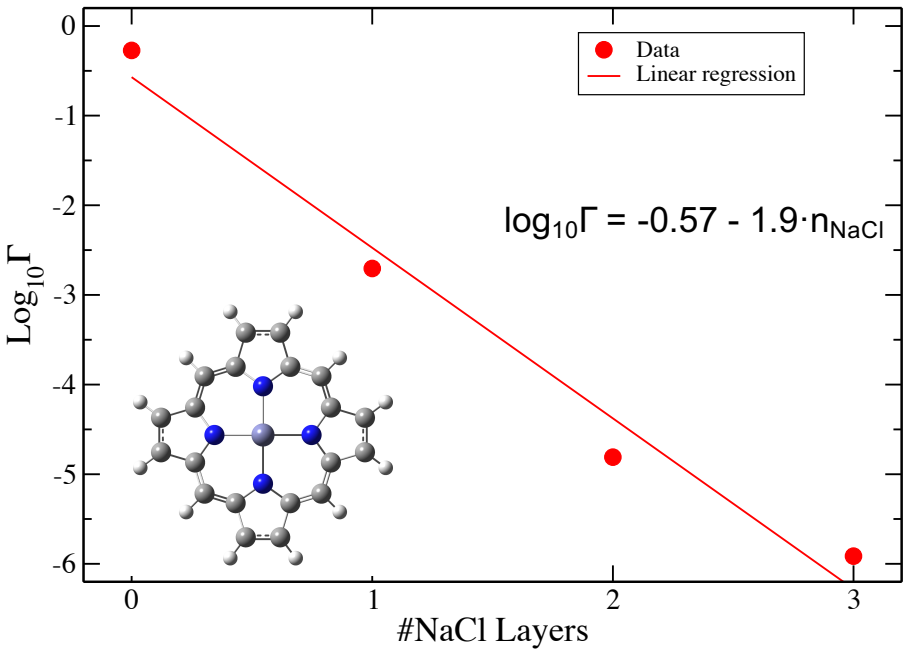

Figure 6.22: Logarithm of the width of the π^*-anionic state of the Zn-porphyrin on nNaCl/Cu(100) as function of the number of salt layers.

As in the case of the nitroethylene, the logarithm of the width of the π^*-molecular resonance follows a linear dependence on the number of NaCl layers. Even the lifetimes in the absence of salt layers are similar for both molecules. This is due to the previously mentioned high efficiency of a metal surface as decay channel for extra electrons deposited on organic molecules leading to nearly universal $\sim 0.4 - 0.5$ eV decay rates in all considered cases.

Surprisingly, not only the intercept but also the slope of the $\log_{10}\Gamma$ dependence on the film thickness is similar for nitroethylene and Zn-porphyrin molecules. If we consider the sodium chloride as a barrier, the transmission coefficient, in atomic units, is given by (see Complement H_I in [272])

$$T = \frac{4E(V-E)}{4E(V-E) + V^2 sinh^2[\sqrt{2m(V-E)}l]} \tag{6.19}$$

where E is the energy of the incident wave (the energy of the state of interest in our case), V is the potential of the barrier (conduction band of NaCl in this case), l is the length of the barrier (thickness of the salt) and m is the mass of the particle. If $\left[\sqrt{2m(V-E)} \cdot l\right] >> 1$ we can write Equation 6.19 approximately as:

$$T \approx \frac{16E(V-E)}{V^2} e^{-2\sqrt{2m(V-E)}\cdot l} \tag{6.20}$$

Now, if we take the logarithm of both sides (the basis of the logarithm only would affect the slope, not the shape):

$$ln(T(l)) = ln\frac{16E(V-E)}{V^2} - 2\sqrt{2m(V-E)} \cdot l \tag{6.21}$$

Therefore, this simple model shows how the transmission probability (and thus, the lifetime) follows an exponential decay, which is a function of the thickness (or number of layers) of the salt, explaining the trends obtained with the WPP simulations.

Chapter 7

Conclusiones

En esta tesis se ha presentado un estudio teórico de la estructura y estabilidad de moléculas orgánicas adsorbidas en superficies metálicas. Concretamente se han estudiado tres derivados del vinilo (acrilamida, acrilonitrilo y acroleína) sobre dos superficies de Cu: Cu(100), de simetría cuadrada, y Cu(111), de simetría hexagonal. Para ello, los cálculos han sido realizados en el marco de la teoría del funcional de la densidad (DFT), con funcionales de la familia GGA (PBE y derivados del mismo). De esta parte del trabajo se han obtenido las siguientes conclusiones:

- La inclusión de interacciones débiles resulta de gran importancia para la correcta descripción de la adsorción de las moléculas estudiadas sobre superficies metálicas, llegando a obtener estructuras cualitativamente distintas si estas fuerzas no son consideradas.

- El método D2 de Grimme sistemáticamente predice energías de adsorción superiores a las obtenidas con funcionales de van der Waals, incluso aunque la corrección D2 sea incluida únicamente en los átomos de la molécula y en los átomos de la última capa de la superficie metálica.

- La geometría de estos sistemas es poco dependiente de la precisión con la que se explora el espacio reciproco, por lo que en una celda de tamaño 5x5, como las utilizadas en esta tesis, el punto Γ es suficiente para obtener geometrías correctas.

- Por el carácter metálico del sustrato, es necesario mejorar la descripción del espacio reciproco para obtener energías de adsorción convergidas. Por ello,

obtener la energía con un grid más fino del espacio K, como 331, sobre una geometría obtenida con el punto Γ, parece ser un buen compromiso entre la calidad del calculo y el tiempo requerido.

- Los derivados de vinilo interaccionan principalmente a través del enlace π, que se sitúa en posición top. En estos sistemas, también se aprecia una preferencia por una interacción en top con pares de electrones sin compartir.

- El análisis de la densidad de estados proyectada muestra que los estados moleculares más implicados en la interacción con la superficie son los de simetría π. La interacción por tanto tiene una componente importante de efecto de donación de la molécula al metal (orbitales π ocupados y pares sin compartir) y retrodonación de la superficie a la molécula, a través del orbital π^*.

- Debido a la interacción hay un flujo neto de densidad electrónica del metal a la molécula. Esta carga se sitúa espacialmente en una región muy similar al orbital LUMO en cada caso, con independencia de la superficie (cuadrada o hexagonal) de adsorción. Sin embargo, no existe una tendencia clara en el valor de la carga transferida con la superficie ni existe una correlación con la energía de adsorción.

- Las energías de adsorción en Cu(111) son menores que en Cu(100). La diferencia entre la adsorción más favorable de cada molécula entre ambas superficies es superior a 100 meV en los tres casos. Por ello, frente a derivados del vinilo, la cara (100) del cobre se muestra más reactiva que la cara (111).

- Debido a la interacción de las moléculas con la superficie, la energía asociada a los modos normales de vibración cambia. Por ese motivo, diferentes energías son necesarias para promover excitaciones vibracionales en las moléculas cuando éstas están adsorbidas respecto a la que sería necesaria fase gas.

- Los cálculos de dinámica molecular basados en la aproximación de Born-Oppenheimer han demostrado que la distribución de la energía cinética depositada inicialmente en estas moléculas es muy rápida y una situación cuasiestacionaria se alcanza en aproximadamente 100 fs.

- A pesar de que la superficie toma parte de la energía aportada a las moléculas, la fragmentación es más habitual cuando la molécula interacciona con el

substrato, debido al efecto catalítico que éste presenta.

- La superficie no sólo aumenta la probabilidad de ruptura, sino que además favorece ciertos fragmentos que se estabilizan por la interacción con el metal, como radicales, que son altamente inestables en fase gas.

Posteriormente, sobre las estructuras obtenidas en la primera parte de la tesis, se ha realizado un estudio de dinámica electrónica, con técnicas de propagación de paquetes de onda (WPP), con la cual se han estudiado los estados aniónicos de las moléculas adsorbidas en Cu(100) y Cu(100) recubierto de capas ultrafinas (1, 2 y 3 capas atómicas de espesor) de NaCl. En esta parte del trabajo las conclusiones obtenidas han sido:

- El tiempo de vida de un electrón en una molécula adsorbida directamente sobre una superficie metálica es extremadamente corto, del orden de los fs: el metal se muestra como un muy eficiente canal de salida del electrón activo.

- En el decaimiento del electrón extra hacia el metal, existe un patrón angular con nodos similares a los que presenta la función de onda del orbital donde se sitúa el electrón extra: la simetría de la molécula determina la simetría del canal de salida del electrón.

- La existencia de un gap proyectado en Γ en la estructura electrónica de la superficie metálica afecta al decaimiento del electrón hacia el sólido. Si el estado aniónico se encuentra dentro del gap, el electrón no puede avanzar perpendicularmente respecto la superficie. Esto afecta al mecanismo de relajación y, por tanto, al tiempo de vida del electrón en la molécula.

- En la superficie (111) del Cu el estado de superficie se encuentra dentro del gap proyectado. Esto hace que estados aniónicos en este rango de energías se acoplen preferiblemente con este estado, a diferencia del caso de la superficie (100), donde el acoplamiento es directamente con el continuo metálico. Por este motivo, en la superficie de Cu(111) el decaimiento es principalmente paralelo a la superficie, con una penetración menor que en Cu(100).

- La presencia de capas aislantes iónicas desacoplan los estados moleculares de los del metal. Una capa de espesor atómico es suficiente para que los tiempos

de vida del electrón en la molécula sean del orden de cientos de fs, suficiente para inducir reactividad con la inyección de electrones.

- El desacoplamiento genera un cambio del tiempo de vida que resulta exponencial con el grosor de la capa de aislante (con el número de capas). Esta tendencia no depende del sistema que soporte el electrón extra y parece ser un comportamiento universal en moléculas de muy diferente naturaleza.

Chapter 8

Conclusions

In this thesis a theoretical study of the structure and stability of organic molecules adsorbed on metal surfaces is presented. Specifically, we have studied three vinyl-derivatives (acrylamide, acrylonitrile and acrolein) on two copper surfaces: Cu(100), with square symmetry, and Cu(111), with hexagonal symmetry. To this, the calculations have been performed in the framework of the Density Functional Theory (DFT), with functionals based in the Generalized Gradient Approximation (GGA), mainly PBE and variations. From this part of the work we have obtained the following conclusions:

- The inclusion of weak interactions is of great importance for a correct description of the adsorption of organic molecules on metal surfaces, with qualitatively different structures if these forces are considered or not.
- Grimme's D2 method systematically predicts higher adsorption energies than those obtained with van der Waals functionals, even if the D2 correction is included only in the atoms of the molecule and in the atoms of the outer layer of the metal surface.
- The geometry of these systems has few dependence on the precision used to explore the reciprocal space, so in a 5x5 size cell, like those used in this thesis, the Γ-point is enough to obtain correct geometries.
- Due to the metallic nature of the substrate, it is necessary to improve the description of the reciprocal space to obtain converged adsorption energies. Therefore, obtaining the energy with a finer grid of K-space, such as 331, over

a geometry obtained with the Γ-point, seems to be a good compromise between quality of the calculation and computational effort.

- Vinyl-derivatives interact mainly through the π bond on the top position of the metal. In these systems, a preference for a top interaction with lone pair electrons is also observed.

- The analysis of the Projected Density Of States (PDOS) shows that the molecular states involved in the interaction with the surface are those of π symmetry. Therefore, the interaction has an important component of donation of electron density from the molecule (occupied π and lone pair orbitals) to the metal, and backdonation from the surface to the molecule (π^* orbital).

- Due to the interaction there is a flux of electron density from the metal to the molecule. This charge is distributed in a very similar region to the LUMO orbital, regardless of the adsorption surface (square or hexagonal). However, we do not observe a clear trend between the value of the transferred charge with the surface neither with the adsorption energy.

- The adsorption energies on Cu(100) are, at least, 100 meV higher than in Cu(111) for the three molecules. Therefore, showing that, for vinyl derivatives, the Cu(100) surface is more reactive than the Cu(111) one.

- Due to the interaction of the molecules with the surface, the energies associated to the vibrational normal modes change. For this reason, different energies are necessary to promote vibrational excitations in the molecules when they are adsorbed with respect to the energies which would be required in the gas phase.

- Molecular dynamics calculations based on the Born-Oppenheimer approach (BOMD) have shown that the distribution of kinetic energy which was initially deposited in these molecules is very fast and a quasi-stationary regime is reached in approximately 100 fs.

- Although the surface takes part of the energy given to the vinyl-derivatives, fragmentation is more common when molecules interact with the substrate, due to the catalytic effect of the metal.

- The rol of the surface is not only to increase the probability of molecular fragmentation. It also favors certain fragments that are stabilized by the interaction with the metal, such as radicals, which are highly unstable in the gas phase.

Subsequently, on the structures obtained in the first part of the thesis, we have carried out an electron dynamics study, with Wave Packet Propagation (WPP) techniques. With this methodology, we have studied the anionic states of the adsorbed molecules on Cu(100) and on Cu(100) coated with ultra-thin NaCl layers (thickness: 1, 2 and 3 atomic layers). In this part of the work the conclusions which have been obtained are:

- The lifetime of an electron in a molecule which is directly adsorbed on a metal surface is extremely short, of the order of few fs: the metal is shown as a very efficient output channel of the active electron.

- In the decay of the extra electron towards the metal, there is an angular pattern with nodes similar to the one of the wavefunction of the orbital where the extra electron is located: the symmetry of the molecule determines the symmetry of the relaxation channel of the electron.

- The existence of a projected gap in Γ in the electronic structure of the metal surface affects the decay of the electron towards the bulk. If the anionic state is inside the gap, the electron cannot penetrate perpendicularly with respect to the surface. This affects the relaxation mechanism and, therefore, the lifetime of the electron in the molecule.

- On the Cu(111) surface, the surface state is inside the projected gap. This causes that the anionic states in this range of energies couple mainly with this state. On the other hand, in the case of the Cu(100) surface, the coupling is directly with the metal continuum. For this reason, on the Cu(111) surface the decay is mainly parallel to the surface, with smaller penetration than in Cu(100).

- The presence of ionic insulating layers decouples the molecular states from the metallic states. A single layer of atomic thickness is enough to enhance the lifetime of the electron in the molecule up to hundreds of fs, which would be enough to induce reactivity with electron injection.

- The decoupling generates a change in lifetime that is exponential with the thickness of the insulating layer (with the number of NaCl layers). This trend does not depend on the system that supports the extra electron and seems to be a universal behavior in molecules of very different nature.

Bibliography

[1] R. P. Feynman, "Feynman and computation," ch. There's Plenty of Room at the Bottom, pp. 63–76, Cambridge, MA, USA: Perseus Books, 1999.

[2] T. Appenzeller, "The man who dared to think small," *Science*, vol. 254, no. 5036, pp. 1300–1300, 1991.

[3] G. E. Moore, "Cramming more components onto integrated circuits, reprinted from electronics, volume 38, number 8, april 19, 1965, pp.114 ff.," *IEEE Solid-State Circuits Society Newsletter*, vol. 11, pp. 33–35, Sep. 2006.

[4] K. S. Novoselov, A. K. Geim, S. V. Morozov, D. Jiang, Y. Zhang, S. V. Dubonos, I. V. Grigorieva, and A. A. Firsov, "Electric field effect in atomically thin carbon films," *Science*, vol. 306, no. 5696, pp. 666–669, 2004.

[5] A. Castellanos-Gomez, "Black phosphorus: Narrow gap, wide applications," *J. Phys. Chem. Lett.*, vol. 6, no. 21, pp. 4280–4291, 2015.

[6] K. Watanabe, T. Taniguchi, and H. Kanda, "Direct-bandgap properties and evidence for ultraviolet lasing of hexagonal boron nitride single crystal," *Nat. Mater.*, vol. 3, pp. 404–409, 2004.

[7] P. Ares, F. Aguilar-Galindo, D. Rodriguez-San-Miguel, D. A. Aldave, S. Diaz-Tendero, M. Alcami, F. Martin, J. Gomez-Herrero, and F. Zamora, "Mechanical isolation of highly stable antimonene under ambient conditions," *Adv. Mater.*, vol. 28, no. 30, pp. 6332–6336, 2016.

[8] J. Repp, G. Meyer, S. M. Stojković, A. Gourdon, and C. Joachim, "Molecules on insulating films: Scanning-tunneling microscopy imaging of individual molecular orbitals," *Phys. Rev. Lett.*, vol. 94, p. 026803, Jan 2005.

[9] B. C. Stipe, M. A. Rezaei, and W. Ho, "Inducing and viewing the rotational motion of a single molecule," *Science*, vol. 279, no. 5358, pp. 1907–1909, 1998.

[10] B. C. Stipe, M. A. Rezaei, and W. Ho, "Single-molecule vibrational spectroscopy and microscopy," *Science*, vol. 280, no. 5370, pp. 1732–1735, 1998.

[11] B. Doppagne, M. C. Chong, H. Bulou, A. Boeglin, F. Scheurer, and G. Schull, "Electrofluorochromism at the single-molecule level," *Science*, vol. 361, no. 6399, pp. 251–255, 2018.

[12] D. M. Eigler and E. K. Schweizer, "Positioning single atoms with a scanning tunnelling microscope," *Nature*, vol. 344, pp. 524–526, 1990.

[13] M. F. Crommie, C. P. Lutz, and D. M. Eigler, "Confinement of electrons to quantum corrals on a metal surface," *Science*, vol. 262, no. 5131, pp. 218–220, 1993.

[14] N. Nilius, T. M. Wallis, and W. Ho, "Development of one-dimensional band structure in artificial gold chains," *Science*, vol. 297, no. 5588, pp. 1853–1856, 2002.

[15] T. M. Wallis, N. Nilius, and W. Ho, "Electronic density oscillations in gold atomic chains assembled atom by atom," *Phys. Rev. Lett.*, vol. 89, p. 236802, Nov 2002.

[16] K. Giesen, F. Hage, F. J. Himpsel, H. J. Riess, and W. Steinmann, "Two-photon photoemission via image-potential states," *Phys. Rev. Lett.*, vol. 55, pp. 300–303, Jul 1985.

[17] U. Höfer, I. L. Shumay, C. Reuß, U. Thomann, W. Wallauer, and T. Fauster, "Time-resolved coherent photoelectron spectroscopy of quantized electronic states on metal surfaces," *Science*, vol. 277, no. 5331, pp. 1480–1482, 1997.

[18] B. L. Darby, P. G. Etchegoin, and E. C. Le Ru, "Single-molecule surface-enhanced Raman spectroscopy with nanowatt excitation," *Phys. Chem. Chem. Phys.*, vol. 16, pp. 23895–23899, 2014.

[19] M. D. Sonntag, E. A. Pozzi, N. Jiang, M. C. Hersam, and R. P. Van Duyne, "Recent advances in Tip-Enhanced Raman Spectroscopy," *J. Phys. Chem. Lett.*, vol. 5, no. 18, pp. 3125–3130, 2014.

[20] F. Aguilar-Galindo, S. Diaz-Tendero, and A. G. Borisov, "Electronic structure effects in the coupling of a single molecule with a plasmonic antenna," *J. Phys. Chem. C.*, vol. 123, no. 7, pp. 4446–4456, 2019.

[21] S. Grimme, "Semiempirical GGA-type density functional constructed with a long-range dispersion correction," *J. Comp. Chem.*, vol. 27, no. 15, pp. 1787–1799, 2006.

[22] M. Dion, H. Rydberg, E. Schröder, D. C. Langreth, and B. I. Lundqvist, "Van der Waals density functional for general geometries," *Phys. Rev. Lett.*, vol. 92, p. 246401, Jun 2004.

[23] K. R. Rusimova, R. M. Purkiss, R. Howes, F. Lee, S. Crampin, and P. A. Sloan, "Regulating the femtosecond excited-state lifetime of a single molecule," *Science*, vol. 361, no. 6406, pp. 1012–1016, 2018.

[24] J. Kroger, B. Doppagne, F. Scheurer, and G. Schull, "Fano description of single-hydrocarbon fluorescence excited by a scanning tunneling microscope," *Nano Lett.*, vol. 18, no. 6, pp. 3407–3413, 2018.

[25] J. Lee, N. Tallarida, X. Chen, L. Jensen, and V. A. Apkarian, "Microscopy with a single-molecule scanning electrometer," *Sci. Adv.*, vol. 4, no. 6, 2018.

[26] H. Imada, K. Miwa, M. Imai-Imada, S. Kawahara, K. Kimura, and Y. Kim, "Single-molecule investigation of energy dynamics in a coupled plasmon-exciton system," *Phys. Rev. Lett.*, vol. 119, p. 013901, Jul 2017.

[27] M. Rashidi, W. Vine, T. Dienel, L. Livadaru, J. Retallick, T. Huff, K. Walus, and R. A. Wolkow, "Initiating and monitoring the evolution of single electrons within atom-defined structures," *Phys. Rev. Lett.*, vol. 121, p. 166801, Oct 2018.

[28] L. Zhang, Y.-J. Yu, L.-G. Chen, Y. Luo, B. Yang, F.-F. Kong, G. Chen, Y. Zhang, Q. Zhang, Y. Luo, J.-L. Yang, Z.-C. Dong, and J. G. Hou, "Electrically driven single-photon emission from an isolated single molecule," *Nat. Commun.*, vol. 8, p. 580, 2017.

[29] L. L. Patera, F. Queck, P. Scheuerer, N. Moll, and J. Repp, "Accessing a charged intermediate state involved in the excitation of single molecules," *Phys. Rev. Lett.*, vol. 123, p. 016001, Jul 2019.

[30] M. Planck, "Ueber das gesetz der energieverteilung im normalspectrum," *Annalen der Physik*, vol. 309, no. 3, pp. 553–563, 1901.

[31] E. Schrödinger, "Quantisierung als eigenwertproblem," *Annalen der Physik*, vol. 384, no. 4, pp. 361–376, 1926.

[32] M. Born and R. Oppenheimer, "Zur quantentheorie der molekeln," *Annalen der Physik*, vol. 389, no. 20, pp. 457–484, 1927.

[33] W. Pauli, "Über den zusammenhang des abschlusses der elektronengruppen im atom mit der komplexstruktur der spektren," *Zeitschrift für Physik*, vol. 31, pp. 765–783, Feb 1925.

[34] J. C. Slater, "Cohesion in monovalent metals," *Phys. Rev.*, vol. 35, pp. 509–529, Mar 1930.

[35] D. R. Hartree, "The wave mechanics of an atom with a non-coulomb central field. part i. theory and methods," *Mathematical Proceedings of the Cambridge Philosophical Society*, vol. 24, no. 1, p. 89–110, 1928.

[36] V. Fock, "Näherungsmethode zur lösung des quantenmechanischen mehrkörperproblems," *Zeitschrift für Physik*, vol. 61, pp. 126–148, Jan 1930.

[37] C. C. J. Roothaan, "New developments in molecular orbital theory," *Rev. Mod. Phys.*, vol. 23, pp. 69–89, Apr 1951.

[38] G. G. Hall and J. E. Lennard-Jones, "The molecular orbital theory of chemical valency VIII. A method of calculating ionization potentials," *Proceedings of the Royal Society of London. Series A. Mathematical and Physical Sciences*, vol. 205, no. 1083, pp. 541–552, 1951.

[39] C. Møller and M. S. Plesset, "Note on an approximation treatment for many-electron systems," *Phys. Rev.*, vol. 46, pp. 618–622, Oct 1934.

[40] J. Cizek, "On the correlation problem in atomic and molecular systems. calculation of wavefunction components in ursell-type ezpansion using quantum-field theoretical methods," *J. Chem. Phys.*, vol. 45, no. 11, pp. 4256–4266, 1966.

[41] T. Kato, "On the eigenfunctions of many-particle systems in quantum mechanics," *Communications on Pure and Applied Mathematics*, vol. 10, no. 2, pp. 151–177, 1957.

[42] S. F. Boys and A. C. Egerton, "Electronic wave functions - I. A general method of calculation for the stationary states of any molecular system," *Proceedings of the Royal Society of London. Series A. Mathematical and Physical Sciences*, vol. 200, no. 1063, pp. 542–554, 1950.

[43] P. Hohenberg and W. Kohn, "Inhomogeneous electron gas," *Phys. Rev.*, vol. 136, pp. B864–B871, Nov 1964.

[44] W. Kohn and L. J. Sham, "Self-consistent equations including exchange and correlation effects," *Phys. Rev.*, vol. 140, pp. A1133–A1138, Nov 1965.

[45] J. P. Perdew, K. Burke, and M. Ernzerhof, "Generalized gradient approximation made simple," *Phys. Rev. Lett.*, vol. 77, pp. 3865–3868, Oct 1996.

[46] Y. Zhao and D. G. Truhlar, "A new local density functional for main-group thermochemistry, transition metal bonding, thermochemical kinetics, and noncovalent interactions," *J. Chem. Phys.*, vol. 125, no. 19, p. 194101, 2006.

[47] A. D. Becke, "Density-functional thermochemistry. III. The role of exact exchange," *J. Chem. Phys.*, vol. 98, no. 7, pp. 5648–5652, 1993.

[48] C. Lee, W. Yang, and R. G. Parr, "Development of the Colle-Salvetti correlation-energy formula into a functional of the electron density," *Phys. Rev. B*, vol. 37, pp. 785–789, Jan 1988.

[49] S. Grimme, "Density functional theory with London dispersion corrections," *Wiley Interdisciplinary Reviews: Computational Molecular Science*, vol. 1, no. 2, pp. 211–228, 2011.

[50] S. Grimme, "Accurate description of van der waals complexes by density functional theory including empirical corrections," *J. Comp. Chem.*, vol. 25, no. 12, pp. 1463–1473, 2004.

[51] F. Bloch, "Über die quantenmechanik der elektronen in kristallgittern," *Zeitschrift für Physik*, vol. 52, pp. 555–600, Jul 1929.

[52] T. Helgaker, E. Uggerud, and H. J. A. Jensen, "Integration of the classical equations of motion on ab initio molecular potential energy surfaces using gradients and hessians: application to translational energy release upon fragmentation," *Chem. Phys. Lett.*, vol. 173, no. 2, pp. 145 – 150, 1990.

[53] E. Uggerud and T. Helgaker, "Dynamics of the reaction CH2OH+ → CHO+ + H2. Translational energy release from ab initio trajectory calculations," *Journal of the American Chemical Society*, vol. 114, no. 11, pp. 4265–4268, 1992.

[54] R. F. W. Bader, "A quantum theory of molecular structure and its applications," *Chem. Rev.*, vol. 91, no. 5, pp. 893–928, 1991.

[55] R. F. W. Bader, *Atoms in Molecules: A Quantum Theory.* Oxford University Press, USA, June 1994.

[56] J. Zhang, *Theory and Application of Quantum Molecular Dynamics.* World Scientific Publishing Co, 1999.

[57] G.-J. Kroes, "Six-dimensional quantum dynamics of dissociative chemisorption of H2 on metal surfaces," *Prog. Surf. Sci.*, vol. 60, no. 1, pp. 1 – 85, 1999.

[58] E. V. Chulkov, A. G. Borisov, J. P. Gauyacq, D. Sánchez-Portal, V. M. Silkin, V. P. Zhukov, and P. M. Echenique, "Electronic excitations in metals and at metal surfaces," *Chem. Rev.*, vol. 106, no. 10, pp. 4160–4206, 2006.

[59] M. Beck, A. Jackle, G. Worth, and H.-D. Meyer, "The multiconfiguration time-dependent Hartree (MCTDH) method: a highly efficient algorithm for propagating wavepackets," *Physics Reports*, vol. 324, no. 1, pp. 1 – 105, 2000.

[60] A. G. Borisov, A. K. Kazansky, and J. P. Gauyacq, "Resonant charge transfer in ion–metal surface collisions: Effect of a projected band gap in the $H^- - Cu(111)$ system," *Phys. Rev. B*, vol. 59, pp. 10935–10949, Apr 1999.

[61] F. Martín and M. F. Politis, "Multicenter-gaussian representation of resonant charge transfer in atom-surface interaction," *Surf. Sci.*, vol. 356, pp. 247–256, 1996.

[62] C. Lanczos, "An iteration method for the solution of the eigenvalue problem of linear differential and integral operators," *Journal of Research of the National Bureau of Standards*, vol. 45, no. 4, pp. 255–282, 1950.

[63] M. Braun, S. Sofianos, D. Papageorgiou, and I. Lagaris, "An efficient Chebyshev–Lanczos method for obtaining eigensolutions of the Schrödinger equation on a grid," *Journal of Computational Physics*, vol. 126, no. 2, pp. 315 – 327, 1996.

[64] J. Crank and P. Nicolson, "A practical method for numerical evaluation of solutions of partial differential equations of the heat-conduction type," *Mathematical Proceedings of the Cambridge Philosophical Society*, vol. 43, no. 1, p. 50–67, 1947.

[65] M. Feit, J. Fleck, and A. Steiger, "Solution of the Schrödinger equation by a spectral method," *Journal of Computational Physics*, vol. 47, no. 3, pp. 412 – 433, 1982.

[66] R. Kosloff, "Quantum molecular dynamics on grids," *Dynamics of molecules and chemical reactions*, pp. 185–230, 1996.

[67] E. O. Brigham, *The Fast Fourier Transform and Its Applications*. Upper Saddle River, NJ, USA: Prentice-Hall, Inc., 1988.

[68] M. Frigo and S. G. Johnson, "The design and implementation of FFTW3," *Proceedings of the IEEE*, vol. 93, no. 2, pp. 216–231, 2005. Special issue on "Program Generation, Optimization, and Platform Adaptation".

[69] E. Chulkov, V. Silkin, and P. Echenique, "Image potential states on metal surfaces: binding energies and wave functions," *Surf. Sci.*, vol. 437, no. 3, pp. 330 – 352, 1999.

[70] A. G. Borisov, A. K. Kazansky, and J. P. Gauyacq, "Resonances induced by Cs adsorbates on Cu(100): Localization of image potential states," *Phys. Rev. B*, vol. 65, p. 205414, May 2002.

[71] X. Gonze, F. Jollet, F. Abreu Araujo, D. Adams, B. Amadon, T. Applencourt, C. Audouze, J.-M. Beuken, J. Bieder, A. Bokhanchuk, E. Bousquet, F. Bruneval, D. Caliste, M. Côté, F. Dahm, F. Da Pieve, M. Delaveau, M. Di Gennaro, B. Dorado, C. Espejo, G. Geneste, L. Genovese, A. Gerossier, M. Giantomassi, Y. Gillet, D. Hamann, L. He, G. Jomard, J. Laflamme Janssen, S. Le Roux, A. Levitt, A. Lherbier, F. Liu, I. Lukačević, A. Martin, C. Martins, M. Oliveira, S. Poncé, Y. Pouillon, T. Rangel, G.-M. Rignanese, A. Romero, B. Rousseau, O. Rubel, A. Shukri, M. Stankovski, M. Torrent, M. Van Setten, B. Van Troeye, M. Verstraete, D. Waroquiers, J. Wiktor, B. Xu, A. Zhou, and J. Zwanziger, "Recent developments in the

ABINIT software package," *Comput. Phys. Commun.*, vol. 205, pp. 106–131, August 2016.

[72] D. R. Hamann, "Optimized norm-conserving Vanderbilt pseudopotentials," *Phys. Rev. B*, vol. 88, p. 085117, Aug 2013.

[73] T. Koopmans, "Uber die zuordnung von wellenfunktionen und eigenwerten zu den einzelnen elektronen eines atoms," *Physica*, vol. 1, no. 1, pp. 104 – 113, 1934.

[74] H. Koch and P. Jorgensen, "Coupled cluster response functions," *J. Chem. Phys.*, vol. 93, no. 5, pp. 3333–3344, 1990.

[75] M. J. Frisch, G. W. Trucks, H. B. Schlegel, G. E. Scuseria, M. A. Robb, J. R. Cheeseman, G. Scalmani, V. Barone, B. Mennucci, G. A. Petersson, H. Nakatsuji, M. Caricato, X. Li, H. P. Hratchian, A. F. Izmaylov, J. Bloino, G. Zheng, J. L. Sonnenberg, M. Hada, M. Ehara, K. Toyota, R. Fukuda, J. Hasegawa, M. Ishida, T. Nakajima, Y. Honda, O. Kitao, H. Nakai, T. Vreven, J. A. Montgomery, Jr., J. E. Peralta, F. Ogliaro, M. Bearpark, J. J. Heyd, E. Brothers, K. N. Kudin, V. N. Staroverov, R. Kobayashi, J. Normand, K. Raghavachari, A. Rendell, J. C. Burant, S. S. Iyengar, J. Tomasi, M. Cossi, N. Rega, J. M. Millam, M. Klene, J. E. Knox, J. B. Cross, V. Bakken, C. Adamo, J. Jaramillo, R. Gomperts, R. E. Stratmann, O. Yazyev, A. J. Austin, R. Cammi, C. Pomelli, J. W. Ochterski, R. L. Martin, K. Morokuma, V. G. Zakrzewski, G. A. Voth, P. Salvador, J. J. Dannenberg, S. Dapprich, A. D. Daniels, Ö. Farkas, J. B. Foresman, J. V. Ortiz, J. Cioslowski, and D. J. Fox, "Gaussian 09 Revision E.01, gaussian inc. wallingford ct 2013," 2013.

[76] J. Nørskov, T. Bligaard, A. Logadottir, S. Bahn, L. Hansen, M. Bollinger, H. Bengaard, B. Hammer, Z. Sljivancanin, M. Mavrikakis, Y. Xu, S. Dahl, and C. Jacobsen, "Universality in heterogeneous catalysis," *J. Catal.*, vol. 209, no. 2, pp. 275 – 278, 2002.

[77] S. J. Tauster, S. C. Fung, R. T. K. Baker, and J. A. Horsley, "Strong interactions in supported-metal catalysts," *Science*, vol. 211, no. 4487, pp. 1121–1125, 1981.

[78] E. L. Muetterties, "Metal clusters in catalysis III. - Clusters as models for chemisorption processes and heterogeneous catalysis," *B. Soc. Chim. Belg.*, vol. 84, no. 10, pp. 959–986, 1975.

[79] A. T. Bell, "The impact of nanoscience on heterogeneous catalysis," *Science*, vol. 299, no. 5613, pp. 1688–1691, 2003.

[80] J. Moffat, *Theoretical Aspects of Heterogeneous Catalysis*. Van Nostrand Reinhold Electrical/Computer Science and Engineering Series, Springer Netherlands, 2013.

[81] R. Joyner and R. van Santen, *Elementary Reaction Steps in Heterogeneous Catalysis*. Nato Science Series C:, Springer Netherlands, 2012.

[82] L. Salem, "The mechanism of the chemical reaction, with recent developments pertaining to heterogeneous catalysis," *Int. J. Quantum Chem.*, vol. 16, no. S13, pp. 321–330, 1979.

[83] N. Armbrust, F. Schiller, J. Güdde, and U. Höfer, "Model potential for the description of metal/organic interface states," *Sci. Rep.-UK*, vol. 7, p. 46561, 2017.

[84] S. Chen, Z. Zhao, and H. Liu, "Charge transport at the metal-organic interface," *Ann. Rev. Phys. Chem.*, vol. 64, no. 1, pp. 221–245, 2013.

[85] J. C. Scott, "Metal-organic interface and charge injection in organic electronic devices," *J. Vac. Sci. Technol. A*, vol. 21, no. 3, pp. 521–531, 2003.

[86] J. Hwang, A. Wan, and A. Kahn, "Energetics of metal-organic interfaces: New experiments and assessment of the field," *Mat. Sci. Eng. R*, vol. 64, no. 1, pp. 1 – 31, 2009.

[87] M. J. Zaworotko, "A reversible step forward," *Nat. Chem.*, vol. 1, p. 267, 2009.

[88] H. Furukawa, K. E. Cordova, M. O'Keeffe, and O. M. Yaghi, "The chemistry and applications of metal-organic frameworks," *Science*, vol. 341, no. 6149, 2013.

[89] H.-C. Zhou, J. R. Long, and O. M. Yaghi, "Introduction to metal-organic frameworks," *Chem. Rev.*, vol. 112, no. 2, pp. 673–674, 2012.

[90] C. Sánchez, B. Julian, P. Belleville, and M. Popall, "Applications of hybrid organic-inorganic nanocomposites," *J. Mater. Chem.*, vol. 15, pp. 3559–3592, 2005.

[91] H. Ishii, K. Sugiyama, E. Ito, and K. Seki, "Energy level alignment and interfacial electronic structures at organic/metal and organic/organic interfaces," *Adv. Mater.*, vol. 11, no. 8, pp. 605–625, 1999.

[92] G. Ferey, "Hybrid porous solids: past, present, future," *Chem. Soc. Rev.*, vol. 37, pp. 191–214, 2008.

[93] G. Yu, J. Gao, J. C. Hummelen, F. Wudl, and A. J. Heeger, "Polymer photovoltaic cells: Enhanced efficiencies via a network of internal donor-acceptor heterojunctions," *Science*, vol. 270, no. 5243, pp. 1789–1791, 1995.

[94] S. Günes, H. Neugebauer, and N. S. Sariciftci, "Conjugated polymer-based organic solar cells," *Chem. Rev.*, vol. 107, no. 4, pp. 1324–1338, 2007.

[95] C. W. Tang, "Two-layer organic photovoltaic cell," *Appl. Phys. Lett.*, vol. 48, no. 2, pp. 183–185, 1986.

[96] M. Grätzel, "Dye-sensitized solar cells," *J. Photoch. PhotoBio. C*, vol. 4, no. 2, pp. 145 – 153, 2003.

[97] T. P. I. Saragi, T. Spehr, A. Siebert, T. Fuhrmann-Lieker, and J. Salbeck, "Spiro compounds for organic optoelectronics," *Chem. Rev.*, vol. 107, no. 4, pp. 1011–1065, 2007.

[98] O. Shekhah, J. Liu, R. A. Fischer, and C. Woll, "Mof thin films: existing and future applications," *Chem. Soc. Rev.*, vol. 40, pp. 1081–1106, 2011.

[99] K. Choy, "Chemical vapour deposition of coatings," *Prog. Mat. Sci.*, vol. 48, no. 2, pp. 57 – 170, 2003.

[100] H. Sirringhaus, N. Tessler, and R. H. Friend, "Integrated optoelectronic devices based on conjugated polymers," *Science*, vol. 280, no. 5370, pp. 1741–1744, 1998.

[101] J. A. Rogers, T. Someya, and Y. Huang, "Materials and mechanics for stretchable electronics," *Science*, vol. 327, no. 5973, pp. 1603–1607, 2010.

[102] M. Law, L. E. Greene, J. C. Johnson, R. Saykally, and P. Yang, "Nanowire dye-sensitized solar cells," *Nat. Mater.*, vol. 4, p. 455, 2005.

[103] A. Hagfeldt, G. Boschloo, L. Sun, L. Kloo, and H. Pettersson, "Dye-sensitized solar cells," *Chem. Rev.*, vol. 110, no. 11, pp. 6595–6663, 2010.

[104] L. Bogani and W. Wernsdorfer, "Molecular spintronics using single-molecule magnets," *Nat. Mater.*, vol. 7, p. 179, 2008.

[105] A. R. Rocha, V. M. Garcia-Suarez, S. W. Bailey, C. J. Lambert, J. Ferrer, and S. Sanvito, "Towards molecular spintronics," *Nat. Mater.*, vol. 4, p. 335, 2005.

[106] S. Sanvito, "Molecular spintronics," *Chem. Soc. Rev.*, vol. 40, pp. 3336–3355, 2011.

[107] M. Mannini, F. Pineider, P. Sainctavit, C. Danieli, E. Otero, C. Sciancalepore, A. M. Talarico, M.-A. Arrio, A. Cornia, D. Gatteschi, and R. Sessoli, "Magnetic memory of a single-molecule quantum magnet wired to a gold surface," *Nat. Mater.*, vol. 8, p. 194, 2009.

[108] J. Gray and B. Luan, "Protective coatings on magnesium and its alloys - a critical review," *J. Alloy. Compd.*, vol. 336, no. 1, pp. 88 – 113, 2002.

[109] D. L. Huber, "Synthesis, properties, and applications of iron nanoparticles," *Small*, vol. 1, no. 5, pp. 482–501, 2005.

[110] I. Chung, B. Lee, J. He, R. P. H. Chang, and M. G. Kanatzidis, "All-solid-state dye-sensitized solar cells with high efficiency," *Nature*, vol. 485, p. 486, 2012.

[111] H. Hakkinen, "The gold-sulfur interface at the nanoscale," *Nat. Chem.*, vol. 4, p. 443, 2012.

[112] F. Tautz, "Structure and bonding of large aromatic molecules on noble metal surfaces: the example of PTCDA," *Prog. Surf. Sci.*, vol. 82, no. 9, pp. 479 – 520, 2007.

[113] I. Temprano, G. Thomas, S. Haq, M. S. Dyer, E. G. Latter, G. R. Darling, P. Uvdal, and R. Raval, "1D self-assembly of chemisorbed thymine on Cu(110) driven by dispersion forces," *J. Chem. Phys.*, vol. 142, no. 10, p. 101916, 2015.

[114] F. Schreiber, "Structure and growth of self-assembling monolayers," *Prog. Surf. Sci.*, vol. 65, no. 5, pp. 151 – 257, 2000.

[115] A. C. Templeton, W. P. Wuelfing, and R. W. Murray, "Monolayer-protected cluster molecules," *Acc. Chem. Res.*, vol. 33, no. 1, pp. 27–36, 2000.

[116] J. C. Love, L. A. Estroff, J. K. Kriebel, R. G. Nuzzo, and G. M. Whitesides, "Self-assembled monolayers of thiolates on metals as a form of nanotechnology," *Chem. Rev.*, vol. 105, no. 4, pp. 1103–1170, 2005.

[117] A. Ulman, "Formation and structure of self-assembled monolayers," *Chem. Rev.*, vol. 96, no. 4, pp. 1533–1554, 1996.

[118] L. H. Dubois and R. G. Nuzzo, "Synthesis, structure, and properties of model organic surfaces," *Annu. Rev. Phys. Chem.*, vol. 43, no. 1, pp. 437–463, 1992.

[119] H. Bin, Y. Yang, Z.-G. Zhang, L. Ye, M. Ghasemi, S. Chen, Y. Zhang, C. Zhang, C. Sun, L. Xue, C. Yang, H. Ade, and Y. Li, "9.73% efficiency non-fullerene all organic small molecule solar cells with absorption-complementary donor and acceptor," *J. Am. Chem. Soc.*, vol. 139, no. 14, pp. 5085–5094, 2017.

[120] S. Díaz-Tendero, M. Alcamí, and F. Martín, "Density functional theory study of the structure and vibrational modes of acrylonitrile adsorbed on Cu(100)," *Phys. Chem. Chem. Phys.*, vol. 15, pp. 1288–1295, 2013.

[121] R. Meyer, C. Lemire, S. K. Shaikhutdinov, and H. J. Freund, "Surface chemistry of catalysis by gold," *Gold Bull.*, vol. 37, pp. 72–124, Mar 2004.

[122] M. X. Yang, J. Eng, P. W. Kash, G. W. Flynn, B. E. Bent, M. T. Holbrook, S. R. Bare, J. L. Gland, and D. A. Fischer, "Generation and reaction of vinyl groups on a Cu(100) surface," *J. Phys. Chem.*, vol. 100, no. 30, pp. 12431–12439, 1996.

[123] A. B. Gurevich, A. V. Teplyakov, M. X. Yang, B. E. Bent, M. T. Holbrook, and S. R. Bare, "Synthesis, bonding, and reactions of π-bonded allyl groups on Cu(100): allyl radical ejection," *Langmuir*, vol. 14, no. 6, pp. 1419–1427, 1998.

[124] J.-L. Lin, H.-P. Lin, C.-M. Yang, T.-Y. Chen, S.-H. Lee, and C.-M. Chiang, "Reactions of CH2=CHBr and CH3CHBr2 on Cu(100) and O/Cu(100)," *J. Phys. Chem. C*, vol. 121, no. 33, pp. 17990–17998, 2017.

[125] B. Voigtländer, *Scanning Probe Microscopy: Atomic Force Microscopy and Scanning Tunneling Microscopy*. NanoScience and Technology, Springer Berlin Heidelberg, 2015.

[126] H.-J. Butt, B. Cappella, and M. Kappl, "Force measurements with the atomic force microscope: Technique, interpretation and applications," *Surf. Sci. Rep.*, vol. 59, no. 1, pp. 1 – 152, 2005.

[127] G. Binnig, H. Rohrer, C. Gerber, and E. Weibel, "Surface studies by scanning tunneling microscopy," *Phys. Rev. Lett.*, vol. 49, pp. 57–61, Jul 1982.

[128] "Methods of experimental physics," in *Scanning Tunneling Microscopy* (J. A. Stroscio and W. J. Kaiser, eds.), p. ii, San Diego: Academic Press, 1993.

[129] E. Meyer, H. J. Hug, and R. Bennewitz, *Introduction to Scanning Tunneling Microscopy*, pp. 15–44. Berlin, Heidelberg: Springer Berlin Heidelberg, 2004.

[130] J. Zegenhagen and A. Kazimirov, *The X-Ray Standing Wave Technique*. World Scientific, 2013.

[131] D. Woodruff, "Surface structural information from photoelectron diffraction," *J. Electron. Spectros. Relat. Phenom.*, vol. 178-179, pp. 186 – 194, 2010. Trends in X-ray Photoelectron Spectroscopy of solids (theory, techniques and applications).

[132] S. Hüfner, *Photoelectron Diffraction*, pp. 597–634. Berlin, Heidelberg: Springer Berlin Heidelberg, 2003.

[133] V. Rakić and L. Damjanović, *Temperature-Programmed Desorption (TPD) Methods*, pp. 131–174. Berlin, Heidelberg: Springer Berlin Heidelberg, 2013.

[134] J. L. Falconer and J. A. Schwarz, "Temperature-programmed desorption and reaction: Applications to supported catalysts," *Cataly. Rev.*, vol. 25, no. 2, pp. 141–227, 1983.

[135] V. Nefedov and N. Shartse, *X-Ray Photoelectron Spectroscopy of Solid Surfaces*. Taylor & Francis, 1988.

[136] D. Briggs and M. Seah, *Practical Surface Analysis, Auger and X-ray Photoelectron Spectroscopy*. Practical Surface Analysis, Wiley, 1996.

[137] W. Liu, A. Tkatchenko, and M. Scheffler, "Modeling adsorption and reactions of organic molecules at metal surfaces," *Acc. Chem. Res.*, vol. 47, no. 11, pp. 3369–3377, 2014.

[138] A. Nilsson, L. G. Pettersson, and J. K. Nørskov, *Chemical bonding at surfaces and interfaces*. Amsterdam: Elsevier, 2008.

[139] S. Díaz-Tendero, A. G. Borisov, and J.-P. Gauyacq, "Theoretical study of the electronic excited states in ultrathin ionic layers supported on metal surfaces: NaCl/Cu(111)," *Phys. Rev. B*, vol. 83, p. 115453, Mar 2011.

[140] S. Díaz-Tendero, S. Foelsch, F. E. Olsson, A. G. Borisov, and J.-P. Gauyacq, "Electron propagation along Cu nanowires supported on a Cu(111) surface," *Nano Lett.*, vol. 8, no. 9, pp. 2712–2717, 2008.

[141] S. Díaz-Tendero, A. G. Borisov, and J.-P. Gauyacq, "Extraordinary electron propagation length in a metallic double chain supported on a metal surface," *Phys. Rev. Lett.*, vol. 102, p. 166807, Apr 2009.

[142] F. Chiter, V. B. Nguyen, N. Tarrat, M. Benoit, H. Tang, and C. Lacaze-Dufaure, "Effect of van der Waals corrections on DFT-computed metallic surface properties," *Mater. Res. Express*, vol. 3, no. 4, p. 046501, 2016.

[143] Y. Andersson, E. Hult, H. Rydberg, P. Apell, B. I. Lundqvist, and D. C. Langreth, *Van der Waals Interactions in Density Functional Theory*, pp. 243–260. Boston, MA: Springer US, 1998.

[144] V. G. Ruiz, W. Liu, E. Zojer, M. Scheffler, and A. Tkatchenko, "Density-functional theory with screened van der Waals interactions for the modeling of hybrid inorganic-organic systems," *Phys. Rev. Lett.*, vol. 108, p. 146103, Apr 2012.

[145] V. G. Ruiz, W. Liu, and A. Tkatchenko, "Density-functional theory with screened van der Waals interactions applied to atomic and molecular adsorbates on close-packed and non-close-packed surfaces," *Phys. Rev. B*, vol. 93, p. 035118, Jan 2016.

[146] K. Berland, V. R. Cooper, K. Lee, E. Schröder, T. Thonhauser, P. Hyldgaard, and B. I. Lundqvist, "Van der Waals forces in density functional theory: a

review of the vdW-DF method," *Rep. Prog. Phys.*, vol. 78, no. 6, p. 066501, 2015.

[147] M. Robledo and S. Díaz-Tendero, "Exploring the adsorption and the potential energy surface of acrylonitrile on Cu(100) and Cu(100) coated with NaCl layers," *J. Phys. Chem. C*, vol. 119, no. 27, pp. 15125–15136, 2015.

[148] M. Robledo, G. Pacchioni, F. Martín, M. Alcamí, and S. Díaz-Tendero, "Adsorption of benzene on Cu(100) and on Cu(100) covered with an ultrathin NaCl film: molecule-substrate interaction and decoupling," *J. Phys. Chem. C*, vol. 119, no. 8, pp. 4062–4071, 2015.

[149] S. Grimme, J. Antony, S. Ehrlich, and H. Krieg, "A consistent and accurate ab initio parametrization of density functional dispersion correction (DFT-D) for the 94 elements H-Pu," *J. Chem. Phys.*, vol. 132, no. 15, p. 154104, 2010.

[150] J. c. v. Klimeš, D. R. Bowler, and A. Michaelides, "Van der Waals density functionals applied to solids," *Phys. Rev. B*, vol. 83, p. 195131, May 2011.

[151] G. Román-Pérez and J. M. Soler, "Efficient implementation of a van der Waals density functional: application to double-wall carbon nanotubes," *Phys. Rev. Lett.*, vol. 103, p. 096102, Aug 2009.

[152] K. Berland and P. Hyldgaard, "Exchange functional that tests the robustness of the plasmon description of the van der Waals density functional," *Phys. Rev. B*, vol. 89, p. 035412, Jan 2014.

[153] K. Berland, C. A. Arter, V. R. Cooper, K. Lee, B. I. Lundqvist, E. Schroder, T. Thonhauser, and P. Hyldgaard, "Van der Waals density functionals built upon the electron-gas tradition: facing the challenge of competing interactions," *J. Chem. Phys.*, vol. 140, no. 18, p. 18A539, 2014.

[154] A. D. Becke and E. R. Johnson, "Exchange-hole dipole moment and the dispersion interaction," *J. Chem. Phys.*, vol. 122, no. 15, p. 154104, 2005.

[155] F. O. Kannemann and A. D. Becke, "Van der Waals interactions in density-functional theory: intermolecular complexes," *J. Chem. Theory Comput.*, vol. 6, no. 4, pp. 1081–1088, 2010.

[156] S. N. Steinmann and C. Corminboeuf, "Comprehensive benchmarking of a density-dependent dispersion correction," *J. Chem. Theory Comput.*, vol. 7, no. 11, pp. 3567–3577, 2011.

[157] A. Tkatchenko and M. Scheffler, "Accurate molecular van der Waals interactions from ground-state electron density and free-atom reference data," *Phys. Rev. Lett.*, vol. 102, p. 073005, Feb 2009.

[158] R. J. Maurer, V. G. Ruiz, J. Camarillo-Cisneros, W. Liu, N. Ferri, K. Reuter, and A. Tkatchenko, "Adsorption structures and energetics of molecules on metal surfaces: Bridging experiment and theory," *Prog. Surf. Sci.*, vol. 91, no. 2, pp. 72 – 100, 2016.

[159] G. Mercurio, E. R. McNellis, I. Martin, S. Hagen, F. Leyssner, S. Soubatch, J. Meyer, M. Wolf, P. Tegeder, F. S. Tautz, and K. Reuter, "Structure and energetics of azobenzene on Ag(111): Benchmarking semiempirical dispersion correction approaches," *Phys. Rev. Lett.*, vol. 104, p. 036102, Jan 2010.

[160] P. Sony, P. Puschnig, D. Nabok, and C. Ambrosch-Draxl, "Importance of van der Waals interaction for organic molecule-metal junctions: adsorption of thiophene on Cu(110) as a prototype," *Phys. Rev. Lett.*, vol. 99, p. 176401, Oct 2007.

[161] M. Mura, A. Gulans, T. Thonhauser, and L. Kantorovich, "Role of van der Waals interaction in forming molecule-metal junctions: flat organic molecules on the Au(111) surface," *Phys. Chem. Chem. Phys.*, vol. 12, pp. 4759–4767, 2010.

[162] G. Li, I. Tamblyn, V. R. Cooper, H.-J. Gao, and J. B. Neaton, "Molecular adsorption on metal surfaces with van der Waals density functionals," *Phys. Rev. B*, vol. 85, p. 121409, Mar 2012.

[163] A. Bilic, J. R. Reimers, and N. S. Hush, "Adsorption of pyridine on the gold(111) surface: Implications for alligator clips for molecular wires," *J. Phys. Chem. B*, vol. 106, no. 26, pp. 6740–6747, 2002.

[164] G. Kresse and J. Furthmühller, "Efficiency of ab-initio total energy calculations for metals and semiconductors using a plane-wave basis set," *Comput. Mat. Sci.*, vol. 6, pp. 15–50, 1996.

[165] G. Kresse and J. Furthmühller, "Efficient iterative schemes for ab initio total-energy calculations using a plane-wave basis set," *Phys. Rev. B*, vol. 54, p. 11169, 1996.

[166] J. c. v. Klimeš, D. R. Bowler, and A. Michaelides, "Chemical accuracy for the van der Waals density functional," *J. Phys.-Condens. Mat.*, vol. 22, no. 2, p. 022201, 2010.

[167] W. Tang, E. Sanville, and G. Henkelman, "A grid-based bader analysis algorithm without lattice bias," *J. Phys. Condens. Mat.*, vol. 21, no. 8, p. 084204, 2009.

[168] E. Sanville, S. D. Kenny, R. Smith, and G. Henkelman, "Improved grid-based algorithm for Bader charge allocation," *J. Comput. Chem.*, vol. 28, no. 5, pp. 899–908, 2007.

[169] G. Henkelman, A. Arnaldsson, and H. Jonsson, "A fast and robust algorithm for Bader decomposition of charge density," *Comp. Mat. Sci.*, vol. 36, no. 3, pp. 354 – 360, 2006.

[170] V. M. Geskin, R. Lazzaroni, M. Mertens, R. Jérôme, and J. L. Brédas, "Acrylonitrile on Cu(100): a density functional theoretical study of adsorption and electrochemical grafting," *J. Chem. Phys.*, vol. 105, no. 8, pp. 3278–3289, 1996.

[171] X. Crispin, C. Bureau, V. M. Geskin, R. Lazzaroni, W. R. Salaneck, and J. L. Brédas, "Chemisorption of acrylonitrile on the Cu(100) surface: a local density functional study," *J. Chem. Phys.*, vol. 111, no. 7, pp. 3237–3251, 1999.

[172] X. Crispin, V. Geskin, A. Crispin, J. Cornil, R. Lazzaroni, W. R. Salaneck, and J.-L. Brédas, "Characterization of the interface dipole at organic/ metal interfaces," *J. Am. Chem. Soc.*, vol. 124, no. 27, pp. 8131–8141, 2002.

[173] J. Carrasco, W. Liu, A. Michaelides, and A. Tkatchenko, "Insight into the description of van der Waals forces for benzene adsorption on transition metal (111) surfaces," *J. Chem. Phys.*, vol. 140, no. 8, p. 084704, 2014.

[174] S. Lukas, S. Vollmer, G. Witte, and C. Woll, "Adsorption of acenes on flat and vicinal Cu(111) surfaces: step induced formation of lateral order," *J. Chem. Phys.*, vol. 114, no. 22, pp. 10123–10130, 2001.

[175] J. c. v. Klimeš and A. Michaelides, "Perspective: advances and challenges in treating van der Waals dispersion forces in density functional theory," *J. Chem. Phys.*, vol. 137, no. 12, p. 120901, 2012.

[176] E. R. McNellis, J. Meyer, and K. Reuter, "Azobenzene at coinage metal surfaces: role of dispersive van der Waals interactions," *Phys. Rev. B*, vol. 80, p. 205414, Nov 2009.

[177] K. Berland, T. L. Einstein, and P. Hyldgaard, "Rings sliding on a honeycomb network: adsorption contours, interactions, and assembly of benzene on Cu(111)," *Phys. Rev. B*, vol. 80, p. 155431, Oct 2009.

[178] R. S. Mulliken, "Electronic population analysis on LCAO-MO molecular wave functions. I," *J. Chem. Phys.*, vol. 23, no. 10, pp. 1833–1840, 1955.

[179] F. L. Hirshfeld, "Bonded-atom fragments for describing molecular charge densities," *Theor. Chim. Acta*, vol. 44, pp. 129–138, Jun 1977.

[180] A. E. Reed, R. B. Weinstock, and F. Weinhold, "Natural population analysis," *J. Chem, Phys.*, vol. 83, no. 2, pp. 735–746, 1985.

[181] C. Fonseca Guerra, J.-W. Handgraaf, E. J. Baerends, and F. M. Bickelhaupt, "Voronoi Deformation Density (VDD) charges: assessment of the Mulliken, Bader, Hirshfeld, Weinhold, and VDD methods for charge analysis," *J. Comput. Chem.*, vol. 25, no. 2, pp. 189–210, 2004.

[182] K. B. Wiberg and P. R. Rablen, "Comparison of atomic charges derived via different procedures," *J. Comput. Chem.*, vol. 14, no. 12, pp. 1504–1518, 1993.

[183] E. Reguera, "Materials for hydrogen storage in nanocavities: Design criteria," *Int. J. Hydrogen Energ.*, vol. 34, no. 22, pp. 9163 – 9167, 2009.

[184] J. Gladh, H. Öberg, J. Li, M. P. Ljungberg, A. Matsuda, H. Ogasawara, A. Nilsson, L. G. M. Pettersson, and H. Öström, "X-ray emission spectroscopy and density functional study of CO/Fe(100)," *J. Chem. Phys.*, vol. 136, no. 3, p. 034702, 2012.

[185] M. Dell'Angela, T. Anniyev, M. Beye, R. Coffee, A. Föhlisch, J. Gladh, T. Katayama, S. Kaya, O. Krupin, J. LaRue, A. Møgelhøj, D. Nordlund, J. K.

Nørskov, H. Öberg, H. Ogasawara, H. Öström, L. G. M. Pettersson, W. F. Schlotter, J. A. Sellberg, F. Sorgenfrei, J. J. Turner, M. Wolf, W. Wurth, and A. Nilsson, "Real-time observation of surface bond breaking with an X-ray laser," *Science*, vol. 339, no. 6125, pp. 1302–1305, 2013.

[186] C. B. Verma, M. Quraishi, and A. Singh, "2-Aminobenzene-1,3-dicarbonitriles as green corrosion inhibitor for mild steel in 1 M HCl: electrochemical, thermodynamic, surface and quantum chemical investigation," *J. Taiwan Inst. Chem. E.*, vol. 49, pp. 229 – 239, 2015.

[187] S. Simpson, J. Hooper, D. P. Miller, D. A. Kunkel, A. Enders, and E. Zurek, "Modulating bond lengths via backdonation: A first-principles investigation of a quinonoid zwitterion adsorbed to coinage metal surfaces," *J. Phys. Chem. C*, vol. 120, no. 12, pp. 6633–6641, 2016.

[188] M. Toader, P. Shukrynau, M. Knupfer, D. R. T. Zahn, and M. Hietschold, "Site-dependent donation/backdonation charge transfer at the CoPc/Ag(111) interface," *Langmuir*, vol. 28, no. 37, pp. 13325–13330, 2012.

[189] J. Rodriguez-Fernandez, M. Robledo, K. Lauwaet, A. Martin-Jimenez, B. Cirera, F. Calleja, S. Diaz-Tendero, M. Alcami, L. Floreano, M. Dominguez-Rivera, A. L. Vazquez de Parga, D. Ecija, J. M. Gallego, R. Miranda, F. Martin, and R. Otero, "Tuning intermolecular charge transfer in donor-acceptor two-dimensional crystals on metal surfaces," *J. Phys. Chem. C*, vol. 121, no. 42, pp. 23505–23510, 2017.

[190] A. Zangwill, *Physics at Surfaces*. Cambridge University Press, 1988.

[191] H. Vazquez, F. Flores, R. Oszwaldowski, J. Ortega, R. Perez, and A. Kahn, "Barrier formation at metal-organic interfaces: dipole formation and the charge neutrality level," *Appl. Surf. Sci.*, vol. 234, no. 1, pp. 107 – 112, 2004.

[192] O. Ostroverkhova, "Organic optoelectronic materials: Mechanisms and applications," *Chem. Rev.*, vol. 116, no. 22, pp. 13279–13412, 2016.

[193] F. Cotton, *Advanced Inorganic Chemistry*. A Wiley-Interscience Publication, Wiley, 1999.

[194] L. N. Lewis, "Chemical catalysis by colloids and clusters," *Chem. Rev.*, vol. 93, no. 8, pp. 2693–2730, 1993.

[195] G. Schmid, V. Maihack, F. Lantermann, and S. Peschel, "Ligand-stabilized metal clusters and colloids: properties and applications," *J. Chem. Soc., Dalton Trans.*, pp. 589–595, 1996.

[196] P. Raveendran, J. Fu, and S. L. Wallen, "Completely green synthesis and stabilization of metal nanoparticles," *J. Am. Chem. Soc.*, vol. 125, no. 46, pp. 13940–13941, 2003.

[197] L. Nicolais and G. Carotenuto, *Metal-Polymer Nanocomposites*. Wiley, 2004.

[198] F. Rosei, M. Schunack, Y. Naitoh, P. Jiang, A. Gourdon, E. Laegsgaard, I. Stensgaard, C. Joachim, and F. Besenbacher, "Properties of large organic molecules on metal surfaces," *Prog. Surf. Sci.*, vol. 71, no. 5, pp. 95 – 146, 2003. Proceedings of the IXth Symposium on Surface Physics, Trest Castle 2002.

[199] R. Otero, A. V. de Parga, and J. Gallego, "Electronic, structural and chemical effects of charge-transfer at organic/inorganic interfaces," *Surf. Sci. Rep.*, vol. 72, no. 3, pp. 105 – 145, 2017.

[200] L. Brillson, *Surfaces and Interfaces of Electronic Materials*. Wiley - IEEE, Wiley, 2012.

[201] N. Koch, N. Ueno, and A. Wee, *The Molecule-Metal Interface*. Wiley, 2013.

[202] K. Wandelt, *Encyclopedia of interfacial chemistry: Surface science and electrochemistry*. Elsevier Science, 2018.

[203] B. Hammer and J. K. Nørskov, "Why gold is the noblest of all the metals," *Nature*, vol. 376, p. 238, 1995.

[204] B. Hammer and J. Nørskov, "Electronic factors determining the reactivity of metal surfaces," *Surf. Sci.*, vol. 343, no. 3, pp. 211 – 220, 1995.

[205] B. Hammer, Y. Morikawa, and J. K. Nørskov, "Co chemisorption at metal surfaces and overlayers," *Phys. Rev. Lett.*, vol. 76, pp. 2141–2144, Mar 1996.

[206] B. Hammer and J. Nørskov, "Theoretical surface science and catalysis-calculations and concepts," in *Impact of surface science on catalysis*, vol. 45 of *Advances in Catalysis*, pp. 71 – 129, Academic Press, 2000.

[207] F. Aguilar-Galindo and S. Díaz-Tendero, "Theoretical insights into vinyl derivatives adsorption on a Cu(100) surface," *J. Phys. Chem. C*, vol. 122, no. 48, pp. 27301–27313, 2018.

[208] B. Jiang and H. Guo, "Dynamics in reactions on metal surfaces: A theoretical perspective," *J. Chem. Phys.*, vol. 150, no. 18, p. 180901, 2019.

[209] H. Petek, H. Nagano, M. J. Weida, and S. Ogawa, "Quantum control of nuclear motion at a metal surface," *J. Phys. Chem. A.*, vol. 104, no. 45, pp. 10234–10239, 2000.

[210] H. Petek and S. Ogawa, "Surface femtochemistry: Observation and quantum control of frustrated desorption of alkali atoms from noble metals," *Annu. Rev. Phys. Chem.*, vol. 53, no. 1, pp. 507–531, 2002. PMID: 11972017.

[211] T. Szakacs, T. Lucza, and A. Lorincz, "Optimal control of quantum systems on metallic surfaces," *Surf. Sci.*, vol. 296, no. 2, pp. 251 – 260, 1993.

[212] P. Nuernberger, D. Wolpert, H. Weiss, and G. Gerber, "Femtosecond quantum control of molecular bond formation," *Proc. Natl. Acad. Sci.*, vol. 107, no. 23, pp. 10366–10370, 2010.

[213] C. Reuß, I. L. Shumay, U. Thomann, M. Kutschera, M. Weinelt, T. Fauster, and U. Höfer, "Control of the dephasing of image-potential states by CO adsorption on Cu(100)," *Phys. Rev. Lett.*, vol. 82, pp. 153–156, Jan 1999.

[214] J. Güdde, M. Rohleder, T. Meier, S. W. Koch, and U. Höfer, "Time-resolved investigation of coherently controlled electric currents at a metal surface," *Science*, vol. 318, no. 5854, pp. 1287–1291, 2007.

[215] P. Nuernberger, D. Wolpert, H. Weiss, and G. Gerber, "Femtosecond laser-assisted catalytic surface reactions of syngas and their optimization by tailored laser pulses," in *Ultrafast Phenomena XV* (P. Corkum, D. M. Jonas, R. J. D. Miller, and A. M. Weiner, eds.), (Berlin, Heidelberg), pp. 237–239, Springer Berlin Heidelberg, 2007.

[216] X. Cui, C. Wang, A. Argondizzo, S. Garrett-Roe, B. Gumhalter, and H. Petek, "Transient excitons at metal surfaces," *Nat. Phys.*, vol. 10, p. 505, 2014.

[217] M. Beye, T. Anniyev, R. Coffee, M. Dell'Angela, A. Föhlisch, J. Gladh, T. Katayama, S. Kaya, O. Krupin, A. Møgelhøj, A. Nilsson, D. Nordlund, J. K. Nørskov, H. Öberg, H. Ogasawara, L. G. M. Pettersson, W. F. Schlotter, J. A. Sellberg, F. Sorgenfrei, J. J. Turner, M. Wolf, W. Wurth, and H. Öström, "Selective ultrafast probing of transient hot chemisorbed and precursor states of CO on Ru(0001)," *Phys. Rev. Lett.*, vol. 110, p. 186101, May 2013.

[218] S.-W. Hla, G. Meyer, and K.-H. Rieder, "Inducing single-molecule chemical reactions with a UHV-STM: a new dimension for nano-science and technology," *ChemPhysChem*, vol. 2, no. 6, pp. 361–366, 2001.

[219] J. Henzl, M. Mehlhorn, H. Gawronski, K.-H. Rieder, and K. Morgenstern, "Reversible cis-trans isomerization of a single azobenzene molecule," *Angew. Chem. Int. Edit.*, vol. 45, no. 4, pp. 603–606, 2006.

[220] A. Safiei, J. Henzl, and K. Morgenstern, "Isomerization of an azobenzene derivative on a thin insulating layer by inelastically tunneling electrons," *Phys. Rev. Lett.*, vol. 104, p. 216102, May 2010.

[221] R. Martel, P. Avouris, and I.-W. Lyo, "Molecularly adsorbed oxygen species on Si(111)-(7x7): STM-induced dissociative attachment studies," *Science*, vol. 272, no. 5260, pp. 385–388, 1996.

[222] P. Avouris, R. Walkup, A. Rossi, H. Akpati, P. Nordlander, T.-C. Shen, G. Abeln, and J. Lyding, "Breaking individual chemical bonds via STM-induced excitations," *Surf. Sci.*, vol. 363, no. 1, pp. 368 – 377, 1996. Dynamical Quantum Processes on Solid Surfaces.

[223] P. Auburger, I. Kemeny, C. Bertram, M. Ligges, M. Bockstedte, U. Bovensiepen, and K. Morgenstern, "Microscopic insight into electron-induced dissociation of aromatic molecules on ice," *Phys. Rev. Lett.*, vol. 121, p. 206001, Nov 2018.

[224] L. J. Lauhon and W. Ho, "Single-molecule chemistry and vibrational spectroscopy: pyridine and benzene on Cu(001)," *J. Phys. Chem. A*, vol. 104, no. 11, pp. 2463–2467, 2000.

[225] S. Li, G. Czap, H. Wang, L. Wang, S. Chen, A. Yu, R. Wu, and W. Ho, "Bond-selected photodissociation of single molecules adsorbed on metal surfaces," *Phys. Rev. Lett.*, vol. 122, p. 077401, Feb 2019.

[226] M. Morin, N. J. Levinos, and A. L. Harris, "Vibrational energy transfer of CO/Cu(100): nonadiabatic vibration/electron coupling," *J. Chem. Phys.*, vol. 96, no. 5, pp. 3950–3956, 1992.

[227] J. D. Beckerle, M. P. Casassa, R. R. Cavanagh, E. J. Heilweil, and J. C. Stephenson, "Ultrafast infrared response of adsorbates on metal surfaces: vibrational lifetime of CO/Pt(111)," *Phys. Rev. Lett.*, vol. 64, pp. 2090–2093, Apr 1990.

[228] J. D. Beckerle, R. R. Cavanagh, M. P. Casassa, E. J. Heilweil, and J. C. Stephenson, "Subpicosecond transient infrared spectroscopy of adsorbates. Vibrational dynamics of CO/Pt(111)," *J. Chem. Phys.*, vol. 95, no. 7, pp. 5403–5418, 1991.

[229] P. R. Shirhatti, I. Rahinov, K. Golibrzuch, J. Werdecker, J. Geweke, J. Altschäffel, S. Kumar, D. J. Auerbach, C. Bartels, and A. M. Wodtke, "Observation of the adsorption and desorption of vibrationally excited molecules on a metal surface," *Nat. Chem.*, vol. 10, pp. 592–598, 2018.

[230] H. Ueba, "Vibrational state of the chemisorbed molecule on metal surfaces: Role of electron-hole pair excitation," *J. Chem. Phys.*, vol. 77, no. 7, pp. 3759–3766, 1982.

[231] K. Schönhammer and O. Gunnarsson, "Energy dissipation at metal surfaces: Electronic versus vibrational excitations," *J. Electron Spectrosc. Relat. Phenom.*, vol. 29, no. 1, pp. 91 – 103, 1983. The International Journal on Theoretical and Experimental Aspects of Electron Spectroscopy.

[232] Q. Ran, D. Matsiev, D. J. Auerbach, and A. M. Wodtke, "Observation of a change of vibrational excitation mechanism with surface temperature: HCl collisions with Au(111)," *Phys. Rev. Lett.*, vol. 98, p. 237601, Jun 2007.

[233] M. Grotemeyer and E. Pehlke, "Electronic energy dissipation during scattering of vibrationally excited molecules at metal surfaces: Ab initio simulations for HCl/Al(111)," *Phys. Rev. Lett.*, vol. 112, p. 043201, Jan 2014.

[234] S. P. Rittmeyer, V. J. Bukas, and K. Reuter, "Energy dissipation at metal surfaces," *Adv. Phys.-X*, vol. 3, no. 1, p. 1381574, 2018.

[235] D. Novko, J. C. Tremblay, M. Alducin, and J. I. Juaristi, "Ultrafast transient dynamics of adsorbates on surfaces deciphered: the case of CO on Cu(100)," *Phys. Rev. Lett.*, vol. 122, p. 016806, Jan 2019.

[236] A. Ge, B. Rudshteyn, J. Zhu, R. J. Maurer, V. S. Batista, and T. Lian, "Electron-hole-pair-induced vibrational energy relaxation of rhenium catalysts on gold surfaces," *J. Phys. Chem. Lett.*, vol. 9, no. 2, pp. 406–412, 2018. PMID: 29227669.

[237] J. Björk and S. Stafström, "Adsorption of large hydrocarbons on coinage metals: a van der Waals density functional study," *ChemPhysChem*, vol. 15, no. 13, pp. 2851–2858, 2014.

[238] S. Gautier, S. N. Steinmann, C. Michel, P. Fleurat-Lessard, and P. Sautet, "Molecular adsorption at Pt(111). How accurate are DFT functionals?," *Phys. Chem. Chem. Phys.*, vol. 17, pp. 28921–28930, 2015.

[239] P. E. Blöchl, "Projector augmented-wave method," *Phys. Rev. B*, vol. 50, pp. 17953–17979, Dec 1994.

[240] G. Kresse and D. Joubert, "From ultrasoft pseudopotentials to the projector augmented-wave method," *Phys. Rev. B*, vol. 59, pp. 1758–1775, Jan 1999.

[241] H. J. Monkhorst and J. D. Pack, "Special points for Brillouin-zone integrations," *Phys. Rev. B*, vol. 13, pp. 5188–5192, Jun 1976.

[242] M. Methfessel and A. T. Paxton, "High-precision sampling for Brillouin-zone integration in metals," *Phys. Rev. B*, vol. 40, pp. 3616–3621, Aug 1989.

[243] S. J. Blanksby and G. B. Ellison, "Bond dissociation energies of organic molecules," *Acc. Chem. Res.*, vol. 36, no. 4, pp. 255–263, 2003.

[244] H. Vázquez, Y. J. Dappe, J. Ortega, and F. Flores, "Energy level alignment at metal/organic semiconductor interfaces: "pillow" effect, induced density of interface states, and charge neutrality level," *J. Chem. Phys.*, vol. 126, no. 14, p. 144703, 2007.

[245] Y. Hamada, Y. Nishimura, and M. Tsuboi, "Infrared spectrum of trans-acrolein," *Chem. Phys.*, vol. 100, no. 3, pp. 365 – 375, 1985.

[246] J. Tornero, H. Telle, G. García, and A. González-Ureña, "Vibrational excitation of adsorbed molecules by photoelectrons of very low energy: acrylonitrile on Cu(100)," *Phys. Chem. Chem. Phys.*, vol. 13, pp. 8475–8484, 2011.

[247] H. Guo, P. Saalfrank, and T. Seideman, "Theory of photoinduced surface reactions of admolecules," *Prog. Surf. Sci.*, vol. 62, no. 7, pp. 239 – 303, 1999.

[248] B. Doppagne, M. C. Chong, E. Lorchat, S. Berciaud, M. Romeo, H. Bulou, A. Boeglin, F. Scheurer, and G. Schull, "Vibronic spectroscopy with submolecular resolution from stm-induced electroluminescence," *Phys. Rev. Lett.*, vol. 118, p. 127401, Mar 2017.

[249] D. Pommier, R. Bretel, L. E. P. López, F. Fabre, A. Mayne, E. Boer-Duchemin, G. Dujardin, G. Schull, S. Berciaud, and E. Le Moal, "Scanning tunneling microscope-induced excitonic luminescence of a two-dimensional semiconductor," *Phys. Rev. Lett.*, vol. 123, p. 027402, Jul 2019.

[250] E. V. Chulkov, I. Sarría, V. M. Silkin, J. M. Pitarke, and P. M. Echenique, "Lifetimes of image-potential states on copper surfaces," *Phys. Rev. Lett.*, vol. 80, pp. 4947–4950, Jun 1998.

[251] J. Bardeen, "Tunnelling from a many-particle point of view," *Phys. Rev. Lett.*, vol. 6, pp. 57–59, Jan 1961.

[252] M. C. Payne, "Transfer hamiltonian description of resonant tunnelling," *J. Phys. C: Solid State Phys*, vol. 19, pp. 1145–1155, mar 1986.

[253] J. Tersoff and D. R. Hamann, "Theory of the scanning tunneling microscope," *Phys. Rev. B*, vol. 31, pp. 805–813, Jan 1985.

[254] T. Hecht, H. Winter, A. G. Borisov, J. P. Gauyacq, and A. K. Kazansky, "Role of the 2d surface state continuum and projected band gap in charge transfer in front of a Cu(111) surface," *Phys. Rev. Lett.*, vol. 84, pp. 2517–2520, Mar 2000.

[255] A. G. Borisov, J. P. Gauyacq, A. K. Kazansky, E. V. Chulkov, V. M. Silkin, and P. M. Echenique, "Long-lived excited states at surfaces: Cs/Cu(111) and Cs/Cu(100) systems," *Phys. Rev. Lett.*, vol. 86, pp. 488–491, Jan 2001.

[256] F. Matino, G. Schull, F. Köhler, S. Gabutti, M. Mayor, and R. Berndt, "Electronic decoupling of a cyclophane from a metal surface," *Proc. Natl. Acad. Sci.*, vol. 108, no. 3, pp. 961–964, 2011.

[257] T. G. Gopakumar, T. Brumme, J. Kröger, C. Toher, G. Cuniberti, and R. Berndt, "Coverage-driven electronic decoupling of Fe-phthalocyanine from a Ag(111) substrate," *J. Phys. Chem. C.*, vol. 115, no. 24, pp. 12173–12179, 2011.

[258] W. Steurer, J. Repp, L. Gross, I. Scivetti, M. Persson, and G. Meyer, "Manipulation of the charge state of single Au atoms on insulating multilayer films," *Phys. Rev. Lett.*, vol. 114, p. 036801, Jan 2015.

[259] X. Kang and M. Zhu, "Tailoring the photoluminescence of atomically precise nanoclusters," *Chem. Soc. Rev.*, vol. 48, pp. 2422–2457, 2019.

[260] M. Allan, M. Lacko, P. Papp, v. Matejčík, M. Zlatar, I. I. Fabrikant, J. Kočišek, and J. Fedor, "Dissociative electron attachment and electronic excitation in $Fe(CO)_5$," *Phys. Chem. Chem. Phys.*, vol. 20, pp. 11692–11701, 2018.

[261] J. Lengyel, J. Fedor, and M. Fárník, "Dissociative electron attachment to HNO_3 and its hydrates: energy-selective electron-induced chemistry," *Phys. Chem. Chem. Phys.*, vol. 21, pp. 8691–8697, 2019.

[262] F. Forster, S. Hufner, and F. Reinert, "Rare gases on noble-metal surfaces. An Angle-Resolved Photoemission study with high energy resolution," *J. Phys. Chem. B.*, vol. 108, no. 38, pp. 14692–14698, 2004.

[263] J. Güdde and U. Höfer, "Femtosecond time-resolved studies of image-potential states at surfaces and interfaces of rare-gas adlayers," *Prog. Surf. Sci.*, vol. 80, no. 3, pp. 49 – 91, 2005.

[264] M. Wolf, E. Knoesel, and T. Hertel, "Ultrafast dynamics of electrons in image-potential states on clean and Xe-covered Cu(111)," *Phys. Rev. B*, vol. 54, pp. R5295–R5298, 1996.

[265] J. Repp, W. Steurer, I. Scivetti, M. Persson, L. Gross, and G. Meyer, "Charge-state-dependent diffusion of individual gold adatoms on ionic thin NaCl films," *Phys. Rev. Lett.*, vol. 117, p. 146102, Sep 2016.

[266] I. Scivetti and M. Persson, "Frontier molecular orbitals of a single molecule adsorbed on thin insulating films supported by a metal substrate: electron and hole attachment energies," *J. Phys. Condens. Matter*, vol. 29, p. 355002, aug 2017.

[267] X. H. Qiu, G. V. Nazin, and W. Ho, "Vibrationally resolved fluorescence excited with submolecular precision," *Science*, vol. 299, no. 5606, pp. 542–546, 2003.

[268] Y.-M. Kuang, Y.-J. Yu, J.-Z. Zhu, Y. Zhang, and Z.-C. Dong, "Tunneling electron induced fluorescence from single porphyrin molecules decoupled by striped-phase octanethiol self-assembled monolayer," *Chin. J. Chem. Phys.*, vol. 29, no. 2, pp. 157–160, 2016.

[269] G. de la Torre, P. Vazquez, F. Agullo-López, and T. Torres, "Phthalocyanines and related compounds:organic targets for nonlinear optical applications," *J. Mater. Chem.*, vol. 8, pp. 1671–1683, 1998.

[270] G. de la Torre, P. Vazquez, F. Agullo-López, and T. Torres, "Role of structural factors in the nonlinear optical properties of phthalocyanines and related compounds," *Chem. Rev.*, vol. 104, no. 9, pp. 3723–3750, 2004. PMID: 15352778.

[271] M. V. Martinez-Diaz, G. de la Torre, and T. Torres, "Lighting porphyrins and phthalocyanines for molecular photovoltaics," *Chem. Commun.*, vol. 46, pp. 7090–7108, 2010.

[272] C. Cohen-Tannoudji, B. Diu, F. Laloe, N. Ostrowsky, and D. Ostrowsky, *Quantum Mechanics*. Wiley-VCH Verlag GmbH, 2019.

Publications

List of publications related to this thesis

1. Fernando Aguilar-Galindo and Sergio Díaz-Tendero.
   Theoretical Insights into Vinyl Derivatives Adsorption on a Cu(100) Surface
   Journal of Physical Chemistry C, **122**, 27301 (2018)

2. Fernando Aguilar-Galindo and Sergio Díaz-Tendero.
   Outstanding energy exchange between organic molecules and metal surfaces: decomposition kinetics of excited vinyl derivatives driven by the interaction with a Cu(111) surface
   Journal of Physical Chemistry C, **123**, 19625 (2019)

3. Fernando Aguilar-Galindo, Sergio Díaz-Tendero and Andrei G. Borisov.
   Unraveling the extraordinary enhance of the lifetime of molecular anions due to isulating layers
   (In preparation)

List of publications not related to this thesis

1. Fernando Aguilar-Galindo, M. Merced Montero-Campillo, Manuel Yáñez and Otilia Mó.
   On the Stability Of [Pb(Proline)]2+ Complexes. Reconciling Theory With Experiment
   Chemical Physics Letters, **598**, 91 (2014)

2. Pablo Ares, Fernando Aguilar-Galindo, David Rodríguez-San-Miguel, Diego A. Aldave, Sergio Díaz-Tendero, Manuel Alcamí, Fernando Martín, Julio Gómez-Herrero and Félix Zamora.
   Mechanical Isolation of Highly Stable Antimonene under Ambient Conditions
   Advanced Materials, **28**, 6332 (2016)

3. Enrique Arpa, Fernando Aguilar-Galindo and Sergio Díaz-Tendero.
Unravelling the Mechanism of Non-photoactivated [2+2] Cycloaddition Reactions: Relevance of Orbital Interactions and Zwitterionic Intermediates
ChemistrySelect, **2**, 1089 (2017)

4. Fernando Aguilar-Galindo, Pilar Ocón and José Manuel López Poyato.
Exploring the catalytic efficiency of X-doped (X=B, N, P) graphene in oxygen reduction reaction: Influence of solvent and border effects
International Journal of Quantum Chemistry, **118**, 25579 (2018)

5. Fernando Aguilar-Galindo, Sergio Díaz-Tendero and Andrei G. Borisov.
Electronic Structure Effects in the Coupling of a Single Molecule with a Plasmonic Antenna
Journal of Physical Chemistry C, **123**, 4446 (2019)

6. Antonio Casado-Sánchez, Mustafa Uygur, Daniel González-Muñoz, Fernando Aguilar-Galindo, José Luis Nova-Fernández, Judith Arranz-Plaza, Sergio Díaz-Tendero, Silvia Cabrera, Olga Garcia Mancheno, and José Alemán.
8-Mercaptoquinoline as Ligand for Enhancing the Photocatalytic Activity of Pt(II) Coordination Complexes: Reactions and Mechanistic Insights
Journal of Organic Chemistry, **84**, 6437 (2019)

7. Fernando Aguilar-Galindo, Ana María Tuñón, Alberto Fraile, José Alemán, Sergio Díaz-Tendero.
Role of intramolecular hydrogen bonds and electron withdrawing groups in the acidity of aldimines and ketimines: a density functional theory study
Theoretical Chemistry Accounts, **138**, 59 (2019)